

**PROGRESS IN RESEARCH**

**APRIL 1, 2004 - MARCH 31, 2005**

**Prepared By**

**The Cyclotron Institute Staff**

**Texas A&M University**

**College Station, TX 77843-3366**

**Phone: (979) 845-1411**

**Fax: (979) 845-1899**

**Web: <http://cyclotron.tamu.edu>**

**July 2005**

## TABLE OF CONTENTS

<b>Introduction .....</b>	<b>viii</b>
R.E. Tribble, Director	

### SECTION I: NUCLEAR STRUCTURE, FUNDAMENTAL INTERACTIONS AND ASTROPHYSICS

<b><math>{}^6\text{Li}</math> Elastic and Inelastic Scattering on <math>{}^{116}\text{Sn}</math> .....</b>	<b>I-1</b>
X. Chen, Y. -W. Lui, H. L. Clark, Y. Tokimoto, and D. H. Youngblood	
<b>Elastic Scattering of Drip Line Nucleus <math>{}^{17}\text{F}</math> .....</b>	<b>I-6</b>
F. Carstoiu, L. Trache, J.C. Blackmon, D.W. Bardayan, C.R. Brune, C.A. Gagliardi, U. Greife, C.J. Gross, C.C. Jewett, R.L. Kozub, T.A. Lewis, J.F. Liang, B.H. Moazen, A.M. Mukhamedzhanov, C.D. Nesarja, F.M. Nunes, P.D. Parker, L. Sahin, J.P. Scott, D. Shapira, M.S. Smith, J.S. Thomas, and R.E. Tribble	
<b>Scattering of <math>{}^7\text{Be}</math> and <math>{}^8\text{B}</math> and Consequences for the Astrophysical <math>S_{17}</math> Factor .....</b>	<b>I-8</b>
G. Tabacaru, A. Azhari, J. Brinkley, V. Burjan, F. Carstoiu, C. Fu, C. A. Gagliardi, V. Kroha, A.M. Mukhamedhanov, X. Tang, L. Trache and R. E. Tribble	
<b>Asymptotic Normalization Coefficients for <math>{}^{13}\text{C} \rightarrow {}^{12}\text{C}+n</math> .....</b>	<b>I-10</b>
T. Al-Abdullah, F. Carstoiu, X. Chen, C. Fu, C. A. Gagliardi, Y.-W. Lui, G. Tabacaru, Y. Tokimoto, L. Trache, and R. E. Tribble	
<b>Determining the <math>{}^{22}\text{Mg}(p,\gamma){}^{23}\text{Al}</math> Reaction Rate Through a Measurement of the ANCs in the Mirror System .....</b>	<b>I-12</b>
T. Al-Abdullah, F. Carstoiu, X. Chen, H. Clark, C. Fu, C. A. Gagliardi, Y.-W. Lui, S. Piskor, G. Tabacaru, Y. Tokimoto, L. Trache, and R. E. Tribble	
<b>Status of <math>{}^{14}\text{O} + \alpha</math> Experiment .....</b>	<b>I-14</b>
Changbo Fu, V. Z. Goldberg, G. G. Chubaryan, G. Tabacaru, L. Trache, and R.E. Tribble	
<b><math>{}^{12}\text{N}</math> Structure in the Resonance <math>{}^{11}\text{C}+p</math> Interaction .....</b>	<b>I-15</b>
V. Z. Goldberg, G. Tabacaru, Changbo Fu, G. Chubaryan, R. E. Tribble, G. V. Rogachev, A. B. Volya B. A. Brown B. B. Skorodumov, and X. D. Tang	
<b>Alpha Cluster Structure in <math>{}^{18}\text{O}</math> .....</b>	<b>I-16</b>
Changbo Fu, V. Z. Goldberg, K.-M. Kallman, T. Lonroth, P. Manngard, B. B. Skorodumov, G. V. Rogachev, S. Brown, K. Kemper, B. Green, E. Johnson, O. Momotyuk and B. Roeder	

<b>In a Search for a Way to Study Neutron Rich Drip-Line Nuclei (Studies of Analog States of Drip Line Nuclei) .....</b>	<b>I-17</b>
V. Z. Goldberg, G.Chubaryan, G. V.Rogachev, J. J. Kolata, A. Aprahamian, B. B. Skorodumov, P. Booutachkov, A. Woehr, M. Quinn, L. Lamm, G. M. Ter-Akopian, M. S. Golovkov, a. Fomichev, and A. M. Rodin	
<b>Precise Branching-Ratio Measurement for the <math>\beta</math> Decay of <math>^{21}\text{Na}</math> .....</b>	<b>I-19</b>
V. E. Iacob, J. C. Hardy, C. A. Gagliardi, N. Nica, G. Tabacaru, L. Trache, R. E. Tribble and I. S. Towner	
<b>The Half-Life of <math>^{34}\text{Ar}</math>: A New Technique for Analyzing Combined Parent-Daughter Decay Curves .....</b>	<b>I-21</b>
V. E. Iacob, J. C. Hardy, C. A. Gagliardi, V. E. Mayes, N. Nica, G. Tabacaru, L. Trache and R. E. Tribble	
<b>Relative Efficiency Calibration for a Plastic Scintillator: Source Measurements and Monte Carlo Calculations .....</b>	<b>I-24</b>
V.E. Iacob and J.C. Hardy	
<b>Precise Experimental Tests of Calculated Internal-Conversion Coefficients: the Decays of <math>^{191}\text{Os}</math> and <math>^{193\text{m}}\text{Ir}</math>, and the Fluorescence Yield in Iridium .....</b>	<b>I-26</b>
J.C. Hardy and I.S. Towner	
<b>A New Critical Survey of Superalloyed <math>0^+ \rightarrow 0^+</math> Nuclear <math>\beta</math>-Decay: Improved Limits on Fundamental Weak-Interaction Parameters.....</b>	<b>I-29</b>
J. C. Hardy and I. S. Towner	
<b>TRIUMF: High Precision Measurements of <math>^{26}\text{Na}</math> <math>\beta^-</math> Decay .....</b>	<b>I-33</b>
V. E. Iacob and J. C. Hardy	
<b>Canadian Penning Trap: Q-Value of the Superalloyed Decay of <math>^{22}\text{Mg}</math> .....</b>	<b>I-34</b>
I. S. Towner and J. C. Hardy	
<b>Canadian Penning Trap: Q-Value of the Superalloyed Decay of <math>^{46}\text{V}</math> .....</b>	<b>I-35</b>
J. C. Hardy	
<b>TWIST: Measuring the Space-Time Structure of Muon Decay .....</b>	<b>I-36</b>
C. A. Gagliardi, J. R. Musser, R. E. Tribble, M. A. Vasilev, and the TWIST Collaboration	
<b>The Physics of STAR at RHIC .....</b>	<b>I-39</b>
C. A. Gagliardi, T. W. Henry, R. E. Tribble, and the STAR Collaboration	

## SECTION II: HEAVY ION REACTIONS

<b>Refining Reaction Dynamics in Fermi Energy Heavy Ion Reactions .....</b>	<b>II-1</b>
R. Wada, T. Keutgen, K. Hagel, J. Wang, M. Murray, L. Qin, J. B. Natowitz, T. Materna, and S. Kowalski	
<b>Isoscaling for Heavy Ion Reaction at Intermediate Energies .....</b>	<b>II-3</b>
S. Kowalski, R. Wada, K. Hagel, T. Materna, J. B. Natowitz, J. S. Wang, Y. Ma, T. Keutgen, L. Qin, M. Murray, A. Makeev, P. Smith, J. Cibor, C. Hamilton, A. S. Botvina, E. Bell, S. Liddick, D. Rowland, A. Ruangma, M. Veselsky, E. Winchester, G.A. Souliotis, S. J. Yennello, A. Samant, M. Cinausero, D. Fabris, E. Fioretto, M. Lunardon, G. Nebbia, G. Prete, G. Viesti, Z. Majka, P. Staszal, W. Zipper, M. E. Brandan, A. Martinez-Rocha, A. Menchaca-Rocha, and Y.El Masri	
<b>Reconstruction of the Primary Fragment Distribution in Multi-Fragmentation Reactions.....</b>	<b>II-6</b>
S. Kowalski, R. Wada, K. Hagel, T. Materna, J. B. Natowitz, J. S. Wang, Y. Ma, T. Keutgen, L. Qin, M. Murray, A. Makeev, P. Smith, J. Cibor, C. Hamilton, A. S. Botvina, E. Bell, S. Liddick, D. Rowland, A. Ruangma, M. Veselsky, E. Winchester, G. A. Souliotis, S. J. Yennello, A. Samant, M. Cinausero, D. Fabris, E. Fioretto, M. Lunardon, G. Nebbia, G. Prete, G. Viesti, Z. Majka, P. Staszal, W. Zipper, M. E. Brandan, A. Martinez-Rocha, A. Menchaca-Rocha, and Y.El Masri	
<b>Exploring New Ways to Produce Heavy and Superheavy Nuclei with BigSol .....</b>	<b>II-8</b>
T. Materna, S. Kowalski, K. Hagel, R. Murthy, J. Natowitz, L. Qin, G. Souliotis, R. Wada, J. Wang, D. Fabris, M. Lunardon, M. Morando, S. Moretto, G. Nebbia, S. Pesente, V. Rizzi, G. Viesti, V. Bocci, M. Barbui, A. Andrighetto, M. Cinausero, G. Prete, Z. Majka, and A. Wieloch	
<b>BRAHMS Results.....</b>	<b>II-10</b>
K. Hagel, R. Wada, T. Materna, S. Kowalski, J. B. Natowitz, and the BRAHMS Collaboration	
<b>Density Dependence of the Symmetry Energy and the Equation of State of Isospin Asymmetric Nuclear Matter .....</b>	<b>II-12</b>
D.V. Shetty, S.J. Yennello, and G.A. Souliotis	
<b>Symmetry Energy and the Influence of Neutron Composition and Excitation Energy in Nuclear Multifragmentation.....</b>	<b>II-14</b>
D.V. Shetty, A.S. Botvina, S.J. Yennello, G.A. Souliotis, E. Bell, and A. Keksis	
<b>Production of Very Neutron-Rich Fragments in the Multifragmentation of Neutron-Rich Systems .....</b>	<b>II-16</b>
G. A. Souliotis, D. V. Shetty, M. Veselsky, A. Botvina, A. Keksis, E. Bell, M. Jandel, and S. J. Yennello	

<b>Apparent Critical Behavior in Fragmentation of Z=12-15 Quasi-Projectiles and Its Dependence on N/Z Degree of Freedom .....</b>	<b>II-19</b>
M. Jandel, S. Wuenschel, S. J. Yennello, G. A. Souliotis, D. V. Shetty and A. Keksis	
<b>Additional Tool for the Calibration of FAUST Si-CsI Telescopes Using Inelastic Reactions <math>^3\text{He}+^{13}\text{C}\rightarrow^{3,4}\text{He}+^{12,13}\text{C}</math> at 25 MeV/nucleon.....</b>	<b>II-21</b>
M. Jandel, R. Varner, G. A. Souliotis, A. Keksis, B. Stein, S. Soisson, D. V. Shetty, E. Bell, J. Iglío, S. Wuenschel, M. Sarahan, C. Richers, J. Garey and S. J. Yennello	
<b><math>\gamma</math>-ray Emission Characteristics in the Peripheral Reaction of <math>^{36}\text{Ar}+^{197}\text{Au}, ^{\text{nat}}\text{Th}</math> at 25 and 45 MeV/nucleon.....</b>	<b>II-22</b>
M. Jandel, R. Varner, G. A. Souliotis, A. Keksis, B. Stein, S. Soisson, D. V. Shetty, E. Bell, J. Iglío, S. Wuenschel, J. Garey, C. Richers and S. J. Yennello	
<b>Using Light Cluster Production to Determine the Density Dependence of Nuclear Symmetry Energy .....</b>	<b>II-23</b>
S. N. Soisson, E. Bell, L. W. Chen, S. J. Yennello and the NIMROD Collaboration	
<b>(N/Z) Equilibration .....</b>	<b>II-24</b>
E. Bell, J. Garey, K. Hagel, D. Shetty, S. Soisson, R. Wada, S. J. Yennello, and the NIMROD Collaboration	
<b>Angular Distributions of Fragments from the Reaction 32 MeV/u <math>^{48}\text{Ca}</math> on <math>^{112}\text{Sn}</math>.....</b>	<b>II-25</b>
A. L. Keksis, M. Veselsky, G. A. Souliotis, E. Bell, M. Jandel, A. Ruangma, D. Shetty, E. M. Winchester and S. J. Yennello	
<b>Forward Indiana Ring Silicon Telescope (FIRST): An Array for the Study of Peripheral Heavy-Ion Collisions at Intermediate Energies .....</b>	<b>II-27</b>
T. Padaszynski, P. Sprunger, R. T. de Souza, S. Hudan, A. Alexander, B. Davin, G. Fleener, A. McIntosh, C. Metelko, R. Moore, N. Peters, J. Poehlman, J. Gauthier, F. Grenier, R. Roy, D. Theriault, E. Bell, J. Garey, J. Iglío, A. L. Keksis, S. Parketon, C. Richers, D. V. Shetty, S. N. Soisson, G. A. Soulioutis, B. Stein, and S. J. Yennello	
<b>Probing the Density Dependence of the Nuclear Symmetry Energy via Heavy Residue Isoscaling .....</b>	<b>II-29</b>
G.A. Souliotis, D.V. Shetty, A. Keksis, E. Bell, M. Jandel, M. Veselsky and S.J. Yennello	
<b>p-A, A-A Collisions with NIMROD.....</b>	<b>II-31</b>
L. J. Qin, R.Wada, K. Hagel, J. S. Wang, T. Keutgen, S. Kowalski, Y. Ma, M. Murray, A. Makeev, P. Smith, J. B. Natowitz, J. Cibor, C. Hamilton, E. Bell, S. Liddick, D. Rowland, A. Ruangma, M. Veselsky, E. Winchester, G.A. Souliotis, S. J. Yennello, A. Samant, M. Cinausero, D. Fabris, E. Fioretto, M. Lunardon, G. Nebbia, G. Prete, G. Viesti, Z. Majka, P. Staszal, W. Zipper, M. E. Brandan, A. Martinez-Rocha, A. Menchaca-Rocha, and Y.El Masri	

### SECTION III: NUCLEAR THEORY

<b>Charm Elliptic Flow at RHIC</b> .....	III-1
B. Zhang, L. W. Chen, and C. M. Ko	
<b>Pseudorapidity Dependence of Anisotropic Flows in Relativistic Heavy Ion Collisions</b> .....	III-2
L. W. Chen, V. Greco, C. M. Ko, and P. F. Kolb	
<b>Determination of the Stiffness of the Nuclear Symmetry Energy from Isospin Diffusion</b> .....	III-3
L. W. Chen, C. M. Ko, and B. A. Li	
<b>Relativistic Heavy Ion Collisions at the Large Hadron Collider</b> .....	III-4
Z. W. Lin, C. M. Ko, B. Zhang, B. A. Li, and S. Pal	
<b>Hadron Production from Quark Coalescence and Jet Fragmentation</b> .....	III-5
V. Greco, C. M. Ko, and I. Vitev	
<b>In-Medium Modifications of the Nucleon and <math>\Lambda(1232)</math> at RHIC</b> .....	III-6
Hendrik van Hees and Ralf Rapp	
<b>Charm-Quark Thermalization in the Quark-Gluon Plasma</b> .....	III-8
Hendrik van Hees and Ralf Rapp	
<b>Hadronic Modes and Quark Properties in the Quark-Gluon Plasma</b> .....	III-10
M. Mannarelli and R. Rapp	
<b>Meissner Masses in the gCFL Phase of QCD</b> .....	III-12
R. Casalbuoni, R. Gatto, M. Mannarelli, G. Nardulli and M. Ruggieri	
<b>Thermal Photons in Strong Interactions</b> .....	III-14
Ralf Rapp	
<b>In-Medium Effects on Charmonium Production in Heavy-Ion Collisions</b> .....	III-15
L. Grandchamp, R. Rapp and G.E. Brown	
<b>Astrophysical Resonant Reactions in Trojan Horse Method</b> .....	III-16
A.M. Mukhamedzhanov, Sh. M. Allison, S. Sherubini, C. Spitaleri, and A. Tumino	
<b>Theory of the Breakup Reactions for Charged Particles: from Exact to the DWBA Amplitude</b> .....	III-17
A. M. Mukhamedzhanov, F. Pirlpesov, A. S. Kadyrov, A. T. Stelbovics, and I. Bray	

<b>Combined Method to Extract Spectroscopic Information .....</b>	<b>III-18</b>
A. M. Mukhamedzhanov, F. M. Nunes	
<b>Complete Asymptotic Boundary Conditions for the Three Charged Particles Scattering Wave Function .....</b>	<b>III-20</b>
A. M. Mukhamedzhanov, F. Pirlepesov, A. S. Kadyrov, A. T. Stelbovics, and I. Bray	
<b>Asymptotic Scattering Wave Function for Three Charged Particles in the Continuum .....</b>	<b>III-21</b>
A. M. Mukhamedzhanov, F. Pirlepesov, and A. S. Kadyrov	
<b>Determination of the Parameters of a Skyrme Type Effective Interaction Using an Extensive Set of Experimental Data.....</b>	<b>III-23</b>
B. K. Agrawal, S. Shlomo, and V. Kim Au	
<b>Viscosity Effects on Isoscalar Compression Modes .....</b>	<b>III-24</b>
A. G. Pochivalov, S. Shlomo and V. M. Kolomietz	
<b>Structure of Isovector Excitation Mode in Spherical Asymmetric Nuclei.....</b>	<b>III-25</b>
V. M. Kolomietz, A. G. Magner and S. Shlomo	
<b>Effects of Self-Consistency Violations in HF-RPA Calculations for Giant Multipole Resonances.....</b>	<b>III-27</b>
Tapas Sil, S. Shlomo, B. K. Agrawal and P.-G. Reinhard	
<b>Non-Markovian Langevin Dynamics of Nuclear Fermi Liquid Drop.....</b>	<b>III-29</b>
V.M. Kolomietz, S.V. Radionov, and S. Shlomo	

#### SECTION IV: ATOMIC AND MOLECULAR SCIENCE

<b>Ratio of Double to Single <i>L</i>-shell Ionization of Holmium Atoms.....</b>	<b>IV-1</b>
V. Horvat, R. L. Watson, and Yong Peng	
<b>Cross Sections for Electron Stripping of Light Fully Stripped Ions by Hydrogen and Helium Atoms.....</b>	<b>IV-5</b>
I. D. Kaganovich, E. A. Startsev, R. C. Davidson, S. R. Kecskemeti, A. Bin-Nun, D. Mueller, L. Grisham, R. L. Watson, V. Horvat, K. E. Zaharakis, Y. Peng	
<b>A Hybrid Approach to the Calculation of Cross Sections for Electron Stripping.....</b>	<b>IV-7</b>
I. D. Kaganovich, E. A. Startsev, R. C. Davidson, S. R. Kecskemeti, A. Bin-Nun, D. Mueller, L. Grisham, R. L. Watson, V. Horvat, K. E. Zaharakis, Y. Peng	

<b>Systematics of Multiple <i>L</i>-shell Ionization in <i>K</i>-shell Ionizing Collisions .....</b>	<b>IV-9</b>
V. Horvat, R. L. Watson, and Yong Peng	

**SECTION V: SUPERCONDUCTING CYCLOTRON AND INSTRUMENTATION**

<b>K500 Operations and Development.....</b>	<b>V-1</b>
D. P. May, G. J. Kim, H. L. Clark, F. P. Abegglen, G. J. Derrig, and W. H. Peeler	
<b>Radiation Effects Facility .....</b>	<b>V-3</b>
H. L. Clark, V. Horvat, B. Hyman, and D. Utley	
<b>Cyclotron Computing .....</b>	<b>V-5</b>
R. Burch, K. Hagel, and M. Vasilyev	
<b>Cyclotron Institute Upgrade Project.....</b>	<b>V-6</b>
H. L. Clark	

**SECTION VI: PUBLICATIONS**

<b>Papers Published.....</b>	<b>VI-1</b>
------------------------------	-------------

**SECTION VII: APPENDIX**

<b>Talks Presented .....</b>	<b>VII-1</b>
<b>Research Personnel and Engineering Staff .....</b>	<b>VII-8</b>
<b>Students.....</b>	<b>VII-9</b>
<b>Organizational Chart.....</b>	<b>VII-10</b>
<b>Graduate Degree Students .....</b>	<b>VII-11</b>
<b>Institute Colloquia and Seminars .....</b>	<b>VII-12</b>

## Introduction

April 1, 2004 – March 31, 2005

This document summarizes the progress in research and operations at the Texas A&M Cyclotron Institute for the period April, 1, 2004 through March 31, 2005. Sections I through IV contain reports from individual research projects. Operation and technical developments are given in Section V. Section VI lists the publications with Cyclotron Institute authors and the Appendix gives additional information including talks presented by members of the Institute during the past year. This volume of Progress in Research continues our new format where publication will be solely on our web site (<http://cyclotron.tamu.edu>). *Since most of the contributions presented here are truly reports on progress in research, results and conclusions should not be quoted from the report without the consent of the authors.*

This past year has been an extremely busy one for us at the Institute. In the spring 2004, we were notified by the Department of Energy that our proposal for upgrading the Cyclotron Institute had been approved and funding would be provided following the completion of a project management plan and a technical review. The upgrade project involves refurbishing our K150 cyclotron and using it as a driver to produce radioactive isotopes. The radioactivity will be slowed down in gas-filled ion guides and then fed to the K500 cyclotron, through a charge breeding electron cyclotron resonance ion source, for reacceleration. During last spring and summer, an Upgrade Management Plan was developed for the project. Following a technical review in September, 2004, the Management Plan was approved by the Department of Energy and the project officially began in December, 2004. Present plans call for the first reaccelerated beams from the K500 to be available in calendar year 2010.

Even with the upgrade effort underway, Cyclotron Institute research programs have continued to make significant progress. Some recent achievements are noted here.

- (1) The symmetry energy has been extracted from results of experiments on isoscaling of fragments produced in heavy-ion collisions ( $A = 58$  Fe and Ni on Fe and Ni targets at 30, 40 and 47 MeV/A) and the influence of neutron composition and excitation on fragment production and secondary decay has been investigated via statistical multi-fragmentation model calculations.
- (2) Results have been obtained for the  $^{22}\text{Mg}(p,\gamma)^{23}\text{Al}$  reaction at stellar energies using charge symmetry and a measurement of the asymptotic normalization coefficient for  $^{22}\text{Ne} + p \leftrightarrow ^{23}\text{Ne}$ .
- (3) A novel method to determine spectroscopic factors from (d,p) reactions has been developed based on information about asymptotic normalization coefficients.
- (4) Antisymmetrized molecular dynamics investigations of isoscaling techniques for determinations of the symmetry energy at low density demonstrate that secondary decay can not be ignored as has previously been assumed.

- (5) Recent measurements of K and L shell ionization by heavy ions have been used to establish universal scaling parameters for L and M shell spectator vacancy fractions and double to single vacancy population ratios.
- (6) Measurements have been completed by the TWIST collaboration producing new results for the Michel parameters  $\rho$  and  $\delta$  with precisions of  $\approx 0.001$ , factors of 2.5-3 better than the previous world averages.
- (7) Due to violations of self-consistency in Hartree-Fock based RPA calculations, shifts in the centroid energies of compression modes can be as large as 1 MeV, leading to a shift of 30 MeV in the extracted value of the nuclear compressibility.
- (8) Using hadronic (D-meson) resonances in an effective model for a strongly coupled Quark-Gluon Plasma, new results find that charm-quark thermalization times could be reduced by a factor of about 3 compared to predictions from perturbative QCD calculations. This result could change our understanding of D-meson spectra and elliptic flow at RHIC.
- (9) Significant constraints on the isobaric incompressibility of asymmetric nuclear matter have been obtained by a comparison of the predictions from an isospin- and momentum-dependent transport model with isospin diffusion data from heavy-ion collisions at intermediate energies.
- (10) A major new critical survey of superallowed nuclear beta decay has been completed and published, in which tight constraints have been set on several weak-interactions parameters fundamental to the conservation of the vector current and the Standard Model.

As in the past, Institute scientists remain active in a number of collaborative research efforts around the world. Major programs include: experiments at TRIUMF laboratory to measure heavy ( $A > 60$ ) superallowed  $\beta$  decays and a measurement of Michel parameters in normal  $\mu^+$  decay; new mass measurements using the Canadian Penning Trap (CPT) at Argonne National Laboratory; and continued work with both the BRAHMS and STAR collaborations at RHIC.

The K500 cyclotron continues to serve the broader community through testing of radiation effects on electronics components. This past year over 25% of the scheduled accelerator time was devoted to single-event-upset testing. Both U.S. and foreign companies continue to utilize our facility.

As in the past, I am pleased to acknowledge the effort made by Y.-W. Lui in assembling this report. Once again, he has managed it in a very prompt and efficient manner.

R.E. Tribble  
July 19, 2005

## **SECTION I**

# **NUCLEAR STRUCTURE, FUNDAMENTAL INTERACTIONS, AND ASTROPHYSICS**

## ${}^6\text{Li}$ Elastic and Inelastic Scattering on ${}^{116}\text{Sn}$

X. Chen, Y.-W. Lui, H.L. Clark, Y. Tokimoto, and D.H. Youngblood

The compressibility of nuclear matter  $K_{\text{nm}}$  can be related to the energies of the isoscalar giant monopole resonance (ISGMR). Alpha inelastic scattering including  $0^0$  measurements have been successfully used to identify the ISGMR in many nuclei. We have studied elastic and inelastic scattering of 40 MeV/nucleon  ${}^6\text{Li}$  ions on  ${}^{116}\text{Sn}$  to determine their usefulness in giant resonance investigations.  ${}^6\text{Li}$  inelastic scattering might provide additional information on weaker components of the ISGMR, particularly in light nuclei where the strength is badly fragmented. In inverse kinematics ( ${}^6\text{Li}$  target) this scattering might allow investigations of the ISGMR in unstable nuclei. A beam of 240MeV  ${}^6\text{Li}$  ions from the Texas A&M University K500 superconducting cyclotron bombarded self-supporting target foil in the target chamber of the multipole-dipole-multipole (MDM) spectrometer. Elastic and inelastic scattering to low-lying states were measured from  $5^0\sim 35^0$  and inelastic scattering to the GR region was measured from  $0^0\sim 6^0$ .

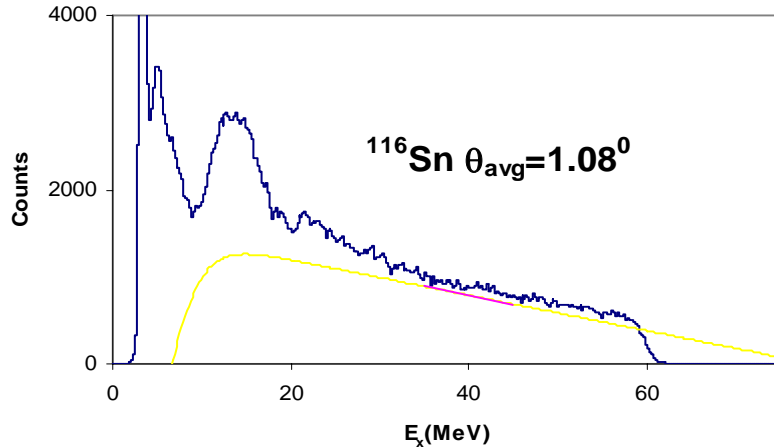


**Figure 1.** Inelastic  ${}^6\text{Li}$  spectrum for  ${}^{116}\text{Sn}$  at  $\theta_{\text{avg}}=1.08^0$ . The yellow line shows the continuum chosen for the analysis.

Woods-Saxon phenomenological potentials were determined from elastic scattering data and inelastic scattering to low-lying states was analyzed by deformed potential model [1]. Using these phenomenological potentials,  ${}^6\text{Li}$  inelastic scattering on  ${}^{116}\text{Sn}$  has been analyzed by the multipole analysis method [2] over a 9 MeV to 26 MeV excitation range. A typical giant resonance spectrum obtained for  ${}^6\text{Li}+{}^{116}\text{Sn}$  is shown in Fig. 1. Angular distributions for a 2 MeV wide bin centered at  $E_x = 15.6$  MeV of the giant resonance peak and the continuum are shown in Fig. 2 along with DWBA fits. The strength distributions of the energy weighted sum rule (EWSR) obtained for ISGMR, ISGDR, ISGQR, and ISGOR of  ${}^{116}\text{Sn}$  are shown in Fig. 3. The peak positions of the ISGMR and ISGQR strength distribution

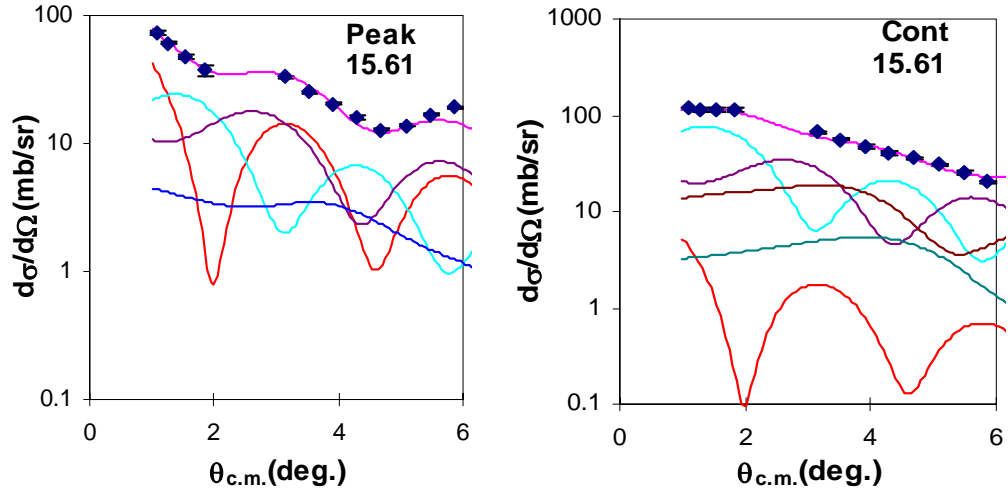


**Figure 2.** The angular distributions of the  $^{116}\text{Sn}$  cross section for a 2 MeV wide bin centered at the excitation energy indicated on the figure (in MeV) for  $^6\text{Li}$  inelastic scattering for GR peak and the continuum. The line through the data points indicates the multipole fits. Contributions of each multipole are shown.

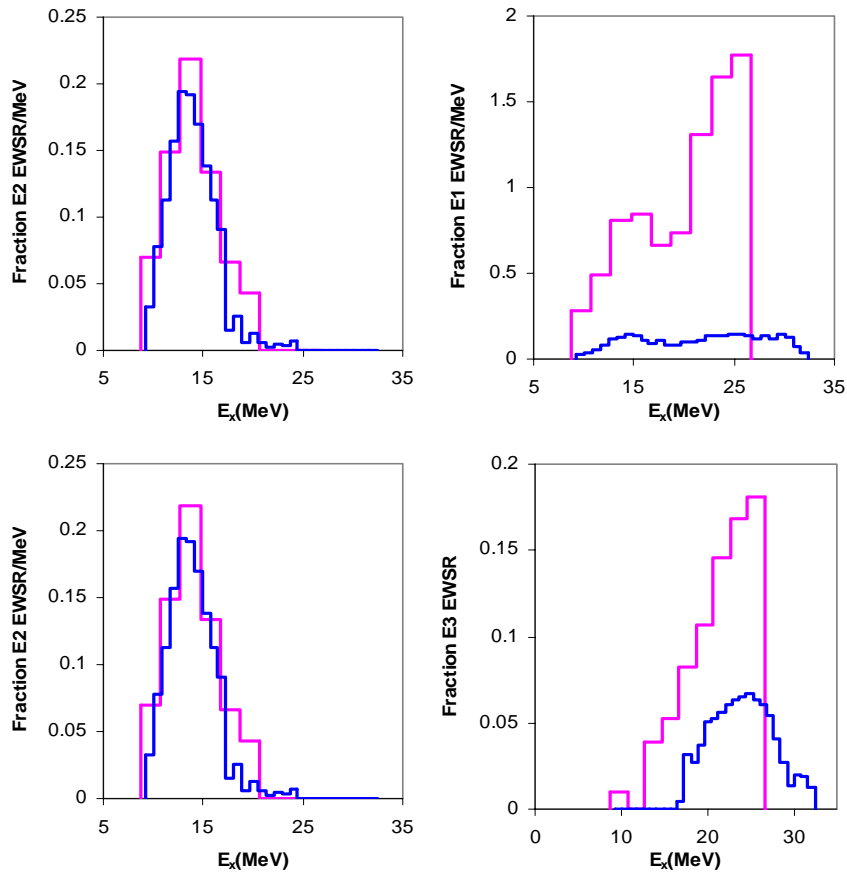


**Figure 3.** Comparison of the strength distribution for E0, E1, E2, E3 extracted from  $^6\text{Li}$  inelastic scattering using the deformed potential model (pink color) with those obtained from  $\alpha$  inelastic scattering[5] using a folding potential (blue color).

are consistent with those obtained from  $\alpha$  inelastic scattering, but there are some differences in sum rule strength. This may be due to different continuum choices or the simplicity of the deformed potential model. No matter how the continuum was reasonably chosen, unlike other multipolarities, the strength of ISGDR was always much higher than 100% of the EWSR. H.L. Clark, et al [3] have pointed out that the predicted cross section for the ISGDR in the deformed potential model is very sensitive to the imaginary component of the optical and transition potential.

${}^6\text{Li}$  elastic scattering on  ${}^{116}\text{Sn}$  was also analyzed using the density-independent folding model. Here the optical potential was obtained by folding the nucleon-nucleon effective interaction M3Y over the target and projectile density distributions. The elastic scattering data was fit in two different ways. First both the real and imaginary part of the potential were obtained from folding. In the second case, a Woods-Saxon (W-S) form was used for the imaginary potential. The parameters obtained are shown in the Table 1 and the calculated angular distributions of cross-sections for both cases are shown with the

**Table 1.** Optical model parameters obtained from the fits of the  ${}^6\text{Li}+{}^{116}\text{Sn}$  elastic scattering. M3Y(R+I) means both the real part and the imaginary part of the optical potential were obtained by double folding. M3Y(R) means a W-S shape was used for the imaginary potential.  $N_R$  and  $N_I$  are real and imaginary renormalization factors for folded potential respectively.

$E_{Li}$ (MeV)	Potential type	$N_R$	V (MeV)	$r_0$ (fm)	A (fm)	$N_I$	W (fm)	$r_{i0}$ (fm)	$a_i$ (fm)
240	Woods- Saxon		188.0	0.837	0.905		28.4	1.17	0.816
240	M3Y(R+I)	0.577				0.68 5			
240	M3Y(R)	0.633					27.6	1.17	0.882

**Table 2.** Parameters used in double folding calculation for inelastic scattering to  $2^+$  and  $3^-$  states of  ${}^{116}\text{Sn}$ .

Low-lying State $E_x(\text{MeV}); J^\pi$							
	$\beta_m$	$N_R$	W (MeV)	$r_{i0}$ (fm)	$a_i$ (fm)	$\beta_n$	$\beta_c$
1.29; $2^+$	0.125	0.633	27.6	1.17	0.882	0.125	0.139
2.27; $3^-$	0.150	0.633	27.6	1.17	0.882	0.150	0.167

elastic scattering data in Fig. 4. Using the potential with the W-S imaginary term the cross section for inelastic scattering to low-lying  $2^+$  and  $3^-$  states were calculated. The parameters used for double folding calculation using Ptolemy [4] are listed in Table 2. Deformation parameters were obtained from electromagnetic B(EL) values by assuming the mass and coulomb deformation lengths are the same. The calculations for the  $2^+$  and  $3^-$  states are shown separately in Fig. 5 and Fig. 6 and are in good agreement with the data. in order to analyze the giant resonance data by double folding model, the transition potentials with folding model for ISGMR and ISGDR are needed. Analysis of the data is in progress.

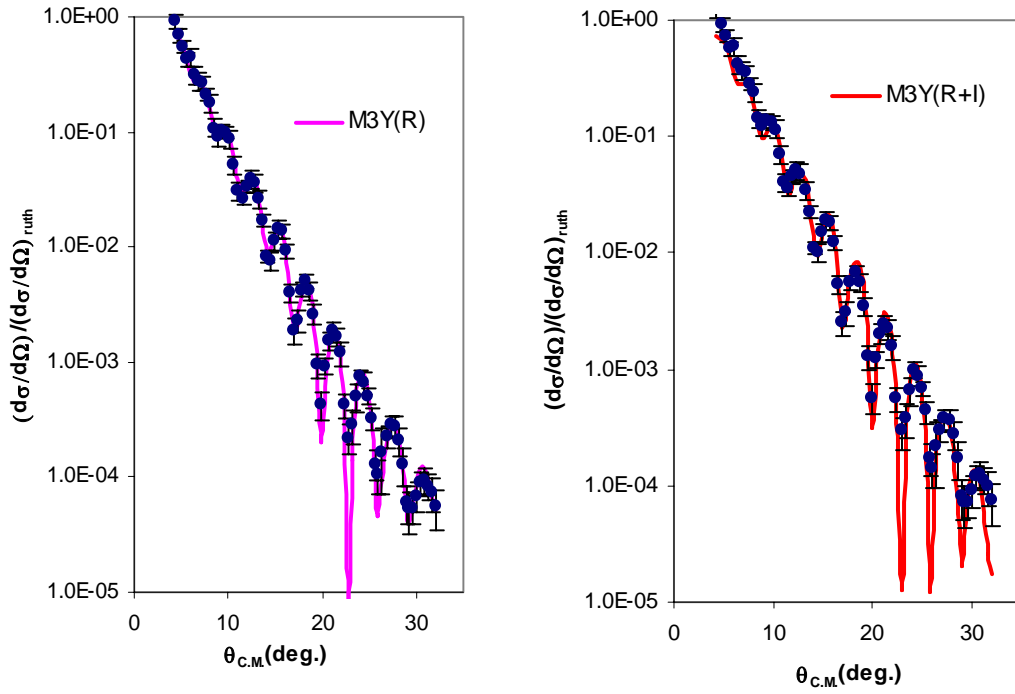


**Figure 2.** Angular distributions for  ${}^6\text{Li}+{}^{116}\text{Sn}$  elastic scattering cross-section (relative to Rutherford cross section) using M3Y(R) and M3Y(R+I) potentials.

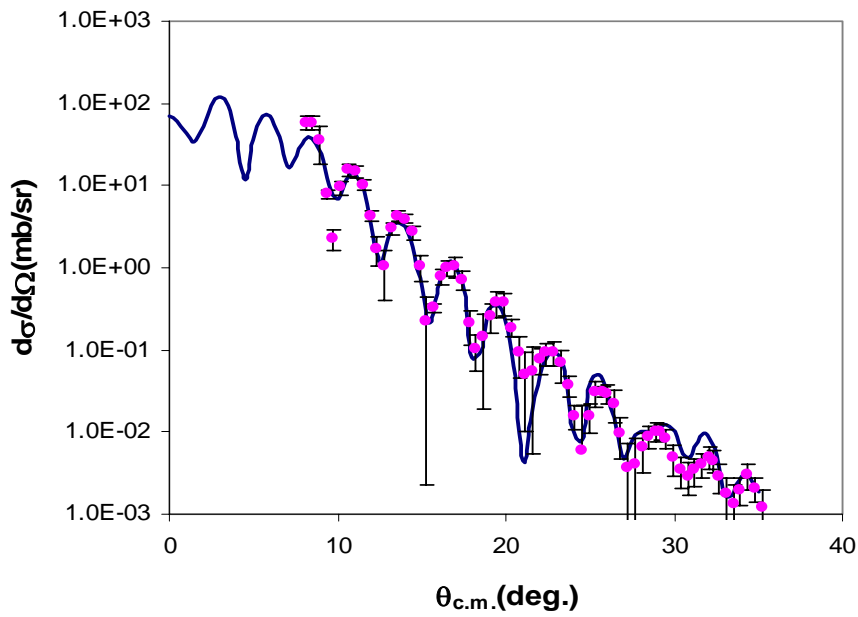


**Figure 5.** The calculated differential cross-section for inelastic scattering to the 1.29 MeV  $2^+$  state in  ${}^{116}\text{Sn}$  is plotted versus average center-of-mass angle along with the data.

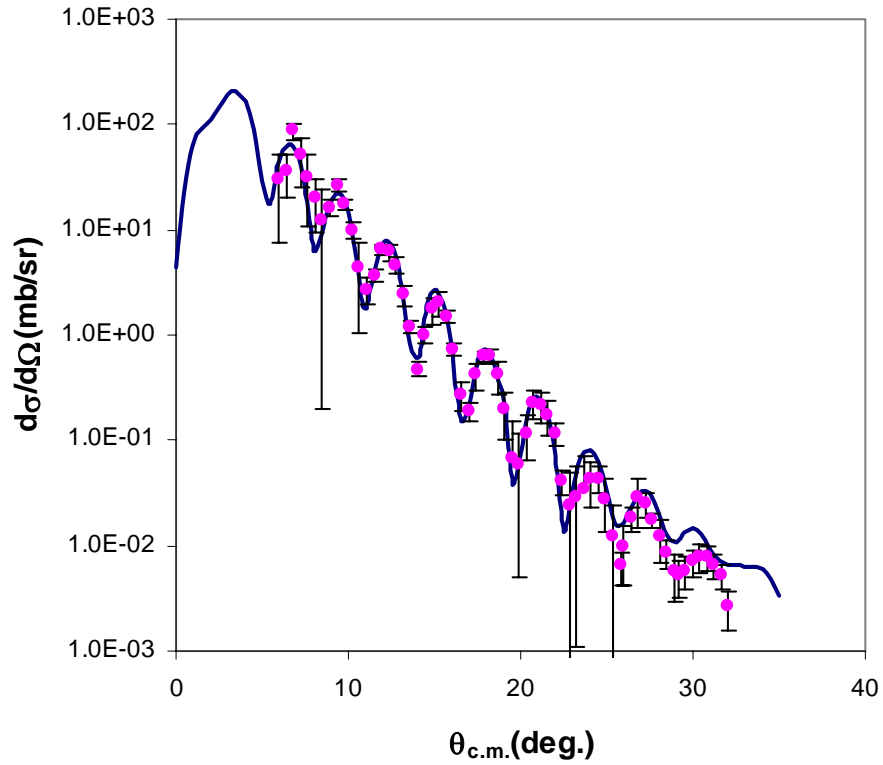


**Figure 6.** The calculated differential cross-section for inelastic scattering to the 2.27 MeV  $3^-$  state in  $^{116}\text{Sn}$  is plotted versus average center-of-mass angle.

Special thank goes to Dr. Florin Carstoiu for his generous help and offer of the computer code to do folding calculation.

- [1] X. Chen, Y.-W. Lui, H. L. Clark, Y. Tokimoto, and D. H. Youngblood, *Progress in Research*, Cyclotron Institute, Texa A&M University (2003-2004), p. I-4
- [2] D. H. Youngblood, Y. -W. Lui, H. L. Clark, *Phys. Rev. C* **60**, 014304 (1999).
- [3] H. L. Clark, Y. -W. Lui, D. H. Youngblood, *Nucl. Phys.* **A687**, 80c (2001).

## Elastic Scattering of Drip Line Nucleus $^{17}\text{F}$

F. Carstoiu,<sup>1</sup> L. Trache, J.C. Blackmon,<sup>2</sup> D.W. Bardayan,<sup>2</sup> C.R. Brune,<sup>3</sup> C.A. Gagliardi, U. Greife,<sup>4</sup> C.J. Gross,<sup>2</sup> C.C. Jewett,<sup>4</sup> R.L. Kozub,<sup>5</sup> T.A. Lewis,<sup>2</sup> J.F. Liang,<sup>2</sup> B.H. Moazen,<sup>5</sup> A.M. Mukhamedzhanov, C.D. Nesarja,<sup>5</sup> F.M. Nunes,<sup>6</sup> P.D. Parker,<sup>7</sup> L. Sahin,<sup>2,8</sup> J.P. Scott,<sup>5</sup> D. Shapira,<sup>2</sup> M.S. Smith,<sup>2</sup> J.S. Thomas,<sup>9</sup> and R.E. Tribble

<sup>1</sup>*Institute of Atomic Physics, Bucharest, Romania*

<sup>2</sup>*Physics Division, Oak Ridge National Laboratory, Oak Ridge, TN 37831*

<sup>3</sup>*Department of Physics and Astronomy, Ohio University, Athens, OH 45701*

<sup>4</sup>*Department of Physics, Colorado School of Mines, Golden, CO 80401*

<sup>5</sup>*Physics Department, Tennessee Technological University, Cookeville, TN 38505*

<sup>6</sup>*NSCL, Michigan State University, East Lansing, MI 48824*

<sup>7</sup>*A. W. Wright Nuclear Structure Laboratory, Yale University, New Haven, CT 06511*

<sup>8</sup>*Department of Physics and Astronomy, University of North Carolina, Chapel Hill, NC 27599*

<sup>9</sup>*Department of Physics and Astronomy, Rutgers University, New Brunswick, NJ 08903*

Heavy ion elastic scattering has been a major source of information on the structure of nuclei and the properties of nucleus-nucleus interactions. Global models have been built based in large part on elastic scattering with stable nuclei and have been used as a basis for extracting structure information from nuclear reaction studies, using Distorted Wave Born Approximation (DWBA) techniques for example. Reaction studies with Radioactive Nuclear Beams (RNB's) are now expanding our understanding of nuclear structure to loosely bound nuclei away from stability. Several recent proton-transfer experiments were performed with RNB's at energies around 10 MeV/nucleon, where reactions are peripheral, with the intention to extract stellar reaction rates. To extract reliable information, good optical potentials are needed. However, nuclear potentials for light nuclei near the drip lines are typically ambiguous and poorly constrained by limited elastic scattering data or by extrapolations of recipes from stable nuclei, facts which raise questions about the accuracy and reliability of nuclear structure information extracted from reaction studies in such cases.

Here precision data have been obtained for the elastic scattering of radioactive nuclear beam  $^{17}\text{F}$ , in an effort to clarify the reaction mechanism for loosely bound nuclei at low energies and to assess the validity of a double folding procedure to predict optical model potentials for use in indirect methods for nuclear astrophysics. A measurement was done to determine the proton radiative capture  $S$ -factor using the ANCs determined from the proton-transfer reaction  $^{14}\text{N}(^{17}\text{F}, ^{18}\text{Ne})^{13}\text{C}$  using a 10 MeV/u beam of isotopically-pure  $^{17}\text{F}$  from the Holifield Radioactive Ion Beam Facility [1]. In the same run elastic scattering cross sections for  $^{14}\text{N}(^{17}\text{F}, ^{17}\text{F})^{14}\text{N}$  and  $^{12}\text{C}(^{17}\text{F}, ^{17}\text{F})^{12}\text{C}$  were measured over an extended angular range. These data were analyzed both in terms of phenomenological Woods-Saxon potentials and with potentials resulting from a double-folding procedure established before [2] and tested on several cases of RNB elastic scattering ( $^7\text{Be}$ ,  $^8\text{B}$ ,  $^{11}\text{C}$ ,  $^{13}\text{N}$  on melamine and C). However the present data represent the best set of experimental elastic data so far, both in terms of resolution of the beam and of the detectors, and in terms of angular coverage.

We found that the OMP parameters extracted from the phenomenological fit have significant ambiguities. Analysis of elastic scattering data in terms of microscopic double folding potentials incorporating density and energy dependent effective nucleon-nucleon interaction and realistic densities consistent with experimentally determined asymptotic normalization coefficient, provides an excellent description of the data and points to a complete dominance of the absorption at the barrier. The semiclassical analysis in terms of multireflection barrier/internal barrier series expansion of the scattering amplitude [3] shows that only the barrier component survives in the scattering process, pointing to a peripheral character of the reactions. The double-folding procedure using the JLM effective interaction and renormalization is shown again to work better.

The paper was submitted for publication in Phys. Rev. C.

[1] J. Blackmon *et al.*, RNB6 Conference, Argonne, Sept. 2003, and Nucl. Phys. A, in press.

[2] L. Trache *et al.*, Phys. Rev. C **61**, 024612 (2000).

[3] F. Carstoiu *et al.*, Phys. Rev. C **70**, 054610 (2004).

## Scattering of ${}^7\text{Be}$ and ${}^8\text{B}$ and Consequences for the Astrophysical $S_{17}$ Factor

G. Tabacaru, A. Azhari,\* J. Brinkley, V. Burjan,<sup>1</sup> F. Carstoiu,<sup>2</sup> C. Fu, C. A. Gagliardi, V. Kroha,<sup>1</sup>

A.M. Mukhamedhanov, X. Tang, L. Trache and R. E. Tribble

<sup>1</sup>*Institute of Nuclear Physics, Czech Academy of Sciences, Prague-Rez, Czech Republic*

<sup>2</sup>*H. Hulubei National Institute for Physics and Nuclear engineering, Bucharest, Romania*

Previously [1,2] we reported the main improvements in a new measurement of the reaction  ${}^7\text{Be}+{}^{14}\text{N}$  to determine the astrophysical  $S_{17}$ -factor. The angular range for elastic scattering and transfer reaction was doubled, and we improved the monitoring of the intensity of the secondary  ${}^7\text{Be}$  radioactive beam. The extension of the measurement's angular range was made in order get a better handle on the optical potential used in the incoming channel and to reduce the uncertainties. Using a direct counting of the  ${}^7\text{Be}$  beam showed that the indirect method used previously to determine the intensity of the secondary beam by means of a Faraday cup for the primary beam overestimated the actual secondary beam intensity with about 5.5% due a tunneling effect discussed in [1,2]. It results that all experimental cross sections were underestimated by about 5.5% in the previous work. This is within reported experimental errors bars, but noticeable. We have therefore to increase the value of the transfer cross section  $\sigma_{\text{exp}}^{\text{tr}}(\text{new})=1.055 \sigma_{\text{exp}}^{\text{tr}}(\text{old})$  due to this difference found in the absolute normalization.

Another development that occurred from the time of the paper of Azhari et al [3] on the above reaction was that the ratio between the ANCs for the  $1p_{1/2}$  and  $1p_{3/2}$  components in the wave function of the ground state of  ${}^8\text{B}$  was established from the mirror neutron transfer reaction  ${}^{13}\text{C}({}^7\text{Li}, {}^8\text{Li}){}^{12}\text{C}$  to be  $\delta^2=C^2({}^8\text{B}, p_{1/2})/C^2({}^8\text{B}, p_{3/2})=0.125(20)$ .

In the Fig. 1 we present the angular distribution for elastic scattering of  ${}^7\text{Be}$  on  ${}^{14}\text{N}$  and  ${}^{12}\text{C}$ : points – experimental data after subtraction of inelastic scattering contribution, continuous line calculation and dashed line – old calculation. The results at small angles are compatible with those reported in [3] and with the predictions of the optical model calculations done at that time. However in the region of larger angles, the new experimental data fall above the predictions, suggesting a smaller absorption than the one assumed initially. This led to a new analysis of the elastic scattering, to new optical potentials, which required new DWBA calculations for the proton transfer.

We have also measured the elastic scattering of  ${}^8\text{B}$  at 95 MeV on a  ${}^{12}\text{C}$  target, in order to check the optical potential we used in the DWBA calculations for the outgoing channel  ${}^8\text{B}+{}^{13}\text{C}$ . From the data we have we verify that the potential obtained from the double folding procedure of the JLM effective interaction, renormalized as in ref. [4] is appropriate.

All the improvements discussed above permit us to re-assess the Asymptotic Normalization Coefficient of  ${}^8\text{B}$  from the  ${}^{14}\text{N}({}^7\text{Be}, {}^8\text{B}){}^{13}\text{C}$  reaction:  $C^2({}^8\text{B}, p_{3/2}; \text{new})=0.414 \pm 0.041 \text{ fm}^{-1}$  and  $C_{\text{tot}}^2({}^8\text{B}; \text{new})=C^2(p_{3/2}) + C^2(p_{1/2})=0.466 \pm 0.047 \text{ fm}^{-1}$ . Consequently a new value of the astrophysical S-factor for the  ${}^7\text{Be}(p, \gamma) {}^8\text{B}$  reaction  $S_{17}=18.0 \pm 1.8 \text{ eV b}$ . This value is in agreement with all the values obtained from indirect methods and with most of those from direct methods, but one.

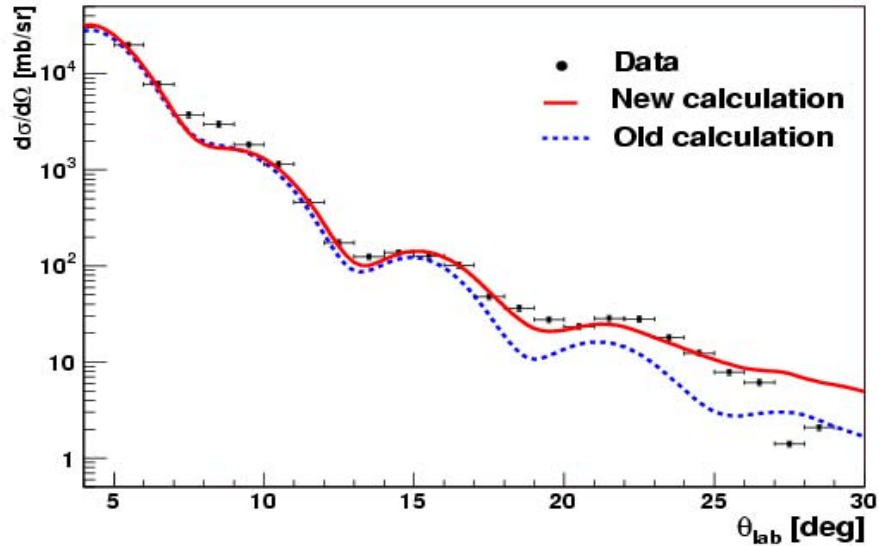


**Figure 1.** Angular distribution for elastic scattering of  $^7\text{Be}$  on  $^{14}\text{N}$  and  $^{12}\text{C}$ : points – experimental data after subtraction of inelastic scattering contribution, continuous line calculation and dashed line – old calculation.

\*Present Address: Alix Partners, Dallas, TX.

- [1] G. Tabacaru *et al.*, *Progress in Research*, Cyclotron Institute, Texas A&M University (2002-2003), p. I-12
- [2] G. Tabacaru *et al.*, *Progress in Research*, Cyclotron Institute, Texas A&M University (2003-2004), p. I-14
- [3] A. Azhari *et al.*, *Phys. Rev. C* **60**, 055803 (1999).
- [4] L. Trache *et al.*, *Phys. Rev. C* **61**, 024612 (2000).

## Asymptotic Normalization Coefficients for $^{13}\text{C} \rightarrow ^{12}\text{C}+n$

T. Al-Abdullah, F. Carstoiu, X. Chen, C. Fu, C. A. Gagliardi, Y.-W. Lui,  
G. Tabacaru, Y. Tokimoto, L. Trache, and R. E. Tribble.

Two different experiments for nuclear astrophysics research purposes were performed to measure the neutron transfer reactions  $^{13}\text{C}(^{22}\text{Ne},^{23}\text{Ne})^{12}\text{C}$  [1] and  $^{13}\text{C}(^{17}\text{O},^{18}\text{O})^{12}\text{C}$  [2], and to determine the asymptotic normalization coefficients (ANCs) for the ground and first excited states in  $^{23}\text{Ne}$  and  $^{18}\text{O}$  respectively. Extracting the ANCs for these nuclei requires the ANCs for the complementary vertex, which comes from the  $^{13}\text{C} \rightarrow ^{12}\text{C}+n$  reaction. Various experiments for  $^{12}\text{C}+^{13}\text{C}$  elastic scattering, elastic transfer, (d,p) and (d,t) reactions are reported in [3], where the nuclear vertex constant  $G^2$  is calculated. An independent experiment was performed to obtain the ANC for  $^{13}\text{C}$  by measuring the neutron exchange reaction  $^{13}\text{C}(^{12}\text{C},^{13}\text{C})^{12}\text{C}$ .

The experiment was carried out using a  $^{12}\text{C}$  beam from K500 cyclotron. The MDM spectrometer was used to study the detailed angular distribution for the elastic scattering and for the exchange reaction  $^{13}\text{C}(^{12}\text{C},^{13}\text{C})^{12}\text{C}$ . A  $104 \mu\text{g}/\text{cm}^2$   $^{13}\text{C}$  target was bombarded with 127 MeV  $^{12}\text{C}$  beam. The Oxford detector was filled with isobutane at a pressure of 20-30 Torr. The detector, which consists of four resistive wires, was used to identify the position of the ejectiles at the focal plane, and to measure the energy loss of particles in ionization chamber, followed by a plastic scintillator to measure the residual energy. The scattering angle at the target was reconstructed as a

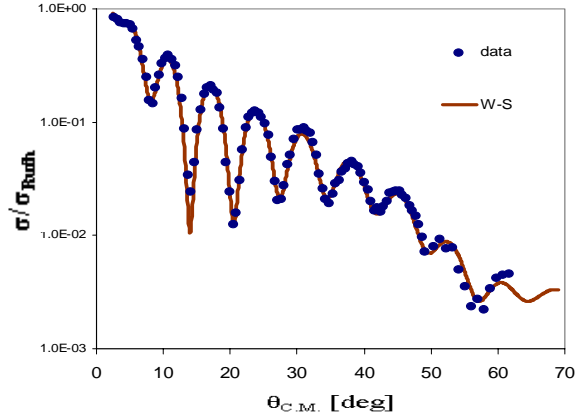


**Figure 1.** The angular distribution for the elastic scattering of 127 MeV  $^{12}\text{C}$  on  $^{13}\text{C}$ . The curve is the fit to the data using OMP obtained from Wood-Saxon potential.

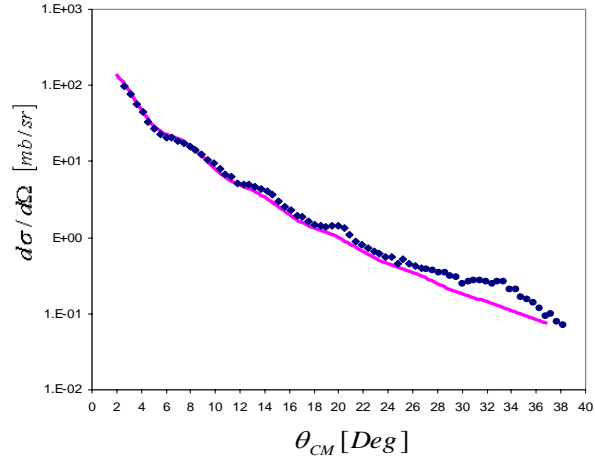


**Figure 2.** The cross section values for the  $^{13}\text{C}(^{12}\text{C},^{13}\text{C})^{12}\text{C}$  reaction. The curve shows the DWBA fit for the  $p_{1/2} \leftrightarrow p_{1/2}$  component.

function of the angle at the first resistive wire in the detector using Raytrace code.

The angular distribution for the elastic scattering data was obtained in the range  $\theta_{\text{C.M.}} = 3^\circ\text{-}63^\circ$ . These data were used to extract the optical model parameters (OMP) for use in DWBA calculations of the  $^{13}\text{C}(^{12}\text{C}, ^{13}\text{C})^{12}\text{C}$  reaction. The OMPs were obtained by fitting the elastic scattering data with a Wood-Saxon form and a folding-model potential. The fit with the least  $\chi^2$  is shown in Fig. 1. The cross section values for the transfer reaction were measured in the forward angles  $\theta_{\text{C.M.}} = 3^\circ\text{-}36^\circ$ . The  $p_{1/2} \rightarrow p_{1/2}$  component, which is the main contribution to the reaction, and the DWBA calculations are shown in Fig. 2. The extracted ANC is  $C^2(^{13}\text{C}) = 2.32 \pm 0.08 \text{ fm}^{-1}$  which agrees with the average  $C^2(^{13}\text{C}) = 2.35 \pm 0.12 \text{ fm}^{-1}$  that is reported in [3]. The uncertainty quoted for  $C^2$  includes contributions from the geometry of the neutron binding energy used in DWBA calculations, in addition to the overall normalization of the cross section values. Other uncertainties considered in [4] have not been included yet. Comparing between the ANC, or the spectroscopic factor  $S$ , as a function of the geometry of the single particle Wood-Saxon well proves that the reaction is peripheral, as seen in Fig. 3, and our approach is valid.

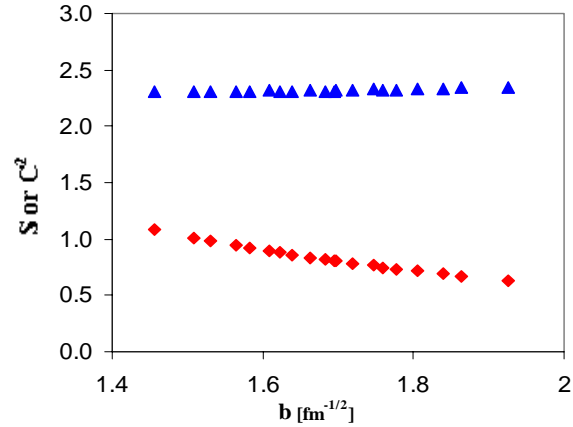


**Figure 3.** Comparison of the spectroscopic factor (diamonds) and of the ANC  $C^2$  (triangles) for different choices of the single particle ANC  $b$  of the Wood-Saxon well.

[1] T. Al-Abdullah, *et al.*, this report.

[2] T. Al-Abdullah, *et al.*, to be published

[3] N. Timofeyuk, *et al.*, Nucl. Phys. **A620**, 29 (1997).

[4] L. Trache, *et al.*, Phys. Rev. C **67**, 062801 (2003).

## Determining the $^{22}\text{Mg}(p,\gamma)^{23}\text{Al}$ Reaction Rate Through a Measurement of the ANCs in the Mirror System

T. Al-Abdullah, F. Carstoiu, X. Chen, H. Clark, C. Fu, C. A. Gagliardi, Y.-W. Lui,  
S. Piskor, G. Tabacaru, Y. Tokimoto, L. Trache, and R. E. Tribble

The long-lived  $^{22}\text{Na}$  ( $T_{1/2}=2.61$  yr) is synthesized during thermonuclear runaways in the Ne-Na cycle. Its  $\beta$ -decay to  $^{22}\text{Ne}$  leads to the emission of a 1.275 MeV  $\gamma$ -ray. However, space based telescopes did not observe this  $\gamma$ -ray production in the ONe novae compared to the model calculations [1]. This can be explained if the parent nucleus  $^{22}\text{Mg}$  is depleted by the fast  $^{22}\text{Mg}(p,\gamma)^{23}\text{Al}$  reaction [2]. An indirect experimental method is applied to determine this astrophysically important reaction rate at stellar energies using stable beam and target. The asymptotic normalization coefficients (ANCs) for the ground state and the first excited state in the peripheral reaction  $^{22}\text{Ne}+n \rightarrow ^{23}\text{Ne}$  have been measured, then transposed to the corresponding states in the mirror nucleus  $^{23}\text{Al}$ , and finally used to calculate the S-factor and the rate of the  $^{22}\text{Mg}(p,\gamma)^{23}\text{Al}$  reaction.

The experiments were performed using the MDM spectrometer. A  $^{22}\text{Ne}$  beam (12 MeV/u) from the K500 cyclotron was transported through the BAS and impinged on  $104 \mu\text{g}/\text{cm}^2$   $^{13}\text{C}$  and  $109 \mu\text{g}/\text{cm}^2$   $^{12}\text{C}$  targets. The angular distributions for the elastic scatterings on both targets and the neutron transfer reaction  $^{13}\text{C}(^{22}\text{Ne}, ^{23}\text{Ne})^{12}\text{C}$  have been measured. The optical model parameters (OMP) for the entrance channel are obtained by fitting the elastic scattering data of  $^{22}\text{Ne}$  on  $^{13}\text{C}$  as shown in Fig. 1 using Woods-Saxon and double-folding potentials. The extracted OMP give a good description also for the elastic scattering data of  $^{22}\text{Ne}$  on  $^{12}\text{C}$ , Fig. 2. Since  $^{23}\text{Ne}$  has a loosely bound neutron in the  $d_{5/2}$  shell around the  $^{22}\text{Ne}$  core, a similar case exists for the last neutron in  $^{13}\text{C}$ , so that DWBA calculations are carried out using the same parameters for the exit channel;  $^{23}\text{Ne}+^{12}\text{C}$ .

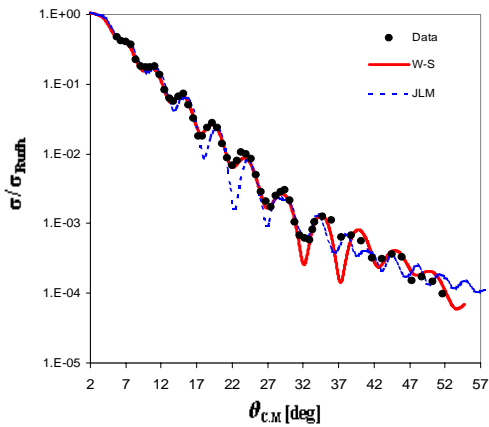


**Figure 1.** The fits of the elastic scattering cross section of 264 MeV  $^{22}\text{Ne}$  on  $^{13}\text{C}$ .

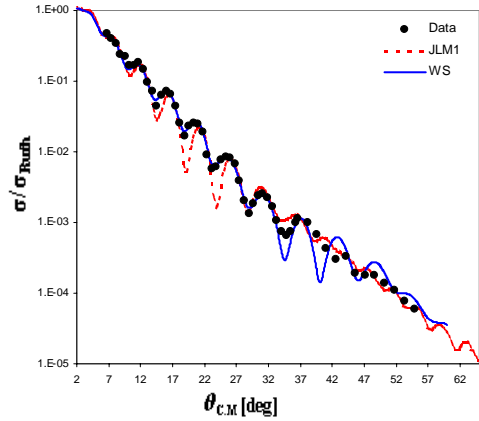


**Figure 2.** The angular distribution of the elastic scattering  $^{22}\text{Ne}+^{12}\text{C}$ .

The ANC in  $^{13}\text{C}$ , which represents the other vertex in the above reaction, is independently measured to be  $C^2(^{13}\text{C}) = 2.32 \pm 0.08 \text{ fm}^{-1}$  [3]. The preliminary result for the  $C^2(^{23}\text{Ne})$  due to the  $p_{1/2} \rightarrow d_{5/2}$  transition is  $0.85 \pm 0.09 \text{ fm}^{-1}$ , Fig. 3. This value is used to obtain the ANC in the mirror nucleus  $^{23}\text{Al}$ ; following the same procedure as was used for the  $(^7\text{Li}, ^8\text{Li})$  reaction [4]. We find  $(C^{^{23}\text{Al}}_{^{22}\text{Mg}, \frac{5}{2}})^2 = (1.22 \pm 0.12) * 10^4 \text{ fm}^{-1}$ . From this, we calculate the non resonant direct capture reaction rate for  $^{22}\text{Mg}(p, \gamma)^{23}\text{Al}$  as seen in Fig. 4. It is the first time to measure the ANCs for  $^{23}\text{Ne}$ , so that more detailed analyses are needed to understand the phase shift between the data and DWBA calculations, in addition to find out the uncertainties for extracting the ANCs.

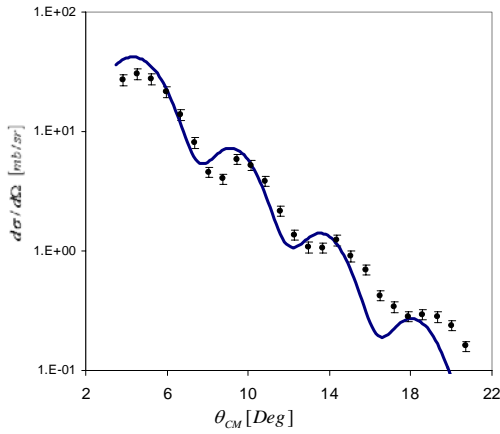


**Figure 3.** The experimental and DWBA calculations for the reaction  $^{13}\text{C}(^{22}\text{Ne}, ^{23}\text{Ne})^{12}\text{C}$ .

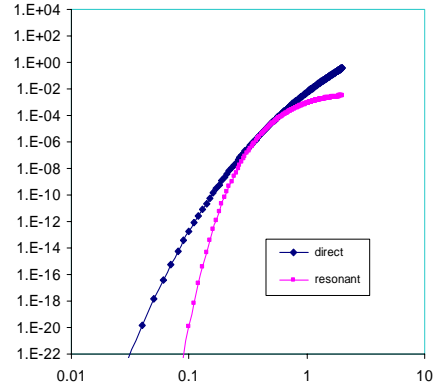


**Figure 4.** The reaction rate  $[\text{cm}^3/\text{mole/s}]$  for  $^{22}\text{Mg}(p, \gamma)^{23}\text{Al}$ .

- [1] I. Iyudin *et al.*, *Astron. Astrophys.* **300**, 422 (1995).
- [2] J.A. Caggiano *et al.*, *Phys. Rev. C* **64**, 025802 (2002).
- [3] T. Al-Abdullah, *et al.*, This report.
- [4] L. Trache *et al.*, *Phys. Rev. C* **67**, 062801 (2003).

## Status of $^{14}\text{O} + \alpha$ Experiment

Changbo Fu, V. Z. Goldberg, G. G. Chubaryan, G. Tabacaru, L. Trache, and R.E. Tribble

Using MARS we obtained an intensity of  $10^5$  /s for an  $^{14}\text{O}$  beam. The  $^{14}\text{O}$  beam with this intensity can be obtained in the energy region from 3 up to 10 MeV/A. The parameters of the  $^{14}\text{O}$  beam correspond to the best achievements of other laboratories for this beam define the promising perspectives of using the beam at Cyclotron Institute.

The study of the  $^{14}\text{O} + \alpha$  interaction is a task with several areas. The astrophysical interest to  $(\alpha, p)$  cross sections is combined with the interest of the  $\alpha$  cluster structure of  $^{18}\text{Ne}$  and with an interest in a possible  $2p$  decay of the excited states in  $^{18}\text{Ne}$ .

It appears that small contaminations in the  $^{14}\text{O}$  beam by lighter ions ( $p$ ,  $d$ ,  $\alpha$ ), at the level of  $10^{-4}$ , preclude observation of the reactions induced by  $^{14}\text{O}$  at small angles. We tried to use an amplitude analysis of a PPAC to discriminate light ions. However, the energy resolution of the PPAC signal appeared to be too poor for a complete solution of the problem.

A new approach based on amplitude of scintillations detected by Photo Multiplier Tube (PMT) from a  $10\ \mu\text{m}$  foil was tested and brought good results. The timing signal from the PMT compared to the cyclotron RF will be used for an analysis of the energy of the secondary  $^{14}\text{O}$  beam. Therefore radioactive beams with poorer energy resolution and a higher intensity can be used. The next step is to test this using a cyclotron beam.

## $^{12}\text{N}$ Structure in the Resonance $^{11}\text{C}+p$ Interaction

V. Z. Goldberg, G. Tabacaru, Changbo Fu, G. Chubaryan, R. E. Tribble  
G. V. Rogachev,<sup>1</sup> A. B. Volya,<sup>1</sup> B. A. Brown, B. B. Skorodumov,<sup>2</sup> and X. D. Tang

<sup>1</sup>*Department of Physics, Florida State University, Tallahassee, FL 32306*

<sup>2</sup>*Department of Physics, University of Notre Dame, South Bend, IN 46556*

Quasistationary states in  $^{12}\text{N}$  were studied by  $^{11}\text{C}+p$  resonance elastic scattering using the thick ( $\text{CH}^4$ ) gas target method [1] in inverse kinematics with a separated  $^{11}\text{C}$  radioactive-ion beam [2]. An analysis of the excitation functions of the elastic scattering in the 3-6 MeV excitation region of  $^{12}\text{N}$  was carried out with the R matrix approach. A common feature of resonance investigations of drip-line nuclei should be the presence of several overlapping resonances even at low excitation energies. However, at low excitation energies, the contemporary shell model calculations (see, as an example,[3,4]) could provide for starting parameters of the fit. A new R-matrix code was made, which gives possibility to take into account a complicated nuclear structure of the levels, as well as the overlapping of the same spin states. We present evidence for all predicted levels in the excitation region in question, including those, which were not experimentally known before.

[1] K. P. Artemov *et al.*, Sov. J. Nucl. Phys. **52**, 408 (1990).

[2] R. E. Tribble *et al.*, Nucl. Phys. **A701**, 278 (2002).

[3] B. A. Brown, Prog. Part. Nucl. Phys. **47**, 517 (2001)

[4] A. Volya and V. Zelevinsky, Phys. Rev. Lett. **94**, 052501 (2005).

## Alpha Cluster Structure in $^{18}\text{O}$

Changbo Fu, V. Z. Goldberg, K.-M. Kallman,<sup>1</sup> T. Lonnroth,<sup>1</sup> P. Manngard,<sup>1</sup> B. B. Skorodumov,<sup>2</sup>  
G. V. Rogachev,<sup>3</sup> S. Brown,<sup>3</sup> K. Kemper,<sup>3</sup> B. Green,<sup>3</sup> E. Johnson,<sup>3</sup> O. Momotyuk,<sup>3</sup> and B. Roeder<sup>3</sup>

<sup>1</sup>*Abo Akademi, Turku, Finland*

<sup>2</sup>*Department of Physics, University of Notre Dame, South Bend, IN 46556*

<sup>3</sup>*Department of Physics, Florida State University, Tallahassee, FL 32306*

Alpha cluster structure in  $^{18}\text{O}$  is of interest from different points of view. (1) There are few data on  $\alpha$ -cluster structure in  $N \neq Z$  nuclei. (2) Recent work [1] demonstrated an unusual doubling of  $\alpha$ -clusters in  $^{22}\text{Ne}$ , and this effect stimulated new theoretical considerations (see [2], for example). (3) There is an astrophysical interest to the lowest  $\alpha$ -cluster states in  $^{18}\text{O}$  as to a possible source of neutrons in stellar reactions. (4) A study of  $^{18}\text{O}$  should complement the current study of the  $^{14}\text{O}+\alpha$  interaction at the Cyclotron Institute.

There has been one experiment on the  $\alpha+^{14}\text{C}$  resonance scattering [3], and only a small part of the data [3] was analyzed. We have analyzed part of the data [3] in the framework of a simplified R-matrix approach and made measurements of  $\alpha+^{14}\text{C}$  resonance scattering in the region 16.3-19.6 MeV, thus extending the energy region of the work [3]. As a result about 30 new levels were identified, and the hypothesis of level doubling was confirmed. These results will be published in [4].

To obtain information on the lowest  $\alpha$ -cluster states in  $^{18}\text{O}$  we made measurements of the excitation functions of  $^{14}\text{C}+\alpha$  elastic scattering at FSU, using the thick target inverse kinematics technique. An example of the excitation function is given in Fig.1. The data is analyzed using R-matrix theory.

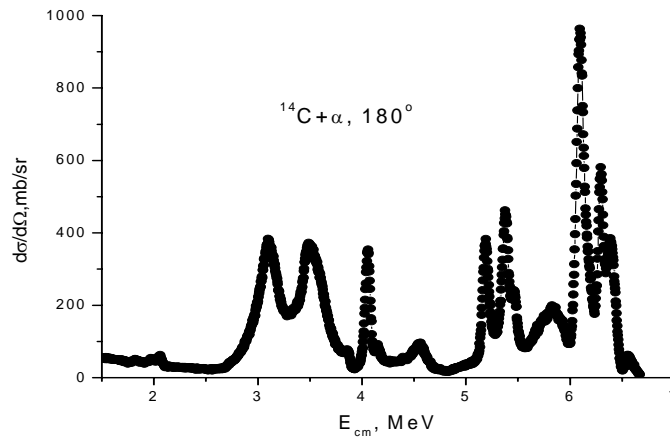


**Figure 1.** Excitation function for  $^{14}\text{C}+\alpha$  elastic scattering at 180 degrees

- [1] G. Rogachev *et al.*, Phys. Rev. C **64**, 051302R (2001)
- [2] M.Dufour and P. Descouvemont, Nucl. Phys. **A726**, 53 (2003)
- [3] G.I. Morgan *et al.*, Phys. Lett. **32B**, 353 (1970)
- [4] V.Z.Goldberg *et al.*, Phys. At. Nucl. **6** (2005) (in press).

## In a Search for a Way to Study Neutron Rich Drip-Line Nuclei (Studies of Analog States of Drip Line Nuclei)

V. Z. Goldberg, G. G. Chubaryan, G. V. Rogachev,<sup>1</sup> J. J. Kolata,<sup>2</sup> A. Aprahamian,<sup>2</sup>  
B. B. Skorodumov,<sup>2</sup> P. Boutachkov,<sup>2</sup> A. Woehr,<sup>2</sup> M. Quinn,<sup>2</sup> L. Lamm,<sup>2</sup>  
G. M. Ter-Akopian,<sup>3</sup> M. S. Golovkov,<sup>3</sup> A. Fomichev,<sup>3</sup> and A. M. Rodin<sup>3</sup>

<sup>1</sup>*Department of Physics, Florida State University, Tallahassee, FL 32306*

<sup>2</sup>*Department of Physics, University of Notre Dame, South Bend, IN 46556*

<sup>3</sup>*Flerov Laboratory of Nuclear Reactions, Joint Institute for Nuclear Research, Dubna, Russia*

We carried out several experiment to study analog states of drip line nuclei in resonance reactions induced by radioactive beams (a part of these studies was published in 2004 [1,2]).

The information, obtained in this way, can be used for reliable predictions (using the Coulomb corrections) of the binding energies and the level schemes of neutron rich drip-line nuclei. If these features of neutron rich nuclei are known, a more detailed analysis can provide data on nuclear radii and density distributions of drip-line nuclei. It is worthwhile to note that resonance reactions usually provide for very exact data.

The  $^8\text{He}+p$  resonance thick target elastic scattering was used to obtain information on the analog states ( $T=5/2$ ) of the ground and excited states in  $^9\text{He}$  [1]. However, the decay of the highly excited analog states of neutron rich nuclei should proceed mainly through neutron decay. Therefore elastic scattering of protons with the excitation of the analog states in question should be correspondingly less probable with the increasing of the neutron excess.

The experiment reported in Ref. 2 was related with observation of neutrons from the decay of the  $^7\text{He}$  analog states in  $^7\text{Li}$  to 3.56 MeV ( $T=1$ ) state in  $^6\text{Li}$  (other neutron decays would violates isospin conservation). The analog states were excited in resonance  $^6\text{He}+p$  interactions using the thick target inverse kinematics method [3]. The  $\gamma$  decay of the 3.56 MeV state served as a tag for the process (see Fig 1).

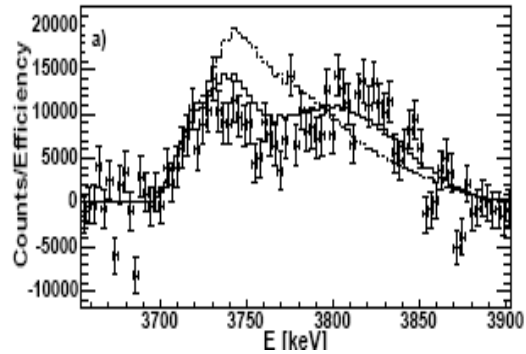


**Figure 1.** The solid curve shows a calculation of the  $\gamma$ -ray spectrum with the analog of the  $7\text{He}_{g.s.}$  and an  $1/2^-$   $E_x=2.7$  MeV,  $\Gamma=6$  MeV excited state.

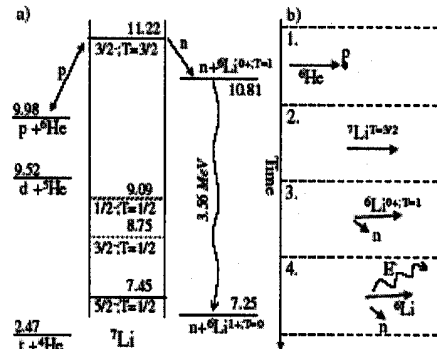


**Figure 2.** a) Decay pathways for the  $T=3/2$  resonance in  $^7\text{Li}$ , and b) the successive kinematics stages of the studied reaction.

In the most recent experiment we tried to use the Doppler shift of the 3.56 MeV  $\gamma$  rays to measure the  $p(^6\text{He},n)$  excitation function to study  $T=3/2$  states in  $^7\text{Li}$  (Fig. 2). It appears that 3.56 MeV  $\gamma$  rays keep the information on the velocity of the  $^6\text{He}$  ions at the moment of its interaction with hydrogen, in spite of the influence of the neutron decay of  $^7\text{Li}$ . This is a result of the inverse kinematics and small ratio of the mass of the neutron to the mass of  $^7\text{Li}$ .

- [1] V.Z.Goldberg *et al.*, Nucl.Phys. **A734**, 349 (2004)
- [2] G.V.Rogachev *et al.*, Phys.Rev.Lett. **92**, 2325 02 (2004)
- [3] K. P. Artemov *et al.*, Sov. J. Nucl. Phys. **52**, 408 (1990).
- [4] P. Boutachkov *et al.*, Phys. Rev. Lett. (submitted)

## Precise Branching-Ratio Measurement for the $\beta$ Decay of $^{21}\text{Na}$

V. E. Iacob, J. C. Hardy, C. A. Gagliardi, N. Nica, G. Tabacaru, L. Trache, R. E. Tribble  
and I. S. Towner<sup>1</sup>

<sup>1</sup> *Queen's University, Kingston, Ontario, Canada and Cyclotron Institute, Texas A&M University,  
College Station, TX*

A recent paper [1] has reported a measurement of the  $\beta$ - $\nu$  correlation coefficient,  $a_{\beta\nu}$ , for the ground-state mirror  $\beta^+$  transition  $^{21}\text{Na} (3/2^+) \rightarrow ^{21}\text{Ne} (3/2^+)$ . The authors compare their result with the standard-model prediction for  $a_{\beta\nu}$  with a view to testing for scalar or tensor currents, the presence of which would signal the need for an extension to the standard model. Although they find a significant discrepancy – the measured value is  $a_{\beta\nu} = 0.5243(91)$  compared with the standard-model prediction of 0.558 – they admit to the possibility of uncontrolled systematic effects in their experiment. Furthermore, both the standard-model prediction and the experimental result depend (in different ways) on the  $\beta$  branching ratio for the ground-state transition, and the authors also note that the currently accepted value for this ratio is based on mutually inconsistent measurements that are between 25 and 45 years old.

As an important part of our program to measure the properties of superallowed  $\beta$  transitions, we have developed a system to measure precise absolute  $\beta$ -branching ratios. We ultimately seek to reach 0.1% precision but, at its current state of development, we are confident of the system's accuracy to  $\sim 0.5\%$ . This is more than enough to settle any significant controversy over the  $^{21}\text{Na}$  branching ratio.

We produced 22.5-s  $^{21}\text{Na}$  using a 28.4-MeV  $^{22}\text{Ne}$  beam from the cyclotron to initiate the  $^1\text{H}(^{22}\text{Ne}, 2n)^{21}\text{Na}$  reaction on an  $\text{LN}_2$ -cooled hydrogen gas target. The ejectiles entered the MARS spectrometer where the fully stripped reaction products were separated, leaving a  $>99\%$  pure  $^{21}\text{Na}$  beam at the extraction slits in the MARS focal plane. This beam, containing  $\sim 10^5$  atoms/s at 24.4 MeV, then exited the vacuum through a 50- $\mu\text{m}$ -thick Kapton window, passed successively through a 0.3-mm-thick BC-404 scintillator and a stack of aluminum degraders, finally stopping in the 75- $\mu\text{m}$ -thick aluminized Mylar tape of a fast tape-transport system. Since the few impurities remaining in the beam had different ranges from  $^{21}\text{Na}$ , most were not collected on the tape; residual collected impurities were concluded to be less than 0.1% of the  $^{21}\text{Na}$  content.

In a typical measurement, we collected  $^{21}\text{Na}$  on the tape for 6 s, then interrupted the beam and triggered the tape-transport system to move the sample in 180 ms to a shielded counting station located 90 cm away, where the sample was positioned between a 1-mm-thick BC404 scintillator to detect  $\beta^+$  particles, and a 70% HPGe detector for  $\gamma$  rays. The sample was counted for 60 s, after which the complete cycle was repeated. The absolute efficiency of the HPGe detector has been calibrated to a precision of 0.2% between 50 and 1400 keV [2]; it was located 15 cm from the sample. The efficiency of the  $\beta^+$  detector, which was located 1.5 cm from the sample, has also been explored *via* measurements and Monte Carlo calculations, and its dependence on  $\beta^+$  energy is now reasonably well understood [3].

The decay scheme of  $^{21}\text{Na}$  appears in the figure. Since no other branch stronger than  $4 \times 10^{-4}\%$  exists [4], the branching ratio to the ground state can be determined from a measurement of the branching

ratio,  $R_I$ , to the 351-keV state. The essence of our measurement is thus to determine the intensity of the 351-keV  $\gamma$  ray relative to the total number of  $^{21}\text{Na}$  decays. We obtain  $R_I$  from the following relationship:

$$R_I = \frac{N_{\gamma\beta}}{N_\beta \varepsilon_\gamma} f,$$

where  $N_{\gamma\beta}$  is the number of 351-keV  $\gamma$  rays observed in coincidence with betas;  $N_\beta$  is the number of (singles) betas observed;  $\varepsilon_\gamma$  is the efficiency of the HPGe detector for 351-keV  $\gamma$  rays; and  $f$  is a correction factor ( $\sim 1$ ) that accounts for random  $\beta$ - $\gamma$  coincidences, real coincident  $\gamma$ -ray summing, differences between the  $\beta^+$  spectra of the two transitions from  $^{21}\text{Na}$ , and the effects of  $\gamma$ -rays recorded in the  $\beta$  detector. Under our experimental conditions,  $f = 0.975(1)$ .

We obtained a total of more than 80,000  $\beta$ - $\gamma$  coincident counts in the 351-keV  $\gamma$ -ray peak. Based on these data, our result for the  $\beta$  branching-ratio to the 351-keV state in  $^{21}\text{Ne}$  is  $R_I = 4.73(5)\%$ , where the quoted uncertainty is dominated by our uncertainty in determining the distance between the source on the tape and the face of the HPGe detector under experimental conditions. Our result is lower than the value 5.03(13)% adopted by Endt [4] from previous mutually inconsistent measurements, and alters the Standard Model prediction for the  $\beta$ - $v$  correlation coefficient of the ground-state decay branch to  $a_{\beta v} = 0.554(2)$ . The effect that this new branching-ratio result has on the experimental measurement of  $a_{\beta v}$  [1] must await reanalysis of that experiment.

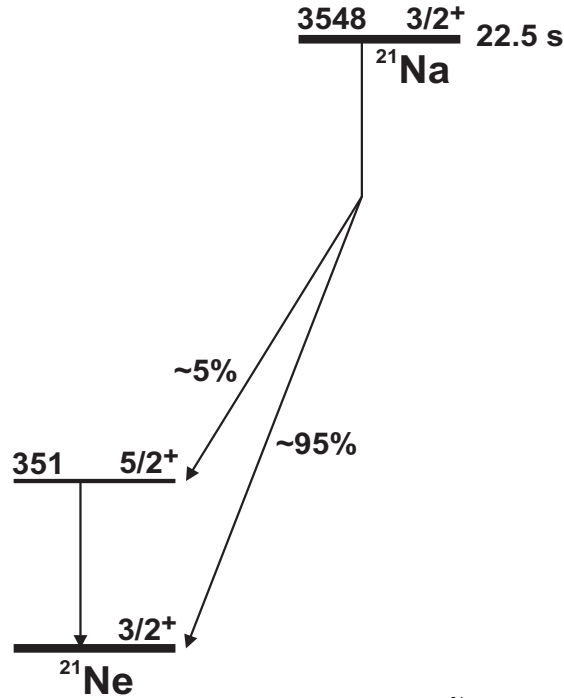


Figure. Decay scheme for the beta-decay of  $^{21}\text{Na}$ .

- [1] N.D. Scielzo, S.J. Freedman, B.K. Fujikawa and P.A. Vetter, Phys. Rev. Lett. **93** 102501 (2004).
- [2] R.G. Helmer, J.C. Hardy, V.E. Jacob, M. Sanchez-Vega, R.G. Neilson and J. Nelson, Nucl. Instrum. Methods. Phys. Res. **A511**, 360 (2003).
- [3] V.E. Jacob and J.C. Hardy, *Progress in Research*, Cyclotron Institute, Texas A&M University (2004-2005), p. I-24.
- [4] P.M. Endt, Nucl. Phys. **A521**, 1 (1990).

## The Half-Life of $^{34}\text{Ar}$ : A New Technique for Analyzing Combined Parent-Daughter Decay Curves

V. E. Iacob, J. C. Hardy, C. A. Gagliardi, V. E. Mayes, N. Nica, G. Tabacaru,  
L. Trache and R. E. Tribble

The half-life of the superallowed  $\beta^+$  emitter  $^{34}\text{Ar}$  has been determined to unprecedented precision as part of our program to test the Standard Model *via* the unitarity of the CKM matrix. For the experimental result to be useful for this test, its precision must be better than 0.1%.

We produced an  $^{34}\text{Ar}$  beam using the reaction  $p(^{35}\text{Cl}, 2n)^{34}\text{Ar}$ , with a 30A MeV  $^{35}\text{Cl}$  beam from the cyclotron incident on an  $\text{LN}_2$ -cooled hydrogen gas target held at 1.5 atm. The fully stripped  $^{34}\text{Ar}$  recoils were separated by the MARS recoil separator, then passed through a 0.3-mm-thick BC-404 scintillator and a stack of aluminum degraders, finally being implanted as a 99.7% pure source in the 76- $\mu\text{m}$ -thick aluminized Mylar tape of our fast tape-transport system. After  $^{34}\text{Ar}$  was collected for a short time (either 0.3 s, 0.7 s or 1.0 s), the beam was turned off and the implanted activity was moved in 175 ms to the center of a shielded  $4\pi$  proportional gas counter located 90 cm away, where the decay positrons were detected and multiscaled for 12 s. The collect-move-detect cycle was then repeated until the desired statistics had been accumulated. To ensure a bias-free result, the experiment was split into numerous different runs, with critical parameters in the detection being modified from one run to another.

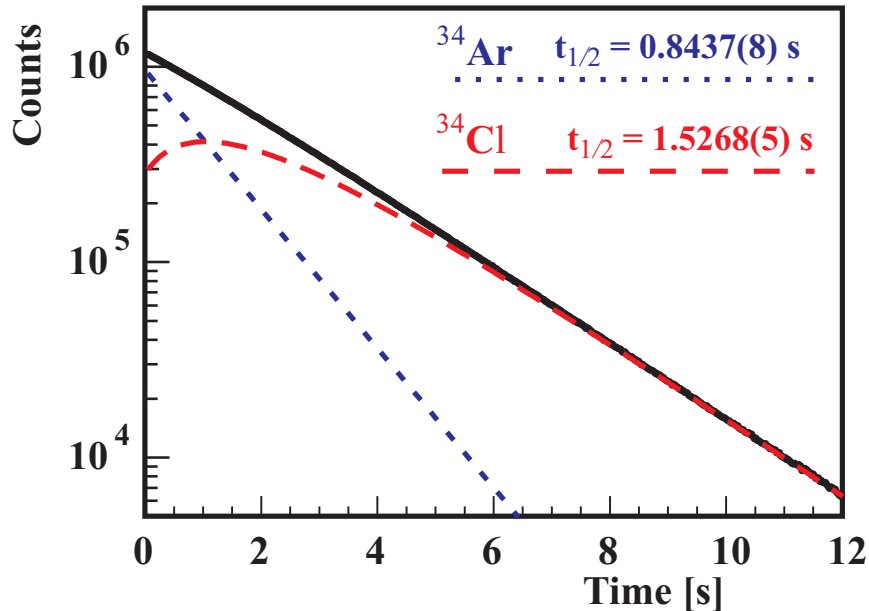


**Figure 1.** Typical multiscaler spectrum of positrons observed following the decay of collected samples of pure  $^{34}\text{Ar}$ . The dashed lines give the fitted contributions of  $^{34}\text{Ar}$  and its daughter  $^{34}\text{Cl}$ .

A typical measured decay spectrum is presented in Fig.1. Note that the decay of  $^{34}\text{Cl}$  appears to dominate the spectrum, the contribution of  $^{34}\text{Ar}$  being almost impossible to detect by eye. The extraction of an accurate half-life for  $^{34}\text{Ar}$  had to face several challenges:

- The daughter nucleus,  $^{34}\text{Cl}$ , is radioactive.
- The detector does not distinguish the  $^{34}\text{Ar}$  decays from the  $^{34}\text{Cl}$  decays.
- The half-lives of the two species are related by a factor close to 2; in fact,  $t_{1/2}(^{34}\text{Cl}) = 1.8 t_{1/2}(^{34}\text{Ar})$ .

The last item is very significant as is illustrated by the decay equations. After the collect interval, the combined  $^{34}\text{Ar}$  and  $^{34}\text{Cl}$  activity is given by

$$\Lambda_{\text{tot}} = N_a \lambda_a \frac{2\lambda_b - \lambda_a}{\lambda_b - \lambda_a} e^{-\lambda_a t} + \left( N_b - \frac{N_a \lambda_a}{\lambda_b - \lambda_a} \right) \lambda_b e^{-\lambda_b t}. \quad (1)$$

In this equation,  $t$  is the time after the end of the collect period,  $N_{a,b}$  are the numbers of  $^{34}\text{Ar}$  and  $^{34}\text{Cl}$  nuclei in the source at  $t = 0$ , and  $\lambda_{a,b}$  are the corresponding decay constants. Note that when  $\lambda_a = 2\lambda_b$  the first term (the component characterized by the  $\lambda_a$  decay constant) vanishes. Although not related by exactly a factor of 2, the actual half-lives of  $^{34}\text{Ar}$  and  $^{34}\text{Cl}$  result in the coefficient of the  $e^{-\lambda_a t}$  term in Eqn (1) being less than one sixth the magnitude of the coefficient of the  $e^{-\lambda_b t}$  term – and being *negative*. This is a serious limiting factor in the extraction of a precise half-life for  $^{34}\text{Ar}$ : a simple two-decay-component fit, even with more than half a billion combined  $^{34}\text{Ar}$  and  $^{34}\text{Cl}$  events recorded, could not do better than 0.4% precision, yielding the value 847.0(37) ms for the half-life of  $^{34}\text{Ar}$  [1].

Our first attempt to overcome this problem was to alter our experimental technique. We increased the ratio of  $^{34}\text{Ar}$  to  $^{34}\text{Cl}$  decay components by making use of the different end-point energies of the associated  $\beta^+$  spectra (5.04 MeV for  $^{34}\text{Ar}$  and 4.47 MeV for  $^{34}\text{Cl}$ ): we introduced a thin Cu foil between the decaying source and the gas counter volume. Thus the positrons originating from  $^{34}\text{Cl}$  decays were attenuated more than those from  $^{34}\text{Ar}$ . We adjusted the foil thickness between 1.25 mm and 1.90 mm to optimize the  $^{34}\text{Ar}$  to  $^{34}\text{Cl}$  ratio while simultaneously avoiding too high a loss of count-rate. For 1.5 mm it was found that the ratio of the coefficients in Eqn (1) is reduced from 6 to about 3, but at the cost of losing about 95% of the unattenuated count-rate. With a total of 9.5 million combined  $^{34}\text{Ar}$  and  $^{34}\text{Cl}$  decay events recorded under this condition, we obtained an  $^{34}\text{Ar}$  half life of 844.4(47) ms. Even though the decay-spectra obtained were qualitatively better at revealing the  $^{34}\text{Ar}$  half-life, this advantage was offset by the loss in statistics.

Our second attempt was computational and was much more successful. We reanalyzed the original experiments using a different approach. A close look at Eqn (1) revealed that the near cancellation of the coefficient of the  $e^{-\lambda_a t}$  term could actually be turned to our advantage: we altered the fitting procedure to focus on the difference between the experimental data and a one-component decay characterized by the exponential  $e^{-\lambda_b t}$ . We also replaced the free fit of the coefficients of the two exponentials in Eqn (1) by one that explicitly connects both coefficients to the experimental implantation time and the half-lives of both nuclides. That is, we required  $N_a$  and  $N_b$  to take the values determined by the known collection time for  $^{34}\text{Ar}$  and the calculated accumulation of  $^{34}\text{Cl}$  as a decay product during the collection time. The associated fitting procedure is more computer-intensive but is effective in increasing the precision of the extracted half-life.

To test the new fitting procedure, we generated a parallel set of artificial spectra by Monte Carlo techniques: these spectra mimicked our experimental data in statistics, background and dead-time, but

with an imposed half-life of 845ms for the parent activity. The results we obtained in fitting the pseudo-data demonstrated our methods to be reliable. Using the new procedure to re-analyze the half-billion combined events in our original experiment we find a preliminary value of 843.8(7) ms for the half-life of  $^{34}\text{Ar}$ . This precision of this result is already below 0.1% and may be further improved by the time analysis is complete.

[1] V.E. Iacob *et al.*, *Bul. Am. Phys. Soc.* **48**, 28 (2003).

## Relative Efficiency Calibration for a Plastic Scintillator: Source Measurements and Monte Carlo Calculations

V.E. Jacob and J.C. Hardy

Precise  $\beta$ -branching-ratio measurements are required to determine  $ft$ -values as part of our program to test the Standard Model via the unitarity of the Cabibbo-Kobayashi-Maskawa matrix. For the measurements to be useful in this test, their precision must be close to 0.1%.

The experimental arrangement we are developing for this purpose is based on the detection of  $\beta$ - $\gamma$  coincidences. The essential idea is that the *absolute* branching ratio,  $R$ , of a particular  $\beta$ -transition to an excited state can be determined from the intensity of the coincident  $\gamma$  rays observed de-exciting that state. The value of  $R$  can be obtained from the following relationship:

$$R = \frac{N_{\gamma\beta}}{N_{\beta}\varepsilon_{\gamma}} f,$$

where  $N_{\gamma\beta}$  is the number of  $\gamma$  rays observed in coincidence with betas;  $N_{\beta}$  is the number of (singles) betas observed;  $\varepsilon_{\gamma}$  is the *absolute* efficiency of the HPGe detector for the  $\gamma$  rays in question; and  $f$  is a correction factor ( $\sim 1$ ) that accounts for random  $\beta$ - $\gamma$  coincidences, real coincident  $\gamma$ -ray summing, differences among the  $\beta^+$  spectra for all transitions from the same parent, and the effects of  $\gamma$ -rays recorded in the  $\beta$  detector.

The absolute efficiency of our HPGe detector has already been determined to 0.2% for all energies between 50 and 1400 keV [1]. Although the absolute efficiency of the  $\beta$  detector does not appear in the equation, the relative efficiency of that detector as a function of  $\beta$  energy is required for a precise determination of the correction factor  $f$ . Our  $\beta$  detector is a 1-mm-thick BC404 plastic scintillator. With few exceptions, the  $\beta^+$  - decays of interest to us populate not only excited states of the daughter but the ground-state as well. Although  $N_{\gamma\beta}$  only includes the positrons populating one or more excited states,  $N_{\beta}$  includes all positrons including those populating the ground state. We need to know the extent to which the detector responds differently to the different transitions.

This requires us also to calibrate precisely the relative efficiency of the

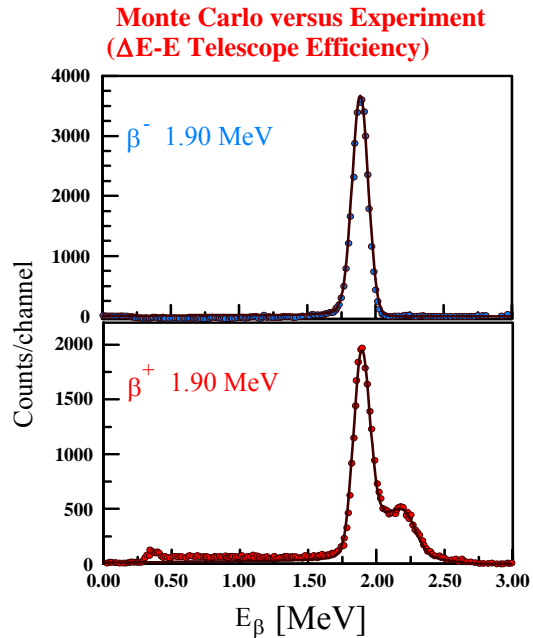


**Figure 1.** Spectra recorded for monoenergetic 1.90-MeV electrons and positrons in a detector telescope (from reference[4]). The experimental points appear as dots. The solid lines correspond to EGS-code Monte Carlo calculations.

plastic scintillator we use to detect the decay positrons. To calibrate precisely the relative efficiency of the plastic scintillator, we performed precise  $\gamma$ -singles and  $\beta$ - $\gamma$  coincidence measurements and combined the data reduction with Monte Carlo calculations. For our HPGe-detector simulations with  $\gamma$  rays we had used the CYLTRAN code (from the Integrated Tiger Series package) [2] but this code does not distinguish between positrons and electrons, so for the  $\beta$  detector we selected instead the DOSRZNR code (from the EGS package) [3]. This package has a complete description of the positron interactions making it suitable for calculations involving these particles. To test its efficacy we first compared its simulations with experimental spectra obtained [4] from monoenergetic  $\beta^+$  and  $\beta^-$  particles; it can be seen in Fig.1 that the agreement is excellent.

We performed another test of the EGS code, this time with continuous  $\beta^+$  spectra. We chose the case of  $^{22}\text{Mg}$ , for which we have

good experimental results from both singles and  $\beta$ - $\gamma$  coincidence measurements [5]. Fig.2 shows the decay scheme of  $^{22}\text{Mg}$  (as an inset) together with the positron spectra measured in coincidence with each of the three  $\gamma$  rays, 583, 74 and 1280 keV. Since the  $\beta^+$  spectrum in coincidence with the 1280 keV gamma has a much lower end-point than the other two, its detection efficiency is less than it is for the other two spectra. This effect manifests itself in the intensity ratio of the 1280- to 583-keV  $\gamma$  rays: when measured in  $\beta$ - $\gamma$  coincidence this ratio is smaller than when the ratio is measured in singles.

The experimental values for this ratio are 0.0510(7) and 0.0540(7) when measured in coincidence and singles, respectively. The difference between these two values is 5.6(1)%. The corresponding difference as determined with the EGS-code Monte Carlo calculation was 5.3(5)%, in complete agreement.

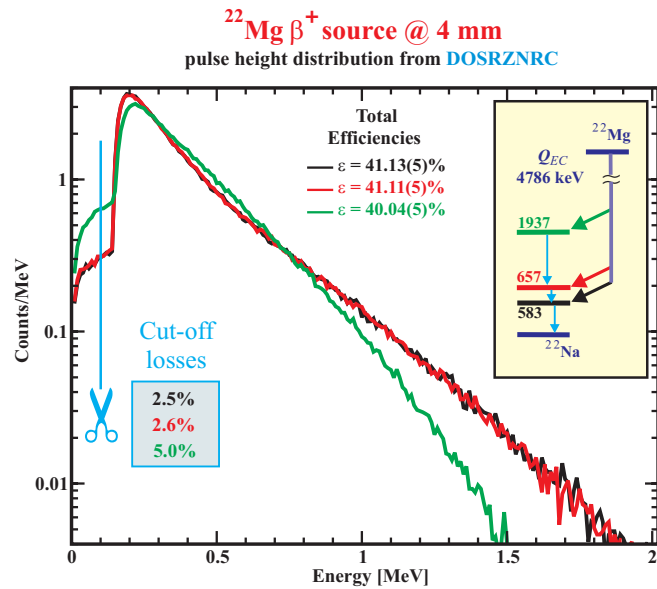


**Figure 2.** Positron spectra measured in coincidence with each of the three  $\gamma$  rays, (583, 74 and 1280 keV) observed following the decay of  $^{22}\text{Mg}$ . The decay scheme of  $^{22}\text{Mg}$  appears in the inset.

- [1] R.G. Helmer, J.C. Hardy, V.E. Jacob, M. Sanchez-Vega, R.G. Neilson and J. Nelson, Nucl. Instrum. Methods Phys. Res. **A511**, 360 (2003).
- [2] Halbleib, J.A., Mehlhorn, T.A., Nucl. Sci. Eng. **92**, 338 (1986).
- [3] NRCC Report PIRS-701 and <http://www.irs.inms.nrc.ca/inms/irs/EGSnrc/EGSnrc.html>.
- [4] E.T.H. Clifford *et al.*, Nucl. Instrum. Methods **224**, 440 (1984).
- [5] J.C. Hardy *et al.*, Phys. Rev. Lett. **91**, 082501 (2003).

**Precise Experimental Tests of Calculated Internal-Conversion Coefficients:  
the Decays of  $^{191}\text{Os}$  and  $^{193\text{m}}\text{Ir}$ , and the Fluorescence Yield in Iridium**

N. Nica, J. C. Hardy, V. E. Iacob, J. R. Montague, S. Raman,<sup>1</sup> C. W. Nestor, Jr.,<sup>1</sup>  
and M. B. Trzhaskovskaya<sup>2</sup>

<sup>1</sup> *Oak Ridge National Laboratory, Oak Ridge, Tennessee 37830*

<sup>2</sup> *Petersburg Nuclear Physics Institute, Gatchina, Russia 188300*

Internal conversion coefficients (ICCs) play an essential role in the analysis of nuclear decay schemes. Even so, tables of ICCs produced over the last five decades differ in detail from one another by a few percent or more, and a recent survey of world data [1] demonstrates similar systematic disagreements of all but the most recent table [2] with measured results. A particularly intriguing outcome of the survey was the apparent experimental preference for a “non-physical” approximation made in this recent table, in which the atomic sub-shell vacancy that occurs as a result of the conversion process is assumed to fill instantaneously: in other words, the hole is ignored. Unfortunately, though, the body of world ICC data includes very few measurements of high precision, say <1%. Thus, it is only in the average over many different transitions that a few-percent discrepancy between experiment and theory can be discerned at all, and it could be argued that the difference in experimental agreement between the two types of calculations – one with the hole, the other without – is hardly a definitive reason to choose an unacceptable physical model. Perhaps, too, there are other deficiencies in the calculation that are playing a role at the 1% level.

In any case, precision  $\gamma$ -ray intensity calibration standards [4] demand reliable ICCs and, in particular, our program to measure precise superallowed  $\beta$ -decay branching ratios relies on such standards (see, for example [3]). Consequently, we have embarked on a program to test the calculated ICCs to sub-percent precision. We began with a measurement [4] of the  $K$ -shell ICC,  $\alpha_K$ , for the 80.2-keV M4 isomeric decay of the second excited state in  $^{193}\text{Ir}$ . The transition energy is very close to the  $K$ -shell binding energy in iridium, which is at 76.112 keV, so the calculated value for  $\alpha_K$  differs by more than 10% depending on whether the hole is incorporated in the calculation or not. Since only a single transition is involved in the decay of this 10.5-day isomeric state, the total number of  $K$  X-rays observed,  $N_K$ , and the total number of  $\gamma$ -rays,  $N_\gamma$ , relate to  $\alpha_K$  by the simple relationship:

$$\alpha_K \omega_K = (N_K / N_\gamma)(\epsilon_\gamma / \epsilon_K), \quad (1)$$

where  $\omega_K$  is the fluorescence yield for iridium, and  $\epsilon_\gamma$  and  $\epsilon_K$  are the detector efficiencies for the  $\gamma$ -rays and X-rays, respectively.

Unfortunately, the  $\omega_K$  for iridium has never been directly measured, so in order to extract  $\alpha_K$  from this equation, we were forced to take the fluorescence yield from tables [5] based on a semi-empirical fit (as a function of  $Z$ ) to existing data, which are actually quite sparse for  $Z > 63$ . The tabulated value,  $\omega_K = 0.958(4)$ , was quoted with sufficient precision that we could comfortably use it to extract a 0.8% result for  $\alpha_K$  but we considered that our conclusions would become even more secure if we could make a direct

measurement of the iridium fluorescence yield and use that value instead. We made this measurement following the same approach we used for the  $^{193}\text{Ir}^m$  decay, measuring the intensity ratio of  $K$  x rays to  $\gamma$  rays, but now focusing on a 129.4-keV ( $M1 + E2$ ) transition in  $^{191}\text{Ir}$ . Since the calculated value of  $\alpha_K$  for this transition is virtually independent of the treatment of the  $K$ -shell vacancy, Eq. (1) can in this case be used to extract an experimental result for  $\omega_K$ . Alternatively, the ratio of the products  $\alpha_K\omega_K$  from the  $^{193}\text{Ir}^m$  and  $^{191}\text{Ir}$  experiments can be used to obtain the ratio of ICCs independent entirely of the fluorescence yield, which cancels in the ratio.

The 15.4-day  $\beta$ -decaying isotope,  $^{191}\text{Os}$ , was prepared from powders of natural osmium oxide and osmium chloride hydrate irradiated at the TRIGA reactor in the Texas A&M Nuclear Science Center. Two weeks after irradiation, when all  $^{193}\text{Os}$  activity had decayed away, the measured spectrum was dominated by the 129.4-keV  $\gamma$  ray and corresponding  $K$  x rays from  $^{191}\text{Ir}$ , the daughter of  $^{191}\text{Os}$ . In all, seven spectra from three different sources, and three background spectra were then recorded over a total period of 70 days, nearly five half-lives of  $^{191}\text{Os}$ . A complete inventory of impurities with activities down to 0.01% of the initial  $^{191}\text{Os}$  activity was made based on observed  $\gamma$ -ray energies and half-lives. The total impurity contribution to the iridium  $K$  X-ray peaks was less than 0.4% in all recorded spectra; no impurities affected the  $\gamma$ -ray peak. Figure 1 shows a spectrum obtained in the energy region of interest.

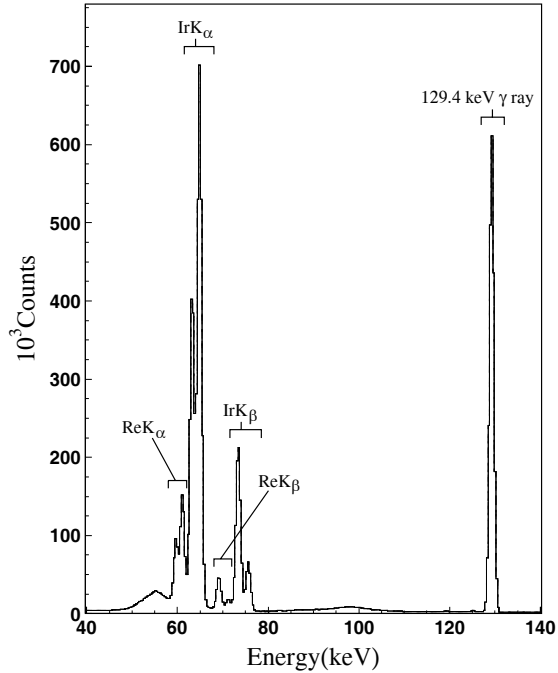


**Figure 1.** Portion of the spectrum of  $\gamma$  and x rays measured following the  $\beta$ -decay of  $^{191}\text{Os}$ .

Our final result for the fluorescence yield of iridium is  $\omega_K = 0.954(9)$ , which agrees well with the predicted value,  $\omega_K = 0.958(4)$ , obtained [5] from the interpolation of a semi-empirical fit to experimental data. The ratio of the products  $\alpha_K\omega_K$  from the  $^{193}\text{Ir}^m$  and  $^{191}\text{Ir}$  experiments yields the value 48.29(39). This number should be compared with 43.0(2), the value taken from the most recent ICC tables [2], in which the atomic hole has been ignored. This 10% disagreement is removed if the same calculations are repeated with the hole included, the calculated result becoming 48.1(2) or 46.4(2) depending on how the hole is incorporated. This result, which is now independent of the fluorescence yield confirms our previous conclusion that the hole must be included.

We will measure other cases to test the universal validity of our conclusion.

[1] S. Raman, C.W. Nestor, Jr., A Ichihara and M.B. Trzhaskovskaya, Phys. Rev. C **66**, 044312 (2002).

- [2] I.M. Band, M.B. Trzhaskovskaya, C.W. Nestor, Jr., P. Tikkanen and S. Raman, *At. Data Nucl. Data Tables* **81**, 1 (2002).
- [3] J.C. Hardy, V.E. Jacob, M. Sanchez-Vega, R.G. Neilson, A. Azhari, C.A. Gagliardi, V.E. Mayes, X. Tang, L. Trache and R.E. Tribble, *Phys. Rev. Lett.* **91**, 082501 (2003).
- [4] N. Nica, J.C. Hardy, V.E. Jacob, S. Raman, C.W. Nestor, Jr. and M.B. Trzhaskovskaya, *Phys. Rev. C* **70**, 054305 (2004).
- [5] E. Schönfeld and H. Janssen, *Nucl. Instrum. Methods Phys. Res.* **A369**, 527 (1996).

## A New Critical Survey of Superaligned $0^+ \rightarrow 0^+$ Nuclear $\beta$ -Decay: Improved Limits on Fundamental Weak-Interaction Parameters

J.C. Hardy and I.S. Towner<sup>1</sup>

<sup>1</sup> *Queen's University, Kingston, Ontario, Canada and Cyclotron Institute,  
Texas A&M University, College Station, TX*

Beta decay between nuclear analog states of spin-parity,  $J^\pi = 0^+$ , and isospin,  $T = 1$ , has been a subject of continuous and often intense study for five decades. The strengths, or  $ft$  values, of such transitions are nearly independent of nuclear-structure ambiguities and depend uniquely on the vector part of the weak interaction. Thus, their measurement has given nuclear physicists access to clean tests of some of the fundamental precepts of weak-interaction theory and, over the years, this strong motivation has led to very high precision being achieved in both the experiments and the theory required to interpret them.

As befits such an important issue, we have undertaken periodic surveys of the relevant world data (see, for example, refs [1-4]). Because the last survey appeared in 1990 and a large amount of new data has appeared in the decade and a half since then, we have just completed a thorough new overview [5] in which we critically survey all relevant measurements formally published before November 2004, adjust original data to take account of the most modern calibration standards, obtain statistically rigorous average results for each transition, and use updated and consistent calculations to extract weak-interaction parameters from those results [5,6].

Eight superallowed  $\beta$ -transitions – from parents  $^{14}\text{O}$ ,  $^{26}\text{Al}^m$ ,  $^{34}\text{Cl}$ ,  $^{38}\text{K}^m$ ,  $^{42}\text{Sc}$ ,  $^{46}\text{V}$ ,  $^{50}\text{Mn}$  and  $^{54}\text{Co}$  – are particularly amenable to experiment and, because of their significance to physics, have consequently received a good deal of attention over the past few decades. In each of these cases, the experimental  $ft$  value is known to better than 0.1%. In the 1990s,  $^{10}\text{C}$  was added to this list, its  $ft$  value now being known to a precision of 0.15%. More recently, three more cases have been added:  $^{22}\text{Mg}$ ,  $^{34}\text{Ar}$  and  $^{74}\text{Rb}$ , with  $ft$ -value standard deviations ranging from 0.24% to 0.40%. In the near future these uncertainties will undoubtedly be reduced and an additional eight cases could well be added to the list. As a result, our new survey includes world data on a total of 20 superallowed transitions.

The final average experimental  $ft$  values obtained from the survey were then converted to corresponding “corrected”  $\mathcal{F}t$  values by the application of small calculated correction terms [7]. In the lower panel of the figure we show results for the twelve superallowed transitions that are now known to 0.4% precision or better. They cover a broad range of nuclear masses from  $A=10$  to  $A=74$ . As anticipated by the Conserved Vector Current hypothesis (CVC) the  $\mathcal{F}t$  values are statistically consistent with one another, yielding an average value of 3072.7(8) s, with a corresponding chi-square per degree of freedom of 0.42. These results have many important outcomes.

First, the CVC prediction that the vector coupling constant,  $G_V$ , is indeed a constant requires that the  $\mathcal{F}t$  values be constant as well. This prediction is confirmed at the level of  $3 \times 10^{-4}$ , which is the fractional uncertainty we obtain on the average  $\mathcal{F}t$  value. Second, another CVC prediction, that the “induced scalar” term must be zero, is also confirmed: in the notation of Behrens and Büring [8], the

upper limit on the magnitude of the induced-scalar coupling constant,  $|f_s|$ , is 0.0013 in electron rest-mass units. Third, we can set an experimental limit on any possible fundamental scalar interaction (assuming maximum parity violation): the Fierz interference constant,  $b_F$ , is determined to be +0.0001(26).

Fourth, with a mutually consistent set of  $\mathcal{F}t$  values, we can determine the value of  $G_V$  and derive an improved value for the up-down mixing element of the Cabibbo-Kobayashi-Maskawa (CKM) matrix: *viz.*  $V_{ud} = 0.9738(4)$ . By more than an order of magnitude,  $V_{ud}$  is the most precisely determined element of the CKM matrix and is an important component of the most demanding test of the unitarity of that matrix: the sum of squares of the top-row elements. With Particle Data Group values [9] for  $V_{us}$  and  $V_{ub}$ , that sum yields 0.9966(14), which fails unitarity by 2.4 standard deviations. However, if the weighted average of two very recent results [10, 11] for  $V_{us}$  is used, then the sum becomes 0.9993(11) and unitarity is fully satisfied.

Fifth, if parity violation were not maximal, then right-hand currents should be included in the derivation of  $V_{ud}$ . Thus, our unitarity results can be used to set an upper limit on the possible role of right-hand currents. Taking the most recent value [10, 11] for  $V_{us}$ , we obtain  $\text{Re}a_{LR}/a_{LL} = -0.0004(6)$ , where  $a_{LR}$  and  $a_{LL}$  are the left-right and left-left coupling constants in the notation of Herczeg [12].

Finally, we can test the efficacy of the nuclear-structure-dependent corrections that must be applied to each experimental  $ft$  value in order to obtain the corresponding  $\mathcal{F}t$  value. The top panel of the figure shows the experimental  $ft$  values corrected only for the transition-dependent “outer” radiative correction,  $\delta_R'$ , a correction that has been calculated from standard QED and is considered unambiguous. The  $\mathcal{F}t$  values in the bottom panel differ from the corresponding values of  $ft(1+\delta_R')$  in the top panel only by the inclusion of the nuclear structure-dependent corrections in the former. The origins of the structure-dependent corrections [7] are completely independent of the superallowed decay data, so the consistency of the corrected  $\mathcal{F}t$  values appearing in the bottom panel of the figure is a powerful validation of the calculated corrections used in their derivation.

Even though the body of world data on superallowed  $0^+$  to  $0^+$  decays already comprises the results of more than 100 measurements, it is still possible for well selected experiments with existing or currently foreseen techniques to make real improvements. For example, the validation of the nuclear-structure-dependent correction terms can be improved by the addition of new transitions selected from amongst those with large calculated corrections. If the  $ft$  values measured for cases with large calculated corrections also turn into corrected  $\mathcal{F}t$  values that are consistent with the others, then this must verify the calculations' reliability for the existing cases, which have smaller corrections. In fact, the cases of  $^{34}\text{Ar}$  and  $^{74}\text{Rb}$ , which have only recently been measured, were chosen for this very reason; their precision can certainly be improved, and other new cases with large calculated corrections, such as  $^{18}\text{Ne}$ ,  $^{30}\text{S}$  and  $^{62}\text{Ga}$ , would be valuable additions.

Another area of potential improvement is in the limit set on scalar currents, which is particularly sensitive to the  $\mathcal{F}t$  values for  $^{10}\text{C}$  and  $^{14}\text{O}$ ; any improvement in their uncertainties could thus reduce the scalar-current limit significantly.

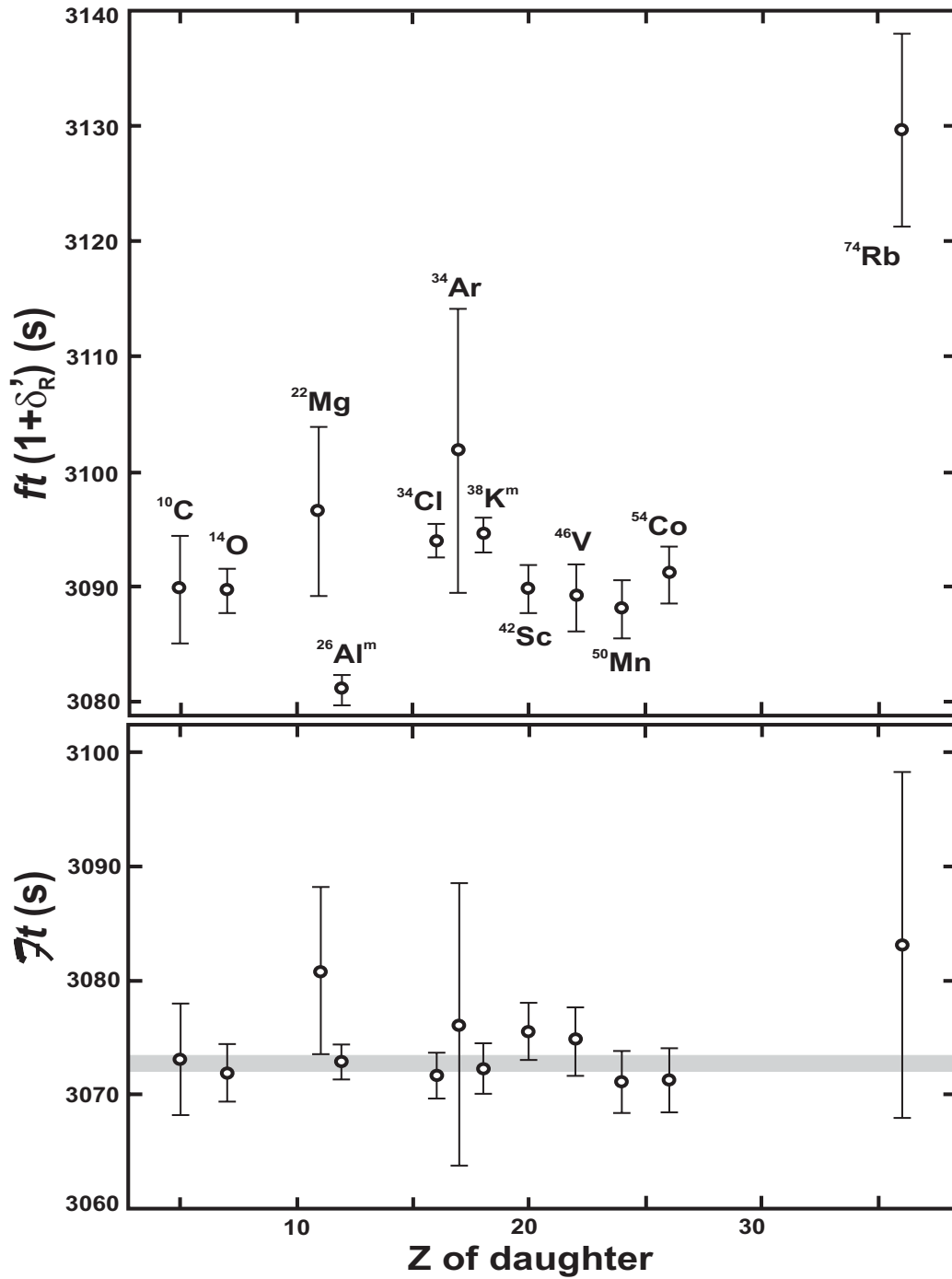


**Figure.** In the top panel are plotted the experimental  $ft$  values corrected only for  $\delta_R'$ , which comprises those radiative effects that are independent of nuclear structure. In the bottom panel, the corresponding  $\mathcal{F}t$  values are given; they differ from the top panel simply by inclusion of the nuclear-structure-dependent corrections. The horizontal grey band in the bottom panel indicates the average  $\mathcal{F}t$  value with its uncertainty.

- [1] I.S. Towner and J.C. Hardy, Nucl. Phys. **A205**, 33 (1973).
- [2] J.C. Hardy and I.S. Towner, Nucl. Phys. **A254**, 221 (1975).
- [3] V.T. Koslowsky, E. Hagberg, J.C. Hardy, H. Schmeing, R.E. Azuma and I.S. Towner, in *Proc. 7th Int. Conf. on atomic masses and fundamental constants, Darmstadt-Seeheim*, ed. O. Klepper (T.H. Darmstadt, 1984) p. 572.
- [4] J.C. Hardy, I.S. Towner, V.T. Koslowsky, E. Hagberg and H. Schmeing, Nucl. Phys. **A509**, 429 (1990).
- [5] J.C. Hardy and I.S. Towner, Phys. Rev. C, in press.
- [6] J.C. Hardy and I.S. Towner, Phys. Rev. Lett **94**, 092502 (2005).
- [7] I.S. Towner and J.C. Hardy, Phys. Rev. C **66**, 035501 (2002).
- [8] H. Behrens and W. Bühring, *Electron Radial Wave Functions and Nuclear Beta-decay*, (Clarendon Press, Oxford, 1982).
- [9] S. Eidelman *et al.*, Phys. Lett. B **592**, 1 (2004).
- [10] A. Sher *et al.*, Phys. Rev. Lett. **91**, 261802 (2003).
- [11] T. Alexopoulos *et al.*, Phys. Rev. Lett. **91**, 261802 (2003).
- [12] P. Herczeg, Phys. Rev. D **34**, 3449 (1986); P. Herczeg, Prog. Part. Nucl. Phys., **46**, 413 (2001).

## TRIUMF: High Precision Measurements of $^{26}\text{Na}$ $\beta^-$ Decay

V. E. Jacob and J. C. Hardy

As a valuable complement to our program to study superallowed  $\beta$  decay at Texas A&M, we are part of a collaboration at TRIUMF that is developing techniques for high-precision lifetime and  $\beta$ -branching-ratio measurements planned for the  $8\pi$   $\gamma$ -ray spectrometer, which has recently been installed on-line with the ISAC radioactive-beam facility at TRIUMF [1]. As a test case of the methodology, a series of experiments was performed with radioactive beams of  $^{26}\text{Na}$ . Although not superallowed, the  $^{26}\text{Na}$   $\beta^-$  decay provides an attractive case to study because beams of  $^{26}\text{Na}$  are readily available from the ISAC surface-ionization source, the daughter  $^{26}\text{Mg}$  is stable, and 100% of the  $\beta$  transitions are followed by  $\gamma$ -ray emission. Under these conditions, precision measurements of the  $\beta$ -branching ratios in the decay of  $^{26}\text{Na}$  can be obtained from the  $\gamma$ -ray activity without requiring an absolute  $\gamma$ -ray efficiency calibration. The results also provide a stringent test of shell-model calculations over a wide range of decay energies and transition intensities.

We measured the half-life of  $^{26}\text{Na}$  by moving collected sources with a fast tape-transport system to a  $4\pi$  continuous-gas-flow proportional counter of identical design to the one we use at Texas A&M. Events were also processed electronically in essentially the same way we do here [2]. The data were then analyzed independently with different software at TRIUMF and at Texas A&M. The results of the two analyses agreed well and yielded a half-life value for  $^{26}\text{Na}$  of  $t_{1/2} = 1.07128 \pm 0.00013 \pm 0.00021$  s, where the first uncertainty is statistical and the second systematic.

Gamma-ray spectra were recorded in the 20 Compton-suppressed HPGe detectors of the  $8\pi$  spectrometer with a continuous beam of  $^{26}\text{Na}$  implanted in a thin aluminum disk at the center of the spectrometer. Relative detector efficiencies were calculated from a GEANT4 simulation normalized to the 1808.7-keV transition in  $^{26}\text{Mg}$ . From the singles and coincidence spectra collected, a total of 84  $\gamma$  rays from 20 levels were identified following the  $\beta^-$  decay of  $^{26}\text{Na}$ . The  $ft$  values were determined for the  $\beta$  transitions populating all 20 levels, and the results were compared with a full  $sd$ -shell-model calculation. There is excellent agreement, with a clear state-by-state correspondence for the first 19 excited states in  $^{26}\text{Na}$ .

These results have been published [3].

[1] C.E. Svensson *et al.*, Nucl. Instrum. Methods Phys. Res. **B204**, 660 (2003).

[2] J.C. Hardy *et al.*, Phys. Rev. Lett. **91**, 082501 (2003).

[3] G.F. Grinyer *et al.*, Phys. Rev. C **71**, 044309 (2005).

## Canadian Penning Trap: Q-Value of the Superallowed Decay of $^{22}\text{Mg}$

J. C. Hardy and V. E. Iacob

As a valuable complement to our program to study superallowed  $\beta$  decay at Texas A&M, we are part of a collaboration based on the Canadian Penning Trap (CPT) Mass Spectrometer, which is situated on-line to the ATLAS facility at the Argonne National Laboratory. The CPT is currently capable of measuring the atomic masses of short-lived isotopes to a precision of  $1 \times 10^{-8}$  and is ideally suited to the measurement of masses of the parents and daughters of superallowed  $\beta$  transitions. Our first reported measurement is of the masses of 3.9-s  $^{22}\text{Mg}$  and 2.6-year  $^{22}\text{Na}$ .

The  $^{22}\text{Mg}$  and  $^{22}\text{Na}$  activities were created by a 3.5-MeV/nucleon beam of  $^{20}\text{Ne}$  passing through a 7-cm long cryogenic target of  $^3\text{He}$  gas held at a pressure of 700 mbar and at liquid-nitrogen temperature. Ejected reaction products proceeded through a focusing magnetic quadrupole triplet, a velocity filter to separate out the primary beam, and an Enge magnetic spectrometer to make the final selection before focusing them on the entrance of an RF gas catcher and injection system. The latter produces a mass-selected beam of the desired product and injects it in pulses into a precision Penning trap [1,2]. Our experiment interleaved measurements of the masses of  $^{22}\text{Na}^+$  and  $^{22}\text{Mg}^+$  with calibrations of the magnetic field of the Penning trap based on molecular ions of  $\text{H}_2^{18}\text{OH}^+$  and  $\text{H}_2^{16}\text{OH}^+$  and ions of  $^{22}\text{Ne}^+$ ,  $^{21}\text{Ne}^+$  and  $^{20}\text{Ne}^+$ .

For the  $A = 22$  radioactive species, we measured mass ratios of 1.000372238(31) and 1.000138820(11) for  $^{22}\text{Mg}^+$  versus  $^{22}\text{Ne}^+$  and  $^{22}\text{Na}^+$  versus  $^{22}\text{Ne}^+$ , respectively. The final mass excesses for the two isotopes of interest, after a -0.01 keV correction for ionization energy differences, were then determined to be  $\Delta M(^{22}\text{Mg}) = -399.73(67)$  keV and  $\Delta M(^{22}\text{Na}) = -5181.12(29)$  keV. They differ by -2.7 keV and +1.3 keV, respectively, from the 2003 mass tables [3], in both cases well outside error bars. Our new mass results yield a  $Q_{\text{EC}}$  value of 4124.39(73) keV for the superallowed  $\beta$  decay of  $^{22}\text{Mg}$ , a decay for which we have recently determined the half-life and branching ratio to high precision at Texas A&M [4]. The  $\mathcal{F}t$  value for the  $^{22}\text{Mg}$  superallowed decay is now known to a precision of 0.2%, which places this decay among the most precisely known superallowed decays used in setting important limits on weak interaction parameters [5].

These results have been published [6].

- [1] J. Clark *et al.*, Nucl. Instrum. Methods Phys. Res. **B204**, 487 (2003).
- [2] G. Savard *et al.*, Nucl. Instrum. Methods Phys. Res. **B204**, 582 (2003).
- [3] G. Audi *et al.*, Nucl. Phys. **A729**, 337 (2003).
- [4] J.C. Hardy *et al.*, Phys. Rev. Lett. **91**, 082501 (2003).
- [5] J.C. Hardy and I.S. Towner, Phys. Rev. Lett **94**, 092502 (2005).
- [6] G. Savard *et al.*, Phys. Rev. C **70**, 042501(R) (2004).

## Canadian Penning Trap: Q-Value of the Superalloyed Decay of $^{46}\text{V}$

J.C. Hardy

The collaboration based on the Canadian Penning Trap (CPT) Mass Spectrometer has completed its second measurement of atomic masses related to superallowed  $\beta$  decay. The masses of 0.42-s  $^{46}\text{V}$  and stable  $^{46}\text{Ti}$  have been determined to a precision of  $1 \times 10^{-8}$ . These results yield a new precise value of the  $Q_{\text{EC}}$  for the superallowed decay of  $^{46}\text{V}$ .

Both isotopes were created by a 3.3-MeV/nucleon beam of  $^{36}\text{Ar}$  impinging on a 0.8-mg/cm<sup>2</sup> rotating target of natural carbon. Ejected reaction products proceeded through a focusing magnetic quadrupole triplet, a velocity filter to separate out the primary beam, and an Enge magnetic spectrometer to make the final selection before focusing them on the entrance of an RF gas catcher and injection system. The latter produces a mass-selected beam of the desired product and injects it in pulses into a precision Penning trap [1,2]. Our experiment interleaved measurements of the masses of  $^{46}\text{V}^{2+}$  and  $^{46}\text{Ti}^{2+}$  with calibrations of the magnetic field of the Penning trap via measurements of  $^{22}\text{Ne}^+$ .

The final masses obtained for the two isotopes of interest were  $M(^{46}\text{V}) = 45.96019909(69)$  amu and  $M(^{46}\text{Ti}) = 45.95262748(62)$  amu. Our result for  $^{46}\text{Ti}$  differs substantially from the value in the 2003 mass tables [3]; however, it should be noted that the latter value is based entirely on a 30-year-old unpublished (p, $\gamma$ ) measurement. Our new masses yield a  $Q_{\text{EC}}$  value of 7052.90(40) keV for  $^{46}\text{V}$ , which differs by 2.19 keV from the number determined in our recent compilation [4], a result that is dominated by a 28-year old measurement [5] of the  $^{46}\text{Ti} (^3\text{He,t}) ^{46}\text{V}$  reaction Q-value. That old measurement included six other Q-value measurements pertaining to superallowed transitions and it now begins to look as though a majority of those results differ significantly from more recent measurements. If all the results in reference [5] are rejected, then the weak-interaction parameters extracted from superallowed decays are noticeably changed from those obtained in our compilation [4], though not outside the uncertainties we quoted there.

These results have been accepted for publication [6].

- [1] J. Clark *et al.*, Nucl. Instrum. Methods Phys. Res. **B204**, 487 (2003).
- [2] G. Savard *et al.*, Nucl. Instrum. Methods Phys. Res. **B204**, 582 (2003).
- [3] G. Audi *et al.*, Nucl. Phys. **A729**, 337 (2003).
- [4] J.C. Hardy and I.S. Towner, Phys. Rev. Lett **94**, 092502 (2005).
- [5] H. Vonach *et al.*, Nucl. Phys. **A278**, 189 (1977).
- [6] G. Savard *et al.*, Phys. Rev. Lett., to be published.

## TWIST: Measuring the Space-Time Structure of Muon Decay

C. A. Gagliardi, J. R. Musser, R. E. Tribble, M. A. Vasiliev, and the TWIST Collaboration

This past year, TWIST published its first physics results for the Michel parameters in normal muon decay, based on the analysis of the data that were taken during Fall, 2002. We find the Michel parameter  $\rho = 0.75080 \pm 0.00032(\text{stat}) \pm 0.00097(\text{syst}) \pm 0.00023$ , where the last uncertainty represents the dependence of  $\rho$  on the Michel parameter  $\eta$  [1]. James Musser led the analysis effort for  $\rho$  as his Ph.D. research. We also find the Michel parameter  $\delta = 0.74964 \pm 0.00066(\text{stat}) \pm 0.00112(\text{syst})$  [2]. Examples of the data vs. Monte Carlo comparisons that led to these results are shown in Figs. 1 and 2. Both results are consistent with the Standard Model expectation that  $\rho = \delta = 3/4$ . The former represents the first successful measurement of  $\rho$  since the mid-1960's, while the latter is the first measurement of  $\delta$  since the mid-1980's. These measurements provide improvements of factors of 2.5-3 compared to the previous accepted values, and they constitute the first time that any Michel parameter has been determined from a blind analysis.

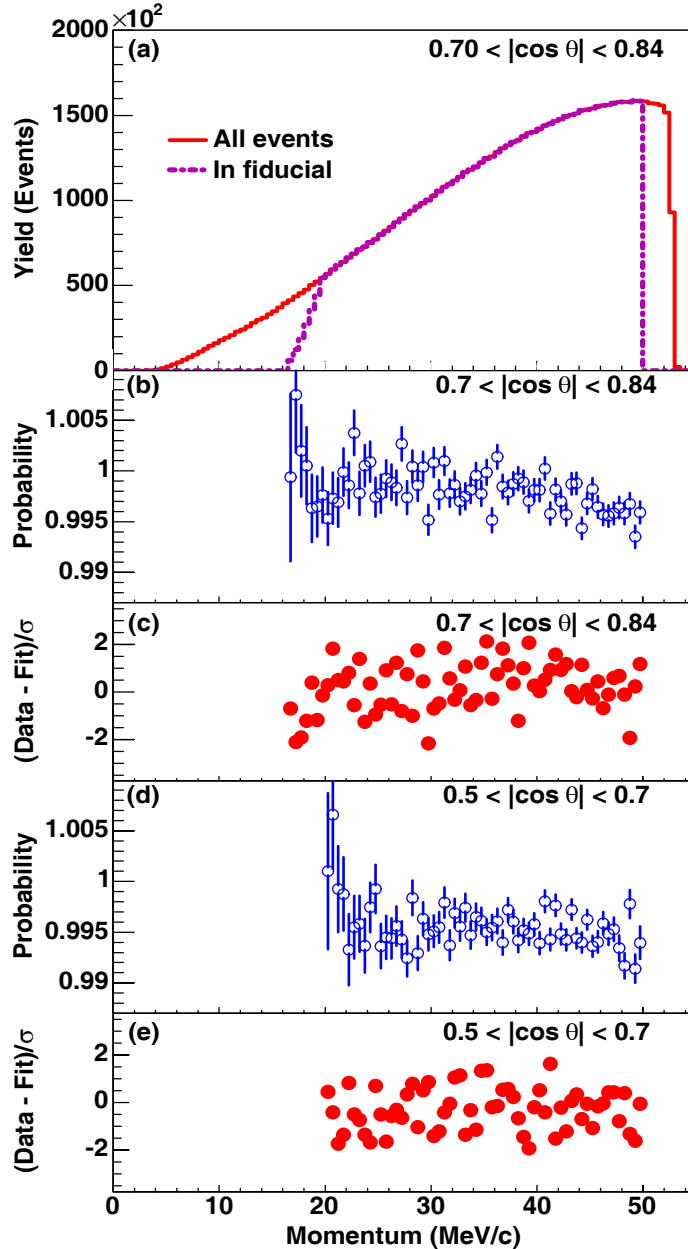


**Figure 1.** (a) The muon decay events within  $0.70 < |\cos(\theta)| < 0.84$  from one data set. (b,d) The probability of reconstructing decays for two different angular regions, as calculated by the Monte Carlo simulation. (c,e) The normalized residuals for the fit of the data spectrum to the Monte Carlo standard spectrum plus derivatives.

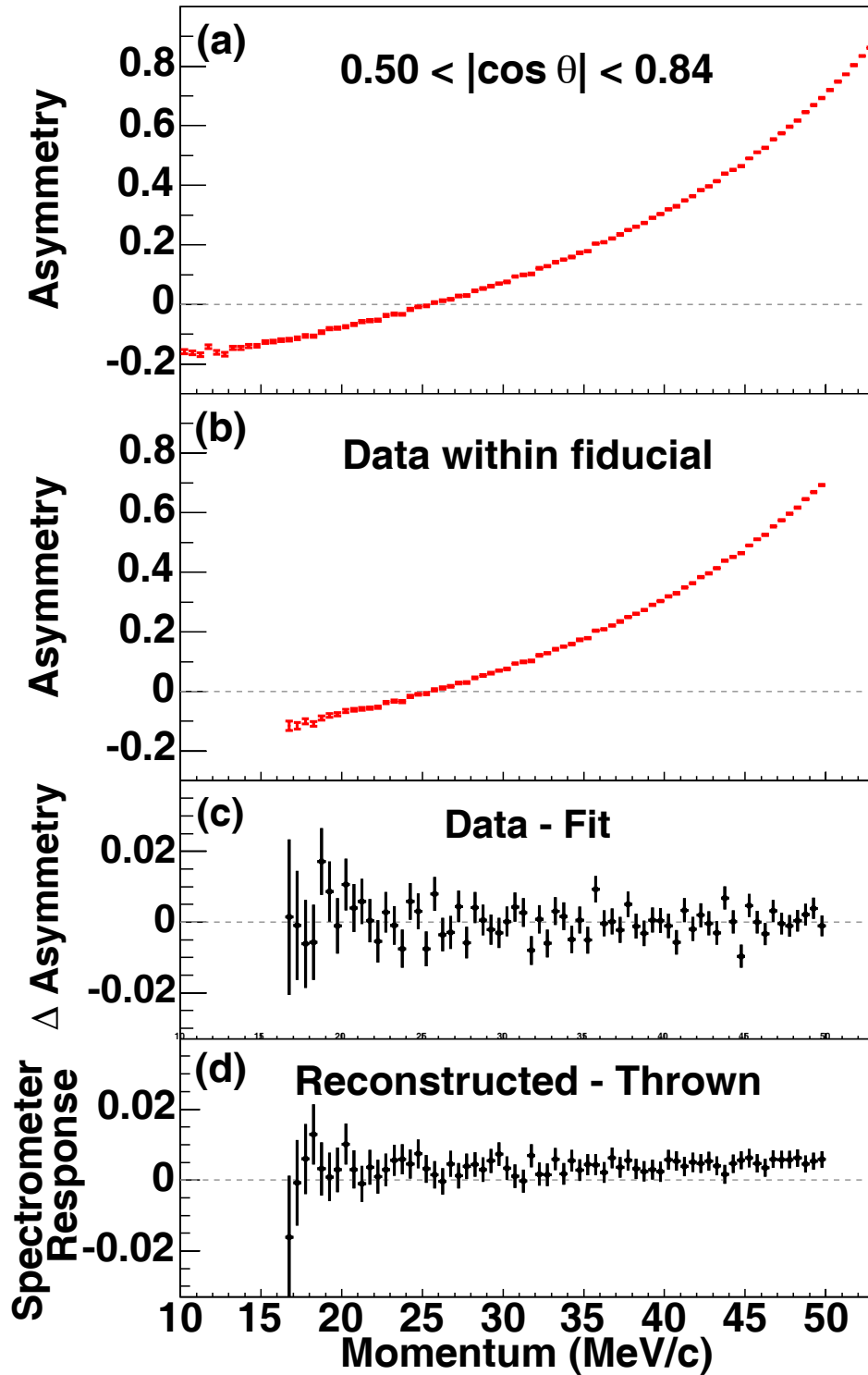


**Figure 2.** (a,b) The observed muon decay asymmetry from one data set. (c) The difference between the asymmetry in panel (b) and the best fit Monte Carlo spectrum. (d) The difference between the asymmetry calculated from the reconstructed Monte Carlo events and as thrown by the Monte Carlo,

The results for  $\rho$  and  $\delta$  can be combined with a previous measurement of the Michel parameter combination  $P_\mu \xi \delta / \rho$  [3] to conclude that  $0.9960 < P_\mu \xi \leq \xi < 1.0040$ , with 90% confidence, which is consistent with the Standard Model prediction and a factor of 3 more precise than the previous best measurement. These results set new, more stringent limits on the  $W_R$  mass and  $W_L - W_R$  mixing in left-right symmetric models. They also provide new, more stringent, model-independent limits on the decay of right-handed muons into left-handed electrons.

Work has also proceeded on the first direct measurement of  $P_\mu \xi$  by TWIST. This measurement is sensitive to several systematic effects related to muon depolarization that are unimportant for the measurements of  $\rho$  and  $\delta$ . The most important are depolarization as the muon crosses the fringe field boundary into the superconducting solenoid magnet and interactions with the detector and target materials that lead to depolarization either during or after stopping. To minimize depolarization in the target, the graphite-coated mylar target that was used in 2002 was replaced by a high-purity Al target in 2003. To minimize the uncertainties in fringe field depolarization, a Time Expansion Chamber (TEC) has been built at TRIUMF to measure the muon beam phase space. The TEC was commissioned during studies in Summer, 2004, then used for the first time during the physics run in Fall, 2004. Data were taken during the Fall, 2004 run that should suffice to determine  $P_\mu \xi$  to  $\sim 0.003$ . The same data should provide a new measurement of  $\rho$  and  $\delta$  with statistical uncertainties comparable to those from the '02 analysis, but with the systematic uncertainties reduced by approximately a factor of 2.

- [1] J.R. Musser *et al.* (TWIST Collaboration), Phys. Rev. Lett. **94**, 101805 (2005).
- [2] A. Gaponenko *et al.* (TWIST Collaboration), Phys. Rev. D **71**, 071101(R) (2005).
- [3] A. Jodidio *et al.*, Phys. Rev. D **34**, 1967 (1986); **37**, 237E (1988).

## The Physics of STAR at RHIC

C.A. Gagliardi, T.W. Henry, R.E. Tribble, and the STAR Collaboration

Our work on STAR continues to address questions in high- $p_T$  and spin physics at RHIC. During the past year, we have been involved in analysis of the Au+Au collision data that were taken during run 4 at a center-of-mass energy of 62.4 GeV/nucleon-nucleon pair, as well as continuing work on the full energy Au+Au data from run 2. A primary motivation for the 62.4 GeV Au+Au run was to explore the energy dependence of high- $p_T$  particle suppression, which has been seen in the 130 and 200 GeV RHIC data. The existing data have been interpreted as evidence for partonic energy loss, often referred to as “jet quenching”, in the dense matter created at RHIC [1]. Figure 1 shows STAR measurements of  $R_{CP}$ , the ratio of charged hadron yields in central versus peripheral collisions, for 62.4 and 200 GeV Au+Au collisions. At intermediate  $p_T$ , the suppression at 62 GeV is not as strong as seen at 200 GeV; at high  $p_T$ , the behavior at the two energies is qualitatively similar. This pattern is consistent with expectations in models that attribute jet quenching to partonic energy loss [2].

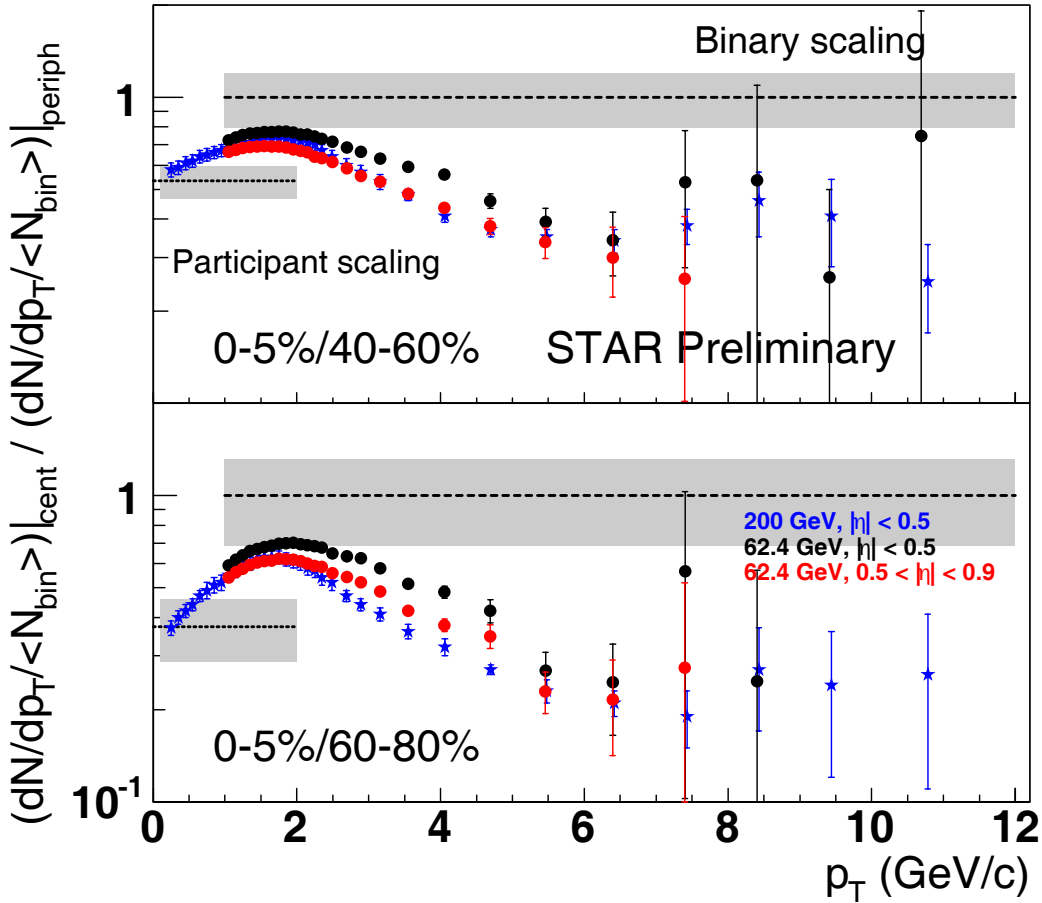


**Figure 1.** Preliminary  $R_{CP}$  measurements in Au+Au collisions at 62.4 GeV (circles) for two different pseudorapidity regions are compared to previous results at 200 GeV (stars) [3].

STAR has also explored high- $p_T$  di-hadron angular correlations in the 62 GeV Au+Au data. At 200 GeV, the near-side, high- $p_T$  jet-like di-hadron angular correlations were found to be very similar in Au+Au collisions to those seen in p+p collisions. In contrast, the back-to-back correlations, which are characteristic of di-jets, were found to be strongly suppressed in central Au+Au collisions [4], as expected if the energetic partons lose energy as they propagate through the dense medium. One way to measure this behavior is to consider the difference in yields on the near- and away-sides. Figure 2 shows the results for Au+Au collisions at 62 and 200 GeV, as functions of centrality. There is a significant difference in the relative yields for peripheral collisions at the two energies. This difference is consistent with predictions from PYTHIA for p+p collisions that the near-side yield should be a factor of  $\sim 3$  smaller at 62 GeV than at 200 GeV, while the away-side yields should be similar. The change in the near-away difference as a function of participant number is very similar at the two energies, which indicates that the interactions of the “associated” parton in the dense medium are similar at the two energies.

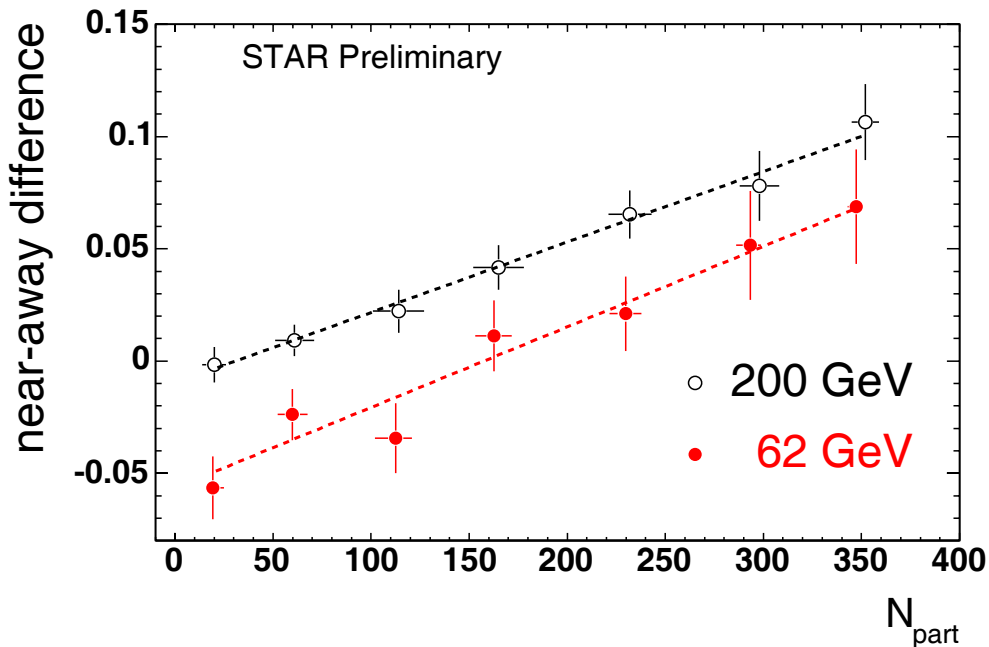


**Figure 2.** Preliminary difference in the near-side and back-to-back di-hadron yields as a function of the number of participants for  $4 < p_T^{trig} < 6$  GeV/c,  $2 < p_T^{assoc} < p_T^{trig}$ , and  $|\eta| < 0.9$  in 62 and 200 GeV Au+Au collisions. The dashed lines show linear fits to the data.

For the past several years, we have been involved in the construction of the STAR Endcap Electromagnetic Calorimeter (EEMC). The EEMC is a critical component of the STAR spin physics program. It provides coverage for direct  $\gamma$ ,  $\pi^0$ , and jet detection at forward pseudorapidity ( $1.09 < \eta < 2$ ), where the sensitivity of these yields to gluon polarization in the proton is large. Over the previous several years, our group built all of the magnetic shielding boxes necessary to house the 720 photomultiplier tubes and 576 multi-anode photomultiplier tubes for the EEMC on the back of the west STAR pole tip. This past year, we assisted with the installation of the last components of the EEMC. The complete EEMC is now in use for the p+p run that is underway.

We also carry administrative responsibilities related to STAR. One of us (CAG) continued to serve as a co-convenor of the High- $p_T$  Physics Working Group, and also served as a member of the NSAC Sub-panel on Heavy Ion Physics (the “Barnes panel”). Members of the group chaired two STAR god-parent committees for papers outside of the spin and high- $p_T$  areas, and participated as members on several other god-parent committees.

- [1] J. Adams *et al.* (STAR Collaboration), Phys. Rev. Lett. **91**, 072304 (2003).
- [2] X.N. Wang, Phys. Lett. B **579**, 299 (2004).
- [3] J. Adams *et al.* (STAR Collaboration), Phys. Rev. Lett. **91**, 172302 (2003).
- [4] C. Adler *et al.* (STAR Collaboration), Phys. Rev. Lett. **90**, 082302 (2003).

**SECTION II**  
**HEAVY ION REACTIONS**

## Refining Reaction Dynamics in Fermi Energy Heavy Ion Reactions

R. Wada, T. Keutgen, K. Hagel, J. Wang, R. Murthy, L. Qin, J. B. Natowitz,  
T. Materna, and S. Kowalski

In the past several years we have made comprehensive studies of the reaction dynamics for several heavy ion induced reactions in the Fermi energy domain. Experiments have been performed using  $4\pi$  detection systems such as NIMROD. To elucidate the underlying reaction dynamics, the experimental results have been compared with predictions of an anti-symmetrized molecular dynamics model (AMD)[1]. While much has been learned about the dynamic evolution of the composite system, our work indicates that the sequential statistical decays of the hot primary fragments produced through a multi-fragmentation process make it difficult to obtain quantitative information about important ingredients of the reaction dynamics such as the stiffness of the equation of state and the in-medium nucleon-nucleon cross sections. Therefore, to further quantify the reaction dynamics model, it is crucial to get more detailed information, such as charge, mass and excitation energy of the *primary* fragments.

For this purpose an experiment has been designed and performed, in which neutrons and charged particles were measured in coincidence with intermediate mass fragments (IMF). Reaction systems with different N/Z ratios have been studied.  $^{64}\text{Zn}$  and  $^{70}\text{Zn}$  beams were incident on  $^{58}\text{Ni}$ ,  $^{64}\text{Ni}$ ,  $^{112}\text{Sn}$ ,  $^{124}\text{Sn}$ ,  $^{197}\text{Au}$  and  $^{232}\text{Th}$  targets at 40 A MeV. Intermediate mass fragments (IMF) were detected by a Si telescope at  $20^\circ$ . The telescope consisted of 129 $\mu\text{m}$  or 65 $\mu\text{m}$ , 300 $\mu\text{m}$ , 1000 $\mu\text{m}$  and 1000  $\mu\text{m}$  Si detectors, each with 5cm x 5cm area and subdivided into four sections. Each quadrant section was backed by a 3cm long CsI(Tl) crystal, read by a PM tube. In Fig. 1 the IMF isotope distributions obtained after linearization are shown for different combinations of Si detectors in the telescope.

For neutron detection, sixteen detectors from the Belgian-French neutron detection array, DEMON, were used. The detectors were set at a distance of 1.0-1.2m from the target, outside the scattering chamber. Neutrons and gammas were identified by a pulse height discrimination method and the neutron energy was calculated from the time of flight, using the cyclotron RF signal as a start signal. In Fig.2 the

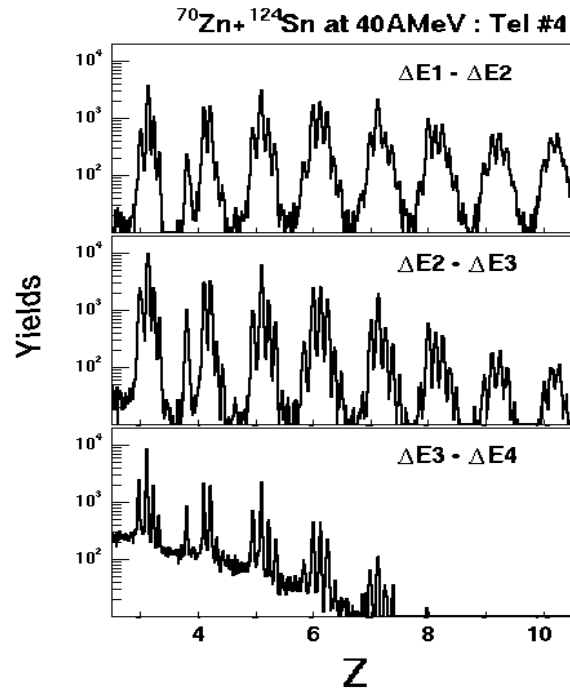


**Figure 1.** IMF isotope distributions after linearization in the Si telescope. From top to bottom, spectra obtained by 129-300, 300-1000, 1000-1000 $\mu\text{m}$  Si. Calculated charge on the X axis represent  $Z+(2Z-A)*0.1$ .

pulse height discrimination spectrum (upper) and the calculated neutron energy spectrum in coincidence with  ${}^9\text{Li}$  are presented.

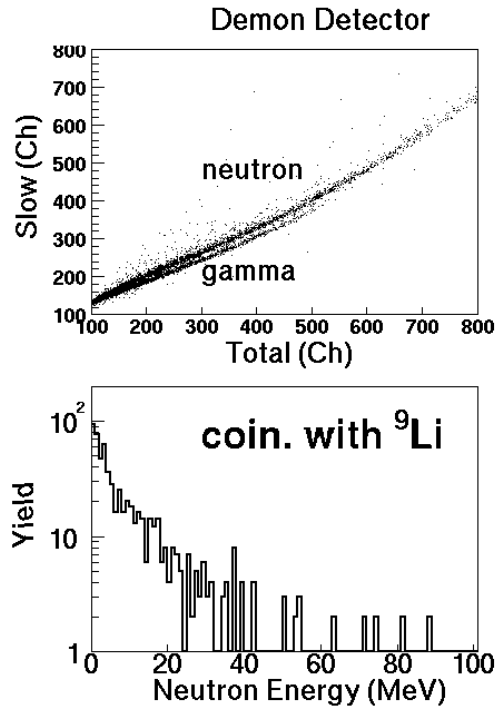


**Figure 2.** (Upper) Total signal vs Slow part of Demon detector signal. (Lower) Neutron energy spectrum at  $35^\circ$  in coincidence with  ${}^9\text{Li}$  in the telescope.

For detection of charged particles, 16 single crystal CsI(Tl) crystals, each read by a PM tube, were set inside the 80cm diameter scattering chamber. Light charged particles were identified by a pulse height discrimination method. Analysis is now underway.

[1] R. Wada *et al.*, Phys. Rev. C **69**, 044610 (2004), Phys.Rev. C **62**, 034601 (2000).

## Isoscaling for Heavy Ion Reaction at Intermediate Energies

S. Kowalski, R. Wada, K. Hagel, T. Materna, J. B. Natowitz, J. S. Wang, Y. Ma, T. Keutgen,  
 L. Qin, M. Murray, A. Makeev, P. Smith, J. Cibor, C. Hamilton, A. S. Botvina, E. Bell, S. Liddick,  
 D. Rowland, A. Ruangma, M. Veselsky, E. Winchester, G. A. Souliotis, S. J. Yennello, A. Samant,<sup>1</sup> M.  
 Cinausero,<sup>1</sup> D. Fabris,<sup>1</sup> E. Fioretto,<sup>1</sup> M. Lunardon,<sup>1</sup> G. Nebbia,<sup>1</sup> G. Prete,<sup>1</sup> G. Viesti,<sup>1</sup> Z. Majka,<sup>2</sup> P.  
 Staszal,<sup>2</sup> W. Zipper,<sup>3</sup> M. E. Brandan,<sup>4</sup> A. Martinez-Rocha,<sup>4</sup> A. Menchaca-Rocha,<sup>4</sup> and Y.El Masri<sup>5</sup>  
<sup>1</sup>INFN-Legnaro, Padova, Italy, <sup>2</sup>Jagiellonian University, Krakow, Poland,  
<sup>3</sup>Institute of Physics Silesia University, Katowice, Poland, <sup>4</sup>IFUNAM, Mexico,  
<sup>5</sup>UCL, Louvain-la-Neuve, Belgium

In many heavy reactions at intermediate energies the scaling factor:

$$R_{12}(N, Z) = \frac{Y_2(N, Z)}{Y_1(N, Z)} = C e^{(\alpha N + \beta Z)} \quad (1)$$

has been observed [1,2], where  $Y_i(N,Z)$  are the fragment yield for systems  $i=1,2$  with different neutron and proton composition. This scaling relation is called isoscaling.

The isoscaling parameters  $\alpha$  and  $\beta$  contain information about proton and neutron composition of the emitting source and may be used to study isospin-dependent properties such as the symmetry energy in the nuclear equation of state [3].in heavy ion reactions

We determined  $\alpha$  and  $\beta$  parameters for comparisons of fragment yields in three different reactions:  $^{64}\text{Zn}+^{197}\text{Au}/^{64}\text{Zn}+^{92}\text{Mo}$ ,  $^{64}\text{Zn}+^{197}\text{Au}/^{64}\text{Zn}+^{58}\text{Ni}$ ,  $^{64}\text{Zn}+^{92}\text{Mo}/^{64}\text{Zn}+^{58}\text{Ni}$  at energies of 47A, 35A and 26A MeV. The data were filtered according to the violence of the collision and designated as “violent” and “semi-violent” reactions [4]. Based on the three-source fit to the data (contributions from three sources; projectile-like (PLF), intermediate velocity (NN) and target-like (TLF)) we selected results from the so-called “midrapidity” region. Fig. 1 shows the fit of formula (1) to the experimental yield ratios for 47A MeV reactions.

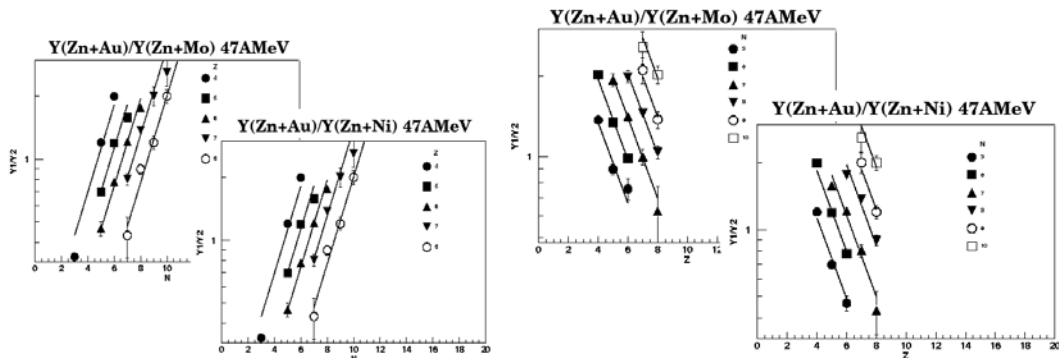


**Figure 1.** Example of the fits of formula (1) to the experimental data.

Fig. 2 presents  $\alpha$  parameters as the function of the incident beam energy for various systems. The  $\alpha$  parameter decreases with increasing beam energy for 47A and 35A MeV. Moreover the  $\alpha$  parameter depends on the  $N/Z$  ratio of the emitting system (decreases with decreasing of the  $N/Z$  of the system).

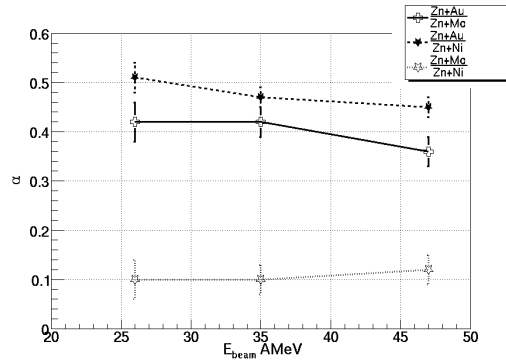


**Figure 2.** The  $\alpha$  parameter obtained from experimental data as function of the energy.

We made a computer simulation using the AMDV [5] code for these reactions. For simulation of secondary decay processes we employed the GEMINI code [6].

Comparisons of the  $\alpha$  and  $\beta$  isoscaling parameters for AMDV “hot fragments” (before secondary decay) and “cold fragments” (after secondary decay) show a difference of a factor around 2. This demonstrates that the influence of the secondary decay on the isoscaling parameters cannot be neglected (see Fig 3).

Fig. 3 shows also the comparison of the  $\alpha$  isoscaling parameters obtained from the experimental data with those obtained from the AMDV and AMDV-GEMINI calculations.

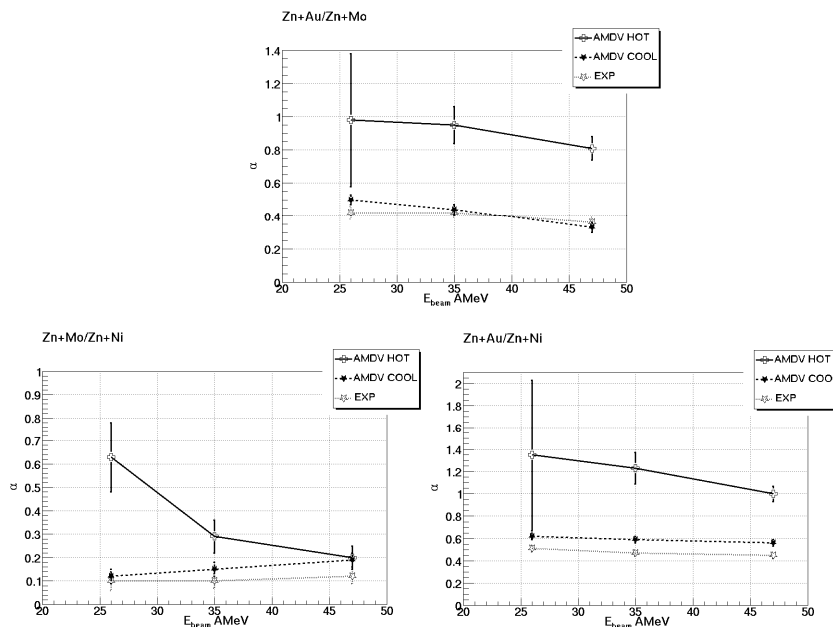


**Figure 3.** Comparison between  $\alpha$  parameters obtained from experimental data and AMDV calculations. AMDV HOT represents data before secondary decay, AMDV COOL – data after secondary decay.

Analysis of the experimental data and AMDV simulations is still in progress with the goal of extracting reliable information on the density dependence of the symmetry energy.

- [1] H. S. Xu, *et al.*, *Rev. Lett.* **85**, 716 (2000).
- [2] M.B. Tsang *et al.*, *Phys. Rev. Lett.* **86**, 5023 (2001).
- [3] A. Ono *et al.*, *Phys. Rev. C* **68**, 051601(R) (2003).
- [4] R. Wada *et al.*, *Phys. Rev. C* **69**, 044610 (2004).
- [5] A. Ono *et al.*, *Phys. Rev. C* **53**, 2958 (1996).
- [6] <http://www.chemistry.wustl.edu/~rc/gemini/>.

## Reconstruction of the Primary Fragment Distribution in Multi-Fragmentation Reactions

S. Kowalski, R. Wada, K. Hagel, T. Materna, J. B. Natowitz, J. S. Wang, Y. Ma, T. Keutgen, L. Qin, M. Murray, A. Makeev, P. Smith, J. Cibor, C. Hamilton, A. S. Botvina, E. Bell, S. Liddick, D. Rowland, A. Ruangma, M. Veselsky, E. Winchester, G. A. Souliotis, S. J. Yennello, A. Samant,<sup>1</sup> M. Cinausero,<sup>1</sup> D. Fabris,<sup>1</sup> E. Fioretto,<sup>1</sup> M. Lunardon,<sup>1</sup> G. Nebbia,<sup>1</sup> G. Prete,<sup>1</sup> G. Viesti,<sup>1</sup> Z. Majka,<sup>2</sup> P. Staszal,<sup>2</sup> W. Zipper,<sup>3</sup> M. E. Brandan,<sup>4</sup> A. Martinez-Rocha,<sup>4</sup> A. Menchaca-Rocha,<sup>4</sup> and Y. El Masri<sup>5</sup>  
<sup>1</sup>*INFN-Legnaro, Padova, Italy*, <sup>2</sup>*Jagiellonian University, Krakow, Poland*,  
<sup>3</sup>*Institute of Physics Silesia University, Katowice, Poland*, <sup>4</sup>*IFUNAM, Mexico*,  
<sup>5</sup>*UCL, Louvain-la-Neuve, Belgium*

In heavy ion reactions at intermediate energies the primary fragment distributions can contain important information on nuclear matter under extreme conditions. Secondary decay processes disturb this information.

We have developed a procedure, which allows the reconstruction of information on the primary fragment distribution (before secondary decay) from experimental observables.

The reconstruction code was tested on computer data taken from an AMD [1] model calculation for the  $^{64}\text{Zn}+^{197}\text{Au}$  reaction at energy 47A MeV. Secondary decay processes were simulated by the GEMINI [2] code.

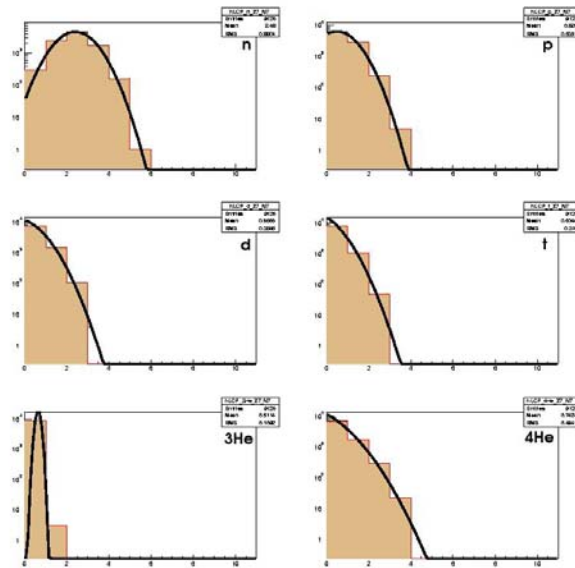


**Figure 1.** Multiplicity distributions for LPs associated with IMF (Z=6 and N=6)

As the input for the procedure we used the identity of the “cold” Intermediate Mass Fragment (IMF) and the associated means and widths of the multiplicity distributions of the evaporated light particles (neutrons, protons, deuterons, tritons,  $^3\text{He}$  and alpha particles) in the decays leading to that fragment. This procedure was adopted because we would like to be as close as is possible to the

experimental conditions. In principle, such mean multiplicities and widths are accessible in fragment particle correlation experiments. (However the widths are not easily determined in complex multi-fragmentation processes.) A Monte-Carlo reconstruction of the primary distribution was then made employing the mean multiplicities, widths and secondary fragment yield distribution.

Fig. 1 shows the (assumed) Gaussian distribution (solid line) and multiplicity distribution obtained from the Monte-Carlo simulation (orange histogram) the cold IMF  $^{12}\text{C}$ . Fig. 2 presents a comparison between output from our reconstruction procedure and the original primary distribution from the AMD simulation. The agreement is very good. As the widths are not easily determined from experiment we are currently exploring GEMINI calculations to determine the correlation between mean multiplicities and widths in hopes that measurements of just the mean multiplicities will suffice to provide the information required for reconstruction.

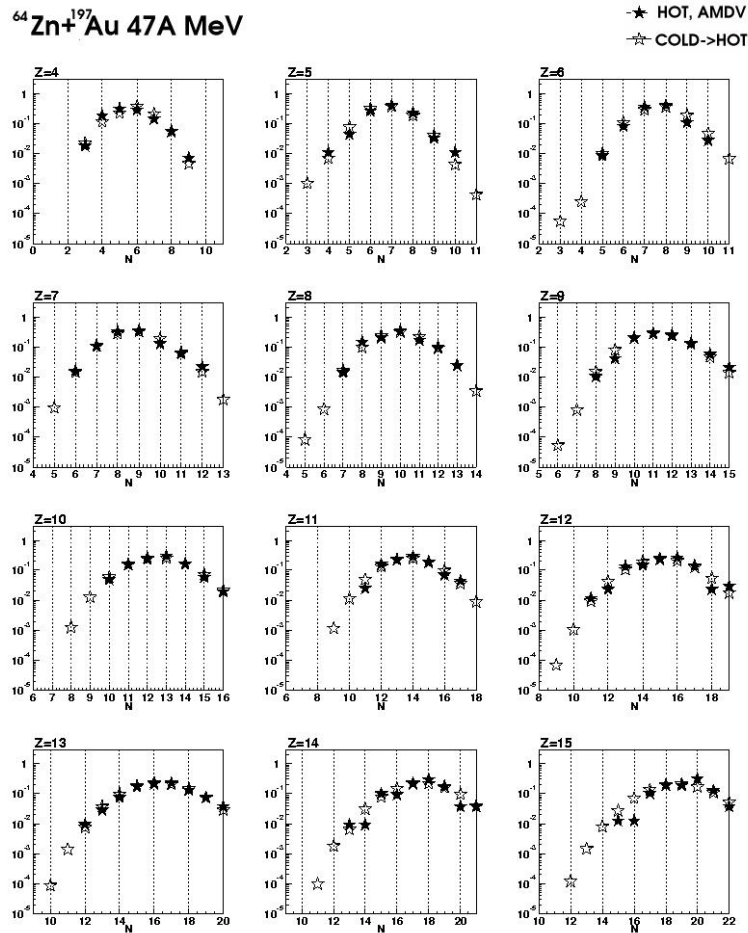


**Figure 2.** Comparison between fragments distribution obtained from AMD simulation (full stars) and reconstructed (open stars)

[1] A. Ono *et al.*, Phys. Rev. C **53**, 2958 (1996).

[2] <http://www.chemistry.wustl.edu/~rc/gemini/>

## Exploring New Ways to Produce Heavy and Superheavy Nuclei with Bigsol

T. Materna, S. Kowalski, K. Hagel, R. Murthy, J. Natowitz, L. Qin,  
G. Souliotis, R. Wada, J. Wang, D. Fabris,<sup>1</sup> M. Lunardon,<sup>1</sup> M. Morando,<sup>1</sup> S. Moretto,<sup>1</sup>  
G. Nebbia,<sup>1</sup> S. Pesente,<sup>1</sup> V. Rizzi,<sup>1</sup> G. Viesti,<sup>1</sup> V. Bocci,<sup>2</sup> M. Barbui,<sup>3</sup>  
A. Andrighetto,<sup>3</sup> M. Cinausero,<sup>3</sup> G. Prete,<sup>3</sup> Z. Majka,<sup>4</sup> and A. Wieloch<sup>4</sup>  
<sup>1</sup>*Dipartimento di Fisica dell'Università di Padova and INFN Sezione di Padova, Italy*  
<sup>2</sup>*Dipartimento di Fisica dell'Università di Brescia and INFN, Italy*  
<sup>3</sup>*INFN Laboratori Nazionali di Legnaro, Italy*  
<sup>4</sup>*Smoluchowski Institute of Physics, Jagiellonian University, Krakow, Poland*

The synthesis of superheavy elements (SHE) has been an important field in both theoretical and experimental nuclear physics for many years. Fusion of the doubly-magic neutron-rich  $^{48}\text{Ca}$  projectiles with transuranium target nuclei has led during the past 5 years to the synthesis of elements with  $Z = 113$ -116 and 118 [1]. The cross-sections involved are at the limit of the sensitivity achievable with the current technology. Our aim is to investigate possible alternative reactions to produce such elements. For example, one of the reactions might be one in which the fissile target nucleus (e.g.  $^{238}\text{U}$  and  $^{232}\text{Th}$ ) would fission as the projectile approaches and where one of the fragments would fuse with the projectile nucleus. The fission fragments being neutron-rich and close to shell closure, they should enhance the fusion and survival probabilities of the formed superheavy nucleus [2].

Experiments have been performed in 2003 and beginning of 2004 in collaboration with the Istituto Nazionale di Fisica Nucleare (INFN, Italy). The superconducting solenoid BigSol was used to collect the reaction products and to focus them towards a Bragg chamber, with a back plane covered with scintillators, at about 4 meters from the magnet. Two position-sensitive PPACs were placed before the Bragg chamber, allowing time of flight measurement and trajectory reconstruction. It was clear from these tests that a better rejection of the high cross-section products (elastics, quasi-elastics,...) had to be achieved.

The possibility of filling BigSol with gas was studied. Unfortunately, the expected mean charge state in gas of the energetic products we hope to observe doesn't allow for an efficient separation. On the other hand, the expected mean charge state in solids is expected to be much more favorable. An improved experimental setup was designed to take advantage of this: 9 foils of mylar ( $0.9\ \mu\text{m}$ ) were inserted throughout BigSol so that the ions would sample the charge state distribution at each passage through a foil, as they would in a gas, but with a more favorable mean charge state. Other improvements have also been implemented: an additional position-sensitive PPAC was inserted about 2 meters after the solenoid and a 16-segment PPAC was placed close to the target.

An experiment was performed with this setup during August 2004, using  $^{172}\text{Yb}$  (7.5, 10 and 15 A.MeV) beams on a  $^{232}\text{Th}$  target and a  $^{238}\text{U}$  (7.5 A.MeV) beam on Ti,  $^{64}\text{Zn}$ ,  $^{90}\text{Zr}$  and  $^{232}\text{Th}$  targets. The analysis of the data is still in progress. An example of data collected is shown on Figure 1.

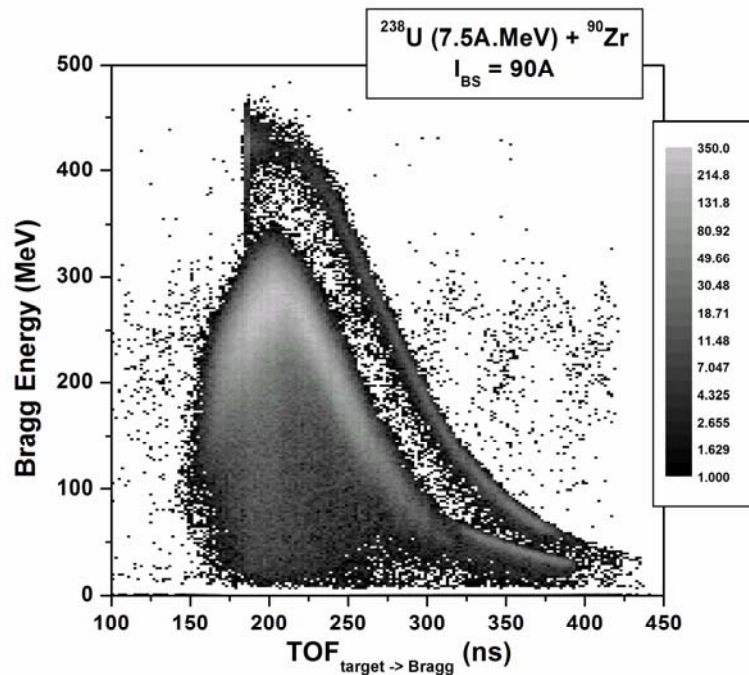


**Figure 1.** Charge collected in the Bragg chamber versus time of flight between the target and the entrance of the Bragg chamber for the reaction  $^{238}\text{U}(7.5\text{A.MeV}) + ^{90}\text{Zr}$ . The current in BigSol was 90A. Two groups of products appear on this figure: one with higher collected charge corresponds to beam-like ions (elastics, quasi-elastics, deep-inelastics, scattered beam,...), the other contains fission fragments from the projectile. A detailed analysis will be required to determine if other kinds of products are also observed.

At the same time as the setup was improved, the simulation and analysis codes were further developed to include the new features as well as to reflect the better understanding we gained of the particularities of our setup. For example, we use the Bragg chamber in an unconventional way such that the ions are not stopped in the gas cell but are allowed to reach the back plane where they are implanted in YAP scintillators. A nonlinear behavior is observed due to the way charge is collected close to anode. The process has been successfully understood and reproduced by the simulation. The improved simulation will allow for a better identification of the ions from the measured parameters.

- [1] Yu. Ts. Oganessian *et al.*, Phys. Rev. C **69**, R021601 (2004); Yu. Ts. Oganessian *et al.*, Nature **400**, 242(1999); Yu. Ts. Oganessian *et al.*, Scientific American **282**, 45 (Jan 2000); Yu. Ts. Oganessian *et al.*, Phys. Rev. C **63**, R011301 (2001); Yu. Ts. Oganessian, “JINR Preprint and Communications”, D7-202-287, Dubna, 2002.
- [2] Y. Aritomo, T. Wada, M. Ohta and Y. Abe, Phys. Rev. C **59**, 796 (1999).

## BRAHMS Results

K. Hagel, R. Wada, T. Materna, S. Kowalski, J. Natowitz and the BRAHMS Collaboration

BRAHMS increased the statistics of the Au+Au measurement at  $\sqrt{s_{mn}} = 200\text{GeV}$  substantially during RHIC Run-IV. In these high statistics measurements, we expect to be able to analyze forward high  $p_t$  data with good statistics as well as extend our measurements definitively to  $y = 4$ . The forward high  $p_t$  data was taken using high field runs with the spectrometer positioned at  $8^\circ$  and the  $y = 4$  data was obtained by positioning the spectrometer at  $2.3^\circ$ , an angle where it was not possible to obtain adequate statistics in the earlier runs due to beam time constraints.

During RHIC Run-V we performed measurements with Cu + Cu at  $\sqrt{s_{mn}} = 200\text{GeV}$  as well as at  $\sqrt{s_{mn}} = 63\text{GeV}$ . The data analysis for Run-V is in the beginning stages. Measurements using the proton beams in the coming period at the end of run V are expected to add to the data we already have to serve as a baseline measurement for heavy ion analyzes. In addition we plan to make a transverse polarization measurement. The infrastructure for the transverse polarization measurement has been developed over the last two p + p runs at RHIC and is now ready for production.

We also continued the analysis of the data from the earlier runs. This resulted in the publication of several papers including *Nuclear Stopping in Au+Au Collisions at  $\sqrt{s_{mn}} = 200\text{GeV}$*  [1], *Centrality dependence of charged-particle pseudorapidity distributions from d+Au collisions at  $\sqrt{s_{mn}} = 200\text{GeV}$*  [2], *On the evolution of the nuclear modification factors with rapidity and centrality in d+Au collisions at  $\sqrt{s_{mn}} = 200\text{GeV}$*  [3], *Charged Meson Rapidity Distributions in central Au+Au Collisions  $\sqrt{s_{mn}} = 200\text{GeV}$*  [4], *Forward and Midrapidity Like-particle Ratios from p+p Collisions at  $\sqrt{s_{mn}} = 200\text{GeV}$*  [5].

The TAMU group has continued the analysis of the p + p data. After completing the analysis paper on ratios p + p collisions[5], we have turned our full attention to generating spectra over a wide range in rapidity. These spectra are important as they serve as the baseline for the results of the heavy ion collisions. In addition, the p + p data are valuable in their own right because come from the first measurement of p+p data at this energy. Results from these measurements are expected to put constraints on pQCD models.

To generate the spectra, we have developed a method of making acceptance corrections on an event by event basis. This is an idealized geometrical acceptance correction, but requires much less computer time than the standard method of performing geant calculations and analyzing the model data in the same way as the real data. Of course, any idealized prescription must be checked by the results from a geant simulation. We compared the results for selected angles and field settings and found the agreement to be quite good. Other advantages to such a method include the fact that statistics from the acceptance correction are no longer an issue. The correction is more or less analytical. In addition, the differences in the acceptance correction due to the different vertices of each event are taken into account with no bin

size. All of these issues are directly related to the savings in computer time, but there is also an overall savings in bookkeeping.

Preliminary spectra from the MRS extracted using this method are shown in figure 1 for rapidities ranging from  $y \sim 0$  ( $\theta = 90^\circ$ ) to  $y \sim 1$  ( $\theta = 35^\circ$ ). Measurements from each angle setting are scaled by a relative factor of 10. The closed symbols represent results from Run-II and the open symbols at ( $\theta = 90^\circ$ ) and ( $\theta = 40^\circ$ ) represent results from Run-III for comparison. We note a fairly good agreement indicating that the correction factors for the different acceptances from the two runs are under control. The magenta open symbols in the bottom row (protons) show the results of an independent analysis which used the “traditional” method for making acceptance corrections. We show, likewise, good agreement adding confidence to this method of acceptance correction.

We are currently working on extracting spectra from the Forward Spectrometer (FS) in the same way. Once these spectra are finalized and the FS spectra generated, we expect them to be used as a basis for different analysis in the same spirit as the publications from the Au + Au data [1,4]. These data, when analyzed, will also provide new information as they are the first measurements of p+p at  $\sqrt{s_{nn}} = 200\text{GeV}$ .

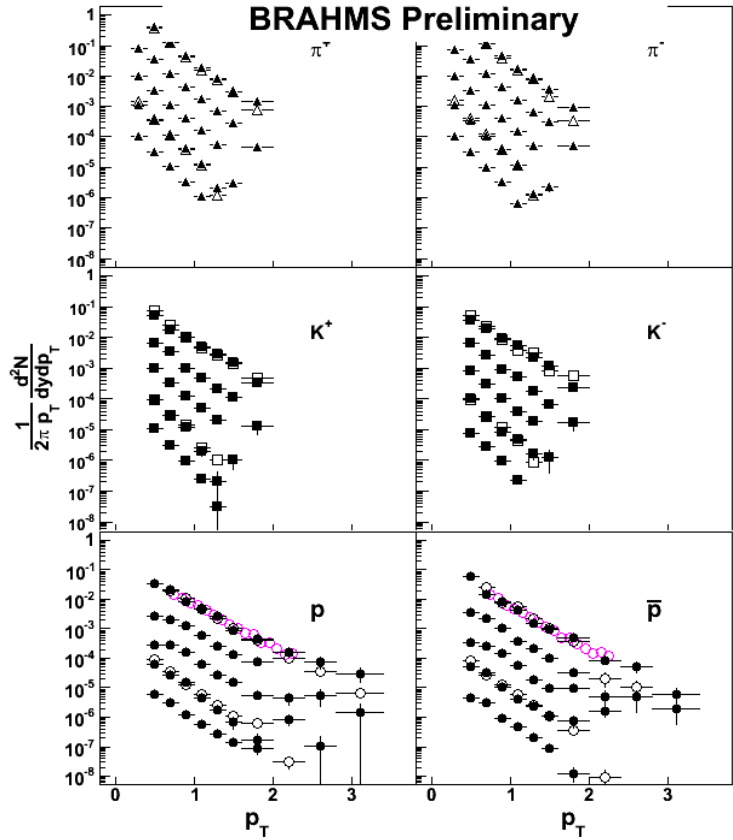


**Figure 1.** Transverse momentum spectra at different angle/field settings of the mid-rapidity spectrometer. Starting with the top distribution in each panel is  $y \sim 0$ ,  $y \sim 0.5$ ,  $y \sim 0.8$ ,  $y \sim 0.9$ ,  $y \sim 1.0$ . The open symbols represent a comparison of measurements taken in different runs. Each distribution for a different angle is divided by a successive factor of 10.

- [1] I. G. Bearden *et al.*, Phys. Rev. Lett. **93**, 102301 (2004).
- [2] I. Arsene *et al.*, Phys. Rev. Lett. **94**, 032301 (2005).
- [3] I. Arsene *et al.*, Phys. Rev. Lett. **93**, 242303 (2004).
- [4] I. G. Bearden *et al.*, Phys. Rev. Lett. **94**, 162301 (2005).
- [5] I. G. Bearden *et al.*, Phys. Lett. B **607**, 42 (2005).

## Density Dependence of the Symmetry Energy and the Equation of State of Isospin Asymmetric Nuclear Matter

D.V. Shetty, S.J. Yennello, and G.A. Souliotis

The density dependence of the nuclear symmetry energy is important for understanding the equation of state of systems as diverse as the atomic nuclei and neutron stars. The properties and the structure of these systems depend heavily on the exact form of the density dependence of the symmetry energy. Theoretical studies based on microscopic and phenomenological approaches predict widely different forms of the density dependence of the symmetry energy. The figure below (left) shows the isoscaling parameter  $\alpha$ , as a function of the fragment asymmetry studied in  $^{40}\text{Ar}$ ,  $^{40}\text{Ca}$ ,  $^{58}\text{Fe}$ ,  $^{58}\text{Ni} + ^{58}\text{Fe}$ ,  $^{58}\text{Ni}$  reactions at beam energies from 25 – 53 MeV/nucleon. The solid and the dotted lines are the predictions of the AMD calculations assuming a “soft” and “stiff” density dependence of the symmetry energy, respectively. As observed the experimental data are well explained by the stiff density dependence of the symmetry energy. The form of this dependence is shown in the figure

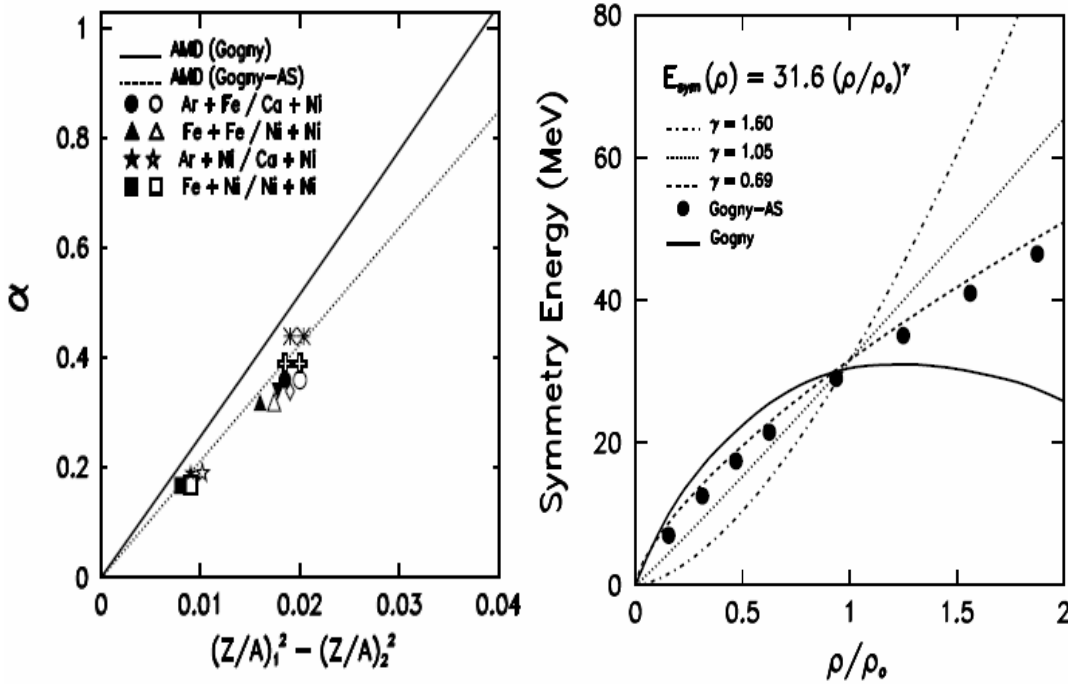


**Figure 1.** (Left) Scaling parameter as a function of beam energy. (Right) parameterization of the density dependence of the nuclear symmetry energy used in the analysis of the present measurements and the isospin diffusion measurements of NSCL-MSU.

(right) by the solid points, and can be parameterized as,  $E_{\text{sym}} = 31.6 (\rho/\rho_0)^{0.69}$ . This form of the dependence of symmetry energy is consistent with the parameterization adopted by Heiselberg and Hjorth-Jensen, in their work on neutron stars. By fitting predictions of the variational many-body calculations they obtained a value of  $E_{\text{sym}}(\rho_0) = 32$  MeV and  $\gamma = 0.6$ , similar to those obtained from

the present measurements. Recently, Chen *et al.* also reported a similar observation from their analysis of the MSU-NSCL isospin diffusion data. The dependence however, is observed to be somewhat stiffer at higher densities with respect to those observed from the present study. This is shown by the dotted curve in the figure and given as,  $E_{\text{sym}} = 31.6(\rho/\rho_0)^{1.05}$ .

Both measurements yield nearly similar results at low densities but are significantly different at higher densities. Given the fact that both measurements probe the low density part of the symmetry energy and are insensitive to the high density region, it appears that a best estimate of the density dependence of the symmetry energy that can be presently obtained is,  $E_{\text{sym}} = 31.6(\rho/\rho_0)^\gamma$ , where  $\gamma = 0.6 - 1.05$ .

[1] D.V. Shetty *et al.*, Phys. Rev. C **70**, 011601 (2004).

[2] L.W. Chen *et al.*, Phys.Rev. Lett. **94**, 032701 (2005).

## Symmetry Energy and the Influence of Neutron Composition and Excitation Energy in Nuclear Multifragmentation

D.V. Shetty, A.S. Botvina, S.J. Yennello, G.A. Souliotis, E. Bell, and A. Keksis

Hot nuclei are routinely produced in the interior of a collapsing star and its subsequent supernova explosion. The production of these nuclei depends strongly on their internal excitation and is sensitive to the symmetry energy part of the binding energy. A slight decrease in the symmetry energy coefficient and subsequent de-excitation can significantly alter the elemental abundance and the synthesis of heavy elements. In this work, we study the symmetry energy of the hot primary fragments produced in a multifragmentation reaction, and their dependence on the excitation energy and the isotopic compositions. The figure below (left) shows the fragment yield distribution for some of the elements produced in  $^{58}\text{Fe}$ ,  $^{58}\text{Ni} + ^{58}\text{Fe}$ ,  $^{58}\text{Ni}$  reactions at various beam energies. The figure on the right (top panel) shows the isoscaling parameter  $\alpha$  (solid points) obtained from the fragment yield distribution, as a function of the excitation energy of the

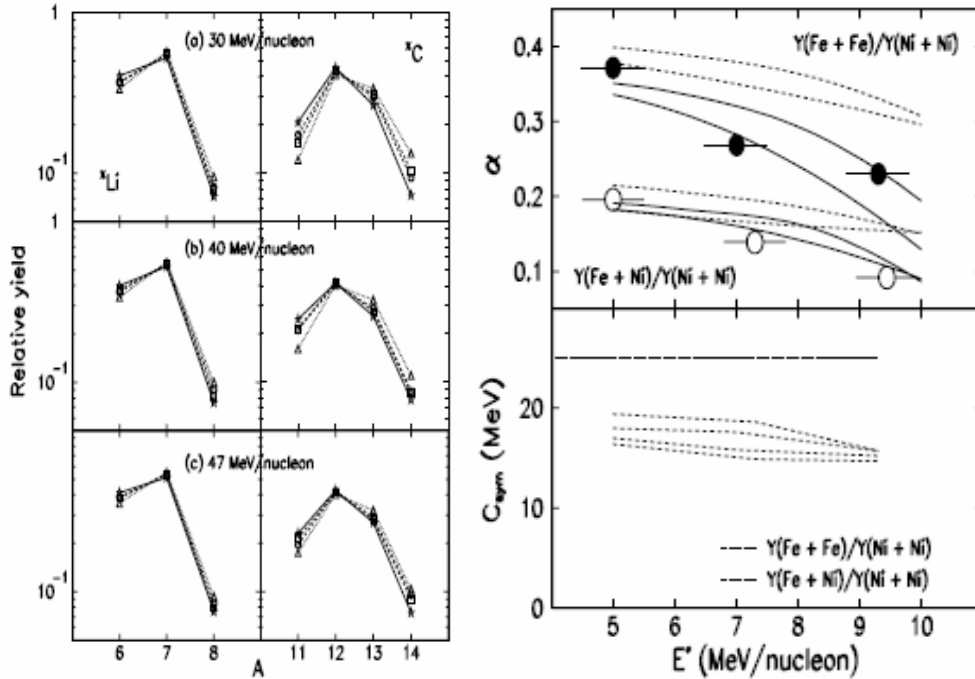


**Figure.** (Left) Relative yield distribution of the fragments for the lithium and carbon isotopes. (Right) Isoscaling parameter (top) and symmetry energy (bottom) as a function of the excitation energy of the fragmenting source.

fragmenting system. The values of the  $\alpha$ 's, from the Statistical Multifragmentation Model (SMM) calculation for the primary and the secondary fragments, are also shown in the figure by the

dotted and the solid curves, respectively. It is observed that the experimentally determined  $\alpha$ 's are well reproduced by the secondary fragment yields from the SMM calculations. The calculated values from the primary and the secondary fragments are not very different at lower excitation and  $\Delta N/Z$  of the fragmenting systems. However, they differ significantly with increasing excitation energy and the  $\Delta N/Z$  of the system. The symmetry energy deduced from the primary fragment  $\alpha$ 's (bottom panel) is significantly lower than the often-assumed value of 25 MeV from the ground state binding energy of stable nuclei. Furthermore, their magnitude decreases slowly with increasing excitation energy.

[1] D.V. Shetty *et al.*, Phys. Rev. C **71**, 024602 (2005).

## Production of Very Neutron-Rich Fragments in the Multifragmentation of Neutron-Rich Systems

G. A. Souliotis, D. V. Shetty, M. Veselsky, A. Botvina, A. Keksis, E. Bell,  
M. Jandel, and S. J. Yennello

The yield distributions of isotopically resolved projectile residues from semi-peripheral collisions of  $^{86}\text{Kr}$  (25MeV/nucleon),  $^{64}\text{Ni}$  (25MeV/nucleon) and  $^{136}\text{Xe}$  (20MeV/nucleon) beams on a variety of targets were studied in this work. The reactions of  $^{86}\text{Kr}$  with  $^{64,58}\text{Ni}$ ,  $^{124,112}\text{Sn}$  and  $^{208}\text{Pb}$  were studied with the MARS recoil separator of the Cyclotron Institute of Texas A&M University [1]. The reactions of  $^{64}\text{Ni}$  and  $^{136}\text{Xe}$  with  $^{64,58}\text{Ni}$  and  $^{124,112}\text{Sn}$ , as well as  $^{208}\text{Pb}$ ,  $^{232}\text{Th}$  were studied with the recently commissioned Superconducting Solenoid (BigSol) Line [2]. In this work, special attention is given to projectile residues, especially the most neutron-rich ones, produced at excitation energies near the multifragmentation threshold ( $\sim 2$  MeV/nucleon). Both the N/Z and the kinematical properties of the observed fragments are well described by a hybrid calculation involving a deep inelastic transfer model [3] for the dynamical stage of the collision and the statistical multifragmentation model (SMM) [4] for the de-excitation stage.

In the following figures, representative results for projectile fragment distributions from the  $^{86}\text{Kr}$  (25MeV/nucleon) +  $^{64}\text{Ni}$  reaction are presented. Calculated angular distributions (Fig.1), isobaric yield distributions (Fig. 2) and mass distributions of several elements (Fig. 3) are shown (see figure captions). The results of the other reactions are similar and their systematic analysis is still underway. Apart from a nuclear reaction standpoint, the observed production of very neutron-rich fragments also addresses the practical issue of the production of neutron-rich rare isotopes in multifragmentation reactions.

As an example of rare isotope production, we may consider  $^{28}\text{Ne}$  produced with cross section of  $\sim 1\mu\text{b}$  (Fig. 3). Assuming a beam of 20 pA of  $^{86}\text{Kr}$  (25 MeV/nucleon) impinging on a  $^{64}\text{Ni}$  (30 mg/cm<sup>2</sup>) target and a separator collection efficiency of  $\sim 30\%$ , a counting rate of  $\sim 1$  pps is expected. Such rates

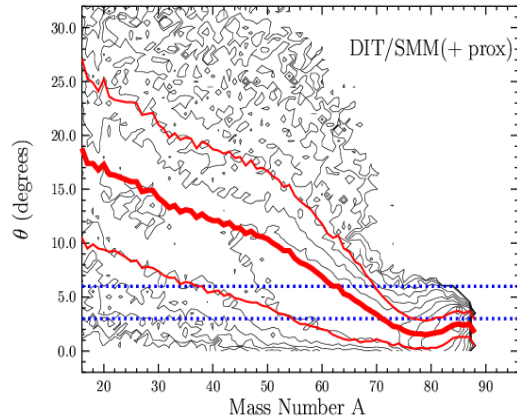


**Figure 1.** Example of calculated (DIT/SMM + target proximity effect) angular distribution of projectile fragments from  $^{86}\text{Kr}$  (25MeV/nucleon) +  $^{64}\text{Ni}$ . The yields are given by the contours (successive contours correspond to a decrease in yield by a factor of 2). Dotted (blue) lines indicate the angular acceptance of the MARS spectrometer for these measurements [1]. The thick (red) line represents the average emission angle for each mass, whereas the thin (red) lines are one standard deviation above and below the average. The large angular spread indicates that, for efficient collection of the multifragmentation products, a large acceptance separator,

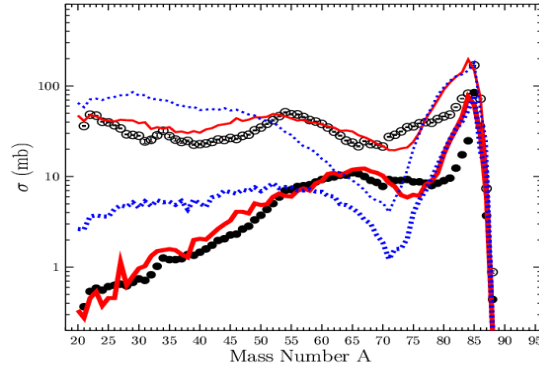


**Figure 2.** Isobaric yield distribution of projectile fragments from  $^{86}\text{Kr}$  (25MeV/nucleon) +  $^{64}\text{Ni}$ . Solid points: measured yields. Open points: total yields obtained from measured ones after correction for the spectrometer angular and momentum acceptance. Dotted (blue) lines: yield calculations from DIT/SMM without target proximity; thin line: total yield; thick line: yield filtered by the angle and magnetic rigidity acceptance of the spectrometer. Solid (red) lines: yield calculations from DIT/SMM with target proximity; thin line: total yield; thick line: filtered yield (as above).

suff  
ice for spectroscopic studies of such neutron-rich isotopes. Thus, multifragmentation may be considered as a new route, complementary to fragmentation (or fission), to access extremely neutron rich nuclei.

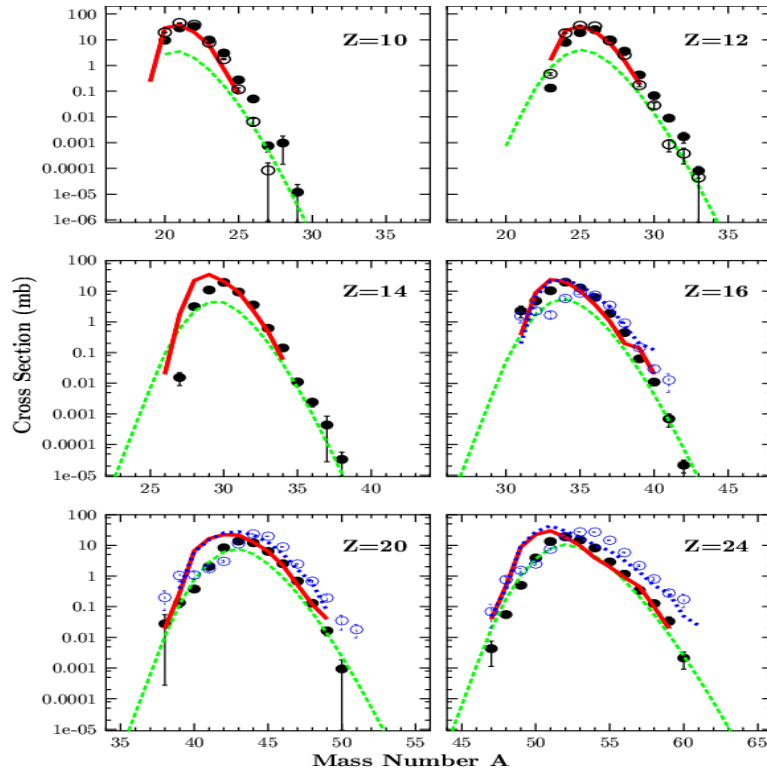


**Figure 3.** Representative results of mass distributions of several elements. Solid (black) points: data from  $^{86}\text{Kr}$  (25 MeV/nucleon) +  $^{64}\text{Ni}$ . Open points for  $Z=10,12$ : data from  $^{86}\text{Kr}$  (25 MeV/nucleon) +  $^{58}\text{Ni}$ . Open (blue) points for  $Z=16,20,24$ : data from  $^{86}\text{Kr}$  (25 MeV/nucleon) +  $^{208}\text{Pb}$ . Solid (red) line: DIT/SMM (with proximity) calculation for  $^{86}\text{Kr}$  +  $^{64}\text{Ni}$ . Dotted (blue) line: same calculation for  $^{86}\text{Kr}$  +  $^{208}\text{Pb}$ . Dashed (green) line: EPAX predictions [5] for  $^{86}\text{Kr}$  +  $^{64}\text{Ni}$ .

- [1] G.A. Souliotis *et al.*, Phys. Rev. Lett. **91**, 022701 (2003); Nucl. Instrum. Methods Phys. Rev. **B204**, 166 (2003).
- [2] G.A. Souliotis *et al.*, *Progress in Research*, Cyclotron Institute, Texas A&M University (2003-2004), p. II-26; *ibid* (2002-2003), p. V-5; *ibid* (2001-2002) p. V-19.
- [3] L. Tassan-Got and C. Stephan, Nucl. Phys. **A524**, 121 (1991).
- [4] A.S. Botvina *et al.*, Phys. Rev. C **65**, 044610 (2002), and references therein.
- [5] K. Summerer and B. Blank, Phys. Rev. C **61**, 034607 (2000).

## Apparent Critical Behavior in Fragmentation of Z=12-15 Quasi-Projectiles and Its Dependence on N/Z Degree of Freedom

M. Jandel, S. Wuenschel, S. J. Yennello, G. A. Souliotis, D. V. Shetty and A. Keksis

Data from the reaction  $^{28}\text{Si}+^{112}\text{Sn}$  at 50 MeV/nucleon [1] was used for analysis of the apparent critical behavior in the disassembly of quasi-projectiles with charge  $Z=12-15$ . Charge distributions were fitted using a power law function  $Z^{-\tau}$  in the region  $Z=2-7$ , for obtaining the critical exponent  $\tau$ . The dependence of  $\tau$  on the apparent excitation energy was obtained for different experimental N/Z bins ranging from  $N/Z = 0.7 - 1.2$  (Fig.1 left). Similarly, the second moment of the charge

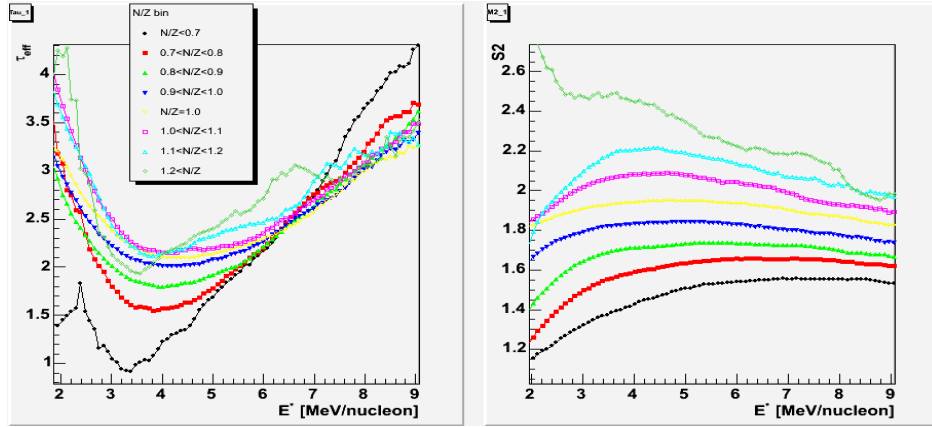


**Figure 1.** Fisher critical exponent  $\tau$  and second moment of the charge distribution  $S_2$ , as a function of the apparent excitation energy of quasi-projectiles ( $Z=12-15$ ). Different curves correspond to different N/Z bins.

distribution  $S_2 = \sum_{Z_i \neq Z_{\text{max}}} Z_i^2 n_i / \sum_{Z_i \neq Z_{\text{max}}} Z_i n_i$ , was obtained as a function of the apparent excitation energy

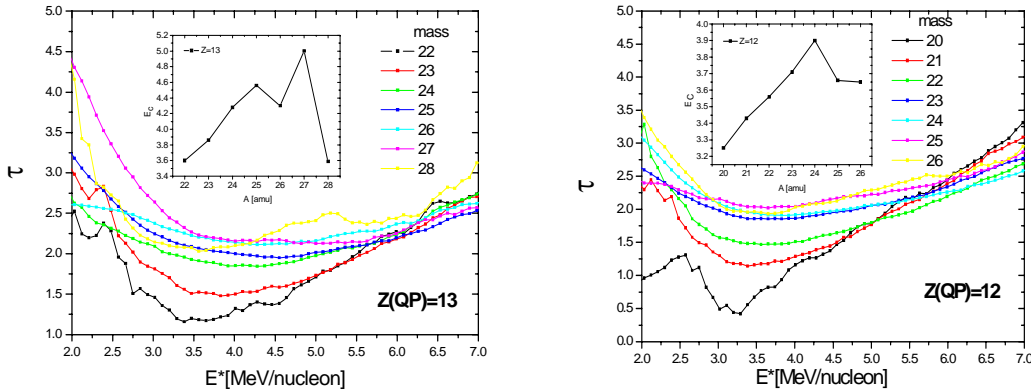


**Figure 2.**  $\tau$  as a function of excitation energy for fixed quasi-projectile charge and mass. Insets show the dependence of transition energy (where  $\tau$  reached the minimum)  $E_C$  on quasi-projectile mass for fixed charges, 12 and 13.

for the same  $N/Z$  bins (Fig.1, right). We observe a general trend of an increase in the transition energy  $E_C$  with increasing  $N/Z$  of the fragmenting system towards  $N/Z=1$  and decrease of  $E_C$  for  $N/Z>1$ . A more constrained analysis was also done by extraction the  $\tau$  values for specific charge and mass of the quasi-projectile. These are as shown in Fig. 2. A similar trend is observed in absolute values of  $\tau$  as in Fig.1 (left). Further analysis to asses the effects of secondary emission on the experimental charge distributions is underway.

[1] A. Laforest *et al.*, Phys. Rev. C **59**, 2567 (1999).

**Additional Tool for the Calibration of FAUST Si-CsI Telescopes Using Inelastic Reactions**  
 ${}^3\text{He}+{}^{13}\text{C}\rightarrow{}^{3,4}\text{He}+{}^{12,13}\text{C}$  at 25 MeV/nucleon

M. Jandel, R. Varner,<sup>1</sup> G. A. Souliotis, A. Keksis, B. Stein, S. Soisson, D. V. Shetty, E. Bell,  
 J. Iglío, S. Wuenschel, M. Sarahan, C. Richers, J. Garey and S. J. Yennello  
<sup>1</sup>Oak Ridge National Laboratory, Oak Ridge, Tennessee 37830

Multi-detector arrays like INDRA, CHIMERA, NIMROD, FAUST are built for detecting charged particles produced in intermediate energy heavy ion reactions. The energy calibration of these devices is an important issue in the analysis of data obtained from these arrays. Usually, radioactive alpha sources like  ${}^{212}\text{Th}$  are used for the calibration of Si detectors, which have a response that is linear to first approximation over a large range of charges that are detected. The response of the CsI detectors is however not linear, because the light output of the CsI crystal is dependent on mass and charge of detected particles. Various formulas for the light output have therefore been proposed and calibration of the CsI detectors has to be performed more carefully.

In this work, we propose measurement of  ${}^{3,4}\text{He}$  particles using inelastic reactions  ${}^3\text{He}+{}^{13}\text{C}\rightarrow{}^{3,4}\text{He}+{}^{12,13}\text{C}$  as a tool for accurate calibration of the CsI detectors.  ${}^{3,4}\text{He}$  particle spectra show peaks with energies corresponding to excited levels in  ${}^{12,13}\text{C}$  as shown in Fig 1 in  $\Delta E$ -E plot taken from one telescope in ring D of FAUST. Spectra of  ${}^3\text{He}$  particles are shown in Fig. 2. The energies of He particles can be found from kinematics calculations using for example LISA software. After calculations of losses in the material (SRIM2000), in our case mylar foils in front of each Si detector, and in the Si detector itself, one can precisely calculate the total energy of corresponding peaks in CsI spectra after subtracting the excitation energy of excited  ${}^{12,13}\text{C}$  states. In this manner, one can use exact calibration points for CsI detectors to assure the correctness of overall calibration procedure in heavy ion reactions.

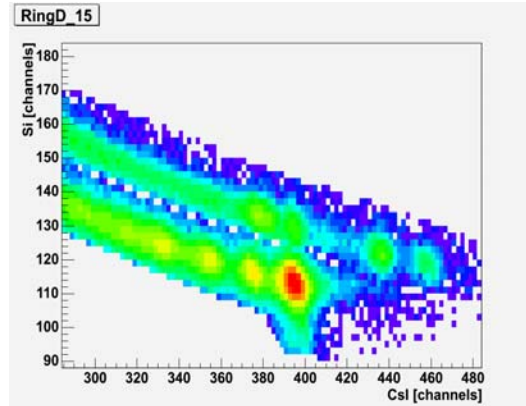


**Figure 1.**  $\Delta E$ -E spectra for  ${}^3\text{He}$  and  ${}^4\text{He}$  particles from  ${}^3\text{He}+{}^{13}\text{C}$  (25 MeV/nucleon) reaction. Structure in the spectra seen is due to excited states of  ${}^{13}\text{C}$  and  ${}^{12}\text{C}$

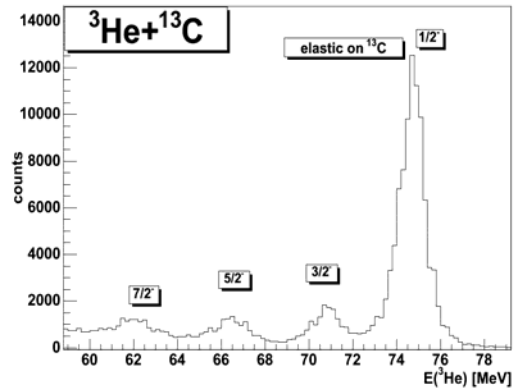


**Figure 2.** Energy spectrum of  ${}^3\text{He}$  particles. The evident domination of excited collective states is observed in inelastic scattering of  ${}^3\text{He}$  on  ${}^{13}\text{C}$ .

**$\gamma$ -ray Emission Characteristics in the Peripheral Reaction of  $^{36}\text{Ar}+^{197}\text{Au}$ ,  $^{\text{nat}}\text{Th}$   
at 25 and 45 MeV/nucleon**

M. Jandel, R. Varner,<sup>1</sup> G. A. Souliotis, A. Keksis, B. Stein, S. Soisson, D. V. Shetty, E. Bell,  
J. Igllo, S. Wuenschel, J. Garey, C. Richers and S. J. Yennello  
<sup>1</sup>*Oak Ridge National Laboratory, Oak Ridge, Tennessee 37830*

The ‘caloric curve’, a relation between the thermal excitation of an excited nucleus and its temperature can provide information on whether the nucleus undergoes a phase transition. The “thermometers” that are used to construct the caloric curve are often based on three different approaches: the slopes of the kinetic energy spectra of the light particles, the double isotope ratio of the isotopes, and the relative population of the excited states. In this work, we propose to exploit gamma-rays as a thermometer for studying the caloric curve. Additionally, the weak electromagnetic interaction of gamma-rays with surroundings provides an important tool for probing the space-time evolution of colliding nuclei.

We carried out an experiment where the information on gamma-rays and charge particles was collected using ORNL-MSU-TAMU BaF<sub>2</sub> array (150 BaF detectors for gamma-ray detection) and 48 Si-CsI FAUST telescopes (for charged particles detection). We intend to derive mean multiplicities and mean energies of gamma-rays as a function of reaction (possible N/Z effect, beam energy); excitation energy and Z, A of quasi-projectile. Gamma-rays are part of the cooling mechanism and especially dipole giant resonances with high energy of gamma-rays can effect the caloric curve construction. Special interest in this way will be paid to the region of  $E^*=4-7$  MeV/nucleon of quasi-projectile, where the phase transition in question may be seen. In addition, the charged particle data will be analyzed to study the Coulomb proximity effect. Analysis of the complex multi-parameter data is underway.

## Using Light Cluster Production to Determine the Density Dependence of Nuclear Symmetry Energy

S. N. Soisson, E. Bell, L. W. Chen, S. J. Yennello and the NIMROD Collaboration

The multiplicities and the energy spectra of light clusters have been shown to be sensitive to the density dependence of the nuclear symmetry energy but not to the isospin-independent part of the nuclear equation of state or the in-medium nucleon-nucleon cross sections using an iBUU-coalescence model [1, 2]. One of the more sensitive probes for the density dependence of the nuclear symmetry energy has been the ratio of triton to  ${}^3\text{He}$  energy spectra. These spectra and subsequent ratios have been measured experimentally for systems of  ${}^{58}\text{Ni} + {}^{58}\text{Ni}$  and  ${}^{58}\text{Fe} + {}^{58}\text{Fe}$  at 45 MeV/A from NIMROD. The iBUU-coalescence model has been run for both momentum-dependent and momentum-independent collisions with a hard ( $x = -2$ ) and soft ( $x = 1$ ) equation-of-state at an impact parameter of  $b = 4$ . The experimental results have been compared directly to these calculations.

We have shown that the measured triton to  ${}^3\text{He}$  ratio shows no significant dependence on centrality. By doing direct comparisons of the ratios of the  ${}^{58}\text{Ni} + {}^{58}\text{Ni}$  and  ${}^{58}\text{Fe} + {}^{58}\text{Fe}$  systems, we see an increase in the ratio by a factor of approximately 2 for the neutron-rich system (Figure 1, Left). However, as seen in Figure 1 (Right), the iBUU-coalescence model does not reproduce the measured ratio for either system, particularly at low kinetic energies, regardless of the equation-of-state parameters used. By taking the double ratio of  $(t/{}^3\text{He})_{\text{FeFe}} / (t/{}^3\text{He})_{\text{NiNi}}$ , the iBUU-coalescence model predictions have the same dependence on the particle kinetic energy as the experimental data but do not match the absolute value.

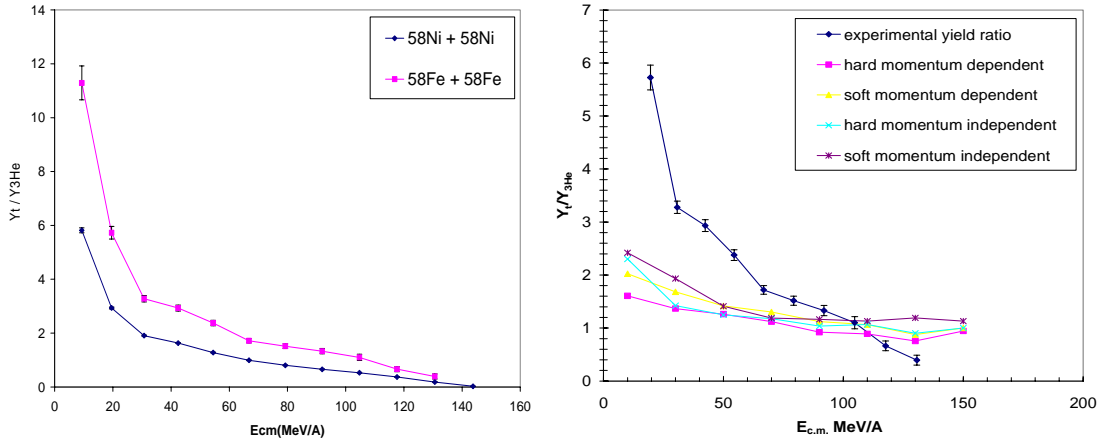


**Figure 1.** (Left) Comparison of the isobaric yield ratios. The pink (upper) line represents the  ${}^{58}\text{Fe} + {}^{58}\text{Fe}$  system and the blue (lower) line represents the  ${}^{58}\text{Ni} + {}^{58}\text{Ni}$  system. (Right). Comparison of the isobaric yield ratio of the  ${}^{58}\text{Fe} + {}^{58}\text{Fe}$  system to the iBUU-coalescence calculations at different equation of state parameters.

- [1] Lie-Wen Chen, C. M. Ko, Bao-An Li, Phys. Rev. C **68**, 017601 (2003).
- [2] Lie-Wen Chen, C. M. Ko, Bao-An Li, Nucl. Phys. **A729**, 809 (2003).
- [3] Lie-Wen Chen, C. M. Ko, Bao-An Li, Phys. Rev. C **69**, 054606 (2004).

## (N/Z) Equilibration

E. Bell, J. Garey, K. Hagel, D. Shetty, S. Soisson, R. Wada, S. J. Yennello,  
and the NIMROD Collaboration

NIMROD, or the Neutron Ion Multi-detector for Reaction Oriented Dynamics [1], was used to examine the reactions of 35 and 45 MeV/nucleon  $^{58}\text{Fe}$  and  $^{58}\text{Ni}$  on  $^{58}\text{Fe}$  and  $^{58}\text{Ni}$  in order to study (N/Z) equilibration. The beams were produced by the K500 Superconducting Cyclotron at the Cyclotron Institute of Texas A&M.

Isotope and isobar ratios are being used to investigate (N/Z) equilibration [2]. Seen in Figure 1 are  $t^3\text{He}$  isobar yield ratios plotted as a function of the combined systems' N/Z content for the 10% most central events at a lab angle of 40 degrees. The  $t^3\text{He}$  ratios show a lack of N/Z equilibration at both energies, but more so at 35 MeV/nucleon.

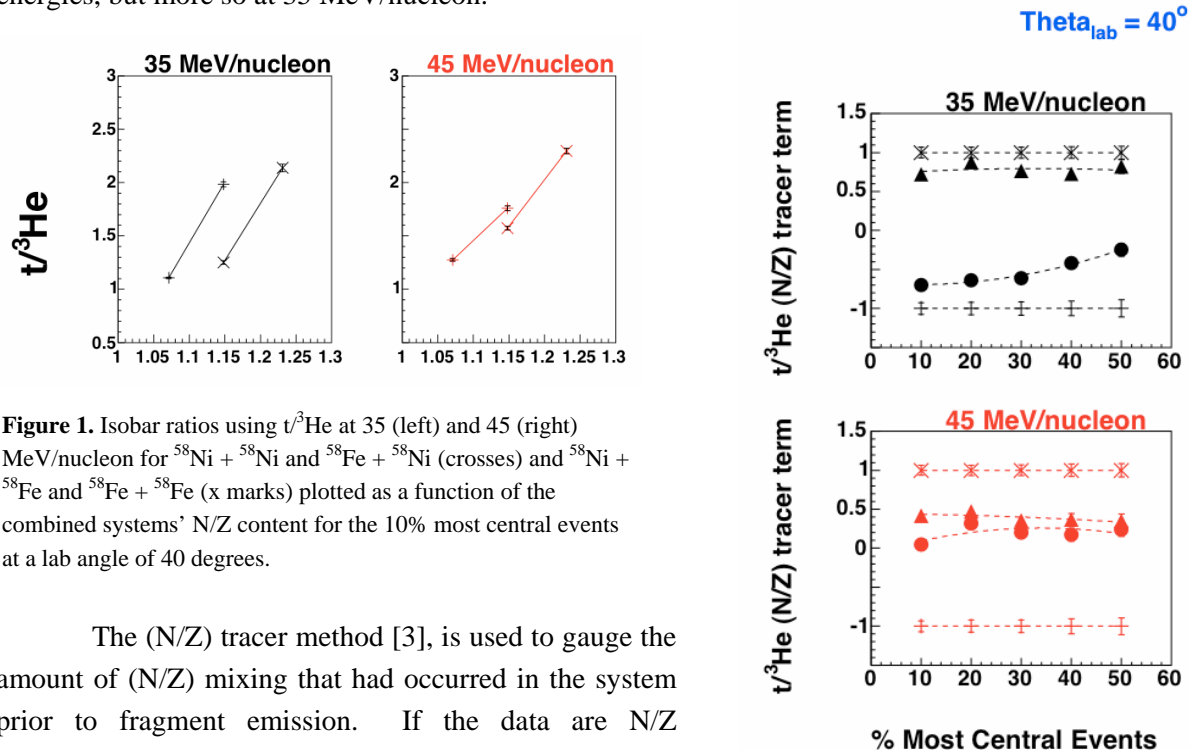


**Figure 1.** Isobar ratios using  $t^3\text{He}$  at 35 (left) and 45 (right) MeV/nucleon for  $^{58}\text{Ni} + ^{58}\text{Ni}$  and  $^{58}\text{Fe} + ^{58}\text{Ni}$  (crosses) and  $^{58}\text{Ni} + ^{58}\text{Fe}$  and  $^{58}\text{Fe} + ^{58}\text{Fe}$  (x marks) plotted as a function of the combined systems' N/Z content for the 10% most central events at a lab angle of 40 degrees.

The (N/Z) tracer method [3], is used to gauge the amount of (N/Z) mixing that had occurred in the system prior to fragment emission. If the data are N/Z equilibrated, the N/Z tracer term takes on a value of zero. In Figure 2, the N/Z tracer terms using  $t^3\text{He}$  are shown at a lab angle of 40 degrees. Again, the 35 MeV/nucleon data are less equilibrated than the 45 MeV/nucleon data.

**Figure 2.** N/Z tracer term using the  $t^3\text{He}$  ratio for  $^{58}\text{Fe} + ^{58}\text{Fe}$  (x),  $^{58}\text{Fe} + ^{58}\text{Ni}$  (triangles),  $^{58}\text{Ni} + ^{58}\text{Fe}$  (circles), and  $^{58}\text{Fe} + ^{58}\text{Fe}$  (crosses) at 35 (top) and 45 (bottom) MeV/nucleon.

[1] N. Marie *et al.*, *Progress in Research*, Cyclotron Institute, Texas A&M University (1997-1998), p. V-19; R. Wada *et al.*, *Progress in Research*, Cyclotron Institute, Texas A&M University (1998-1999), p. V-15; T. Keutgen *et al.*, *Progress in Research*, Cyclotron Institute, Texas A&M University (1999-2000), p. V-11.

[2] H. Johnston, *et al.*, *Phys. Lett. B* **371** 186 (1996); H. Johnston, *et al.*, *Phys. Rev. C* **56**, 1972 (1997).

[3] F. Rami, *et al.*, *Phys. Rev. Lett.* **84**, 1120 (2000).

## Angular Distributions of Fragments from the Reaction 32 MeV/u $^{48}\text{Ca}$ on $^{112}\text{Sn}$

A. L. Keksis, M. Veselsky, G. A. Souliotis, E. Bell, M. Jandel, A. Ruangma, D. Shetty,  
E. M. Winchester and S. J. Yennello

FAUST, the Forward Array Using Silicon Technology [1], was used to collect fragments from quasiprojectile fragmentation reaction  $^{48}\text{Ca}$  on  $^{112}\text{Sn}$  at 32 MeV/nucleon. See [2-4] for details on calibrations, gating, analysis and information on other systems. Recently the isotopic yields have been extracted. In figure 1, the angular dependence of a single isotope from each element Hydrogen to Carbon is shown. The yields from each angle have been scaled for comparison between angles.

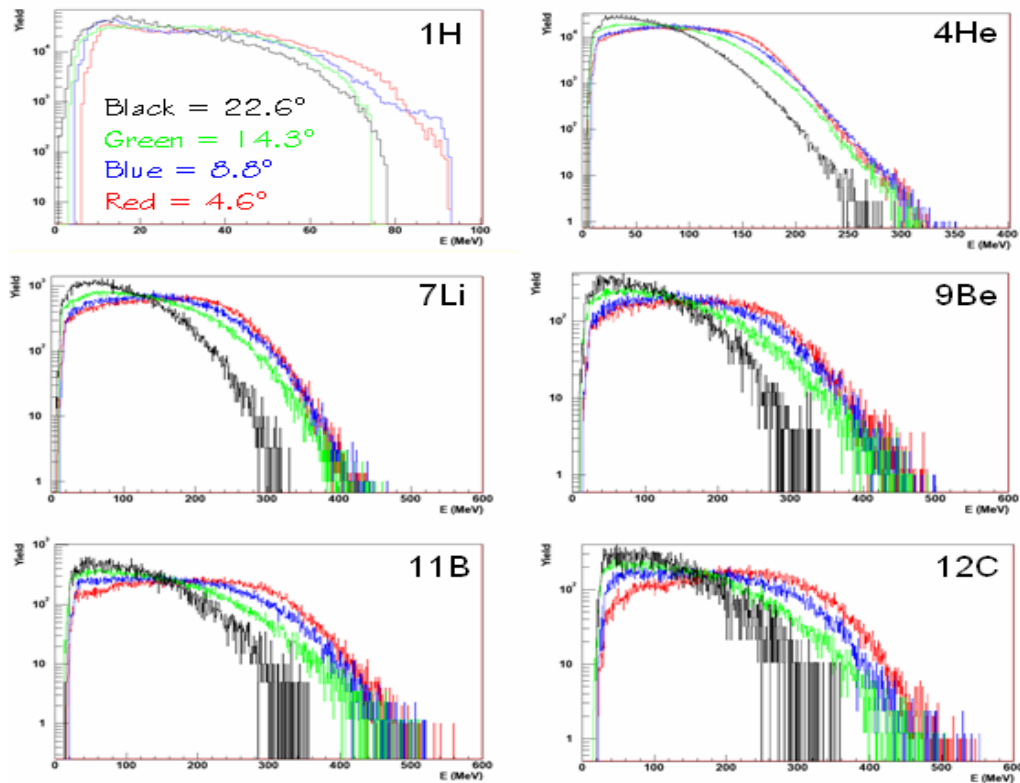


**Figure 1.** The yield versus excitation energy of a specific isotope of hydrogen to carbon as a function of angle.

The Figure 1 shows that the peak of the distribution shifts from near beam energy (32MeV/nucleon) towards lower energy, with increasing angle, for each nuclide. This is expected since the smaller angles will have more earlier emitted fragments moving close to beam velocity, while larger angles capture later emitted fragments.

[1] F. Gimeno-Nogues *et al.*, Nucl. Instrum. Methods Phys. Res. **A399**, 94 (1997).

- [2] A.L. Keksis *et al.*, *Progress in Research*, Cyclotron Institute, Texas A&M University (2001-2002), p.II-38.
- [3] A.L. Keksis *et al.*, *Progress in Research*, Cyclotron Institute, Texas A&M University (2002-2003), p.II-11.
- [4] A.L. Keksis *et al.*, *Progress in Research*, Cyclotron Institute, Texas A&M University (2003-2004), p.II-23.

## Forward Indiana Ring Silicon Telescope (FIRST): An Array for the Study of Peripheral Heavy-Ion Collisions at Intermediate Energies

T. Padaszynski,<sup>1</sup> P. Sprunger,<sup>1</sup> R. T. de Souza,<sup>1</sup> S. Hudan,<sup>1</sup> A. Alexander,<sup>2</sup> B. Davin,<sup>1</sup> G. Fleener,<sup>2</sup> A. Mcintosh,<sup>1</sup> C. Metelko,<sup>1</sup> R. Moore,<sup>2</sup> N. Peters,<sup>1</sup> J. Poehlman,<sup>2</sup> J. Gauthier,<sup>3</sup> F. Grenier,<sup>3</sup> R. Roy,<sup>3</sup> D. Theriault,<sup>3</sup> E. Bell, J. Garey, J. Igljo, A. L. Keksis, S. Parketon, C. Richers, D. V. Shetty, S. N. Soisson, G. A. Soulioutis, B. Stein, and S. J. Yennello

<sup>1</sup> *Department of Chemistry and Indiana University Cyclotron Facility,  
Indiana University, Bloomington, IN 47405*

<sup>2</sup> *Department of Chemistry, Indiana University, Bloomington IN 47405*

<sup>3</sup> *Departement de Physique, Universite Laval, Quebec, Canada*

The Forward Indiana Ring Silicon Telescope (FIRST) is a segmented charged particle detector array that was designed to study peripheral and mid-central heavy-ion collisions at intermediate energies ( $E/A \sim 50$  MeV). It was commissioned in an experiment at the Cyclotron Institute, Texas A&M University in 2003. FIRST consists of three annular Si(IP)-CsI(Tl) telescopes (designated T1, T2, and T3) with good segmentation in polar angle (80 segments in  $2^\circ \leq \theta_{\text{lab}} \leq 28^\circ$ ) and moderate segmentation in azimuth (16 segments in  $0^\circ \leq \phi_{\text{lab}} \leq 360^\circ$ ) provided by the Si(IP) detectors. The  $\Delta E$ -E technique was used to identify particles with good isotopic resolution up to Al ( $Z=13$ ). To achieve this isotopic identification [2], it was necessary to correct for thickness variations in the  $\Delta E$  detector. The phenomenon of charge splitting between adjacent segments, due to limited inter-strip isolation, was investigated by examining the energy signal obtained from adjacent rings in the detector. As FIRST is intended to identify multiple particles incident on a single telescope, it is important to be able to resolve multiple particles that are incident on a single pie. By cross-comparing the energy signals of rings and pies, it was possible to distinguish coincidence summing due to multiple particles in the same pie from charge splitting. Once the identity of each particle has been determined, its angle and energy are assigned. We have determined that the PID resolution for the case of multiple particles incident on the same pie is only slightly worse than if only one particle is incident on an individual pie.

Two independent approaches were used to calibrate the CsI(Tl) detectors. The first method was to have accelerated low-intensity beams of  $^4\text{He}$ ,  $^{12}\text{C}$ ,  $^{16}\text{O}$ , and  $^{20}\text{Ne}$  at  $E/A=24.95$  and  $59.9$  MeV directly incident on the detectors. Additional calibration points were provided by further degrading these beams using known thickness aluminum degraders. In addition to the direct beams at the end of the experiment, we also utilized data acquired during the experiment to provide calibration points for the CsI(Tl) detectors [3]. In this second approach, we selected discrete points in the  $\Delta E$ -E map, and used the measured energy loss in the Si detectors, the  $Z$  and  $A$  of the identified ion, together with the determined Si detector thickness to calculate the energy deposited into the CsI(Tl) crystal.

Preliminary analysis of the experimental data has yielded the charged particle multiplicity distribution for the reaction  $^{64}\text{Zn}+^{64}\text{Zn}$  at  $E/A=45$  MeV. This distribution is the measured distribution for all identified particles. The total charged particle multiplicity in FIRST has an average value of 2.8 and a maximum of 12 as indicated by this distribution. In the case of T3, the maximum observed multiplicity of

9 would correspond to more than 50% occupancy. However, comparison for  $N_c=9$  to  $N_c=1$  in T3 reveals that the relative probability for  $N_c=9$  occurs at approximately the  $10^{-6}$  level. Hence, the granularity of FIRST is more than acceptable for the investigation of peripheral heavy ion collisions.

In order to compare the experimental data with the predictions of theoretical models, a detector filter has been constructed for FIRST. This filter is a software representation of the actual detector system and accounts for the geometrical efficiency of the array.

- [1] T. Padaszynski *et al.*, Nucl. Instrum. Methods Phys. Res. A (in press).
- [2] B. Davin *et al.*, Nucl. Instrum. Methods Phys. Res. **A473**, 301 (2001).
- [3] TRIM, J.F. Ziegler, <http://www.research.ibm.com/ionbeams/home/htm>.
- [4] M. Parlog *et al.*, Nucl. Instrum. Methods Phys. Res. **A482**, 693 (2002).

## Probing the Density Dependence of the Nuclear Symmetry Energy via Heavy Residue Isoscaling

G.A. Souliotis, D.V. Shetty, A. Keksis, E. Bell, M. Jandel, M. Veselsky and S.J. Yennello

The isoscaling properties of isotopically resolved projectile residues from peripheral collisions of  $^{86}\text{Kr}$  (25MeV/nucleon),  $^{64}\text{Ni}$  (25MeV/nucleon) and  $^{136}\text{Xe}$  (20MeV/nucleon) beams on various target pairs were employed to probe the symmetry energy term of the nuclear binding energy.

The reactions of  $^{86}\text{Kr}$  with  $^{64,58}\text{Ni}$  and  $^{124,112}\text{Sn}$  were previously studied with the MARS recoil separator [1]. The reactions of  $^{64}\text{Ni}$  and  $^{136}\text{Xe}$  with  $^{64,58}\text{Ni}$  and  $^{124,112}\text{Sn}$ , as well as heavier targets ( $^{197}\text{Au}$ ,  $^{208}\text{Pb}$ ,  $^{232}\text{Th}$ ) were studied with the Superconducting Solenoid Line (BigSol) [2] and their analysis was completed recently. In the present isoscaling study, special attention is given to heavy projectile fragments produced in peripheral and semiperipheral collisions near the onset of multifragment emission ( $E^*/A = 2\text{-}3$  MeV). For these fragments, the measured average velocities are used to extract excitation energies. The excitation energies, in turn, are used to estimate the temperatures and densities of the fragmenting quasiprojectiles within an expanding correlated Fermi gas model [3]. The isoscaling analysis of the fragment yields provided the isoscaling parameters  $\alpha$  (Fig. 1) which, in combination with isospin asymmetries and temperatures, provided the values of the nuclear symmetry energy. In this analysis, the following formula was employed [4]:  $\alpha = 4C_{\text{sym}}/T [(Z/A)_1^2 - (Z/A)_2^2]$  in which  $Z/A$  is the isotopic composition of each system 1, 2 of each reaction pair and  $T$  the temperature. The extracted values of the symmetry energy (Fig. 2c) at this excitation energy range (2-3 MeV/nucleon) are lower than the value  $C_{\text{sym},0} \sim 23$  MeV corresponding to ground-state nuclei in agreement with recent works [5,6]. In addition, as expected, and as suggested by the calculation, the density of the fragmenting quasiprojectiles is reduced compared to the normal nuclear density (Fig. 2d).

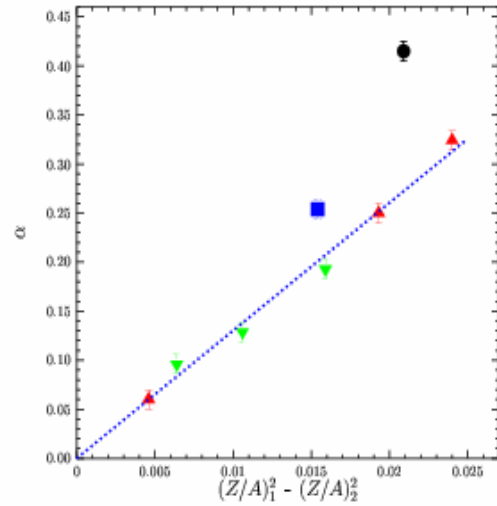


**Figure 1.** Isoscaling parameter  $\alpha$  as a function of  $(Z/A)_1^2 - (Z/A)_2^2$  for each reaction pair studied in this work. Circle:  $^{86}\text{Kr} + ^{124,112}\text{Sn}$ . Square:  $^{86}\text{Kr} + ^{64,58}\text{Ni}$ . Upright triangles:  $^{64}\text{Ni} + ^{124,112}\text{Sn}$ ,  $^{64,58}\text{Ni}$ ,  $^{232}\text{Th}-^{208}\text{Pb}$ , respectively in decreasing values of  $\alpha$ . Inverted triangles:  $^{136}\text{Xe} + ^{124,112}\text{Sn}$ ,  $^{64,58}\text{Ni}$ ,  $^{232}\text{Th}-^{197}\text{Au}$ , respectively, in decreasing values of  $\alpha$ . The line indicates the linear relationship in the  $^{64}\text{Ni}$  points.

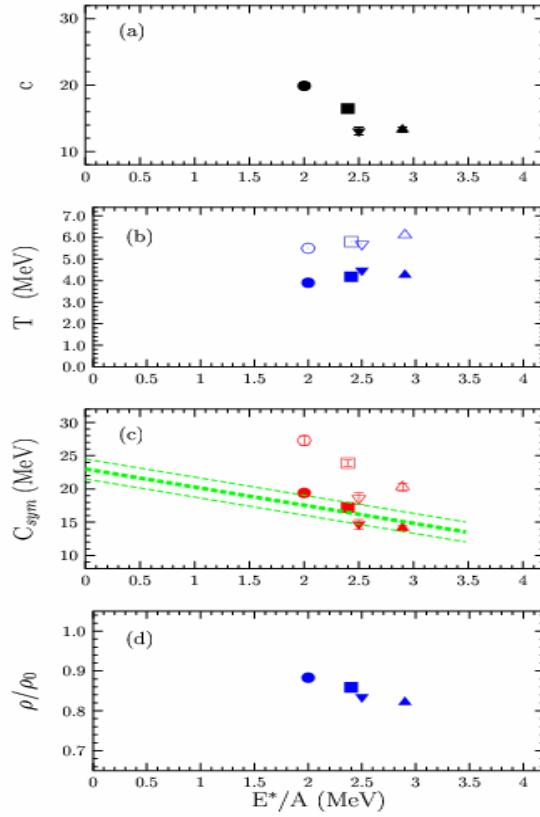


**Figure 2.** (a) Reduced isoscaling parameter  $c \equiv \alpha [(Z/A)_1^2 - (Z/A)_2^2]$  as a function of the excitation energy per nucleon  $E^*/A$  (MeV). Symbols as before. (b) Temperature as a function of  $E^*/A$ . Open symbols: Fermi gas. Closed symbols: expanding mononucleus model [3]. Symbol types as before. (c) Symmetry energy  $C_{sym}$  of the nuclear binding energy as a function of  $E^*/A$ .  $C_{sym} = c T / 4$ . The open and closed symbols correspond to the two estimates of the temperature as in (b). The symbol types correspond to the reaction systems as before. The lines indicate the decrease of  $C_{sym}$  with respect to the ground state value. (d) Calculated density; symbols as before.

- [1] G. A. Souliotis *et al.*, Phys. Rev. C **68**, 024605 (2003).
- [2] G.A. Souliotis *et al.*, *Progress in Research*, Cyclotron Institute, Texas A&M University (2003-2004), p. II-25
- [3] L.G. Sobotka *et al.*, Phys. Rev. Lett. **93**, 132702 (2004).
- [4] A.S. Botvina *et al.*, Phys. Rev. C **65**, 044610 (2002).
- [5] D.V. Shetty *et al.*, Phys. Rev. C **71**, 024602 (2005).
- [6] A. LeFevre *et al.*, Phys. Rev. Lett. **94**, 162701 (2005).

## p-A, A-A Collisions with NIMROD

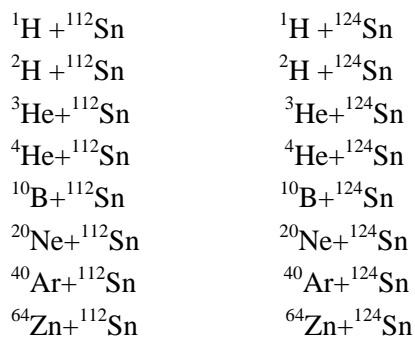
L. J. Qin, R. Wada, K. Hagel, J. S. Wang, T. Keutgen, S. Kowalski, Y. Ma, M. Murray, A. Makeev, P. Smith, J. B. Natowitz, J. Cibor, C. Hamilton, E. Bell, S. Liddick, D. Rowland, A. Ruangma, M. Veselsky, E. Winchester, G. A. Souliotis, S. J. Yennello, A. Samant,<sup>1</sup> M. Cinausero,<sup>1</sup> D. Fabris,<sup>1</sup> E. Fioretto,<sup>1</sup> M. Lunardon,<sup>1</sup> G. Nebbia,<sup>1</sup> G. Prete,<sup>1</sup> G. Viesti,<sup>1</sup> Z. Majka,<sup>2</sup> P. Staszal,<sup>2</sup> W. Zipper,<sup>3</sup> M. E. Brandan,<sup>4</sup> A. Martinez-Rocha,<sup>4</sup> A. Menchaca-Rocha,<sup>4</sup> and Y. El Masri<sup>5</sup>

<sup>1</sup>*INFN-Legnaro, Padova, Italy, <sup>2</sup>Jagiellonian University, Krakow, Poland,*

<sup>3</sup>*Institute of Physics Silesia University, Katowice, Poland, <sup>4</sup>IFUNAM, Mexico,*

<sup>5</sup>*UCL, Louvain-la-Neuve, Belgium*

In recent years, investigation of the dynamics of a large series of heavy ion collisions indicates that much of the early particle emission may be attributed to nucleon-nucleon collisions occurring during the thermalization stage of the reaction. In order to better characterize the early stage emission we have carried out a series of experiments in which the reactions of  $^{112}\text{Sn}$  and  $^{124}\text{Sn}$  with a wide range of projectiles, ranging from p to  $^{64}\text{Zn}$ , all at the same energy, 47 AMeV, were studied. The systems studied includes:



By careful comparisons of the yields, spectra and angular distributions observed for these different systems we expect to be able to cleanly separate emission resulting from early non-equilibrium emission from that resulting from the thermalized system and obtain a much cleaner picture of the dynamic evolution of the hotter systems. Guided by QMD calculations, information on the symmetry potential of the mean field can be extracted. In this series of experiment, we expect to reach different densities in different collisions together with different N/Z ratios. Isospin dependent effects on NN cross sections are expected to be extracted, which can be compared with IQMD model results [1][2][3].

In our data analysis, Self-consistent coalescence model analyses are to be applied to the light cluster yields in an attempt to probe emitter source sizes and to follow the evolution of the temperatures and densities from the time of first particle emission to equilibration. A common technique i.e Three Source Fitting is used to characterize the light particle emission in this energy range. This assumes a projectile like fragment (PLF) source, an intermediate velocity (NN) source, and a target like fragment (TLF) source and provides us a schematic picture of the emission process and estimation of the multiplicities and energy emitted at each stage of the reaction [4].

The calibration of CsI detector has been completed for all light particles . Light particle angular distributions for each system have been generated , Results for a typical system are shown in Figure 1 for  ${}^4\text{He}$  and  ${}^1\text{H}$ .

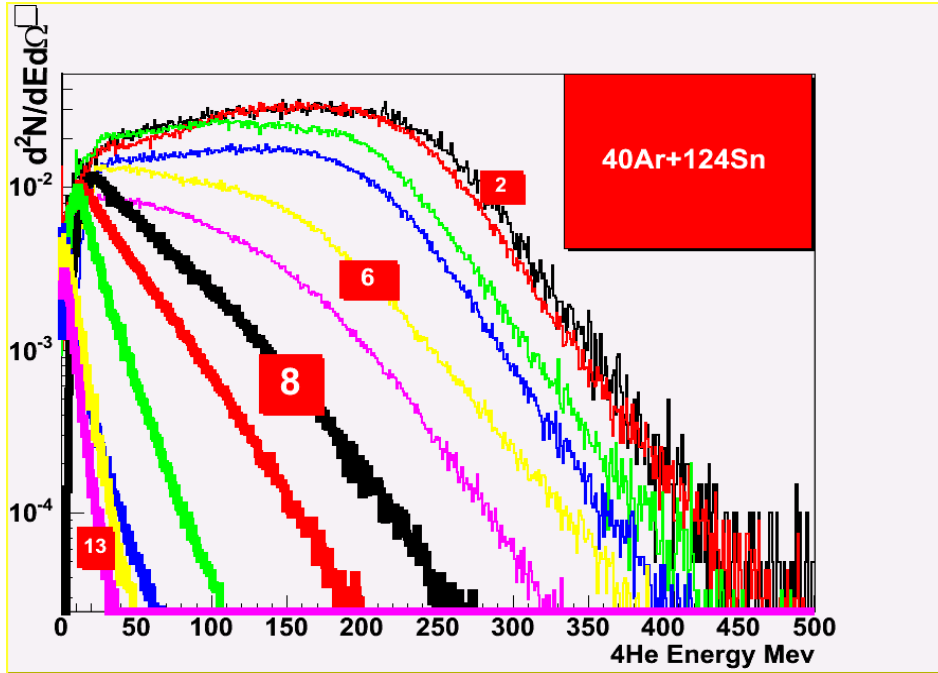


**Figure 1a.** Angular Distribution of  ${}^4\text{He}$  Yields  ${}^{40}\text{Ar}+{}^{124}\text{Sn}$ . Numbers indicate rings in NIMROD detector. Ring 2 is the most forward ring. Ring 13 is the most backward ring.

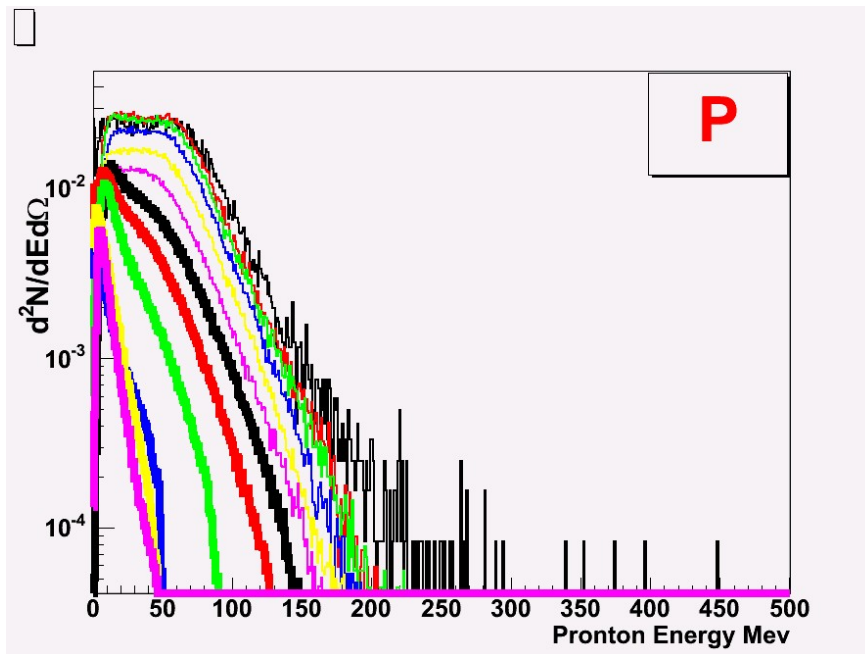


**Figure 1b.** Angular Distribution of  ${}^1\text{H}$  Yields  ${}^{40}\text{Ar}+{}^{124}\text{Sn}$ .

In a first approach, we have selected the most violent events by taking into account only the 30% largest Transverse Energy. Figure 2 shows the correlation of total charged particles plus neutron multiplicity measured with Nimrod which corresponds to the events selected for Figure 1. as a function of the transverse energy of light particles. The low transverse energy region can be associated with a larger impact parameters and the high transverse energy region with the high excitation energies and smaller impact parameters which are generally more central events.

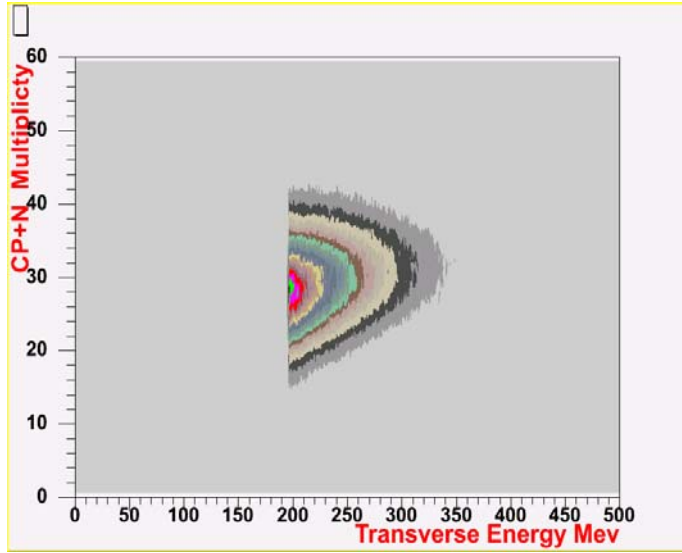


Figure 2. Event selections with transverse energy.

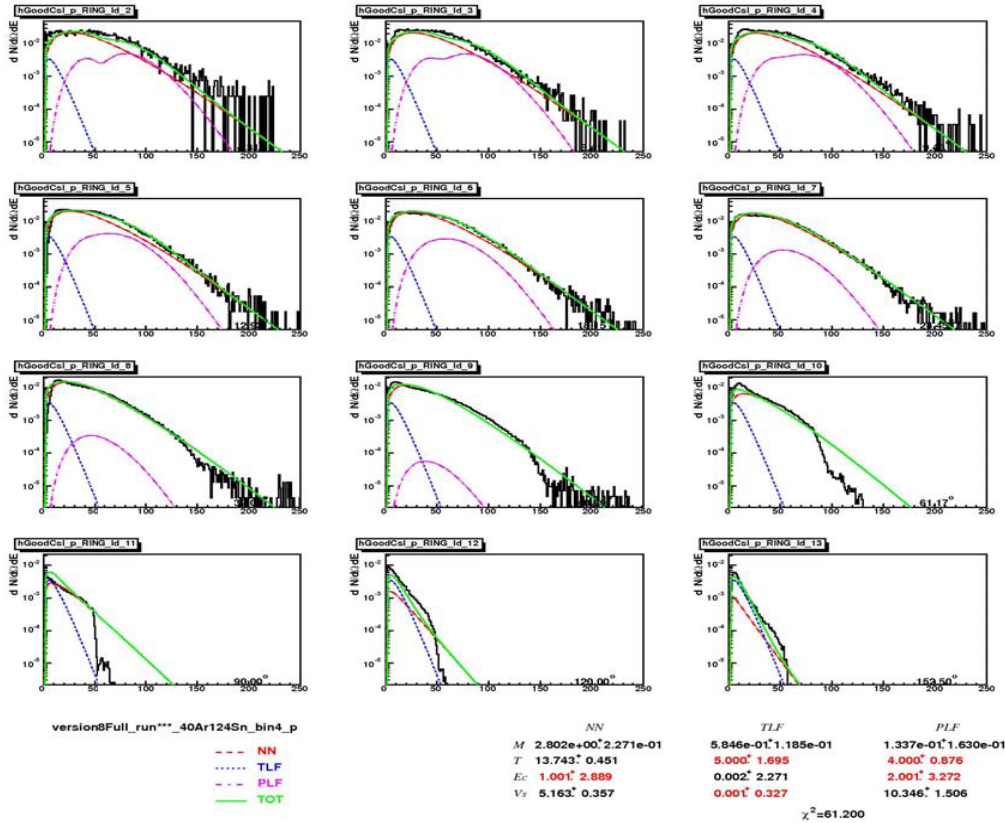


Figure 3. Three source fit representations of the laboratory kinetic energy spectra of protons emitted in violent collisions of  $^{40}\text{Ar} + ^{124}\text{Sn}$  for twelve angular ranges from  $4^\circ$  to  $170^\circ$ . The summed contributions from the PLF, NN, and TLF sources are represented by solid lines.

Figure 3 shows the preliminary result of  $^1\text{H}$  three source fitting from the system  $^{40}\text{Ar}+^{124}\text{Sn}$ . The finalization of parameter extraction is in progress.

[1] Jian-Ye Liu *et al.*, Phys. Rev. Lett. **86**, 975 (2001).

[2] Lie-Wen Chen *et al.*, Phys. Rev. Lett. **90**, 162701 (2003).

[3] Ph. Chomaz *et al.*, Phys Lett B **447**, 221 (1999).

[4] K. Hagel *et al.*, Phys. Rev. C **62**, 034607 (2000)

**SECTION III**  
**NUCLEAR THEORY**

## Charm Elliptic Flow at RHIC

B. Zhang,<sup>1</sup> L. W. Chen, and C. M. Ko

<sup>1</sup>*Department of Chemistry and Physics, Arkansas State University, State University, AR 72467*

Using a multiphase transport (AMPT) model, we have studied charm elliptic flow in heavy ion collisions at the Relativistic Heavy Ion Collider [1]. Assuming that the cross section for charm quark scattering with light quarks is the same as that between light quarks, we find that both charm and light quark elliptic flows are sensitive to the value of the cross section. Compared to that of light quarks, the elliptic flow of charm quarks is smaller at low transverse momentum but approaches comparable values at high transverse momentum as a result of their large masses. Similar features are seen in the elliptic flow of charmed mesons as well as that of the electrons from their semileptonic decays when the charmed mesons are produced from quark coalescence during hadronization of the partonic matter. To describe the large electron elliptic flow observed in the experimental data requires a charm quark scattering cross section that is much larger than that given by the perturbative QCD as shown in Fig.1.

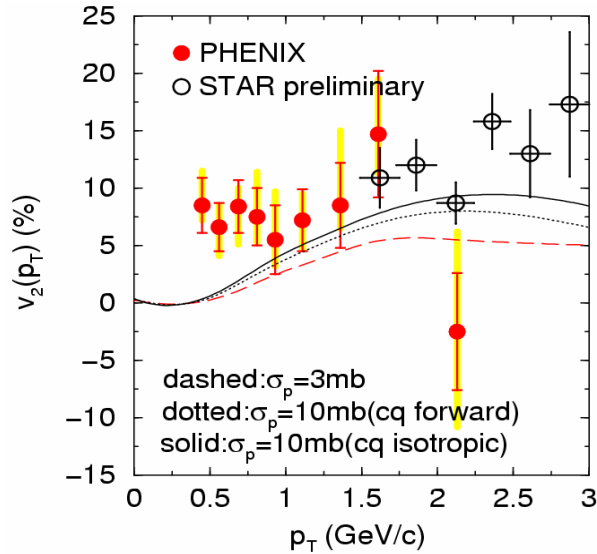


**Figure 1.** Transverse momentum dependence of the elliptic flow of electrons from charmed meson decays from the AMPT model for different parton scattering cross sections of 3 (dashed curve) and 10 (dotted curve) mb with forward peaking angular distribution as well as 10 mb with isotropic angular distribution (solid curve) from minimum-bias Au + Au collisions at  $s_{NN}^{1/2} = 200$  GeV.

[1] B. Zhang, L.W. Chen, and C.M. Ko, nucl-th/0502056.

## Pseudorapidity Dependence of Anisotropic Flows in Relativistic Heavy Ion Collisions

L. W. Chen, V. Greco, C. M. Ko, and P. F. Kolb<sup>1</sup>

<sup>1</sup>*Physik Department, Technische Universitat Munchen, D-85747 Garching, Germany*

The pseudorapidity dependence of anisotropic flows  $v_1$ ,  $v_2$ ,  $v_3$ , and  $v_4$  of charged hadrons in heavy-ion collisions at the Relativistic Heavy Ion Collider has been studied in a multi-phase transport (AMPT) model [1]. We find that while the string melting scenario, in which hadrons that are expected to be formed from initial strings are converted to their valence quarks and antiquarks, can explain the measured  $p_T$ -dependence of  $v_2$  and  $v_4$  of charged hadrons at midrapidity with a parton scattering cross section of about 10 mb, the scenario without string melting reproduces better recent data on  $v_1$  and  $v_2$  of charged hadrons at large pseudorapidity in Au + Au collisions at  $s^{1/2} = 200$  AGeV as shown in Figs. 1 and 2. Our results thus suggest that a partonic matter is produced only around midrapidity and that strings remain dominant at large rapidities. The  $p_T$ -dependence of  $v_1$ ,  $v_2$ ,  $v_3$ , and  $v_4$  for charged hadrons at forward pseudorapidity has also been predicted.

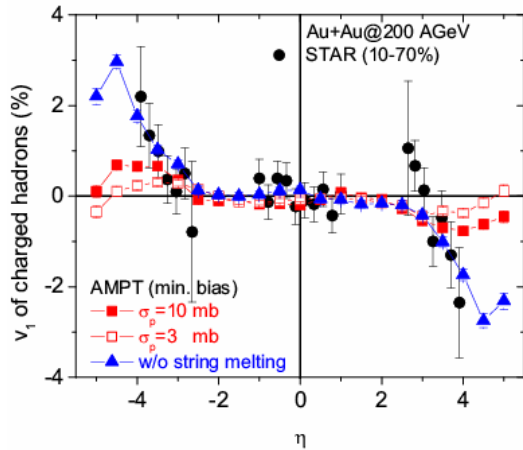


**Figure 1.** Pseudorapidity dependence of  $v_1$  in the string melting scenario with parton cross sections  $\sigma_p=3$  (open squares) and 10 (solid squares) mb as well as the scenario without string melting (triangles).

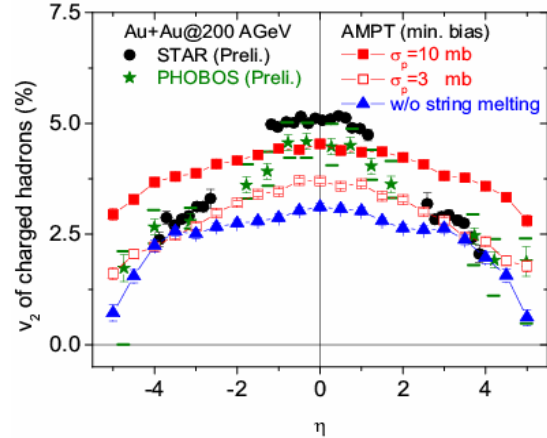


**Figure 2.** Same as Fig.1 for pseudorapidity dependence of  $v_2$ .

[1] L.W. Chen, V. Greco, C.M. Ko, and P.F. Kolb, Phys. Lett. B **605**, 95 (2005).

## Determination of the Stiffness of the Nuclear Symmetry Energy from Isospin Diffusion

L. W. Chen, C. M. Ko, and B. A. Li<sup>1</sup>

<sup>1</sup>*Department of Chemistry and Physics, Arkansas State University, State University, AR 72467*

Using an isospin- and momentum-dependent transport (IBUU) model, we have studied the effect of both the stiffness of the nuclear symmetry energy and the momentum dependence of the nucleon potential on the degree of isospin diffusion in heavy ion collisions at intermediate energies [1]. Using a momentum dependence derived from the Gogny effective interaction as shown in Fig.1 for different symmetry energy, recent experimental data from NSCL/MSU on isospin diffusion [2] are shown to be consistent with a nuclear symmetry energy given by  $E_{\text{sym}}(\rho) \sim 31.6 (\rho/\rho_0)^\gamma$  with  $\gamma = 1.05$  at subnormal densities, which is much softer than that extracted using the momentum independent interaction SBKD as shown in Fig.2. This leads to a significantly constrained value of about -550 MeV for the isospin-dependent part of the isobaric incompressibility  $K_{\text{asy}}$  of isospin asymmetric nuclear matter.

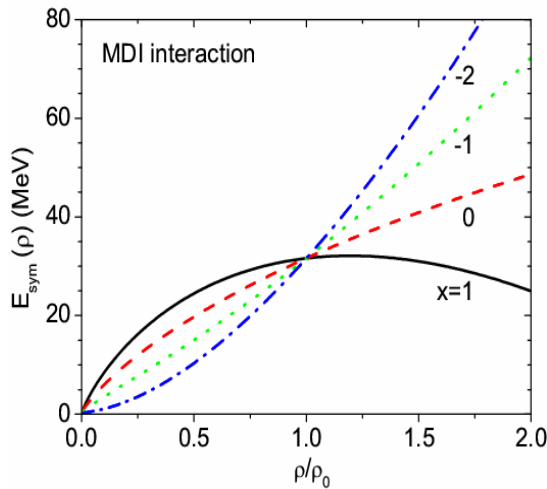


**Figure 1.** Density dependence of the nuclear symmetry energy for different  $x$  parameters in the momentum-dependent interaction (MDI).

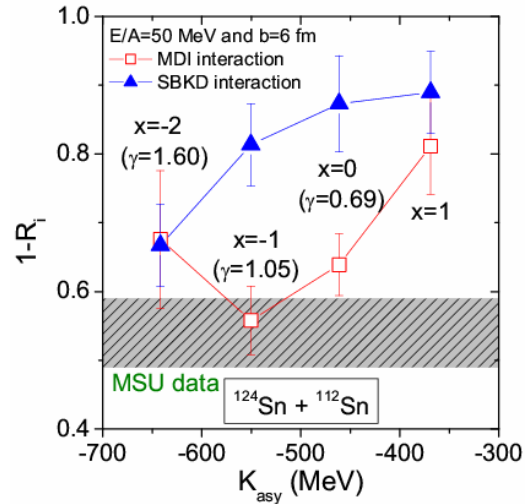


**Figure 2.** Degree of isospin diffusion as a function of  $K_{\text{asy}}$  with the MDI and SBKD interactions.

[1] L.W. Chen, C.M. Ko, and B. A. Li, Phys. Rev. Lett. **94**, 032701 (2005).

[2] M.B. Tsang *et al.*, Phys. Rev. Lett. **92**, 062701 (2004).

## Relativistic Heavy Ion Collisions at the Large Hadron Collider

Z. W. Lin,<sup>1</sup> C. M. Ko, B. Zhang,<sup>2</sup> B. A. Li,<sup>2</sup> and S. Pal<sup>3</sup>

<sup>1</sup>Center for Materials Research, University of Alabama in Huntsville, Huntsville, AL 35899

<sup>2</sup>Department of Chemistry and Physics, Arkansas State University, State University, AR 72467

<sup>3</sup>Department of Physics, Michigan State University, East Lansing, MI 48824

Using a multi-phase transport (AMPT) model, we have studied the rapidity and transverse momentum distributions in central ( $b < 3$  fm) Pb + Pb collisions at  $s_{NN}^{1/2} = 5.5$  TeV at the Large Hadron Collider (LHC) [1]. As shown in Fig.1 for the charged particle pseudo-rapidity distribution and the rapidity distributions of charged pions, kaons, protons, and antiprotons, the distributions are significantly wider and higher than corresponding distributions at RHIC. At mid-rapidity, the distributions without shadowing are higher than the ones with shadowing by about 80%. The highest value at mid-rapidity is about 4500, more than a factor of three higher than that at RHIC. The predicted transverse momentum spectra at LHC are shown in Fig.2, and it is seen that the inverse slope parameters, particularly for kaons and protons, are larger than those at RHIC as a result of stronger transverse flow. Similar to that observed at RHIC, the proton spectrum is below that of pions at low transverse momentum but they become comparable at about 2 GeV/c.

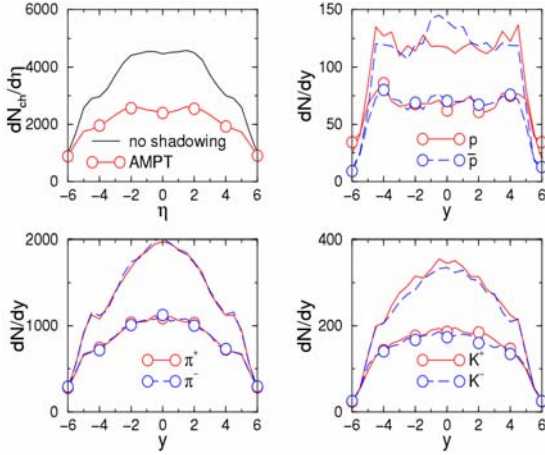


**Figure 1.** Rapidity distributions in central ( $b < 3$ ) Pb + Pb collisions at  $s_{NN}^{1/2} = 5.5$  TeV from the default AMPT model with (curves with circles) and without (curves without symbols) nuclear shadowing.

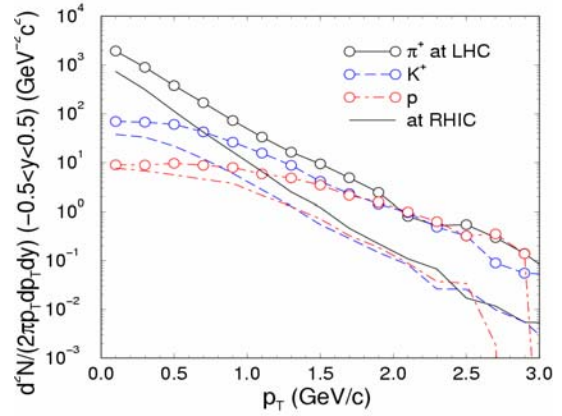


**Figure 2.** Same as Fig.1 for the transverse momentum spectra. Curves without symbols are from the default AMPT model for central ( $b < 3$  fm) Au + Au collisions at  $s_{NN}^{1/2} = 200$  GeV at RHIC.

[1] Z.W. Lin, C.M. Ko, B.A. Li, B. Zhang, and S. Pal, nucl-th/0411110.

## Hadron Production from Quark Coalescence and Jet Fragmentation

V. Greco, C. M. Ko, and I. Vitev<sup>1</sup>

<sup>1</sup>*Theory Division and Physics Division, Los Alamos National Laboratory, Mail Stop H846,  
Los Alamos, New Mexico 87545*

Using a hadronization model based on quark coalescence and minijet fragmentation, we have studied hadron production in central Au + Au collisions at  $s_{\text{NN}}^{1/2} = 62$  GeV at RHIC [1]. The predicted transverse momentum spectra of pions, protons and antiprotons are shown in Fig.1. We find a larger enhancement of the  $p/\pi$  ratio with respect to the one seen in nuclear collisions at  $s_{\text{NN}}^{1/2} = 200$  GeV as shown in Fig.2. This is mainly due to a steeper pion spectrum that is dominated by minijet fragmentation already at  $p_{\text{T}} \approx 4$  GeV and a proton spectrum that is instead still dominated by contributions from the quark coalescence up to  $p_{\text{T}} \approx 6.5$  GeV. Experimental confirmation of this prediction will provide a stronger evidence for quark coalescence as a likely non-perturbative mechanism for hadronization, especially for protons at transverse momentum up to about 6 GeV.

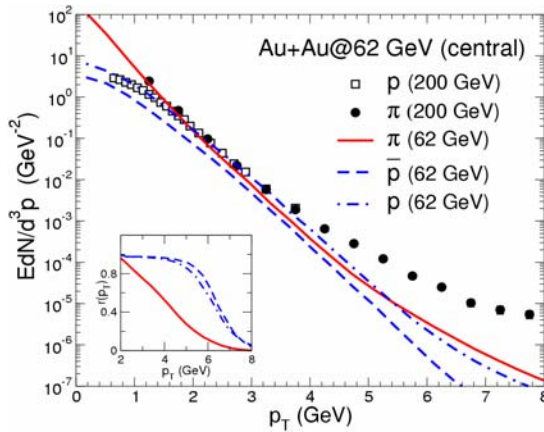


**Figure 1.** Hadron transverse momentum spectra. Data for  $\pi^0$  (filled circles) and proton (open squares) are for  $s_{\text{NN}}^{1/2} = 200$  GeV. Inset: The fraction of quark coalescence contribution for  $\pi$  (solid line),  $p$  (dash-dotted line), and anti- $p$  (dashed line).

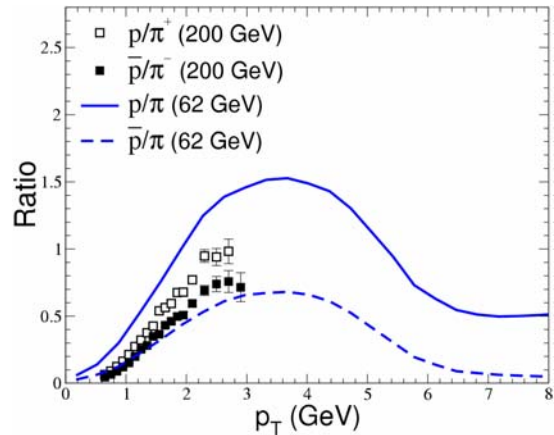


**Figure 2.** Same as Fig.1 for the ratios of proton (solid line) and antiproton (dashed line) to pion spectra.

[1] V. Greco, C.M. Ko, and I. Vitev, Phys. Rev. C **71**, 041901 (2005).

# In-Medium Modifications of the Nucleon and $\Delta(1232)$ at RHIC

Hendrik van Hees and Ralf Rapp

From asymptotic freedom of QCD, at sufficiently high temperatures and densities of nuclear matter, one expects a (pseudo-)phase transition to a quark-gluon plasma (QGP). Lattice calculations show that this transition is closely related with the restoration of the approximate chiral symmetry in the light-quark sector of QCD. Since in the restored phase the spectral functions of chiral-partner hadrons become degenerate, one expects significant medium modifications which one hopes to observe in ultra-relativistic heavy-ion collisions [1].

In this work, we employ a hadronic model to describe interacting pions, nucleons, and baryon resonances to investigate their properties within a hot and dense medium, particularly for the  $\Delta(1232)$  resonance, which recently became accessible to experiment through the measurement of  $\pi N$ -invariant mass spectra at RHIC [2].

The  $\pi N \Delta$ -coupling is taken as a p-wave interaction with a monopole form factor with a three-momentum cutoff of 290 MeV, which fits the  $\pi N$ -phase shift in the  $\Delta(1232)$  channel [3].

To assess medium modifications, we dressed the  $\Delta(1232)$  with self-energy contributions from scattering off thermal pions, including the baryon resonances  $N(1440)$ ,  $N(1520)$ ,  $N(1700)$ ,  $\Delta(1600)$ ,  $\Delta(1620)$ , and  $\Delta(1700)$ . We furthermore included  $\pi N$  interactions as well as vertex corrections in the  $\Delta$ -self-energy loop, employing standard Migdal parameters to account for short-range  $NN$  and  $N\Delta$  correlations, to suppress an artificial threshold enhancement due to the in-medium pion-dispersion relation. The resulting model has been checked to approximately agree with photo-absorption data on nuclei.

As shown in Fig. 1, under RHIC conditions the peak position of the  $\Delta$ -spectral function shifts to higher masses with increasing temperature and density, and the width increases as compared to the vacuum. The broadening is mainly caused by a Bose enhancement of the pion in the decay of the  $\Delta$  and by resonant  $\pi\Delta$  interactions. For conditions resembling thermal freeze out (dashed line in Fig. 1), the peak position is located at about  $M \cong 1.226$  GeV and the width has increased to  $\Gamma \cong 177$  MeV to be compared to the vacuum values of  $M \cong 1.219$  GeV and  $\Gamma \cong 110$  MeV respectively, which is in qualitative agreement with preliminary data from the STAR collaboration [2].

We have also calculated the in-medium modifications of the nucleon with  $\pi N$ - and  $\pi\Delta$ -loops. As shown in Fig. 2, the nucleon-spectral function becomes substantially broadened.

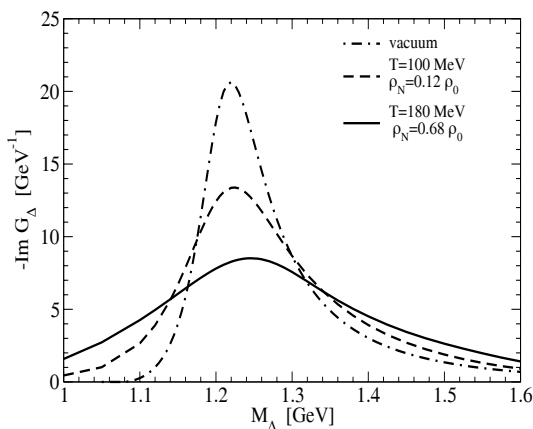


**Figure 1.** The  $\Delta$ -spectral function at finite temperature and density in comparison to the vacuum.

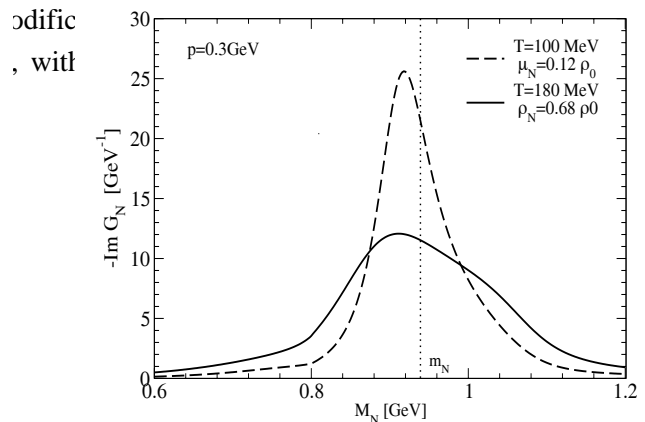


**Figure 2.** The nucleon-spectral function at finite temperature and density.

- [1] R. Rapp, J. Wambach, *Adv. Nucl. Phys.* **25**, 1 (2000).
- [2] H. van Hees, R. Rapp, *Phys. Lett. B* **606**, 59 (2005).
- [3] P. Fachini, *J. Phys. G* **30**, S735 (2004).
- [4] W. Weinhold, B. Friman, W. Nörenberg, *Phys. Lett. B* **433**, 236 (1998).

# Charm-Quark Thermalization in the Quark-Gluon Plasma

Hendrik van Hees and Ralf Rapp

Hadrons containing heavy quarks are believed to be valuable probes [1] for the investigation of the properties of the quark-gluon plasma (QGP), the hot and dense state of matter which is apparently created in ultrarelativistic heavy-ion collisions.

In this work [2] we address the interactions of anti-/charm quarks with thermal light anti-/quarks and gluons, which constitute the QGP. The  $c$ -quark  $p_T$ -distributions and elliptic flow,  $v_2$ , are believed to be reflected by the corresponding observables of  $D$ -mesons. Recent experimental data from the Relativistic Heavy-Ion Collider (RHIC) indicate that the  $v_2$  of  $D$ -mesons is comparable to that of light hadrons [3,4].

As a non-perturbative mechanism for charm-quark thermalization, we have suggested rescattering off partons through mesonic resonances, whose survival in the QGP up to temperatures  $T \cong 1 - 2T_c$  is motivated by pertinent findings from lattice-QCD calculations for light-light and heavy-heavy quark pairs, as well as from Nambu-Jona-Lasinio models for heavy-light mesonic systems.

Here, we use an effective heavy-quark model, which respects chiral and isospin symmetry for the light quarks and includes pseudoscalar  $D$ -mesons, their scalar chiral partners,  $D_0^*$ , and the vector and axialvector mesons,  $D^*$  and  $D_1^*$ . In the strange-quark sector we only include the pseudoscalar and the vector states since we expect the chiral  $s-\bar{s}$  condensate to persist up to temperatures considerably higher than  $T_c$ . Within this model, we have calculated drag and diffusion coefficients for elastic  $c-q$  scattering, complemented by perturbative-QCD (pQCD)  $c-q$  and  $c-g$  cross sections, and assessed pertinent thermalization time scales employing a Fokker-Planck equation [5].

The resonance-scattering contribution leads to an equilibration time for charm quarks which is by a factor  $\sim 3$  lower than with the pQCD cross sections alone, see Fig. 1. For the analogous case of bottom quarks the effect is much smaller due to their higher mass. The equilibration times for  $c$ -quarks are comparable to the typical lifetime of the QGP fireball, and thus (partial) thermalization becomes likely. Solving the time-dependent Fokker-Planck equation with an initial  $c$ -quark distribution from PYTHIA indeed shows that including the resonance scattering cross sections leads to a final distribution which is approximately thermal with a temperature of about 290 MeV.

In subsequent (ongoing) work, we use a Langevin simulation for a relativistic Fokker-Planck equation and include asymmetric flow for the QGP medium of light quarks and gluons, supplemented by

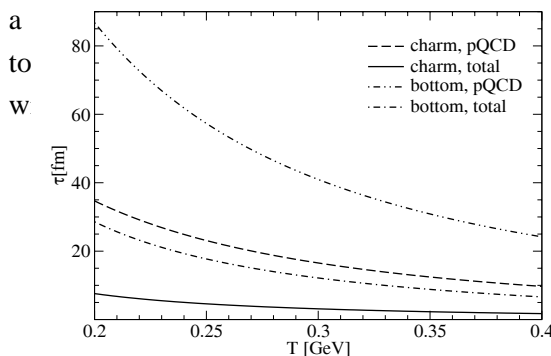


**Figure 1.** Equilibration times for charm and bottom quarks; the case of using pQCD cross sections only is compared to a scenario including resonance scattering contributions.

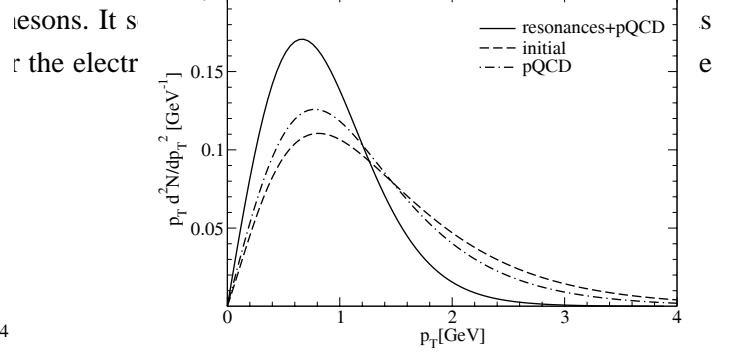


**Figure 2.** Equilibration times for charm and bottom quarks; the case of using pQCD cross sections only is compared to a scenario including resonance scattering contributions.

- [1] R. Rapp, L. Grandchamp, J. Phys. G **30**, S305 (2004)
- [2] H. van Hees, R. Rapp, Phys. Rev. C **71**, 034907 (2005)
- [3] S. Kelly *et al.* (PHENIX Collaboration), J. Phys. G **30**, S1189 (2004)
- [4] F. Laue *et. al.* (STAR Collaboration), J. Phys. G **31**, S27 (2005)
- [5] B. Svetitsky, Phys. Rev. D **37**, 2484 (1988)

## Hadronic Modes and Quark Properties in the Quark-Gluon Plasma

M. Mannarelli and R. Rapp

A central goal of the relativistic heavy-ion collision program is the creation and identification of new forms of highly excited nuclear matter, in particular a deconfined and chirally symmetric Quark-Gluon Plasma (QGP). Recent data from the Relativistic Heavy-Ion Collider (RHIC) indicate that the produced matter exhibits strong collective behavior which is incompatible with expectations based on a weakly interacting QGP: standard perturbative QCD (pQCD) cross sections for quarks and gluons do not allow for rapid thermalization [1] as required in hydrodynamic models to reproduce the observed magnitude of the elliptic flow. The question thus arises what the nature of the produced medium at temperatures  $T \approx 1-2 T_c$  is ( $T_c \approx 170$  MeV: critical temperature). Of particular importance is the identification of the relevant interactions that can provide sufficiently large scattering rates while maintaining consistency with the QGP equation of state (EoS), as determined in lattice QCD (lQCD). Recent (quenched) lQCD calculations found intriguing evidence that mesonic correlation functions, after transformation into Minkowski space, exhibit resonance (or bound-state) like structures for temperatures up to  $\sim 2T_c$  [2]. As is well known, resonance scattering is typically characterized by isotropic angular distributions and thus more efficient in randomizing momentum distributions than forward-dominated pQCD cross sections. Indeed, a recent calculation [3] based on the assumption of resonant “D”-meson states in the QGP has shown that thermal relaxation times for charm quarks are reduced by a factor of  $\sim 3$  as compared to using perturbative rescattering cross sections.

In the present work [4] we have set up a Brueckner-type many-body scheme, utilizing (heavy) quark-antiquark (q-qbar) interaction potentials as extracted from lQCD (supplemented by relativistic effects), to study the properties of light (anti-) quarks in a Quark-Gluon Plasma at moderate temperatures,  $T \sim 1-2 T_c$ . The q-qbar  $T$ -matrix (including color-singlet and -octet channels) has been evaluated self-consistently with corresponding quark self-energies and spectral functions. Quark interactions with gluons are introduced through a “gluon-induced” quark mass  $m$  which is a parameter in our model.

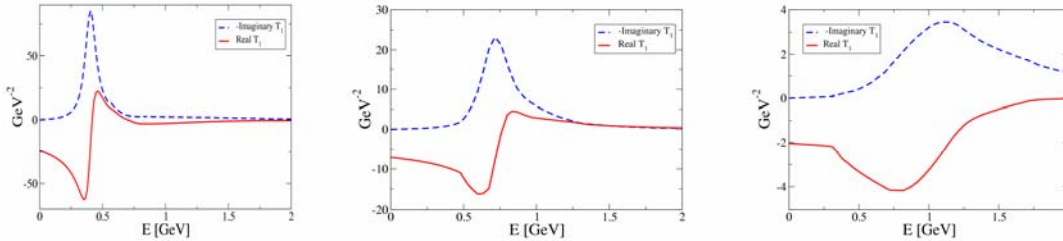


**Figure 1.** Real (full lines) and (absolute value of the) imaginary part (dashed lines) of the light-quark (on-shell)  $T$ -matrix in the color-singlet channel at temperatures  $T=1.2T_c$ ,  $1.5T_c$  and  $1.75T_c$  (left, middle and right panel, respectively) vs. q-qbar CM energy  $E$ , with a “gluon-induced” quark-mass term  $m=0.1$  GeV.

Our main results are the following: (i) the attractive color-singlet potential generates light mesonic states in the q-qbar  $T$ -matrix which persist as resonances up to temperatures  $\sim 1.75 T_c$ ; (ii) the

repulsive octet potential induces quasiparticle masses of up to 150 MeV; (iii) the resonance structures in the  $T$ -matrix entail quark-quasiparticle widths of  $\sim 200$  MeV, corresponding to scattering rates of  $\sim 1\text{fm}^{-1}c$  possibly reflecting liquid-like properties of the system.

The real and imaginary part of the on-shell  $T$ -matrix in the color-singlet channel for quasiparticles with a gluon-induced mass-term of  $m=0.1\text{GeV}$  are shown in Fig.1 for temperatures  $T=1.2-1.75 T_c$ . At  $T=1.2T_c$  the color-singlet  $T$ -matrix exhibits a relatively narrow bound state located below the  $q$ - $\bar{q}$  threshold energy of  $E_{\text{thr}}\sim 0.52$  GeV (corresponding to twice the real part of the total quark self-energy discussed below). When increasing the temperature to  $1.5T_c$  and  $1.75T_c$ , the state moves above the threshold ( $E_{\text{thr}} \sim 0.48$  GeV), accompanied by a significant broadening.

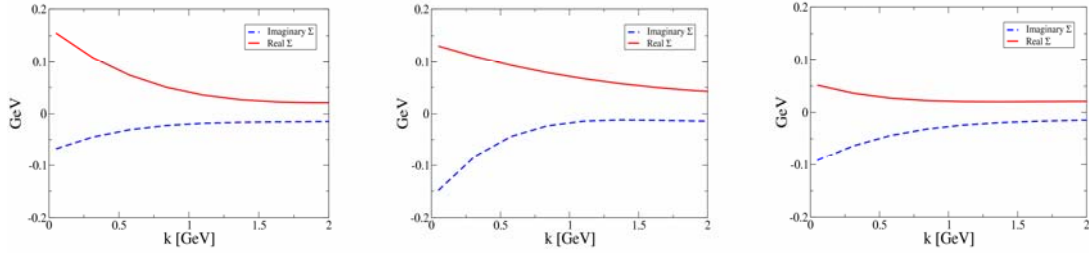


**Figure 2.** Real (solid lines) and imaginary (dashed lines) parts of the on-shell quark self-energy vs. quark 3-momentum at temperatures  $T=1.2T_c$ ,  $1.5T_c$  and  $1.75 T_c$  (left to right) with  $m=0.1\text{GeV}$ .

In Fig. 2 the real and imaginary parts of the self-consistently determined self-energy are displayed. The imaginary parts translate into widths of about 200 MeV at low momenta and for temperatures around  $1.5 T_c$ , and are mostly due to resonant scattering in the singlet channel. This is further illustrated by the significant increase in  $\text{Im } \Sigma$  when going from  $1.2$  to  $1.5 T_c$  (cf. left and middle panel in Fig. 2), during which the state in the  $T$ -matrix moves from below to above threshold (cf. left and middle panel in Fig. 2), *i.e.*, converts from bound state to resonance. The magnitude of the quark widths is quite comparable to the thermal masses, qualitatively supporting the notion that the QGP could be in a liquid-like regime.

- [1] R. Baier, A. H. Mueller, D. Schiff, and D. T. Son, Phys. Lett. B **502**, 51 (2001).
- [2] F. Karsch and E. Laermann, LANL e-print arxiv hep-lat/0305025.
- [3] H. van Hees and R. Rapp, Phys. Rev. C **71**, 034907 (2005).
- [4] M. Mannarelli and R. Rapp, LANL e-print arxiv hep-ph/0505080.

## Meissner Masses in the gCFL Phase of QCD

R.Casalbuoni, R.Gatto, M.Mannarelli, G.Nardulli and M.Ruggieri

At asymptotic densities cold quark matter is in the Color Flavor Locked (CFL) phase of QCD [1-2]. This state is characterized by nine gapped fermionic quasi-particles ( $3 \times 3$ , for color and flavor) and by electric neutrality, even for non vanishing quark masses  $M_j$ , provided the CFL phase persists. At lower densities, including the strange quark mass  $M_s$ , requiring electrical and color neutrality, and imposing weak equilibrium, a phase transition from the CFL phase to a new phase, called gapless CFL (gCFL), occurs. In the gCFL phase seven fermionic quasiparticles have a gap in the dispersion law, but the remaining two are gapless. At zero temperature the transition from the CFL to the gCFL phase takes place at  $M_s^2/\mu_b \approx 2\Delta$ , where  $\mu_b$  is the quark chemical potential and  $\Delta$  is the gap parameter. The next phase at still lower densities is difficult to determine, with the crystalline color superconductive phase being a candidate [3].

In this work, we investigate the dependence of Meissner masses on  $M_s$  in the gCFL phase. Imposing weak equilibrium and neutrality we numerically evaluate the gluon Meissner masses in the gCFL phase and show that an instability arises in a certain range of values of the  $M_s$ , with the masses of gluons with color  $a=1,2,3,8$  becoming imaginary. Our calculation scheme is the High Density Effective Theory (HDET) which allows a significant reduction of the computational complexity.

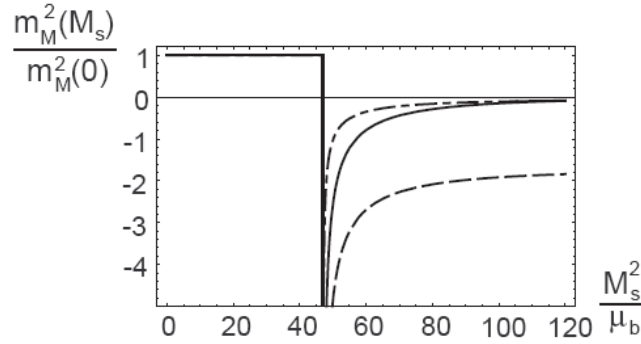


**Figure 1.** Squared values of the Meissner masses (in units of the squared Meissner mass for  $M_s=0$ ) as a function of  $M_s^2/\mu_b$  (in MeV) for gluons  $a = 1, 2, 3, 8$ . The solid line denotes the gluons with colors  $a = 1, 2$ . The dashed line denotes the gluons with color  $a = 3$ ; the dot-dashed line is for  $a = 8$ .

In Fig. 1 we present the results for the squared Meissner masses of gluons with color  $a = 1, 2, 3, 8$  in units of the squared Meissner mass at zero strange quark mass. The solid line denotes gluons with color  $a = 1, 2$ ; the dashed line gluons with color  $a = 3$ ; dot-dashed line gluons with  $a = 8$ . We find that increasing  $M_s^2/\mu_b$  the degeneracy in the Meissner masses is partially removed. Moreover there is a discontinuity of the squared Meissner mass of gluons of colors  $a = 1, 2, 3, 8$ , which at the onset of the gCFL phase, i.e. for  $M_s^2/\mu_b \approx 2\Delta$  (here  $\Delta=25$  MeV ) drop to negative values, leading to an instability.

The next step will be the determination of the actual color superconductive ground state in this range of parameters, to remove the instability determined by the imaginary Meissner masse of the gluons.

- [1] M. G. Alford, K. Rajagopal and F. Wilczek, Nucl. Phys. **B537**, 443 (1999).
- [2] R. Rapp, T. Schafer, E. V. Shuryak and M. Velkovsky, Ann. Phys. **280**, 35 (2000).
- [3] R. Casalbuoni, M. Ciminale, M. Mannarelli, G. Nardulli, M. Ruggieri and R. Gatto, Phys. Rev. D **70**, 054004 (2004).
- [4] R. Casalbuoni, R. Gatto, M. Mannarelli, G. Nardulli and M. Ruggieri, Phys. Lett. B **605**, 362 (2005),  
Erratum- ibid. B 615, 297 (2005).

## Thermal Photons in Strong Interactions

Ralf Rapp

Electromagnetic probes have a long history as valuable probes of the structure of strongly interacting systems. In this brief review [1] we focus on the properties of thermal photon rates in a hot and dense hadron gas (HG) as well as in the Quark-Gluon Plasma (QGP), as well as their role in providing pertinent signatures in ultrarelativistic heavy-ion collisions (URHICs).

Concerning thermal emission rates from the QGP, a recent analysis succeeded in resumming collinear singularities to arrive at the complete in-medium result to leading-order (LO) in the strong coupling constant,  $\alpha_s$ . The corresponding rate is enhanced by a factor of 2-3 over the LO Born result, cf. Fig.1. For the HG [3],  $t$ -channel meson-exchange processes (in particular  $\omega$ -exchange in  $\pi\rho \rightarrow \pi\gamma$ ) have

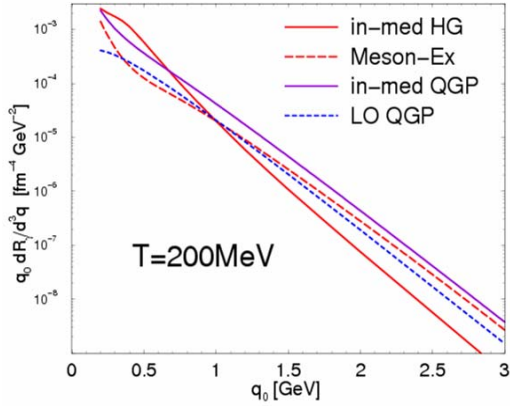


**Figure 1.** Thermal photon rates in hadronic matter (red curves, to be added) and in the QGP (naïve LO compared to full in-med. LO).

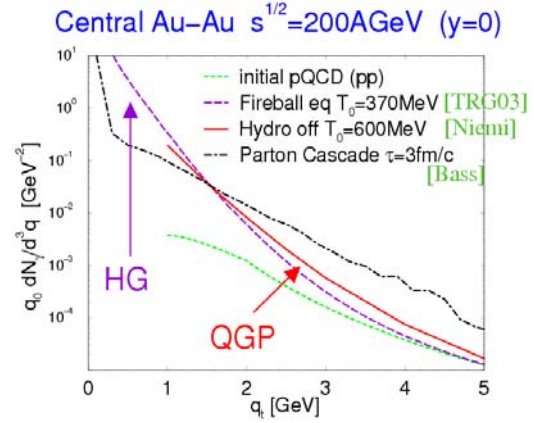


**Figure 2.** Transverse-momentum direct-photon spectra at RHIC from a thermal fireball [3], hydrodynamics [4] and parton-cascade [5].

been found to dominate at large photon energies, whereas processes which are important for low-mass dilepton production are the major source at energies of below  $\sim 1$  GeV. When added together, the total HG rate is surprisingly similar to the in-medium QGP result (Fig. 1), suggestive for a quark-hadron duality as has been found before for dilepton rates.

When applied to direct photon spectra in URHICs, it turns out [3] that at SPS energies, once the Cronin effect for primordial (initial) pQCD photons is accounted for, thermal emission mostly originates from the HG, whereas at RHIC energies, QGP emission dominates for  $q_t=1-3$  GeV.

[1] R. Rapp, Mod. Phys. Lett. **19**, 1717 (2004).

[2] P. Arnold, G.D. Moore and L.G. Yaffe, JHEP **0112**, 009 (2001).

[3] S. Turbide, R. Rapp and C. Gale, Phys. Rev. C **69**, 014903 (2004).

[4] F. Gelis, H. Niemi, P.V. Ruuskanen and S.S. Räsänen, J. Phys. G **31**, S1037 (2004).

[5] S.A. Bass, B. Müller and D.K. Srivastava, Phys. Rev. Lett. **90**, 082301 (2003).

## In-Medium Effects on Charmonium Production in Heavy-Ion Collisions

L. Grandchamp<sup>1</sup>, R. Rapp and G.E. Brown<sup>2</sup>

<sup>1</sup> *Lawrence Berkeley National Laboratory, Berkeley, CA 94720*

<sup>2</sup> *Department of Physics, State University of New York, Stony Brook, NY 11794-3800*

Heavy-quark bound states (charm- and bottom-onium) constitute valuable probes of the highly excited matter as created in high-energy collisions of heavy nuclei. A suppressed production of  $J/\Psi$ 's (relative to expectations from p-p collisions) has been suggested as a signature of the creation of a (deconfined) Quark-Gluon Plasma (QGP). However, it has been realized recently that QGP formation also facilitates the regeneration of charmonium states through recombination of charm and anticharm quarks, provided the latter are produced abundantly.

To study the evolution of charmonium states in the (putative) equilibrium phases of ultrarelativistic heavy-ion reactions we have employed a kinetic theory framework [1] incorporating in-medium properties of open- and hidden-charm states in line with recent QCD lattice calculations. Whereas at SPS energies  $J/\Psi$  suppression is the prevalent effect, at collider energies (RHIC and LHC) secondary production through c-cbar coalescence becomes the dominant production mechanism. The time evolution of the  $J/\Psi$  number as a function of proper time (Fig. 1) in central Au-Au at RHIC indicates that

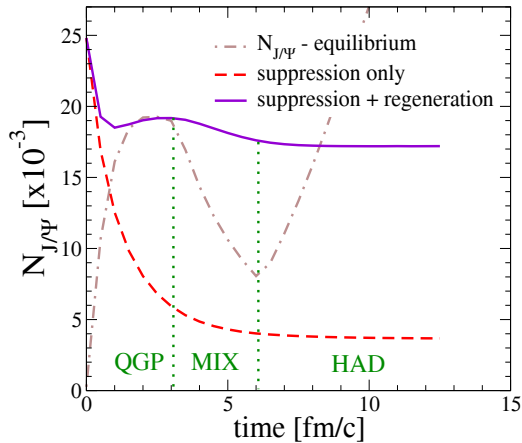


**Figure 1.** Time evolution of  $J/\Psi$  abundances in  $\sqrt{s}=200\text{GeV}$  Au-Au collisions at RHIC through the QGP, mixed and hadronic phase of an expanding fireball model.

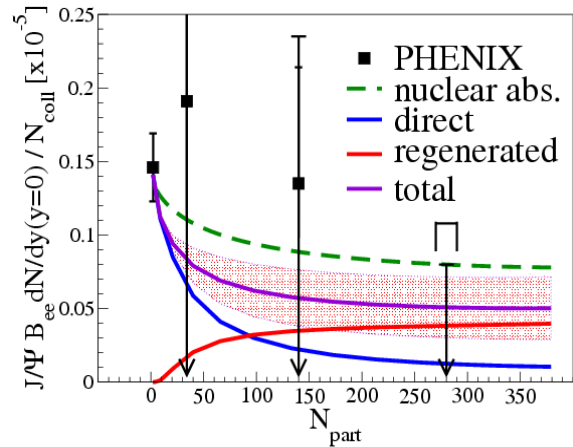


**Figure 2.** Centrality dependence of the  $J/\Psi$  yield in  $\sqrt{s}=200\text{GeV}$  Au-Au collisions, normalized to the number of primordial N-N collisions.

in lattice QCD). The yield appears to chemically equilibrate at  $T_c$ . The pertinent centrality dependence (Fig. 2) reiterates the dominance of the regenerated  $J/\Psi$ 's in central collisions, with appreciable uncertainty due to in-medium charm-quark masses. Future evaluation of bottomonium production, presumably suppressed at RHIC energies, will provide a valuable test of the proposed approach.

[1] L. Grandchamp, R. Rapp and G.E. Brown, Phys. Rev. Lett. **92**, 212301 (2004).

## Astrophysical Resonant Reactions in Trojan Horse Method

A.M. Mukhamedzhanov, Sh. M. Allison,<sup>1,2</sup> S. Sherubini,<sup>3</sup> C. Spitaleri,<sup>3</sup> and A. Tumino<sup>3</sup>

<sup>1</sup>*Cyclotron Institute, Texas A&M University, College Station, Texas 77843*

<sup>2</sup>*Southwestern College, Wienfield, Kansas*

<sup>3</sup>*Laboratori Nazionali del Sud, INFN, Catania, Italy*

Nuclear astrophysical reactions occur at energies significantly below the Coulomb barrier. That is why cross-sections of astrophysical reactions typically are very small, and it is difficult, often impossible, to measure the cross-sections of these reactions at astrophysically relevant energies. There are four widely used indirect techniques: asymptotic normalization coefficient, Coulomb breakup reactions, surrogate reactions and Trojan Horse. The Trojan Horse (TH) method provides astrophysical information about nuclear reactions at stellar energies. In our work we consider the theory of the Trojan Horse for reactions proceeding through the resonance. In the TH method, a projectile impinging on a target has high enough energy to overcome the Coulomb + centrifugal barrier. After penetration through the barrier the projectile virtually breaks into two particles. One of them carries away the energy of the projectile, while the second interacts with the target at astrophysically relevant energies. The advantage of this method is that it allows us to measure astrophysical reactions at energies not available in direct experiments and measure both resonant and direct reactions. However, there is a price we have to pay: the fragment left by the projectile, which interacts with the target, is virtual. Hence the extracted astrophysical cross section is half-off-energy-shell. The question of the impact of the off-shellity in the entrance channel on the cross-section at astrophysical energies has not been studied. The goal of this project is to investigate a relationship between the half-off-energy-shell and on-energy-shell resonant astrophysical cross sections.

To determine the amplitude of the reaction  $x+A \rightarrow F^{(r)} \rightarrow b+B$  in the TH method reaction  $a+A \rightarrow y+b+B$  is measured. We derived the expression for the TH reaction amplitude  $a+A \rightarrow b+B$  assuming that this reaction is a two-step process proceeding through the resonance state  $F^{(r)}$  in the subsystem  $x+A$ . If the interactions in the initial and final states are neglected the amplitude of this process is described by the pole diagram. The resonant reaction amplitude for the subprocess  $x+A \rightarrow F^{(r)} \rightarrow b+B$  is of main interest for us. This amplitude contains the off-shell form factor corresponding to the synthesis  $x + A \rightarrow F^{(r)}$ . The appearance of this off-shell form factor is due to the off-shellity of particle  $x$ . We demonstrate how to derive the on-shell amplitude and cross section of the resonant process  $x+A \rightarrow F^{(r)} \rightarrow b+B$  from the half-off-shell resonant amplitude and cross section, correspondingly, determined from the TH method. It boils down to a simple renormalization of the TH resonant amplitude. We are working on derivation of the relationship between the TH and on-shell resonant amplitudes in the presence of the initial and final-state interactions.

## **Theory of the Breakup Reactions for Charged Particles: from Exact to the DWBA Amplitude**

A. M. Mukhamedzhanov, F. Pirlepesov, A. S. Kadyrov,<sup>1</sup> A. T. Stelbovics,<sup>1</sup> and I. Bray<sup>1</sup>

<sup>1</sup>*Centre for Atomic, Molecular and Surface Physics, Murdoch University, Perth, Australia*

Breakup processes have become an important tool in modern nuclear physics providing viable information ranging from nuclear structure to nuclear astrophysics. However, the theory of the breakup reactions lags behind the demand. A treatment of the breakup processes is always complicated due to the presence of the three-body final-state. It is even more complicated if the Coulomb interactions are not negligible as happens when the Coulomb parameters are large. Evidently, this is the case when the breakup reaction occurs at energies close to the breakup threshold or when charges of the interacting nuclei are high. The correct formulation of the Faddeev integral equations in the momentum space when all three particles are charged is still an open problem. Moreover, in the presence of the Coulomb interaction the exact post form of the breakup amplitude, which is seemingly more convenient than the prior form, has not been derived for general case of arbitrary masses and charges of the interacting particles.

The aim of this work is to present correct expressions for the exact prior and post forms of the breakup amplitude in terms of the three-body wave functions, which have correct asymptotic behavior when Coulomb interactions are taken into account. For the first time we derived the exact post form of the breakup amplitude for general case of charged particles. We demonstrate that this amplitude cannot be written as a volume integral with the transition operator expressed in terms of the interaction potentials. Instead, the amplitude is given by the surface integral in the six-dimensional hyperspace. To calculate this integral one should know the asymptotic behavior of the three-body asymptotic scattered wave of the exact three-body scattering wave function with the boundary conditions given by the initial incident wave. The asymptotic behavior of the three-body scattered wave in all the asymptotic regions has been found by us. We show the flaw in the conventional approach for charged particles. This approach is based on using the channel wave function in the final state, which is not a solution of the asymptotic Schrödinger equation. We demonstrate that in the presence of the Coulomb interactions the transition to the DWBA from the exact amplitudes is not a straightforward procedure. The transition operator, which defines the breakup amplitude, plays a central role in few-body formalism and it is customary to consider it carefully when doing approximations. In particular, it is well known that the long-range nature of the Coulomb interaction is the main reason why the integral Faddeev equations for charged particles have not yet been solved above the breakup threshold. We believe that expressions suggested in this work will be useful not only for the DWBA calculations but also for the most advanced methods to calculate the breakup amplitudes, like the direct, ab-initio calculations of the Schrödinger equation in configuration space, the continuum-discretized coupled-channel method (CDCC), especially when analyzing reactions at energies near the breakup threshold. A similar method has been used very successfully in electron-atom scattering and is known as the convergent close coupling (CCC) method.

## Combined Method to Extract Spectroscopic Information

A. M. Mukhamedzhanov, F. M. Nunes,<sup>1</sup>

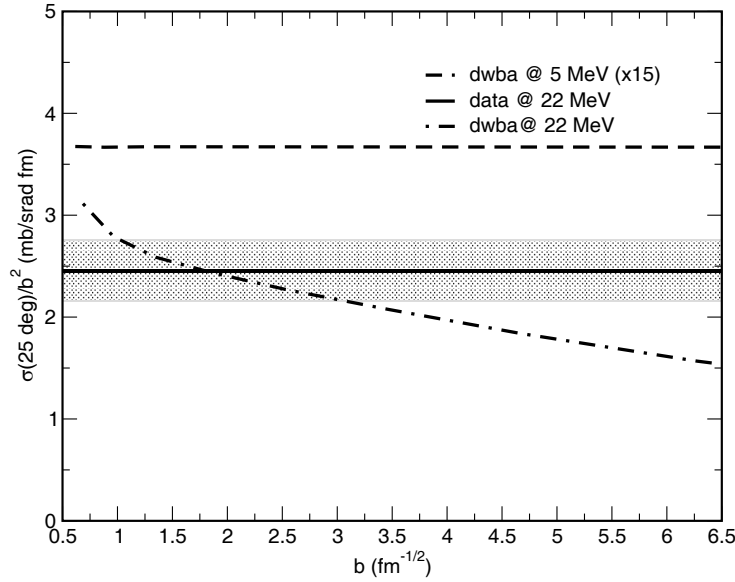
<sup>1</sup>*N.S.C.L. and Department of Physics and Astronomy, Michigan State University,  
East Lansing, MI 48824*

SF was introduced by the shell model formalism and is typically related to the shell occupancy of a state  $n$  in one nucleus relative to a state  $m$  in a nearby nucleus. Today, phenomenological SFs are extensively used in a variety of topics, from nuclear reactions to astrophysics or applied physics, yet the procedure for their extraction from the data has remained essentially the same for decades. For more than forty years since the dawn of nuclear physics, direct transfer reactions, such as  $(d,p)$ ,  $(d,t)$ ,  $({}^3\text{He},d)$ ,  $({}^3\text{He},\alpha)$ , have been the central tool to determine SFs. Extracting SFs with good precision from data is very important to test the validity of today's many body theories. For conventional nuclei there are many experiments available providing SFs, which are often lower than those predicted by shell model. Electron-induced knockout or electron scattering is supposed to provide a better accuracy in extracting SFs than transfer. However, for exotic nuclei near or on the driplines transfer reactions are a unique tool and, hence, can have a large impact in the programs of the new generation rare isotope laboratories. Given the experimental difficulties faced with measurements on the driplines, it is crucial to have a reliable method for analyzing and extracting useful information from each single data set.

Usually, transfer angular distributions are analyzed within the framework of the distorted-wave Born approximation (DWBA). The SF determined by normalizing the calculated DWBA differential cross section to the experimental one is compared with the SF predicted by shell model. Even when error bars in the experimental cross section are low, the uncertainty of the extracted SF resulting from the normalization of the DWBA cross section is often large, regardless of whether it agrees with the shell model prediction. The reasons for this inaccuracy are typically: i) optical potentials ambiguity, ii) the inadequacy of the DWBA reaction theory, or iii) the dependence on the single-particle potential parameters. This work will critically review the standard procedure of extracting SFs from transfer reactions focusing on the third point; the modified method eliminates the dependence of the extracted SFs on the single-particle potentials, the main advantage of the method. We discuss a modified approach to spectroscopy from transfer reaction which includes the asymptotic normalization coefficient (ANC) in the analysis using equation  $C^2 = Sb^2$ . Here,  $C$  is the ANC,  $S$  is the spectroscopic factor and  $b$  is the single-particle ANC, i. e. the amplitude of the tail of the single-particle wave function of the nucleon bound state wave function. Introduction of the information about the ANC allows us to fix the contribution to the DWBA amplitude from the external region. Hence, the spectroscopic factor is determined from the contribution of the nuclear interior. This modified method requires two independent experiments. The goal of the first experiment is to determine the ANC. Sub-Coulomb transfer reactions or transfer reactions induced by heavy ions at energies above the Coulomb barrier. To demonstrate this method we analyzed  $(d,p)$  on targets  ${}^{208}\text{Pb}$ ,  ${}^{12}\text{C}$ ,  ${}^7\text{Li}$  and  ${}^{84}\text{Se}$ . To determine the spectroscopic factor we calculate the

$b$  dependence of the function  $R(b) = \frac{d\sigma^{DW}}{d\Omega} / b^2$ , where  $d\sigma^{DW}/d\Omega$  is the reduced DWBA differential

cross section. From solution of the equation  $R(b) = R^{exp}$ ,  $R^{exp} = \frac{d\sigma^{exp}}{d\Omega} / C^2$ , where  $d\sigma^{exp}/d\Omega$  is the experimental differential cross section, we can determine the single-particle ANC  $b$ , and then the spectroscopic factor. As example we demonstrate the  $R(b)$  function for the  $^{208}Pb(d,p)^{209}Pb$  reaction. The solid line shows the experimental  $R^{exp}$ , and the strip indicates the experimental uncertainty. Experimental data are taken from [1] and ANC  $C^2 = 2.15 \pm 0.16 \text{ fm}^{-1}$  extracted from the sub-Coulomb transfer reaction  $^{208}Pb(d,n)^{209}Pb$  [2]. The dashed-dotted line is the



$E_d = 5 \text{ MeV}$ . Solution of equation  $R(b) = R^{exp}$  gives the  $b = 1.82^{+1.28}_{-0.72} \text{ fm}^{-1}$ , and the spectroscopic factor  $S = 0.74^{+1.46}_{-0.44}$ . As we see, due to the small contribution of the nuclear interior and large experimental uncertainty, the uncertainty of the extracted spectroscopic factor is quite large. The method here presented has the potential of reducing the uncertainty in the overlap function considerably. Results for  $^{208}Pb(d,p)^{209}Pb$  were used to illustrate the method. We also demonstrate that this method can rule out inadequate choices of optical potentials. Considering specific future experiments, we have performed exploratory calculations for  $^{84}Se(d,p)^{85}Se$ . This method will become useful for a broad variety of transfer experiments in the field of rare isotopes. The same method can equally be used for transfer to excited states. These same ideas can be extended to other reactions, in particular breakup reactions which also have an impact on Astrophysics. Finally, it would be helpful if the state-of-the-art reaction codes would incorporate the formalism discussed.

[1] K. Hirota *et al.*, Nucl. Phys. **A628**, 547 (1998).

[2] M.A. Franey, J.S. Liley, W.R. Phillips, Nucl. Phys. **A324**, 193 (1979).

## Complete Asymptotic Boundary Conditions for the Three Charged Particles Scattering Wave Function

A. M. Mukhamedzhanov, F. Pirlepsov, A. S. Kadyrov,<sup>1</sup> A. T. Stelbovics,<sup>1</sup> and I. Bray<sup>1</sup>  
<sup>1</sup>*Centre for Atomic, Molecular and Surface Physics, Murdoch University, Perth, Australia*

We determined the asymptotic behavior of the three charged particles scattering wave functions in all four asymptotic regions. This asymptotic behavior provides complete boundary conditions for solution of the three-body problem with Coulomb interaction. There are two types of the three-body scattering wave function. The scattering wave function of the first type evolves from the initial three-body incident wave (all three incident particles are in continuum). The wave function of the second type evolves from the initial two-body incident wave (the bound state plus particle). There are three different wave functions of the second type corresponding to three different combinations bound state- particle in the three-body system. First we derived all the leading asymptotic terms of the three-body incident wave up to terms of order  $O(1/\rho_\alpha^3)$  in the asymptotic region  $\Omega_\alpha$ , where particles  $\beta$  and  $\gamma$  are close to each other and far away from particle  $\alpha$ . Here,  $\rho_\alpha$  is the distance between the center of mass of the system  $\beta + \gamma$  and the third particle  $\alpha$ . In the asymptotic region, where all three particles are well separated, our found asymptotic form of the incident wave smoothly matches the Redmond's three-body Coulomb distorted wave. The asymptotic behavior of the three-body scattering wave function of the second type is given by the sum of the incident wave, outgoing two-body wave corresponding to elastic, inelastic channels and rearrangement channels, and three-body scattered wave corresponding to the breakup channel. The outgoing three-body scattered wave can be written in form of the integral containing the three-body Green function. The spectral decomposition of this Green function can be expressed in terms of the three-body scattering wave functions of the first type. Thus we derive a fundamental relationship between the three-body scattered wave of the three-body scattering wave function of the second type and the scattering wave function of the first type. From the integral representation of the three-body scattered wave we find its asymptotic behavior for general case of particles with arbitrary masses and charges in all the asymptotic regions. The amplitude of this three-body scattered wave is the breakup amplitude. The three-body scattered wave asymptotically decays as  $1/R^{5/2}$ , but in the asymptotic regions where two particles are close to each other the derived by us asymptotic form contains the correlation of the particles which are close to each other. Thus combining with the asymptotic terms obtained in [1] we completed derivation of the asymptotic behavior of the three-body scattering wave functions in all the asymptotic regions. These asymptotic forms can be used as boundary conditions for breakup and rearrangement channels. It opens up a possibility to find reaction and breakup amplitudes by solving the Schrödinger equation in the interior region. If the radius of the internal region is large enough, then the solution can be matched with the established asymptotic forms. The coefficients in the corresponding channels will provide the reaction amplitudes.

## Asymptotic Scattering Wave Function for Three Charged Particles in the Continuum

A. M. Mukhamedzhanov, F. Pirlepsov, and A. S. Kadyrov<sup>1</sup>

<sup>1</sup>*Centre for Atomic, Molecular and Surface Physics, Murdoch University, Perth, Australia*

The quantum mechanical dynamics of three charged particles is described by the Schrödinger equation which should be supplemented by proper boundary conditions. Merkuriev and Fadeev [1] claimed that solution of this equation exists and is unique if the boundary conditions are known in all asymptotic regions. Three-body scattering theory introduces new challenges compared to the two-body case.

The leading asymptotic term of the three-body incident wave function in the asymptotic region  $\Omega_0$ , where all three particles are well separated, was derived by Redmond [2,3]. It is the three-body Coulomb distorted plane wave. For practical applications Redmond [2,3], Garibotti and Miraglia [4], and Merkuriev and Faddeev [1] extended the asymptotic Redmond's term by substituting the confluent hypergeometric functions for the exponential Coulomb distortion factors. This extended wave function, often called the 3C wave function, is well-behaved even in the singular directions, where the Redmond's asymptotic term is not determined. If any of the particles is neutral, then the resulting asymptotic solution becomes the plane wave for the neutral particle and the exact two-body scattering wave function for the charged pair. However, neither the Redmond's asymptotic term nor the 3C wave function is asymptotic solution of the Schrödinger equation in the asymptotic domains  $\Omega_\nu$ , where particles of pair  $\nu$  are close to each other and far away from particle  $\nu$ ,  $\nu = \alpha, \beta, \gamma$ . Redmond's asymptotic term, by construction, satisfies the asymptotic Schrödinger's equation up to terms  $O(1/r_\alpha^2, 1/r_\beta^2, 1/r_\gamma^2)$ , where  $r_\alpha$  is the distance between particles  $\beta$  and  $\gamma$ . However, in the asymptotic region,  $\Omega_\nu$ , where the distance between the particles of pair  $\nu$  is limited, the terms  $O(1/r_\nu)$  are not small and the potential  $V_\nu^c$  in the Schrödinger's equation has to be compensated exactly rather than asymptotically as happens when we use the Redmond's asymptotic wave function in  $\Omega_0$ . In the 3C wave function two very important effects are absent. Consider, for example, the asymptotic region  $\Omega_\alpha$ . In this region the two-body relative motion of particles  $\beta$  and  $\gamma$  is distorted by the Coulomb field of the third particle  $\alpha$  [5]. The second evident defect in the 3C function is the absence of the nuclear interaction between particles  $\beta$  and  $\gamma$  which can be close enough to each other in  $\Omega_\alpha$ . Nevertheless, the 3C wave function can be used as a starting point to derive the leading asymptotic terms of the three-body incident wave in  $\Omega_\alpha$  [5,6], because this asymptotic three-body incident wave should match the Redmond's asymptotic term in  $\Omega_0$ . We demonstrated how important the condition of the matching of the asymptotic wave functions on the border of different asymptotic regions [5].

In this work the asymptotic wave function derived in [6] has been further improved in the region, where the particles of pair  $\alpha$  remain close to each other while the third particle  $\alpha$  is far away from them. The improved wave function satisfies the Schrödinger equation up to the terms of order  $O(1/\rho_\alpha^3)$ , where  $\rho_\alpha$  is the distance between the center of mass of the system  $\beta + \gamma$  and the third particle  $\alpha$ , and gives further insight into the continuum behavior of the three charged particles wave function. It opens up further possibilities to solve and analyze the three body Schrödinger equation by numerical means. It is

worth mentioning that the asymptotic solution satisfying the Schrödinger equation in the asymptotic region  $\Omega_v$  up to the  $O(1/\rho_v^2)$  can be found analytically [5,6]. To find an asymptotic solution satisfying the Schrödinger equation in  $\Omega_v$  up to terms of  $O(1/\rho_v^3)$  we need to solve the two-body type differential equations numerically. The next order term in the asymptotic three-body scattering wave function represents the outgoing  $3 \rightarrow 3$  scattered wave and can be found only by a numerical solution of the three-body Schrödinger equation or Faddeev equations.

- [1] S. P. Merkuriev and L. D. Faddeev, *Kvantovaya Teoriya Rasseyaniya dlya System Neskol'kich Tschastits* (Nauka, Moscow, 1985) (in Russian).
- [2] P. J. Redmond (unpublished).
- [3] L. Rosenberg, *Phys. Rev. D* **8**, 1833 (1973).
- [4] C. R. Garibotti and I. E. Miraglia, *Phys. Rev. A* **21**, 572 (1980).
- [5] E. O. Alt and A. M. Mukhamedzhanov, *Phys. Rev. A* **47**, 2004 (1993).
- [6] A. M. Mukhamedzhanov and M. Lieber, *Phys. Rev. A* **54**, 3078 (1996).

## Determination of the Parameters of a Skyrme Type Effective Interaction Using an Extensive Set of Experimental Data

B. K. Agrawal, S. Shlomo, and V. Kim Au

We have fitted the values of the Skyrme parameters to an extensive set of experimental data together with few additional constraints: (i) the quantity  $P = 3\rho \frac{dS}{d\rho}$ , directly related to the slope of the symmetry energy  $S$ , must be positive for the densities up to  $3\rho_0$ ; a condition imposed by the neutron star model, (ii) the enhancement factor  $\kappa$ , associated with the Thomas-Reiche-Kuhn sum rule for the isovector giant dipole resonance, should lie in the range of 0.1-0.5 and (iii) the Landau parameter  $G_0'$ , crucial for the spin properties of finite nuclei and nuclear matter, should be positive at  $\rho = \rho_0$ . We have carried out two different fits named as KDE0 and KDE, without and with the exchange Coulomb term, respectively. The nuclear matter properties for both interactions proposed in the present work are obtained directly from the fit. The selection of the experimental data in conjugation with some constraints ensures that these interactions can be used to study the bulk ground state properties of nuclei ranging from the stable to the ones near the proton and neutron drip lines as well as the properties of neutron stars. The interactions obtained in the present work encompasses the merits of the SKX and SLy type of Skyrme interactions. The values obtained for the KDE0 and KDE Skyrme parameters are given in the table [1].

Parameter	KDE0	KDE	SLy7
$t_0$ (MeV.fm <sup>3</sup> )	-2526.5109 (140.63)	-2532.88 (115.32)	-2482.41
$t_1$ (MeV.fm <sup>5</sup> )	430.9417 (16.67)	403.73 (27.63)	457.97
$t_2$ (MeV.fm <sup>5</sup> )	-398.377 (27.31)	-394.56 (14.26)	-419.85
$t_3$ (MeV.fm <sup>3(1+<math>\alpha</math>)</sup> )	14235.5192 (680.73)	14575.0 (641.99)	13677.0
$x_0$	0.75827 (0.0655)	0.7707 (0.0579)	0.8460
$x_1$	-0.308711 (0.0165)	-0.5229 (0.0298)	-0.5110
$x_2$	-0.949459 (0.0179)	-0.8956 (0.0270)	-1.000
$x_3$	1.14447 (0.0862)	1.1716 (0.0767)	1.3910
$W_0$ (MeV.fm <sup>5</sup> )	128.9648 (3.33)	128.06 (4.39)	126.00
$\alpha$	0.01676 (0.0163)	0.1690 (0.0144)	0.1667

[1] B. K. Agrawal, S. Shlomo, and V. Kim Au, Phys. Rev. C (accepted).

## Viscosity Effects on Isoscalar Compression Modes

A. G. Pochivalov, S. Shlomo and V. M. Kolomietz<sup>1</sup>

<sup>1</sup>*Institute for Nuclear Research, Kiev 03680, Ukraine*

Experimental data for the isoscalar giant monopole (ISGMR) and dipole (ISGDR) resonances indicate that the centroid energy  $E1$  of the ISGDR is significantly smaller than those obtained by the self-consistent Hartree Fock (HF) random phase approximation (RPA) calculations with effective interactions, which reproduce the experimental values of the centroid energy  $E0$  of the ISGMR. Moreover, the experimental value  $E1/E0$  is close to the prediction of the liquid drop model (LDM) and lies below the theoretical results for the ratio  $E1/E0$  obtained in both the RPA and the scaling-like calculations. The energies of both ISGMR and ISGDR are shifted to higher values with respect to the LDM prediction because of the Fermi surface distortion effect (FSDE) [1]. On the other hand the FSDE depends significantly on the interparticle collisions and disappears in the limit of short relaxation time. Thus, one can expect the ratio  $E1/E0$  can approach the experimental value if the collisional damping is taken into account.

We aim in this work to investigate the effect of collisional damping on the isoscalar compression modes, and find that one can account for the experimental data for the ratio  $E1/E0$  and for the widths of the ISGMR and the ISGDR in the case of short relaxation time. We apply the nuclear fluid dynamic approach (FDA) [1] with the effect of relaxation (collisional damping effect). We start from the fluid dynamic equations of motion for the viscous Fermi liquid. Within the FDA, the eigenfrequency  $\omega$  of the compression eigenmodes satisfies the dispersion equation

$$\omega^2 - c_0^2(\omega)q^2 + i\omega\gamma(\omega)q^2 = 0, \quad c_0^2(\omega) = [K + 12\mu(\omega)/\rho_0]/9m, \quad \gamma(\omega) = 4\nu(\omega)/3\rho_0m, \quad (1)$$

where  $K$  is the incompressibility,  $\rho_0$  is the bulk particle density and  $m$  is the nucleon mass. The transport coefficients  $\mu(\omega)$  and  $\nu(\omega)$  in Eq. (1) are derived by the Fermi distortion effects [1] and depend on the relaxation time  $\tau$ . The wave number  $q$  in Eq. (1) is derived by the boundary conditions on the free surface of the nucleus which are significantly different for the ISGMR and the ISGDR because the ISGDR appears as the overtone to the spurious mode. We have solved the dispersion equation (1) augmented by the corresponding boundary condition for both ISGMR and ISGDR for several nuclei. We find that the ratio  $(E1/E0)_{\text{FDA}}$  depends on the relaxation time and approaches the experimental value  $(E1/E0)_{\text{exp}} = 1.5 \pm 0.1$  in a short relaxation time limit at  $\tau = 10^{-22}$  s. In rare collision regime ( $\omega\tau \ll 1$ ), the compression mode energies  $E0$  and  $E1$  are saturated at certain values which correspond to the zero sound velocity  $c_0 = [K + (24/5)\epsilon_F/9m]^{1/2}$  ( $\epsilon_F$  is the Fermi energy). In frequent collision regime ( $\omega\tau \gg 1$ , small), the contribution to the sound velocity  $c_0$  from the Fermi surface distortion effect is washed out and both energies  $E0$  and  $E1$  reach the first sound limit (i.e., the LDM regime) at  $c_0 = c_1 = (K/9m)^{1/2}$ . We note also the non-monotonic behavior of the widths  $\Gamma_0$  and  $\Gamma_1$  for the ISGMR and the ISGDR, respectively, which is a consequence of the memory effect ( $\omega$ -dependence) in the friction coefficient  $\gamma(\omega)$  of Eq. (1).

[1] V.M. Kolomietz and S. Shlomo, Phys. Rev. C **61**, 064302 (2000).

## Structure of Isovector Excitation Mode in Spherical Asymmetric Nuclei

V. M. Kolomietz<sup>1</sup>, A. G. Magner<sup>1</sup> and S. Shlomo

<sup>1</sup>*Institute for Nuclear Research, Kiev 03680, Ukraine*

The two bump structure (splitting) of the isovector giant dipole resonance (IVGDR), which is observed in the isospin conjugate photonuclear ( $\gamma, n$ ) and ( $\gamma, p$ ) reactions, is often explained as a phenomenon of the nuclear isospin asymmetry within the isospin splitting model (ISM). The ISM assumes that both the main peak and the satellite correspond, respectively, to the two different isospins  $T_{\square}+1$  and  $T_{\square}$ , where  $T_{\square} = (N-Z)/2$  is the isospin of the ground state of the nucleus. Another IVGDR splitting caused by deformations of the nucleus is observed in the photonuclear and electronic inelastic scattering reactions. In this case, the energy splitting  $\Delta E$  between two component of the IVGDR is proportional to the deformation  $\delta = \Delta R/R$ . However, experimental data indicate that the splitting of the isovector giant resonances into two or more peaks is a more general effect than the one obtained in the conjugate ( $\gamma, n$ ) and ( $\gamma, p$ ) reactions or in deformed nuclei.

We suggest a quite general explanation of the splitting of both the isoscalar and the isovector modes in spherical neutron-rich nuclei within the Fermi-liquid-drop model (FLDM) based on the Landau kinetic theory [1]. The FLDM provides the existence of the isoscalar and isovector vibrations related to the two different dimensionless zero-sound velocities  $s$  and  $s'$ . They are determined by the isoscalar and the isovector Landau interaction amplitudes, respectively. Due to the macroscopic self-consistency and the boundary condition on the free nuclear surface the FLDM shows a new satellite structure of the isovector and isoscalar giant multipole resonances. For large enough nuclear mass number  $A$ , we have obtained a simple estimate for the energy splitting  $\Delta E$  of the IVGDR

$$\Delta E \approx (10/3)^{3/2} \varepsilon_F^2 F_0' / b_{s,-} A^{2/3},$$

where  $\varepsilon_F$  is the Fermi energy,  $F_0'$  is the Landau's interaction amplitude in isovector channel and  $b_{s,-}$  is the isovector surface tension parameter. This result shows that the splitting effect depends significantly on the effective volume ( $F_{\square}'$ ) and surface ( $b_{s,-}$ ) isovector interactions such that it is proportional to their ratio  $F_{\square}'/b_{s,-}$ , and does not depend on the neutron excess  $N-Z$ . We have performed calculations of the characteristics (energy  $E_{\text{GDR}}$  of the main IVGDR and its satellite, their relative strength  $m^{(s)}/m^{(m)}$  and the depletion of the energy weighted sum rule (EWSR),  $m_1/m_{\text{EWSR}}$ ) of the isovector giant dipole resonance (IVGDR) and its satellite for several isotopes of Ca, Sn and Sm nuclei. The splitting magnitude in our FLDM almost does not depend on the neutron excess  $N-Z$ . This is in contrast to another splitting effect predicted by the ISSM which shows an increase of the energy splitting of the IVGDR with the isospin quantum number  $T_3=(N-Z)/2$ . The satellite strength ratio  $m^{(s)}/m^{(m)}$  is small and increases linearly with the asymmetry parameter  $X = (N-Z)/A$  in contrast to both the opposite ISSM-splitting behavior like  $1/T_3$  and the case of splitting due to deformation in the collective model, with approximately equivalent strengths of the peaks. The relative strengths and the depletion of the EWSR for all (Fermi-liquid) satellites turn

into zero and they disappear in the symmetric limit  $N=Z$ . The strength ratios of the two peaks and their depletion of the EWSR are in agreement with the experimental results.

[1] V.M. Kolomietz and S. Shlomo, Phys. Rep. **390**, 133 (2004).

## Effects of Self-Consistency Violations in HF-RPA Calculations for Giant Multipole Resonances

Tapas Sil, S. Shlomo, B. K. Agrawal and P.-G. Reinhard<sup>1</sup>

<sup>1</sup>*Institut für Theoretische Physik, Universität Erlangen, W-8520 Erlangen, Germany.*

The study of collective modes in nuclei provides very important information for understanding the structural and bulk properties of nuclear systems. In particular, the isovector giant dipole (IVGDR) mode is sensitive to the symmetry energy and the centroid energy  $E_{\text{cen}}$  of the isoscalar giant monopole resonance (ISGMR) allows us to extract the value of the incompressibility modulus  $K$  of symmetric nuclear matter. These quantities are important ingredients not only for the description of the finite nuclei but also for the study of heavy-ion-collisions, supernovae and neutron stars. Recent developments in high precision experimental facilities in our Cyclotron Institute make it possible to measure the centroid energy of ISGMR with an error of  $\delta E_{\text{cen}} \sim 0.1-0.3$  MeV. This leads to an error of 7 MeV for  $K=230$  and  $E_{\text{cen}}=13.96\pm 0.20$  MeV for  $^{208}\text{Pb}$ , since one has  $(\delta K)/K = 2(\delta E_{\text{cen}})/E_{\text{cen}}$ . Therefore the theoretical calculation should be highly accurate so that the error in the calculated value of  $E_{\text{cen}}$  is less than the experimental error.

The basic theory for the microscopic description of modes of giant resonances is the Hartree-Fock (HF) based random phase approximation (RPA). A very accurate calculation within HF+RPA demands self-consistency, i.e., exactly the same interaction has to be used in carrying out the HF and the RPA calculations. Most of the presently available HF+RPA calculations are contaminated by the problem of self-consistency violation (SCV) caused by neglecting the particle-hole (ph) spin-orbit and Coulomb interactions in carrying out the RPA calculations. In Ref. [1], results of elaborate studies of the effects of (SCV) on the constrained energy ( $E_{\text{con}}$ ) and scaling energy ( $E_s$ ) have been reported only for the ISGMR. In order to estimate the error due to SCV,  $E_{\text{con}}$  and  $E_s$  were calculated in HF+RPA with some of the interactions (spin-orbit or Coulomb) turned on in HF calculation but missing in the RPA level and the results were compared with those obtained using the fully self-consistent constrained or scaling approaches within Hartree-Fock. It was pointed out [1] that the violation of self-consistency through spin-orbit and Coulomb interactions between the HF and RPA levels might cause an error in  $E_{\text{con}}$  of the ISGMR as large as 5 times the experimental error. We note that in Ref. [1] the effect of SCV on the  $E_{\text{cen}}$  could not be estimated, since fully self-consistent HF-RPA calculation, with the ph spin-orbit and Coulomb interactions included in the RPA, was not carried out. In this work, we investigated the effects of SCV on  $E_{\text{cen}}$ , obtained by carrying out highly accurate fully self-consistent HF-RPA calculations of the response functions and their energy moments. Moreover, we have not restricted our investigation to the ISGMR and considered the isoscalar and isovector modes of multi-polarities  $L=0-3$  in a wide range of nuclei.

We have quantified very accurately [2] the effects of self-consistency violations in the calculations of the energies of giant resonances of nuclei within the Hartree-Fock based random phase approximation. We have studied the cases of SCV due to the omission of the spin-orbit (LS) or/and Coulomb (CO) ph interactions and mainly focus on their effects on the centroid energy  $E_{\text{cen}}$ . Here we

consider both isoscalar and isovector modes of multipolarities  $L=0-3$ . It is found, for the wide range of nuclei considered here, that the effects of violations of self-consistency due to the ph LS or CO interactions are most significant for the ISGMR. For the ISGMR, the absence of the ph LS interaction tends to increase  $E_{\text{cen}}$ , whereas the violation due to ph CO interaction decreases  $E_{\text{cen}}$ . For the spin unsaturated nuclei (such as  $^{56}\text{Ni}$ ,  $^{100}\text{Sn}$ ), the shift of  $E_{\text{cen}}$  is robust ( $\sim 1.5$  MeV) which is almost 5 times larger than the experimental uncertainty. For other higher multi-polarities, the individual effects of the ph LS and CO interactions are somewhat smaller than those for the ISGMR. But for the quadrupole and octopole modes, the LS and CO self-consistency violations both tend to reduce the centroid energy. Hence, the effect of SCV on  $E_{\text{cen}}$  in these modes is significant ( $\sim 0.5$  MeV) if one neglects the ph spin-orbit and Coulomb interactions simultaneously in the RPA calculation.

[1] B. K. Agrawal and S. Shlomo, Phys. Rev. C **70**, 014308 (2004).

[2] T. Sil, S. Shlomo, B. K. Agrawal and P. -G. Reinhard, Phys. Rev. C (submitted).

## Non-Markovian Langevin Dynamics of Nuclear Fermi Liquid Drop

V.M. Kolomietz,<sup>1</sup> S.V. Radionov,<sup>1,2</sup> and S. Shlomo

<sup>1</sup>*Institute for Nuclear Research, Kiev 03680, Ukraine*

<sup>2</sup>*Matematisk Fysik, LTH, Lunds Universitet, Lund, Sweden*

One of the important features of the nuclear large amplitude dynamics is its dissipative character or, the presence of the time irreversible energy flow from the collective degrees of freedom to the nucleonic ones. On the other hand, the experimental observation of the finite variance of the kinetic energy of the fission fragments manifests the fact that fluctuations have to be also associated with the collective variables. Both the dissipation and the fluctuations can be described by the introduction of the friction and random forces connected to each other by the fluctuation-dissipation theorem. In this respect, the Fokker-Planck or Langevin approaches can be used to study the nuclear large scale dynamics (nuclear fission, heavy ion collisions, etc.) [1].

We study the influence of the memory effects on some prescission characteristics of the fissioning nucleus. Starting from the collisional kinetic equation with a random force we derive the memory-dependent Langevin equation of motion for the nuclear shape parameter. Considering a spheroidal nucleus, the nuclear shape is parametrized by the parameter  $q$  of the total elongation and the collective potential energy in the region from the barrier to the scission point is approximated by an inverted oscillator. The position of the nuclear scission  $q_{sc}$  is defined from the difference of 28 MeV in the potential energy between the saddle  $q_f$  and scission  $q_{sc}$  points for the nucleus  $^{236}\text{U}$ . Solving the generalized Langevin equation, we have obtained analytical expressions for the mean value  $\langle E_{kin} \rangle$  and the variance  $\sigma^2(E_{kin})$  of the collective kinetic energy. We have found that both quantities  $\langle E_{kin} \rangle$  and  $\sigma^2(E_{kin})$  are sensitive to the variations of the saddle-to-scission time  $t_{sc}$ , arising from the random force contribution to the equation of motion. We have also studied the pre-scission kinetic energy,  $\langle E_{kin,ps} \rangle$ , of the fissioning nucleus assuming that  $\langle E_{kin,ps} \rangle$  is given by the kinetic energy  $\langle E_{kin,ps} \rangle$  at  $t = t_{sc}$ , where the saddle-to-scission time  $t_{sc}$  is obtained in the absence of the random force. The results of numerical calculations within our non-Markovian Langevin-like approach provide smaller values of  $\langle E_{kin,ps} \rangle$  and  $\sigma^2(E_{kin,ps})$  than those obtained within the traditional Markovian Langevin approach. The lowering of the values of  $\langle E_{kin,ps} \rangle$  and  $\sigma^2(E_{kin,ps})$  for the non-Markovian dynamics can be explained as a result of the presence of the additional elastic force coming from the memory integral in the equation of motion for shape variable  $q$ . The memory integral (retarded force) is split into the dissipative friction and time-reversible elastic forces [2]. The latter is caused by the Fermi-surface distortion and acts against the adiabatic force, slowing down the descent from the barrier. This phenomena reflects itself in the lowering of the mean values and the fluctuations of the velocity at the scission point and leads to the lowering of  $\langle E_{kin,ps} \rangle$  and  $\sigma^2(E_{kin,ps})$ .

[1] V.M. Kolomietz and S. Shlomo, Phys. Rep. **390**, 133 (2004).

[2] V.M. Kolomietz, S.V. Radionov and S. Shlomo, Phys. Rev. C **64**, 054302 (2001).

## **SECTION IV**

# **ATOMIC, MOLECULAR AND MATERIALS SCIENCE**

## Ratio of Double to Single $L$ -shell Ionization of Holmium Atoms

V. Horvat, R. L. Watson, and Yong Peng

Spectra of  $L$  x rays emitted from Ho targets bombarded by 6 MeV/amu C, Ne, Ar, Kr, and Xe ions were measured in high resolution using a curved crystal spectrometer, employing second-order diffraction from a LiF crystal. The spectra were analyzed in order to examine the systematic evolution of the  $L$  x-ray satellite structure as a function of projectile atomic number. A relatively simple interpretation of the structure in the measured spectra, based on the Independent Electron Approximation and Dirac-Fock calculations, was used to develop an analysis procedure that reproduced the shape of the spectra with reasonably good accuracy. It was found that transitions from atoms with single  $L$ - and multiple  $M +$  outer-shell vacancies in the initial state dominate the spectra. In addition, contributions from  $L$  x rays emitted by atoms with two or three  $L$  vacancies in the initial state were clearly identified [1]. These contributions were found to account for up to 21% of the total  $L$  x-ray intensity.

In this reporting period, the results obtained in the analysis of the spectra were used to establish scaling rules for the apparent average double to single  $L$ -vacancy population ratio at the time of  $L$  x-ray emission. The results were then compared with those obtained for  $K$ -vacancy populations at the time of  $K$  x-ray emission for Co, Ni, and Cu atoms, since their  $K$  binding energies are comparable to Ho  $L$  binding energies.

In the Independent Electron Approximation [2], the cross section ( $\sigma_m$ ) for the removal of exactly  $m$  electrons from a shell containing  $N$  electrons ( $m \leq N$ ) is expressed in terms of the single-electron ionization probability  $p(b)$  as

$$\sigma_m = 2\pi \int_0^{\infty} \binom{N}{m} p(b)^m [1 - p(b)]^{N-m} b db, \quad (1)$$

where  $b$  is the impact parameter. If  $p(b)$  is approximated by an exponential decay function [3],

$$p(b) = p_o \exp(-b/r), \quad (2)$$

in which  $p_o$  and  $r$  are parameters that do not depend on  $b$ , then

$$\sigma_m = 2\pi r^2 \binom{N}{m} p_o^m \sum_{i=0}^{N-m} (-1)^i \binom{N-m}{i} p_o^i / (m+i)^2. \quad (3)$$

In this approximation, the ratio  $\sigma_2/\sigma_1$  depends only on  $p_o$  and not on  $r$ . The parameter  $p_o = p(0)$  is the ionization probability per electron at impact parameter equal to zero. The solid lines in Fig. 1(a) represent the values of  $\sigma_2/\sigma_1$  for  $L$ -vacancy production in Ho and  $K$ -vacancy production in Ni, calculated using eq.(3) and plotted as a function of  $p_o$ .

According to the Geometrical Model [4], ionization probabilities per electron ( $p_n$ ) for near-central collisions should lie on a universal curve when plotted as a function of the Universal Variable ( $X_n$ ), given by

$$X_n = 4V[G(V)]^{1/2} Z_1 / (nv_1) \quad (4)$$

In eq.(4),  $Z_1$  is the projectile atomic number,  $v_1$  is its speed in atomic units,  $n$  is the principal quantum number of the ionized target electron,  $V = v_1 / v_2$  is the scaled projectile speed ( $v_2$  is the average target electron speed prior to ionization), and  $G(V)$  is the Binary Encounter Approximation (BEA) scaling function [5], originally formulated to describe universal scaling of the cross sections for inner-shell ionization.

Based on the results obtained in the analysis of Ho  $L$  and Co, Ni, and Cu  $K$  x-ray spectra, the scaling predicted by the Geometrical model was found to apply to  $p_n^x$ , the apparent average  $n$ -vacancy fraction at the time of x-ray emission, provided that the x-ray transition results in filling of a vacancy in the shell specified by a quantum number  $n'$ , such that  $n' < n$ . Specifically, it was found experimentally [6] that

$$p_n^x = a / [1 + (b / X_n)^c] , \quad (5)$$

where  $a = 0.579 \pm 0.016$ ,  $b = 1.86 \pm 0.11$ , and  $c = 1.95 \pm 0.09$ .

The values of  $p_n^x$  obtained using eq.(5) can be compared to the  $p_o$  value obtained using eq.(2) under the assumption that the net effect of post-collision vacancy rearrangement and fluorescence yield enhancement is small. This assumption was found to be reasonably valid (within 10 to 20%) based on a previous analysis of these effects on the  $p_L^x$  values for  $K$ -shell ionizing collisions involving a Cu target and 10 MeV/amu projectiles ranging in atomic number from 10 (Ne) to 83 (Bi) [7].

The apparent average double to single  $K$ -vacancy population ratio at the time of  $K$  x-ray emission in Co, Ni, and Cu ( $R_{2/1}^K$ ), and the apparent average double to single  $L$ -vacancy population ratio at the time of  $L$  x-ray emission in Ho ( $R_{2/1}^L$ ) were determined in analyses of the Co, Ni, and Cu  $K$  x-ray spectra and the Ho  $L$  x-ray spectra, respectively. Under the assumption that the net effects of post-collision vacancy rearrangement and fluorescence yields on the double and single vacancy decays are nearly the same, this ratio is approximately equal to the ratio of the double and single vacancy production cross sections.

The values of  $\sigma_2/\sigma_1$  obtained using eq.(3) (as shown in Fig. 1a) are compared with the measured values of  $R_{2/1}^L$  and  $R_{2/1}^K$ , for which the corresponding values of  $p_o$  (i.e.  $p_n^x$  for  $n = 2$  and  $n = 1$ , respectively) were determined using eq.(5). The calculations agree with both sets of measured data reasonably well. Predicted values of  $\sigma_2/\sigma_1$  can also be presented as universal functions of  $X_n$  [eq.(4)] by expressing  $p_o$  in eq.(3) in terms of the Universal Variable using either the empirical curve [eq.(5)] or the curve predicted by the Geometrical Model, given by

$$p_n = X_n^2 / \{4.2524 + X_n^2 [1 + 0.5 \exp(-X_n^2 / 16)]\} . \quad (6)$$

Both results are shown in Fig. 1(b) and compared with the experimental data. Predictions of this model agree reasonably well with both sets of measured data. The general validity of these results remains to be tested experimentally for different collision parameters.

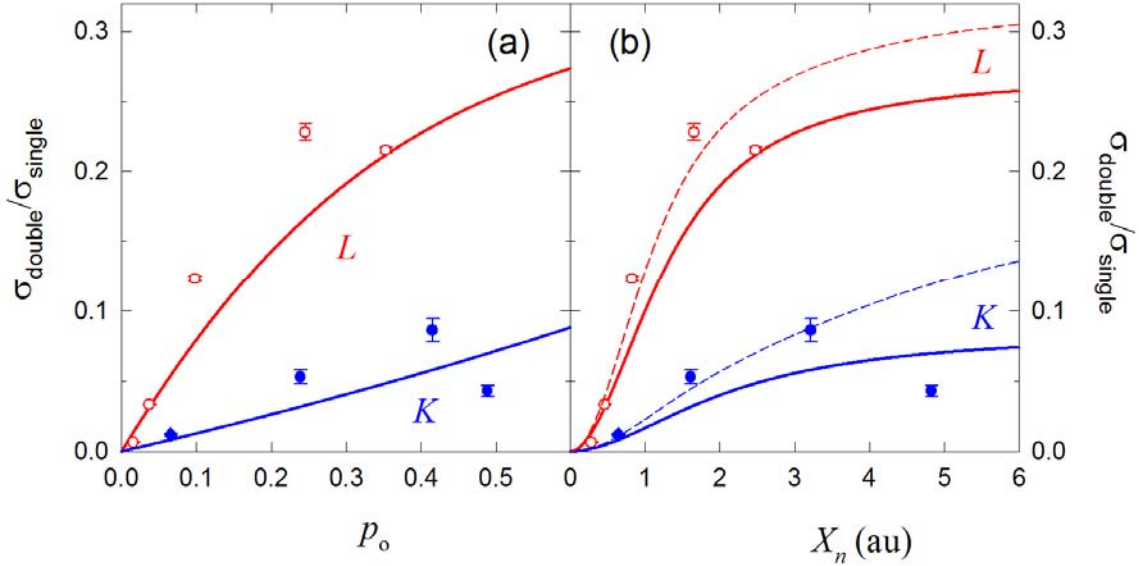


**Figure 1.** Double-vacancy production to single-vacancy production cross section ratios ( $\sigma_2/\sigma_1$ ), calculated using eq.(3), plotted (a) as a function of the single-electron ionization probability at small impact parameters ( $p_0$ ) and (b) as a function of the corresponding Universal Variable ( $X_n$ ) determined using eq.(5). The solid lines represent the results for the  $L$ -shell ionization of Ho (red) and  $K$ -shell ionization of Ni (blue). Also shown are the measured values of  $R_{2/1}^L$  (open circles) and  $R_{2/1}^K$  (solid circles), for which  $X_n$  was determined using eq.(4) and the corresponding values of  $p_0$  were determined as  $p_n^x$  (for  $n = 2$  and  $n = 1$ , respectively) using eq.(5). The data point shown by the solid diamond (measured using a 6 MeV/amu N beam on a Ni target) was taken from Ref.[8]. The dashed lines represent the universal function predicted by the Geometrical Model, as given by eq.(6).

- [1] V. Horvat *et al.*, *Progress in Research*, Cyclotron Institute, Texas A&M University (2003-2004) p. IV-3.
- [2] J. H. McGuire and L. Weaver, *Phys. Rev. A* **16**, 41 (1977).
- [3] T. Tonuma, H. Shibata, S. H. Be, H. Kumagai, M. Kase, T. Kambara, I. Kohno, A. Ohsaki, and H. Tawara, *Phys. Rev. A* **33**, 3047-3053 (1986).
- [4] B. Sulik, I. Kadar, S. Ricz, D. Varga, J. Vegh, G. Hock, and D. Berenyi, *Nucl. Instrum. Methods Phys. Res. B* **28**, 509 (1987).
- [5] J. H. McGuire and P. Richard, *Phys. Rev. A* **9**, 1374 (1973).
- [6] V. Horvat *et al.*, *Progress in Research*, Cyclotron Institute, Texas A&M University (2003-2004) p. IV-6.
- [7] R. L. Watson, J. M. Blackadar, and V. Horvat, *Phys. Rev. A* **60**, 2959 (1999).

[8] Y. Aways, T. Kambara, Y. Kanai, *Int. Jour. Mass Spectrom.* **192**, 49 (1999).

## Cross Sections for Electron Stripping of Light Fully Stripped Ions by Hydrogen and Helium Atoms

I. D. Kaganovich,<sup>1</sup> E. A. Startsev,<sup>1</sup> R. C. Davidson,<sup>1</sup> S. R. Kecskemeti,<sup>1</sup> A. Bin-Nun,<sup>1</sup> D. Mueller,<sup>1</sup>  
L. Grisham,<sup>1</sup> R. L. Watson, V. Horvat, K. E. Zaharakis, Y. Peng  
<sup>1</sup>*Plasma Physics Laboratory, Princeton University, Princeton, NJ 08543*

Ions may lose electrons as they pass through residual gas in accelerators, beam transport lines, and target chambers. As a result, the ion beam transmission and the quality of beam focus are reduced. Therefore, it is important to assess the values of projectile stripping cross sections in ion–atom collisions. In contrast to ionization by electrons and protons, where extensive experimental and theoretical results exist for a large variety of atoms and ions, the knowledge of cross sections for stripping of fast complex ions by atoms is far from complete [1]. Here we use the term “stripping” for projectile electron loss in a collision with a stationary atom or an ion, and the term “ionization” for target electron loss in the collision with a projectile. However, the two terms describe the same process from two different frames of reference, and so the same approach can be used to describe both stripping and ionization.

In Fig. 1, the measured cross sections [2] for ionization of a hydrogen atom in a collision with selected light fully stripped light ions ( $H^+$ ,  $He^{2+}$ ,  $Li^{3+}$ , and  $C^{6+}$ ) are compared with predictions of the existing theories as a function of the projectile scaled speed. The scaled projectile speed is the projectile speed ( $v$ ) divided by the average orbital speed of the target electron ( $v_{nl}$ ). Evidently, the Bethe formula [3] is good for projectile speeds larger than the average electron orbital speed. At large projectile speed, the Gerjuoy, Garcia and Vriens (GGV) formula [4] underestimates the cross sections, whereas the Gryzinski formula [5] yields results close to those of the Bethe formula and the experimental data. The Bethe, GGV and Gryzinski formulas all fail at small projectile speeds because they assume that target electrons are localized and neglect their motion during the collision.

Here we propose a new semiempirical formula that has no fitting parameters and is correct for small and large projectile speeds:

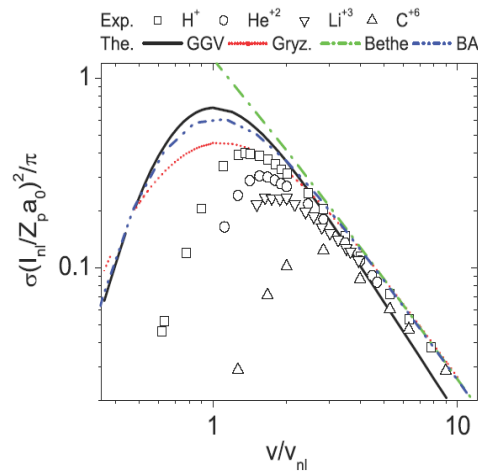


**Figure 1.** Scaled cross-sections for ionization of atomic hydrogen by selected fully stripped ions. Both experimental data [2] and theoretical curves are shown. Bethe stands for Bethe’s quantum-mechanical calculation in the Born approximation [3] limited to  $v > v_{nl}$ . GGV stands for the classical calculation by Gerjuoy using the fitted target electron velocity distribution of Garcia and Vriens [4], and Gryz denotes the Gryzinski approximation [5]. Finally, BA denotes the Born approximation in the general case [6]. All values are in atomic units.

$$\sigma = \pi a_o^2 \frac{Z_p^2 E_o^2}{Z_p + 1 I_{nl}^2} G(V), \quad (1)$$

where

$$G(V) = \exp(-V^{-2})[1.26 + 0.283 \ln(2V^2 + 25)]/V^2 \quad (2)$$

and

$$V = \frac{v}{v_{nl} \sqrt{Z_p + 1}}. \quad (3)$$

Here  $\sigma$  is the cross section for ionization of a hydrogen target atom,  $a_o = 52.9$  pm is the Bohr radius, and  $Z_p$  is the projectile atomic number, and  $I_{nl} / E_o = 0.5$  is the ionization potential of hydrogen in its ground state expressed in atomic units ( $E_o = 27.2$  eV).

The cross sections scaled based on eqs.(1-3) are shown in Fig. 2. Evidently the scaling shown in Fig. 2 is much better than the scaling shown in Fig. 1, as the presented experimental data in Fig. 2 seem to outline a universal curve. The newly proposed semiempirical formula [eqs. (1-3)] was also found to apply to the collisions involving helium target atoms.

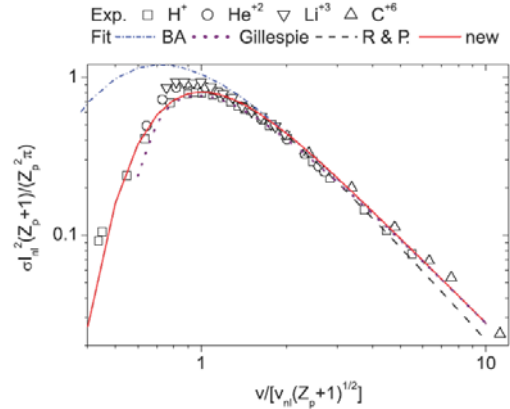


**Figure 2.** Scaled cross-sections for ionization of atomic hydrogen by selected fully stripped ions. Both experimental data [2] and theoretical curves are shown. BA denotes the Born approximation [6]. Gillespie denotes Gillespie's fit [7]. R.&P. denotes the fit proposed by Rost and Pattard [8]. New denotes the newly proposed semiempirical formula [eqs. (1-3)].

- [1] R.K. Janev, L.P. Presnyakov, V.P. Shevelko, *Physics of Highly Charged Ions*, Springer, Berlin, 1999.
- [2] M. B. Shah, D. S. Elliott, and H. B. Gilbody, *J. Phys. B* **20**, 2481 (1987); C. F. Barnett ed., *Atomic Data for Fusion. Volume 1: Collisions of H, H<sub>2</sub>, He and Li Atoms and Ions with Atoms and Molecules*, ORNL-6086 (1990); R. A. Phaneuf, R. K. Janev, and M. S. Pindzola, *Atomic Data for Fusion. Volume 5: Collisions of Carbon and Oxygen Ions with Electrons, H, H<sub>2</sub> and He*, ORNL-6090 (1987); <http://www-cfadc.phy.ornl.gov/redbooks/> (Note that data for carbon ions are semiempirical. Only one data point at 400keV/amu was measured and the rest of the data are reproduced using Gillespie's fit [7].); M. B. Shah and H. B. Gilbody, *J. Phys. B* **15**, 413 (1982).
- [3] H. Bethe, *Ann. Phys. (Leipz.)* **5**, 325 (1930).
- [4] E. Gerjuoy, *Phys. Rev. A* **148**, 54 (1966); L. Vriens, *Proc. R. Soc. London* **90**, 935 (1966).
- [5] M. Gryzinski, *Phys. Rev. A* **138**, 322 (1965).
- [6] H. A. Bethe and R. Jackiw, *Intermediate Quantum Mechanics*, The Benjamin/Cummings Publishing Company, 2<sup>nd</sup> ed., 1968.
- [7] G. Gillespie, *J. Phys. B* **15** (1982) L729; *G. Gillespie, Phys. Lett.* **93A**, 327 (1983).
- [8] J. M. Rost and T. Pattard, *Phys. Rev. A* **55**, R5 (1997).

## A Hybrid Approach to the Calculation of Cross Sections for Electron Stripping

I. D. Kaganovich,<sup>1</sup> E. A. Startsev,<sup>1</sup> R. C. Davidson,<sup>1</sup> S. R. Kecskemeti,<sup>1</sup> A. Bin-Nun,<sup>1</sup> D. Mueller,<sup>1</sup>  
L. Grisham,<sup>1</sup> R. L. Watson, V. Horvat, K. E. Zaharakis, Y. Peng

<sup>1</sup>*Plasma Physics Laboratory, Princeton University, Princeton, NJ 08543*

Recently, we have investigated (theoretically and experimentally) collisions involving more than 18 different pairs of projectile and target species in the energy range of 3–38 MeV/amu and examined the applicability of existing theories to the determination of projectile stripping cross sections. The systems considered included 3.4 MeV/amu Kr<sup>7+</sup> and Xe<sup>11+</sup> in N<sub>2</sub> [1]; and 10.2 MeV/amu Ar<sup>6+</sup>, 19 MeV/amu Ar<sup>8+</sup>, 30 MeV/amu He<sup>+</sup> and 38 MeV/amu N<sup>6+</sup> all in He, N<sub>2</sub>, Ar and Xe [2].

The results for He<sup>+</sup> and N<sup>6+</sup> are shown in Table 1. The trend of all the measured data shows that cross sections calculated in the Born approximation agree better with experimental data for the lightest target atoms (He), while the classical results agree better with the experimental data for heaviest target atoms (Xe). In most other cases (N<sub>2</sub> and Ar targets) the Born approximation and the classical trajectory method yield results that are comparable to each other and in agreement with the measurements. The existing discrepancies for the lightest and the heaviest targets are a consequence of applying a particular theoretical method outside its validity region. In an effort to unify the theoretical approach, a hybrid method was developed that combines the Born approximation and the classical trajectory calculations, and applies one or the other, whichever is more applicable, depending on the collision parameters.

**Table 1.** Stripping cross sections  $\sigma$  (in  $10^{-16}$  cm<sup>2</sup>) of 30 MeV/amu He<sup>+</sup> and 38 MeV/amu N<sup>6+</sup> in collisions with He, Ar, and Xe. Exp. denotes the experimental results [2], BA denotes the cross sections calculated using the Born approximation, and CT refers to the classical trajectory calculations, while Hybrid is a combination of BA and CT, as described in the text.

Projectile	Target	$\sigma_{\text{Exp}}$	$\sigma_{\text{BA}}$	$\sigma_{\text{CT}}$	$\sigma_{\text{Hybrid}}$
30 MeV/amu He <sup>+</sup>	He	0.4 ± 0.1	0.30	0.69	0.30
	Ar	7.3 ± 0.4	9.0	11.5	9.1
	Xe	23 ± 1	47	36	33
38 MeV/amu N <sup>6+</sup>	He	0.06 ± 0.01	0.044	0.046	0.044
	Ar	1.64 ± 0.03	1.58	1.58	1.68
	Xe	6.29 ± 0.04	10.30	6.50	6.9

Cross sections for the removal of an electron from an atom or an ion in a collision can be calculated as an integral of the ionization probability  $P(b)$  over impact parameter  $b$ . Since the classical trajectory calculations yield accurate results at small impact parameters but fail at large impact parameters, while the opposite is true for the Born approximation, it is important to determine the critical value of the impact parameter that marks the transition between the two regimes. When this critical value ( $b_c$ ) is found, the cross section can be calculated by integrating the classical ionization probability over  $b$  from zero to  $b_c$  and adding the integral from  $b_c$  to infinity of the ionization probability obtained in the Born approximation.

The range of validity of the two methods can be estimated by evaluating the action

$$S(b) = \int_{-\infty}^{\infty} V[r(b,t)] dt \quad (1)$$

along the trajectory

$$r(b,t) = [b^2 + (vt)^2]^{1/2}. \quad (2)$$

$b_c$  is then determined from the condition

$$S(b_c) = \hbar.$$

For  $b < b_c$ , the target atom potential  $V(r)$  is strong and the corresponding action is large, so that the classical method is applicable, but the Born approximation is not. Likewise, for  $b > b_c$ , the target atom potential  $V(r)$  is weak and the corresponding action is small, so that the Born approximation is applicable, but the classical method is not. Therefore, we should use the classical approach when  $b < b_c$  and the Born approximation when  $b > b_c$ . Some results of these calculations are listed in the last column of Table 1.

It should be noted that the cross sections involving He as the target atom are identical for calculations making use of the Born approximation and the calculations using the hybrid method. This is because for this case  $S / \hbar$  is smaller than unity and the Born approximation remains valid throughout the entire region of integration. On the other hand, in the case of a xenon target, the hybrid method yields results close to those of the calculations performed using the classical trajectory method, because  $S / \hbar$  remains larger than unity for the most of the range of impact parameters for which ionization occurs. Moreover, the hybrid method can produce more accurate results than either of the two other methods considered (see, for example, the case of  $N^{6+}$  on Ar target in Table 1).

- [1] D. Mueller, L. Grisham, I. Kaganovich, R.L. Watson, V. Horvat, K.E. Zaharakis, *Phys. Plasmas* **8**, 1753 (2001).
- [2] D. Mueller, L. Grisham, I. Kaganovich, R.L. Watson, V. Horvat, K.E. Zaharakis, Y. Peng, *Laser Part. Beams* **20**, 551 (2002).

## Systematics of Multiple $L$ -shell Ionization in $K$ -shell Ionizing Collisions

R V. Horvat, R. L. Watson, and Yong Peng

Spectra of  $K$  x rays emitted from Ti, V, Fe, Co, Ni, and Cu targets bombarded by fast heavy ions were measured in high resolution using a curved crystal spectrometer. The projectiles included C, Ne, Ar, Cr, Kr, Xe, and Bi ions at energies ranging from 2.5 to 25 MeV/amu. The Ti, V, and Fe x rays were measured employing first-order diffraction from a LiF crystal, whereas the Co, Ni, and Cu x rays were measured in second-order using the same crystal. The spectra were analyzed to determine the degree of simultaneous  $L$ -shell ionization produced in (near-central)  $K$ -shell ionizing collisions and to establish its dependence on collision parameters.

A portion of the recorded  $K$  x-ray spectrum of Co induced by 6 MeV/amu Kr ion bombardment, shown in Figure 1, illustrates the interpretation of the observed peak structure. The peaks shown in blue correspond to  $K\alpha_1$  ( $2p_{3/2} \rightarrow 1s$ ) transitions in atoms having zero through seven  $L$ -shell spectator vacancies at the time of x-ray emission. Likewise, the peaks shown in brown correspond to  $K\alpha_2$  ( $2p_{1/2} \rightarrow 1s$ ) transitions. These two sets of peaks (known as  $K\alpha$  x-ray satellites) characterize the distribution of  $L$ -shell vacancies produced in  $K$ -shell ionizing ion-atom collisions. Also, high-energy electrons and x rays, produced in primary collisions or in the relaxation processes that follow, create  $K$ -shell vacancies in neighboring target atoms. In this secondary process, however, simultaneous ionization of the  $L$  shell is very improbable. Therefore, the  $K\alpha_1$  and  $K\alpha_2$  x-ray transitions that result from secondary ionization give rise to the “diagram-line” peaks shown in pink. The three sets of peaks plus a constant background (shown in gray) were fit to the measured spectrum (shown with black dots) using a procedure described in Ref. [1].

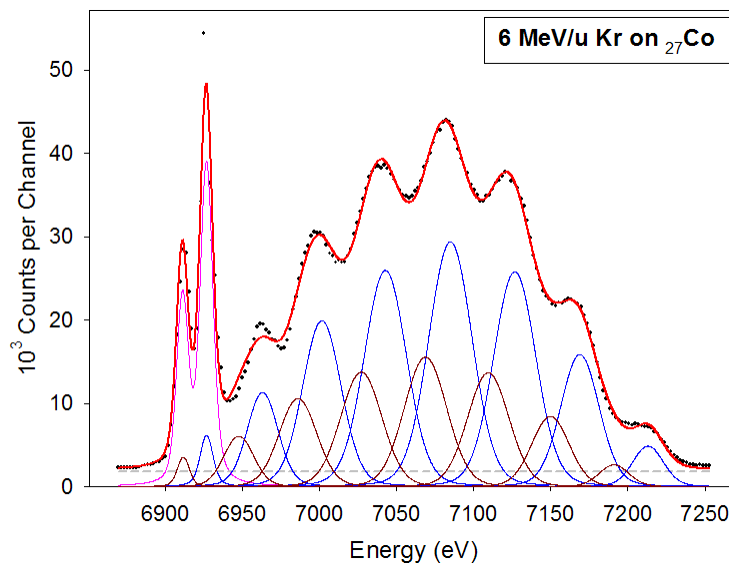


**Figure 1.** Spectrum of  $K\alpha_1$  and  $K\alpha_2$  x rays of Co produced under bombardment by 6 MeV/amu Kr ions.

The degree of  $L$ -shell ionization remaining at the time of  $K$  x-ray emission may be expressed in terms of the apparent average number of  $L$ -shell vacancies ( $n_L$ ). This parameter can be obtained in a straightforward way from the observed peak intensities. The average number of  $L$ -shell vacancies produced in the primary collision ( $N_L$ ) can be deduced from the relative peak intensities corrected for (i) vacancy rearrangement between the time of collision and the time of x-ray emission and (ii) the dependence of fluorescence yield on vacancy configuration. The relative difference between  $n_L$  and  $N_L$  is expected to be on the order of 10 percent.

According to the geometrical model [2],  $N_L$  is a function of a dimensionless universal variable  $X$ , given by

$$X = (4\alpha c / v_1) V [G(V)]^{1/2} Z_1 / n, \quad (1)$$

where  $\alpha$  is the fine structure constant,  $c$  is the speed of light in vacuum,  $Z_1$  is the projectile atomic number,  $v_1$  is the projectile speed,  $n$  is the principal quantum number of the ionized target electron,  $V = v_1 / v_2$  is the scaled projectile speed ( $v_2$  is the average target electron speed prior to ionization), and  $G(V)$  is the binary encounter approximation (BEA) scaling function [3], originally formulated to describe the universal scaling of the cross sections for inner-shell ionization. Our main objective in this work is to examine the dependence of  $n_L$  on the universal variable  $X$ . Preliminary results are shown in Figure 2. In this figure, the solid (blue) line represents the best fit to the experimentally determined  $n_L$  values (shown as filled circles) and the dashed line represents the values of  $N_L$  predicted by the geometrical model.

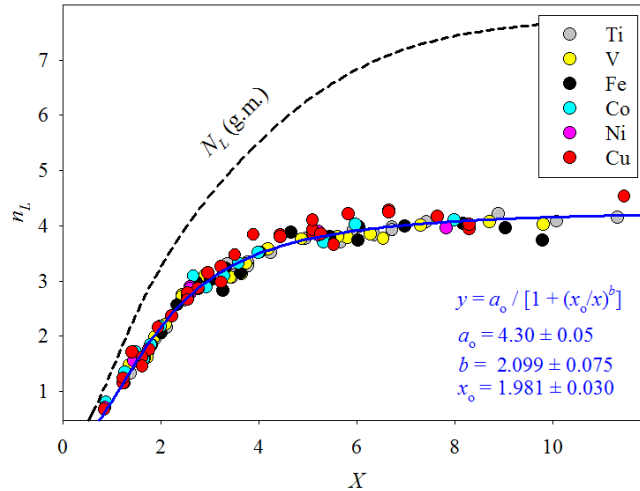


**Figure 2.** Average number of  $L$ -shell vacancies produced in (near-central)  $K$ -shell ionizing collisions

Evidently, the scaling predicted by the geometrical model is appropriate, since the data points do appear to follow a universal curve as a function of  $X$ . However, this empirical universal curve is not in

agreement with the prediction of the geometrical model, which increasingly overestimates the experimental data points as  $X$  increases. The relatively small differences between  $n_L$  and  $N_L$  cannot account for this discrepancy.

- [1] V. Horvat, R. L. Watson, J. M. Blackadar, A. N. Perumal, and Yong Peng, Phys. Rev. A **71** (2005) (in press).
- [2] B. Sulik, I. Kadar, S. Ricz, D. Varga, J. Vegh, G. Hock, and D. Berenyi, Nucl. Instrum. Methods Phys. Res. **B28**, 509 (1987).
- [3] J. H. McGuire and P. Richard, Phys. Rev. A **9**, 1374 (1973).

## **SECTION V**

# **SUPERCONDUCTING CYCLOTRON AND INSTRUMENTATION**

## **K500 Operations and Development**

D. P. May, G. J. Kim, H. L. Clark, F. P. Abegglen, G. J. Derrig,  
R. S. Olsen and W. H. Peeler

### **Introduction**

During the 2004-2005 reporting period a total of 57 different beams, including 28 newly developed beams, were used for experiments. There were a total of 115 beam tunings not counting multiple tunes of beams for the SEE program. The SEE program will be treated separately.

### **Ion Sources**

The January 2004 repair to the damaged hexapole of ECR1 has had positive results as evidenced by operating experience during the last year. ECR1 is much more stable and less critical in its tuning. It also exhibits much less reflected microwave power, and as a result ECR1 can be operated at higher microwave power with higher charge-state output.

The plasma chamber of ECR2 has been redesigned with a possible switch to the new chamber in the summer of 2005. In the new design, small diameter (1.8 mm), water-carrying copper tubes are interposed between the NbFeB permanent magnets and the aluminum plasma-chamber wall. This allows for more protection of the hexapole via water-cooling than the present design, due to higher flow, and also eliminates all of the troublesome water-to-vacuum seals of the present design.

### **Cyclotron Beams**

Of the newly developed beams, two zirconium beams are of note. This element was sputtered into the ECR1 ion source.

### **Operations**

For the period April 1, 2004 through March 31, 2005, the operational time is summarized in Table I, while Table II lists how the scheduled time was divided. There were two major repairs that caused significant losses of time. In February three days were lost due to the failure of a deflector insulator and in April approximately two weeks were lost to a nagging sparking problem on ECR1. The location of the sparks was eventually found to be in an inaccessible position on the hexapole chamber. When the chamber was finally removed, two holes in the insulator sleeve were located. This sleeve had been fabricated with new material when the hexapole had been repaired. The old material was used in fabricating a new sleeve for the repair. Also noted is that the outside use of the cyclotron increased significantly from previous years, indicating a sharp increase in time devoted to SEE testing.

**Table 1.** 2004-2005 Operational Time.

<b>Time</b>	<b>Hrs.</b>	<b>%Time</b>
Beam on target	5138.75	<b>66.5</b>
Tuning, optics, set-up	925.00	<b>12.0</b>
Beam development	236.50	<b>3.0</b>
Scheduled maint.	114.25	<b>1.5</b>
Unscheduled maint.	837.50	<b>10.8</b>
Idle time	477.00	<b>6.2</b>
Cool down	0.00	<b>0.0</b>
<b>Total</b>	<b>7573.00</b>	<b>100.0</b>

**Table 2.** Scheduled Beam Time.

<b>Time</b>	<b>Hrs.</b>	<b>%Time</b>
Nuclear physics	1343.75	<b>18.4</b>
Nuclear chemistry	2246.75	<b>30.8</b>
Atomic physics	404.00	<b>5.6</b>
Outside collaboration	240.00	<b>3.3</b>
Outside users	2815.00	<b>38.6</b>
Beam development	236.50	<b>3.3</b>
<b>Total</b>	<b>7131.00</b>	<b>100.0</b>

## Radiation Effects Facility

H. L. Clark, G. Chubarian, V. Horvat, B. Hyman, G. Souliotis and D. Utley

The activity of the Radiation Effects Facility (REF) increased over the previous reporting year. In this reporting period, the facility was used for 2,012 hours, which is a ~37% increase over the 1,474 hours used in the 2003-2004 reporting period. Users of the facility (and hours used) over the past year were: NASA GSFC (235), NASA JPL (200.5), BAE Systems (182.25), Xilinx (161), Boeing Satellite Systems (160), Aeroflex (122.25), Innovative Concepts (98), NAVSEA (83.5), SEAKR (81), Raytheon (80), Mitsubishi (66), Mission Research Corp. (62.75), General Dynamics (48.5), International Rectifier (47.5), Northrop Grumman (46.5), Honeywell (36.75), Lockheed Martin (32), Prairie View A&M University (32), Science Applications International Corp. (32), ICS Radiation (30.5), Stapor Research (29), Harris (26), Air Force (23.75), Actel (16), NASA JSC (16), Radiation Assured Devices (14.5), Ball Aerospace (12), Aerospace Corp. (11.75), MD Robotics (8.5), Full Circle Research (8) and ITT Aerospace (8). Science Applications International Corp., Stapor Research, MD Robotics and ITT Aerospace were new customers of the facility.

Table 1 compares the facility usage by commercial and government customers. The ratio from

**Table 1.** Radiation Effects Facility usage by commercial and government customers for this and previous reporting years.

Reporting Year	Total Hours	Commercial Hours (%)	Government Hours (%)
2004-2005	2,012	1,421 (71%)	591 (29%)
2003-2004	1,474	785 (53%)	689 (47%)
2002-2003	1,851	1,242 (67%)	609 (33%)
2001-2002	1,327	757 (57%)	570 (43%)
2000-2001	1,500	941 (63%)	559 (37%)
1999-2000	548	418 (76%)	131 (24%)
1998-1999	389	171 (44%)	218 (56%)
1997-1998	434	210 (48%)	224 (52%)
1996-1997	560	276 (49%)	284 (51%)
1995-1996	141	58 (41%)	83 (59%)

this reporting year (71% to 29%) is similar to the trend seen in the 2002-2003 reporting period. The number of commercial hours increased by almost a factor of 2 from 2003-2004 (increase of 636 hours) while the number of government hours decreased by ~100. Much of the testing conducted at the facility has been for defense systems by both government and commercial agencies. It is expected that the facility will continue to be as active in future years.

Table 2 lists the beams used this year and the number of times each was requested. In total, 399 beams were run this year, which is 23% more than the previous year. 10 MeV/nucleon H-<sup>4</sup>He and 40

MeV/nucleon  $^3\text{He}$  were developed for dosimetry and detector tests. No new beams were added to SEELine users list.

**Table 2.** Beams used and the number of times requested for this reporting year and previous years. 399 beams were run this year.

Particle Type	A MeV	Requests 2000-01	Requests 2001-02	Requests 2002-03	Requests 2003-04	Requests 2004-05
$^{20}\text{Ne}$	15	1	13	19	15	23
$^{40}\text{Ar}$	“	4	24	43	46	51
$^{63}\text{Cu}$	“	N/A	N/A	5	14	22
$^{84}\text{Kr}$	“	6	26	55	47	49
$^{109}\text{Ag}$	“	N/A	N/A	6	18	15
$^{129}\text{Xe}$	“	5	18	43	51	50
$^{141}\text{Pr}$	“	N/A	N/A	2	2	1
$^{165}\text{Ho}$	“	3	11	17	7	8
$^{181}\text{Ta}$	“	4	5	4	3	5
$^{197}\text{Au}$	“	12	9	23	34	34
$^{22}\text{Ne}$	25	27	13	19	6	15
$^{40}\text{Ar}$	“	31	20	32	16	25
$^{84}\text{Kr}$	“	32	20	35	26	33
$^{129}\text{Xe}$	“	25	18	24	15	25
H-D	40	1	8	10	4	7
$^{20}\text{Ne}$	“	5	3	5	6	11
$^{40}\text{Ar}$	“	12	8	10	7	13
$^{78}\text{Kr}$	“	13	9	6	5	10
<b>Total</b>		<b>192</b>	<b>207</b>	<b>360</b>	<b>324</b>	<b>399</b>

## Cyclotron Computing

R. Burch, K. Hagel, and M. Vasilyev

In a continuing effort to supply the Institute's growing need for data storage, we moved the file server which we were developing<sup>1</sup> into production and increased the research groups home and data storage allocations. The file server runs Fermi Linux and utilizes the enterprise class logical volume management system, LVM, with the journaling file system EXT3. This configuration allows us to "grow" data storage areas without the need to migrate data from/to different physical mediums. The file server houses and exports the home, data, and opt directories. These directories are made available via NFS v3 to the computational servers via a Gigabit Ethernet connection. The file server also houses the tape-less backup system where we takes snapshots of the user home directories every four hours. We retain the most recent six hourly backups, (one snapshot every four hours) for one day, daily backups for one week, weekly backups for one month, and monthly backups for three months. Additionally, striving to supply the Institute with the necessary computational power it requires, we have replaced two aging computational servers with two newer, faster computational servers. The lab now has five high performance machines available for general use and six data acquisition front-ends for experimental use. Additional servers purchased this year were: AAA server, backup server, web server, and a mail server to replace the current aging mail server. The AAA, backup, and web servers are in full production mode and are running Fermi Linux. The mail server is in development stage and is expected to install anti-Virus, anti-Spam programs, and a webmail application soon. The aging machines were redeployed as a data acquisition frontend, an ssh gateway, a spare firewall, and an intrusion detection system, all of which are in production mode and running Fermi Linux. Additionally, an old Pentium was recovered and redeployed as a network sysloger which collects and stores the log files from all machines we manage. Replacing aged hardware in a timely manner helps to insure the availability of the required institute computational services. Redeployment of the aged hardware to less critical, but important, security related tasks helps to further strengthen our network security posture, a major component of the Texas Administrative Code 202 (TAC 202).

We are evaluating a move to Scientific Linux (a Redhat Enterprise redistribution) as our primary operating system. Scientific Linux (SL) is a descendent of Fermi Linux 3.0.1 (RHE3) and is supported by Fermi Lab, CERN and the scientific community at large. We are evaluating both SL 3 (2.4 kernel) and SL 4 (2.6 kernel). Scientific Linux comes with applications which are very useful to the scientific community and appears to be ideally suited for our work at the institute. Additionally, SL has a patch management system, which we have enabled, that installs patches, including security patches, and updates nightly with little or no administrative intervention.

[1] R.Burch *et al.*, *Progress in Research*, Cyclotron Institute, Texas A&M University (2003-2004), p.V-5.

## Cyclotron Institute Upgrade Project

H. L. Clark

On January 3, 2005 the Cyclotron Institute Upgrade Project (CIUP) began with the approval of the CIUP management plan by the Department of Energy Nuclear Physics Office. The project will extend to the first quarter of calendar year 2011. Funding for the upgrade comes from several sources: the Department of Energy, matching support from TAMU, the Robert A. Welch Foundation and beam time sales for testing electronics components at the Cyclotron Institute.

The CIUP is divided into three major tasks: (1) re-commissioning the K150 (88") cyclotron, coupling it to existing beam lines in order to provide intense stable beams into the K500 experimental areas and using it as a driver to produce radioactive beams; (2) developing light-ion and heavy-ion guides for stopping radioactive ions created with the K150 beams; (3) transporting  $1^+$  ions from ion guides into a charge-breeding electron-cyclotron-resonance ion source to produce highly charged radioactive ions for acceleration in the K500 superconducting cyclotron. When completed in about 6 years, the upgraded facility will provide high-quality re-accelerated secondary beams in a unique energy range in the world.

Most of the work in this reporting period focused on task 1, re-commissioning the K150 cyclotron. Areas of progress included:

- 1) **K150 Coil Power Supplies:** The K150 cyclotron coil power supply bid was awarded to Alpha Scientific for building 23 power supplies for the main coil, trim coils and valley coils. The first set of supplies is scheduled to arrive in early June. In preparation for the supplies, restoration of the K150 pit area began in January.
- 2) **K150 Bus Bar Work:** 1800 feet of copper bus bar arrived in early February. Most of the original bus bar that connected the power supplies to the K150 cyclotron was salvaged for the K500 cyclotron project and needs to be replaced. A hydraulic machine that will be used to bend and reconnect the new bus bar was assembled and tested. Bus bar installation began in early March.
- 3) **K150 RF System:** The RF supply cabinets, racks and console have been welded and painted. A 4-foot steel mezzanine was installed on the south wall of the K150 vault. Low voltage power supplies and some control modules have been built and tested. Most electronic and water cooling components for the RF system have been procured and preassembled. The last major expenses will be the NWL filament supplies and RF ceramic feed-throughs. Cabinet assembly work will begin in July.
- 4) **Building Utilities Upgrade:** The new LCW loop (to feed the K150 cyclotron, RF system, beam lines, ion guides, etc.) design was approved. Some materials have been procured. The cooling tower upgrade was completed in February 2005. Placement of the second building transformer to power the K150 cyclotron and associated equipment is still in discussion with TAMU power people. The size (power output) of the new transformer has been determined.
- 5) **K150 Vacuum System:** The K150 vacuum system design has been approved. The resonator tank will be restored to its original configuration with one 35" diffusion pump, a roots blower package and large mechanical pumps. The beam box will be equipped with three external 10" cryogenic pumps and liquid nitrogen cooled internal cryogenic panels. The internal panels will be similar in design to

panels used on the 88" cyclotron at LBNL. TAMU cyclotron engineers are working with LBNL vacuum engineers to obtain their drawings.

- 6) **K150 Beam Line:** K150 beam line layout has been finalized. Mechanical plans for the new quadrupole magnets and cyclotron exit steering magnet are being drafted. The vacuum chambers for the switching magnets are being drafted. A materials list for the entire beam line is being compiled and includes electrical utility, LCW utility, support structures, vacuum equipment, valves and shield wall plugs. A list of magnet power supplies and switches is also being compiled. The red lines in Figure 1 indicate the new K150 beam lines.
- 7) **K150 Control System:** K150 computer control system design has begun. A test stand is currently being developed.
- 8) **K150 Inflector:** The original K150 cyclotron "mirror" inflector was pulled from the machine, cleaned and tested. The mirror inflector will be used at initial start up of K150 cyclotron. A spiral inflector will be designed during the vertical injection design stage.
- 9) **Light Ion Guide:** Mechanical plans for the prototype LIG & SPIG device have been drafted. The lab space for the prototype is being prepared. Procurement of items will begin in May 2005.
- 10) **Relocation of SEE Line:** Plans for relocating the SEE Line to cave 1 have been approved. The PSP magnet and shielding blocks were removed. Vertical reciprocating conveyors (equipment lifts) and stairways were installed in cave 1 and at the south wall end of cave 2. Flexicor Corp will build the new roof planks and walls for the shielding maze. Relocation of the SEE Line apparatus will commence after installation of the new roof planks and shielding maze. SEE Line should be fully operational in cave 1 by August 2005. The light blue lines in Figure 1 indicate the relocated SEE Line facility.

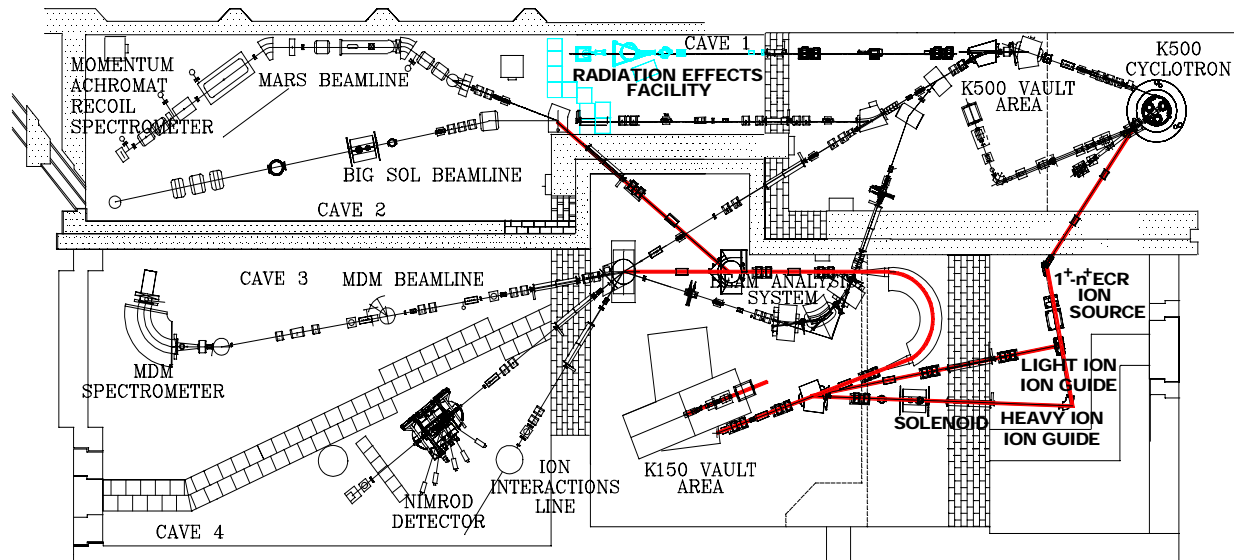


**Figure 1.** Layout for upgraded TAMU Facility. New additions are shown with red lines. The relocated SEE line is shown in light blue. High-intensity stable beams from the re-commissioned K150 Cyclotron will be used with ion guide techniques to produce high quality reaccelerated rare-ion beams from the K500 Cyclotron. K150 beams will be delivered to existing K500 experimental areas.

**SECTION VI**  
**PUBLICATIONS**

## PAPERS PUBLISHED

April 1, 2004 – March 31, 2005

**Giant Resonance in  $^{112}\text{Sn}$  and  $^{124}\text{Sn}$ : Isotopic Dependence of Monopole Resonance Energies**, Y.-W. Lui, D.H. Youngblood, Y. Tokimoto, H.L. Clark, and B. John, Phys. Rev. C **70**, 014307 (2004).

**Refractive Effects in the Scattering of Loosely Bound Nuclei**, F. Carstoiu, L. Trache, R.E. Tribble, and C.A. Gagliardi, Phys. Rev. C **70**, 054610 (2004).

**The  $^{17}\text{F}(p,\gamma)^{18}\text{Ne}$  Direct Capture Cross Section**, J.C. Blackmon, D.W. Bardayan, C.R. Brune, F. Carstoiu, A.E. Champagne, R. Crespo, T. Davinson, J.C. Fernandes, C.A. Gagliardi, U. Greife, C.J. Gross, P.A. Hausladen, C. Iliadis, C.C. Jewett, R.L. Kozub, T.A. Lewis, F. Liang, B.H. Moazen, A.M. Mukhamedzhanov, C.D. Nesaraja, F.M. Nunes, P.D. Parker, D.C. Radford, L. Sahin, J.P. Scott, D. Shapira, M.S. Smith, J.S. Thomas, L. Trache, R.E. Tribble, P.J. Woods, and C.-H. Yu, Nucl. Phys. **A746**, 365c (2004).

**Breakup of Loosely Bound Nuclei at Intermediate Energies as Indirect Method in Nuclear Astrophysics:  $^8\text{B}$ ,  $^9\text{C}$  and the  $S_{17}$ ,  $S_{18}$  Astrophysical Factors**, L. Trache, F. Carstoiu, C.A. Gagliardi, A.M. Mukhamedzhanov, and R.E. Tribble, Nucl. Phys. **A746**, 625c (2004).

**Determination of the Direct Capture Contribution for  $^{13}\text{N}(p,\gamma)^{14}\text{O}$  from the  $^{14}\text{O} \rightarrow ^{13}\text{N} + p$  Asymptotic Normalization Coefficient**, X. Tang, A. Azhari, C. Fu, C.A. Gagliardi, A.M. Mukhamedzhanov, F. Pirlpesov, L. Trache, R.E. Tribble, V. Burjan, V. Kroha, F. Carstoiu, and B.F. Irgaziev, Phys. Rev. C **69**, 055807 (2004).

**Quark Mixing, CKM Unitarity**, H. Abele, E. Barberio, D. Dubbers, F. Gluck, J.C. Hardy, W.J. Marciano, A. Serebrov and N. Severijns, Eur. Phys. J. C **33**, 1 (2004).

**Q-Value of the Superaligned Decay of  $^{22}\text{Mg}$  and the Calibration of the  $^{21}\text{Na}(p,\gamma)$  Experiment**, G. Savard, J.A. Clark, F. Buchinger, J.E. Crawford, S. Gulick, J.C. Hardy, A.A. Hecht, V.E. Jacob, J.K.P. Lee, A.F. Levand, B.F. Lundgren, N. Scielzo, K.S. Sharma, I. Tanihata, I.S. Towner, W. Trimble, J.C. Wang, Y. Wang and Z. Zhou, Phys. Rev. C **70**, 042501(R) (2004).

**Precise Measurement of  $\alpha_K$  for the M4 Transition from  $^{193}\text{Ir}^m$ : A Test of Internal-Conversion Theory**, N. Nica, J.C. Hardy, V.E. Jacob, S. Raman, C.W. Nestor, Jr and M.B. Trzhaskovskaya, Phys. Rev. C **70**, 054305 (2004).

**CVC Tests and CKM Unitarity**, J.C. Hardy, Nucl. Phys. **A752**, 101c (2005).

**Superaligned  $0^+ \rightarrow 0^+$   $\beta$  Decays: A Critical Survey with Tests of CVC and the standard Model**, J.C.

Hardy and I.S. Towner, Phys. Rev. C **71**, 044309 (2005).

**New Limits on Fundamental Weak-Interaction Parameters from Superaligned  $\beta$  Decay**, J.C. Hardy and I.S. Towner, Phys. Rev. Lett. **94**, 092502 (2005).

**Precise  $FT$ -Value Measurement for the Superaligned  $0^+$ -to- $0^+$   $\beta$  Decay of  $^{22}\text{Mg}$** , J.C. Hardy, V.E. Jacob, M. Sanchez-Vega, R.G. Neilson, A. Azhari, C.A. Gagliardi, V.E. Mayes, X. Tang, L. Trache and R.E. Tribble, Proceedings of International Conference on the Labyrinth in Nuclear Structure, Crete, July 2003; AIP Conference Proceedings # **701**, 244 (2004).

**Development Plans – The Texas A&M University Cyclotron Institute**, F. Abegglen, A. Azhari, G. Chubaryan, H. Clark, G. Derrig, C.A. Gagliardi, J.C. Hardy, G. Kim, D. May, M. Murray, J.B. Natowitz, R.P. Schmitt, G. Soliotis, R.E. Tribble, R. Wada, R.L. Watson, D.H. Youngblood, and S.J. Yennello Proceedings of the International Symposium, New Projects and Lines of Research in Nuclear Physics (2003) pg 272.

**New Measurements along the rp- and r-Process Paths**, G. Savard, J.A. Clark, R.C. Barber, B. Blank, F. Buchinger, J.E. Crawford, S. Gulick, J.C. Hardy, A. Heinz, J.K.P. Lee, A.F. Levand, R.B. Moore, D. Seweryniak, K.S. Sharma, G.D. Sprouse, W. Trimble, J. Vaz, J.C. Wang, and Z. Zhou, Hirscheegg '03: Nuclear Structure and Dynamics at the Limits. Proceedings of the International Workshop XXXI on Gross Properties of Nuclei and Nuclear Excitations (2003) pg 269.

**Search for Temperature and N/Z Dependent Effects in the Decay of  $A = 98$  Compound Nuclei**, S. Moretto, D. Fabris, M. Lunardon, S. Pesente, V. Rizzi, G. Viesti, M. Barbui, M. Cinausero, E. Fioretto, G. Prete, A. Brondi, E. Vardaci, F. Lucarelli, A. Azhari, X. D. Tang, K. Hagel, Y. Ma, A. Makeev, M. Murray, J. B. Natowitz, L. Qin, P. Smith, L. Trache, R. E. Tribble, R. Wada, and J. Wang, Phys. Rev. C **69**, 044604 (2004).

**Resonance Scattering  $^8\text{He} + p$  and  $T=5/2$  States in  $^9\text{Li}$** , V.Z. Goldberg, G.V. Rogachev, J.J. Kolata, G. Chubarian, D. Aleksandrov, M.S. Golovkov, Yu.Ts. Oganessian, A. Rodin, B. Skorodumov, R.S. Slepnev, G. Ter-Akopian, R. Wolski, Nucl.Phys. **A734**, 349 (2004).

**Analog States of  $^7\text{He}$  Observed via the  $^6\text{He}(p, n)$  Reaction**, G.V. Rogachev, P. Boutachkov, A. Aprahamian, F.D. Becchetti, J.P. Bychowski, Y. Chen, G. Chubarian, P.A. DeYoung, V.Z. Goldberg, J.J. Kolata, L.O. Lamm, G.F. Peaslee, M. Quinn, B.B. Skorodumov, A. Wohr, Phys.Rev.Lett. **92**, 232502 (2004).

**Structure of Exotic  $^7\text{He}$  and  $^9\text{He}$** , G.V. Rogachev, A. Aprahamian, F.D. Becchetti, P. Boutachkov, Y. Chen, G. Chubarian, P.A. DeYoung, A. Fomichev, V.Z. Goldberg, M.S. Golovkov, J.J. Kolata, Yu.Ts. Oganessian, G.F. Peaslee, M. Quinn, A. Rodin, B.B. Skorodumov, R.S. Slepnev, G. Ter-Akopian, W.H. Trzaska, A. Wohr, R. Wolski, Nucl.Phys. **A746**, 229c (2004).

**Reaction Dynamics and Multifragmentation in Fermi Energy Heavy Ion Reactions**, R. Wada, T. Keutgen, K. Hagel, Y. G. Ma, J. Wang, M. Murray, L. Qin, P. Smith, J. B. Natowitz, R. Alfaro, J. Cibor, M. Cinausero, Y. El Masri, D. Fabris, E. Fioretto, A. Keksis, S. Kowalski, M. Lunardon, A. Makeev, N. Marie, E. Martin, Z. Majka, A. Martinez-Davalos, A. Menchaca-Rocha, G. Nebbia, G. Prete, V. Rizzi, A. Ruangma, D. V. Shetty, G. Souliotis, P. Staszal, M. Veselsky, G. Viesti, E. M. Winchester, S. J. Yennello, W. Zipper, and A. Ono, *Phys. Rev. C* **69**, 044610 (2004).

**Fragment Yield Distribution and the Influence of Neutron Composition and Excitation Energy in Multifragmentation Reaction**, D.V. Shetty, A.S. Botvina, S.J. Yennello, G.A. Souliotis, E. Bell, and A. Keksis, *Phys. Rev. C* **71**, 024602 (2005).

**The Decay Time Scale for Highly Excited Nuclei as seen from Asymmetrical Emission of Particles**, M. Jandel, A.S. Botvina, S.J. Yennello, G.A. Souliotis, D.V. Shetty, E. Bell, and A. Keksis *J. Phys. G* **31**, 29 (2005).

**Thermodynamical Properties of Highly Excited Quasi-Projectiles**, M. Veselsky and S.J. Yennello, *Nucl. Phys. A* **749**, 114c (2005).

**Neutron to Proton Ratios of Quasiprojectile and Midrapidity Emission in the  $^{58}\text{Ni} + ^{58}\text{Ni}$  Reaction at 52 MeV/nucleon**, D. Thériault, A. Vallée, L. Gingras, Y. Larochelle, R. Roy, A. April, L. Beaulieu, F. Grenier, F. Lemieux, J. Moisan, M. Samri, C. St-Pierre, S. Turbide, B. Borderie, R. Bougault, P. Buchet, J. L. Charvet, A. Chbihi, J. Colin, D. Cussol, R. Dayras, D. Durand, J. D. Frankland, E. Galichet, D. Guinet, B. Guiot, P. Lantesse, J. F. Lecolley, N. Le Neindre, O. Lopez, A. M. Maskay, L. Nalpas, M. Parlog, P. Pawlowski, M. F. Rivet, E. Rosato, J. C. Steckmeyer, B. Tamain, E. Vient, C. Volant, J. P. Wieleczko, S. J. Yennello, E. Martin, and E. Winchester, *Phys. Rev. C* **71**, 014610 (2005).

**Symmetry Energy and the Isospin Dependent Equation of State**, D.V. Shetty, S.J. Yennello, A.S. Botvina, G.A. Souliotis, M. Jandel, E. Bell, A. Keksis, S. Soisson, B. Stein, and J. Iglío, *Phys. Rev. C* **70**, 011601(R) (2004).

**Neutron-rich Rare Isotope Production and Studies of the N/Z Degree of Freedom in Binary Collisions at Fermi Energies**, G.A. Souliotis, M. Veselsky, D.V. Shetty, L. Trache, and S.J. Yennello, *Nucl. Phys. A* **746**, 526c (2004).

**Heavy Residue Isoscaling as a Probe of the Process of N/Z Equilibration**, G.A. Souliotis, M. Veselsky, D.V. Shetty, and S.J. Yennello, *Phys. Lett. B* **588**, 35 (2004).

**Mid-Rapidity Emission in  $^{124}\text{Sn}$ ,  $^{124}\text{Xe} + ^{124}\text{Sn}$ ,  $^{112}\text{Sn}$  Reactions at 28 MeV/nucleon**, D.V. Shetty, A. Keksis, E. Martin, A. Ruangma, G.A. Souliotis, M. Veselsky, E. Winchester, S.J. Yennello, K. Hagel, Y.G. Ma, A. Makeev, N. Marie, M. Murray, J.B. Natowitz, L. Qin, P. Smith, R. Wada, J. Wang, M. Cinausero, E. Fioretto, G. Prete, D. Fabris, M. Lunardon, G. Nebbia, V. Rizzi, G. Viesti, J. Cibor, Z. Majka, P. Staszal, R. Alfaro, A. Martinez-Davalos, A. Menchaca-Rocha, Y. El Masri, and T. Keutgen Nucl. Phys. **A734**, E100 (2004).

**Isoscaling Studies of Fission: A Sensitive Probe into the Dynamics of Scission**, M. Veselsky, G.A. Souliotis, and M. Jandel, Phys. Rev. C **69**, 044607 (2004).

**Isoscaling in Peripheral Nuclear Collisions Around the Fermi Energy and a Signal of Chemical Separation from its Excitation Energy Dependence**, M. Veselsky, G.A. Souliotis, and S.J. Yennello, Phys. Rev. C **69**, 031602 (2004).

**Neutron-Rich Rare Isotope Production on the Fermi Energy Domain**, G.A. Souliotis, M. Veselsky, G. Chubarian, L. Trache, and S.J. Yennello, Nucl. Phys. **A734**, 557 (2004).

**Target Proximity Effect and Dynamical Projectile Breakup at Intermediate Energies**, R. Moustabchir, L. Beaulieu, L. Gingras, R. Roy, M. Samri, G. Boudreault, J. Gauthier, G.P. Gelinas, F. Grenier, R. Ibbotson, Y. Larochelle, E. Martin, J. Moisan, D. Ouerdane, D. Rowland, A. Ruangma, C. St-Pierre, D. Theriault, A. Vallee, E. Winchester, and S.J. Yennello, Nucl. Phys. **A739**, 15 (2004).

**Effects of In-Medium Cross Sections and Optical Potential on Thermal-Source Formation in  $p + ^{197}\text{Au}$  Reactions at 6.2-14.6 GeV/c**, S. Turbide, L. Beaulieu, P. Danielewicz, V.E. Viola, R. Roy, K. Kwiatkowski, W.-C. Hsi, G. Wang, T. Lefort, D.S. Bracken, H. Breuer, E. Cornell, F. Gimeno-Nogues, D.S. Ginger, S. Gushue, R. Huang, R. Korteling, W.G. Lynch, K.B. Morley, E. Ramakrishnan, L.P. Remsberg, D. Rowland, M.B. Tsang, H. Xi, and S.J. Yennello, Phys. Rev. C **70**, 014608 (2004).

**Breakup Densities of Hot Nuclei**, V.E. Viola, K. Kwiatkowski, J.B. Natowitz, and S.J. Yennello, Phys. Rev. Lett. **93**, 132701 (2004).

**Forward and Midrapidity Like-Particle Ratios from  $p+p$  Collisions at  $\sqrt{s} = 200$  GeV**, BRAHMS Collaboration, I.G. Bearden, D. Beavis, C. Besliu, B. Budick, H. Bøggild, C. Chasman, C.H. Christensen, P. Christiansen, J. Cibor, R. Debbe, E. Enger, J. J. Gaardhøje, M. Germinario, K. Hagel, A. Holm, A.K. Holme, H. Ito, E. Jakobsen, A. Jipa, F. Jundt, J.I. Jørdre, C.E. Jørgensen, R. Karabowicz, T. Keutgen, E.J. Kim, T. Kozik, T.M. Larsen, J.H. Lee, Y.K. Lee, G. Løvholden, Z. Majka, A. Makeev, M. Mikelsen, M.J. Murray, J. Natowitz, B.S. Nielsen, J. Norris, K. Olchanski, D. Ouerdane, R. Płaneta, F. Rami, C. Ristea, D. Röhrich, B.H. Samset, D. Sandberg, S.J. Sanders, R.A. Scheetz, P. Staszal, T.S. Tveter, F. Videbæk, R. Wada, A. Wieloch, Z. Yin and I.S. Zgura, Phys. Lett. B **607**, 42 (2005).

**Charged Meson Rapidity Distributions in central Au+Au Collisions at  $\sqrt{s} = 200$  GeV**, I. G. Bearden, D. Beavis, C. Besliu, B. Budick, H. Bøggild, C. Chasman, C. H. Christensen, P. Christiansen, J. Cibor, R. Debye, E. Enger, J. J. Gaardhøje, M. Germinario, K. Hagel, O. Hansen, A. Holm, A. K. Holme, H. Ito, A. Jipa, F. Jundt, J. I. Jørdre, C. E. Jørgensen, R. Karabowicz, E. J. Kim, T. Kozik, T. M. Larsen, J. H. Lee, Y. K. Lee, G. Løvhøiden, Z. Majka, A. Makeev, M. Mikelsen, M. Murray, J. Natowitz, B. S. Nielsen, J. Norris, K. Olchanski, D. Ouerdane, R. Płaneta, F. Rami, C. Ristea, D. Röhrich, B. H. Samset, D. Sandberg, S. J. Sanders, R. A. Sheetz, P. Staszczel, T. S. Tveter, F. Videbaek, R. Wada, Z. Yin, and I. S. Zgura (BRAHMS Collaboration), *Phys. Rev. Lett.* **94**, 162301 (2005).

**On the Evolution of the Nuclear Modification Factors with Rapidity and Centrality in d+Au Collisions at  $\sqrt{s} = 200$  GeV**, I. Arsene, I. G. Bearden, D. Beavis, C. Besliu, B. Budick, H. Bøggild, C. Chasman, C. H. Christensen, P. Christiansen, J. Cibor, R. Debye, E. Enger, J. J. Gaardhøje, M. Germinario, K. Hagel, H. Ito, A. Jipa, F. Jundt, J. I. Jørdre, C. E. Jørgensen, R. Karabowicz, E. J. Kim, T. Kozik, T. M. Larsen, J. H. Lee, Y. K. Lee, S. Lindal, R. Lystad, G. Løvhøiden, Z. Majka, A. Makeev, M. Mikelsen, M. Murray, J. Natowitz, B. Neumann, B. S. Nielsen, D. Ouerdane, R. Płaneta, F. Rami, C. Ristea, D. Röhrich, B. H. Samset, D. Sandberg, S. J. Sanders, R. A. Sheetz, P. Staszczel, T. S. Tveter, F. Videbaek, R. Wada, Z. Yin, and I. S. Zgura (BRAHMS Collaboration), *nucl-ex/0403005*, I. Arsene *et al.*, *Phys. Rev. Lett.* **93**, 242303 (2004).

**Centrality Dependence of Charged-Particle Pseudorapidity Distributions from d+Au Collisions at  $\sqrt{s} = 200$  GeV**, I. Arsene, I. G. Bearden, D. Beavis, C. Besliu, B. Budick, H. Bøggild, C. Chasman, C. H. Christensen, P. Christiansen, J. Cibor, R. Debye, E. Enger, J. J. Gaardhøje, M. Germinario, K. Hagel, H. Ito, A. Jipa, J. I. Jørdre, F. Jundt, C. E. Jørgensen, R. Karabowicz, E. J. Kim, T. Kozik, T. M. Larsen, J. H. Lee, Y. K. Lee, S. Lindal, R. Lystad, G. Løvhøiden, Z. Majka, A. Makeev, M. Mikelsen, M. Murray, J. Natowitz, B. Neumann, B. S. Nielsen, D. Ouerdane, R. Płaneta, F. Rami, C. Ristea, D. Röhrich, B. H. Samset, D. Sandberg, S. J. Sanders, R. A. Sheetz, P. Staszczel, T. S. Tveter, F. Videbaek, R. Wada, Z. Yin, and I. S. Zgura (BRAHMS Collaboration), *nucl-ex/0401025*, *Phys. Rev. Lett.* **94**, 032301 (2005).

**Measurement of Muon Decay Parameter  $\delta$** , A. Gaponenko, R. Bayes, Yu.I. Davydov, P. Depommier, J. Doornbos, W. Faszler, M.C. Fujiwara, C.A. Gagliardi, D.R. Gill, P. Green, P. Gumplinger, M.D. Hasinoff, R.S. Henderson, J. Hu, B. Jamieson, P. Kitching, D.D. Koetke, A.A. Krushinsky, Yu.Yu. Lachin, J.A. Macdonald, R.P. MacDonald, G.M. Marshall, E.L. Mathie, L.V. Miasoedov, R.E. Mischke, J.R. Musser, P.M. Nord, M. Nozar, K. Olchanski, A. Olin, R. Openshaw, T.A. Porcelli, J.-M. Poutissou, R. Poutissou, M.A. Quraan, N.L. Rodning, V. Selivanov, G. Sheffer, B. Shin, F. Sobratee, T.D.S. Stanislaus, R. Tacik, V.D. Torokhov, R.E. Tribble, M.A. Vasiliev, and D.H. Wright (TWIST Collaboration), *Phys. Rev. D* **71**, 071101(R) (2005).

**Measurement of the Michel Parameter  $\rho$  in Muon Decay**, J.R. Musser, R. Bayes, Yu.I. Davydov, P. Depommier, J. Doornbos, W. Faszler, C.A. Gagliardi, A. Gaponenko, D.R. Gill, P. Green, P. Gumplinger, M.D. Hasinoff, R.S. Henderson, J. Hu, B. Jamieson, P. Kitching, D.D. Koetke, A.A. Krushinsky, Yu.Yu. Lachin, J.A. Macdonald, R.P. MacDonald, G.M. Marshall, E.L. Mathie, L.V. Miasoedov, R.E. Mischke, P.M. Nord, K. Olchanski, A. Olin, R. Openshaw, T.A. Porcelli, J.-M. Poutissou, R. Poutissou, M.A. Quraan, N.L. Rodning, V. Selivanov, G. Sheffer, B. Shin, F. Sobratee, T.D.S. Stanislaus, R. Tacik, V.D. Torokhov, R.E. Tribble, M.A. Vasiliev, and D.H. Wright (TWIST Collaboration), *Phys. Rev. Lett.* **94**, 101805 (2005). [This paper, together with the companion paper describing the measurement of  $\delta$ , was featured in the News section of the CERN Courier **45**(4), 8 (2005).]

**Open Charm Yields in d+Au Collisions at  $\sqrt{s_{NN}} = 200$  GeV**, J. Adams *et al.* (STAR Collaboration), *Phys. Rev. Lett.* **94**, 062301 (2005).

**Transverse-Momentum Dependent Modification of Dynamic Texture in Central Au+Au Collisions at  $\sqrt{s_{NN}} = 200$  GeV**, J. Adams *et al.* (STAR Collaboration), *Phys. Rev. C* **71**, 031901(R) (2005).

**Pseudorapidity Asymmetry and Centrality Dependence of Charged Hadron Spectra in d+Au Collisions at  $\sqrt{s_{NN}} = 200$  GeV**, J. Adams *et al.* (STAR Collaboration), *Phys. Rev. C* **70**, 064907 (2004).

**Azimuthal Anisotropy and Correlations at Large Transverse Momentum in p+p and Au+Au Collisions at  $\sqrt{s_{NN}} = 200$  GeV**, J. Adams *et al.* (STAR Collaboration), *Phys. Rev. Lett.* **93**, 252301 (2004).

**Measurements of Transverse Energy Distributions in Au+Au Collisions at  $\sqrt{s_{NN}} = 200$  GeV**, J. Adams *et al.* (STAR Collaboration), *Phys. Rev. C* **70**, 054907 (2004).

**Rapidity and Centrality Dependence of Proton and Antiproton Production from  $^{197}\text{Au}+^{197}\text{Au}$  Collisions at  $\sqrt{s_{NN}} = 130$  GeV**, J. Adams *et al.* (STAR Collaboration), *Phys. Rev. C* **70**, 041901(R) (2004).

**Centrality and Pseudorapidity Dependence of Charged Hadron Production at Intermediate  $p_T$  in Au+Au Collisions at  $\sqrt{s_{NN}} = 130$  GeV**, J. Adams *et al.* (STAR Collaboration), *Phys. Rev. C* **70**, 044901 (2004).

**Production of  $e^+e^-$  Pairs Accompanied by Nuclear Dissociation in Ultra-Peripheral Heavy Ion Collisions**, J. Adams *et al.* (STAR Collaboration), *Phys. Rev. C* **70**, 031902(R) (2004).

**Photon and Neutral Pion Production in Au+Au Collisions at  $\sqrt{s_{NN}} = 130$  GeV**, J. Adams *et al.* (STAR Collaboration), *Phys. Rev. C* **70**, 044902 (2004).

**Azimuthally Sensitive Hanbury Brown-Twiss Interferometry in Au+Au Collisions at  $\sqrt{s_{NN}} = 200$  GeV**, J. Adams *et al.* (STAR Collaboration), Phys. Rev. Lett. **93**, 012301 (2004).

**Cross Sections and Transverse Single-Spin Asymmetries in Forward Neutral-Pion Production from Proton Collisions at  $\sqrt{s} = 200$  GeV**, J. Adams *et al.* (STAR Collaboration), Phys. Rev. Lett. **92**, 171801 (2004).

**Kaon Production and Kaon to Pion Ratio in Au+Au Collisions at  $\sqrt{s_{NN}} = 130$  GeV**, C. Adler *et al.* (STAR Collaboration), Phys. Lett. B **595**, 143 (2004).

**Multistrange Baryon Production in Au-Au Collisions at  $\sqrt{s_{NN}} = 130$  GeV**, J. Adams *et al.* (STAR Collaboration), Phys. Rev. Lett. **92**, 182301 (2004).

**Projectile Electron Loss and Capture in MeV/u Collisions of  $U^{28+}$  with  $H_2$ ,  $N_2$ , and Ar**, R. E. Olson, R. L. Watson, V. Horvat, A. N. Perumal, Y. Peng, and Th. Stöhlker, J. Phys. B **37**, 4539 (2004).

**Cross Sections for Charge Change in Argon and Equilibrium Charge States of 3.5 MeV/amu Uranium Ions Passing Through Argon and Carbon Targets**, A. N. Perumal, V. Horvat, R. L. Watson, Y. Peng, and K. S. Fruchey, Nucl. Instrum. Methods Phys. Res. **B227**, 251 (2005).

**Photoproduction of Pentaquark Cascades from Nucleons**, W. Liu and C. M. Ko, Phys. Rev. C **69**, 045204 (2004).

**Effects of Momentum-Dependent Potential on Two-Nucleon Correlation Functions and Light Cluster Production in Intermediate-Energy Heavy-Ion Collisions**, L. W. Chen, B. A. Li, and C. M. Ko, Phys. Rev. C **69**, 054606 (2004).

**Momentum Anisotropies in the Quark Coalescence Model**, P. P. R. Kolb, L. W. Chen, V. Greco, and C. M. Ko, Phys. Rev. C **69**, 051901(R) (2004).

**$\Xi$  Production at AGS Energies**, S. Pal, C. M. Ko, J. M. Alexander, P. Chung, and R. A. Lacey, Phys. Lett. B **595**, 158 (2004).

**Quark Coalescence Model for Charmed Mesons in Ultrarelativistic Heavy Ion Collisions Production**, V. Greco, C. M. Ko, and R. Rapp, Phys. Lett. B **595**, 202 (2004).

**Pentaquark  $\Theta^+$  Production from Photon-Nucleon Reactions**, W. Liu and C. M. Ko, Nucl. Phys. **A741**, 215 (2004).

**Effect of Resonance Decays on Hadron Elliptic Flows**, V. Greco and C. M. Ko, Phys. Rev. C **70**, 024901 (2004).

**Pentaquark Brayon Production at the Relativistic Heavy Ion Collider**, L. W. Chen, V. Greco, C. M. Ko, S. H. Lee, and W. Liu, Phys. Lett. B **601**, 34 (2004).

**Determination of the Stiffness of the Nuclear Symmetry Energy from Isospin Diffusion**, L. W. Chen, C. M. Ko, and B. A. Li, Phys. Rev. Lett. **94**, 032701 (2005).

**Pseudorapidity Dependence of Anisotropic Flows in Relativistic Heavy Ion Collisions**, L. W. Chen, V. Greco, C. M. Ko, and P. Koch, Phys. Lett. B **605**, 95 (2005).

**Partonic Effects on Anisotropic Flows at RHIC**, L. W. Chen and C. M. Ko, J. Phys. G **31**, S49 (2005).

**Quark Coalescence at RHIC**, V. Greco and C. M. Ko, J. Phys. G **31**, S407 (2005).

**In-Medium Effects on Charmonium Production in Heavy-Ion Collisions**, L. Grandchamp, R. Rapp and G.E. Brown, Phys. Rev. Lett. **92**, 212301 (2004).

**Theory Highlights of Quark Matter 2004**, R. Rapp, J. Phys. G **30**, S951 (2004).

**Medium Modifications of Charm and Charmonium in High-Energy Heavy-Ion Collisions**, L. Grandchamp, R. Rapp and G.E. Brown, J. Phys. G **30**, S1355 (2004).

**Thermal Photons in Strong Interactions**, R. Rapp, Mod. Phys. Lett. A **19**, 1717 (2004).

**$\Delta(1232)$  and Nucleon Spectral Functions in Hot Hadronic Matter**, H. van Hees and R. Rapp, Phys. Lett. B **606**, 59 (2005).

**Photon Production in Relativistic Nuclear Collisions at SPS and RHIC Energies**, S. Turbide, R. Rapp and C. Gale, Int. J. Mod. Phys. A **19**, 5351 (2004).

**The  $\Delta(1232)$  at RHIC**, H. van Hees and R. Rapp, J. Phys. G **31**, S203 (2005).

**The Vector Probe in Heavy-Ion Reactions**, R. Rapp, J. Phys. G **31**, S217 (2005).

**Thermalization of Heavy Quarks in the Quark-Gluon Plasma**, H. van Hees and R. Rapp, Phys. Rev. C **71**, 034907 (2005).

**Three-Body Coulomb Final-State Interaction Effects in the Coulomb Breakup of Light Nuclei**, E. O. Alt, B. F. Irgaziev, A. M. Mukhamedzhanov, Mod. Phys. Lett. A **20**, 947 (2005).

**Three-Body Coulomb Interaction Effects in the Final State of the  $^{208}\text{Pb}(^8\text{B}, ^7\text{Be p})^{208}\text{Pb}$  Coulomb Breakup Reaction**, E. O. Alt, B. F. Irgaziev, A. M. Mukhamedzhanov, Phys. Rev. C **71**, 024605 (2005).

**Theory of Electron-Impact Ionization of Atoms**, A.S. Kadyrov, A.M. Mukhamedzhanov, A. T. Stelbovics and I. Bray, Phys. Rev. A **70**, 062703 (2004).

**Insight into Continuum Couplings**, F.M.Nunes, A.M. Mukhamedzhanov, C.C. Rosa, B. F. Irgaziev, Nucl. Phys. **A736**, 255 (2004).

**Hot Nuclei**, S. Shlomo, and V.M. Kolomietz, Rep. Prog. Phys. **68**, 1 (2005).

**Critical Densities for the Skyrme Type Effective Interactions**, B.K. Agrawal, S. Shlomo, and V.K. Au, Phys. Rev. C **70**, 014308 (2004).

**Consequences of Self-Consistency Violations in Hartree-Fock Random-Phase Approximation Calculations of the Nuclear Breathing Mode Energy**, B.K. Agrawal and S. Shlomo, Phys. Rev. C **70**, 014308 (2004).

**Flow Effects on Multifragmentation in the Canonical Model**, S.K. Samaddar, J.N. De, and S. Shlomo, Phys. Rev. C **69**, 064615 (2004).

**Status of the Nuclear Matter Equation of State as Determined from Compression Modes**, S. Shlomo, B.K. Agrawal, and A.V. Kim, Nucl. Phys. **A734**, 589 (2004).

# **SECTION VII**

## **APPENDIX**

**TALKS PRESENTED**  
**April 1, 2004 – March 31, 2005**

*Giant Monopole Resonance in Cd and Sn Isotopes*, **Y.-W. Lui**, D.H. Youngblood, H.L. Clark, Y. Tokimoto and B. John, **Invited Talk**, International Symposium on Atomic Nuclei at Extreme Values of Temperature, Spin and Isospin, Zakopane, Poland, (August 2004).

*Report on BigSol Operations*, **R.E. Tribble**, **Invited Talk**, Workshop on Measuring Transfer reactions with Radioactive Beams, Argonne national Laboratory, Argonne, Illinois, (June 2004).

*Indirect Techniques in Nuclear Astrophysics: The ANC Method*, **R.E. Tribble**, **Invited Talk**, CAARI 2004, Ft. Worth, Texas, (October 2004).

*Quasi-New ANC Results and their Implications in Stellar Evolution, plus a Look to the Future at Texas A&M*, **R.E. Tribble**, **Invited Talk**, Laboratory for Nuclear Studies, Catania, Sicily, Italy (March 2005).

*High- $p_T$  Results from STAR*, **C.A. Gagliardi (for the STAR Collaboration)**, **Invited Talk**, Workshop on Jet Corr. RHIC, Brookhaven, New York, (March 2005).

*Recent High- $p_T$  Results from STAR*, **C.A. Gagliardi (for the STAR Collaboration)**, **Invited Talk**, Int. Conf. on Hard Electromag. Probes High Energy Nucl. Coll., Ericeira, Portugal, (November 2004).

*STAR Forward Detector Upgrades*, **C.A. Gagliardi (for the STAR Collaboration)**, **Invited Talk**, 18<sup>th</sup> Int. Conf. Appl. Accel. Res. Indus., Ft. Worth, Texas, (October 2004).

*Recent Results from RHIC*, **C.A. Gagliardi**, **Invited Talk**, Third Int. Conf. Quarks and Nucl. Phys., invited, Bloomington, Indiana, (May 2004).

*Measuring the Space-Time Structure of Muon Decay with TWIST*, **C.A. Gagliardi**, Physics Division, Brookhaven National Laboratory, Upton, New York, (March 2005).

*Jet Quenching at RHIC*, **C.A. Gagliardi**, Physics Department, University of Texas, Austin, Texas, (April 2004).

*Recent Results from RHIC*, **C.A. Gagliardi**, Abilene Christian University, Abilene, Texas, (September 2004).

*TWIST Measurement of the Decay Parameters  $\rho$  and  $\delta$  of Normal Muon Decay*, **J.R. Musser**, Pennsylvania State University Altoona, Altoona, Pennsylvania, (February 2005).

*TWIST Measurement of the Decay Parameters  $\rho$  and  $\delta$  of Normal Muon Decay*, **J.R. Musser**, Arkansas Technological University, Russellville, Arkansas, (February 2005).

*TWIST Measurement of the Decay Parameters  $\rho$  and  $\delta$  of Normal Muon Decay*, **J.R. Musser**, Valparaiso University, Valparaiso, Indiana, (January 2005).

*TWIST Measurement of the Decay Parameters  $\rho$  and  $\delta$  of Normal Muon Decay*, **J.R. Musser**, Indiana University Cyclotron Facility, Bloomington, Indiana, (January 2005).

*TWIST Measurement of the Michel Parameter  $\rho$* , **J.R. Musser (for the TWIST Collaboration)**, TRIUMF, Vancouver, British Columbia, Canada, (October 2004).

*Extracting the ANC's for  $^{23}\text{Al} \rightarrow ^{22}\text{Mg} + p$  from Its Mirror System  $^{23}\text{Ne} \rightarrow ^{22}\text{Ne} + n$  Reaction*, **T. Al-Abdullah**, X. Chen, H. Clark, C. Fu, C.A. Gagliardi, Y.-W. Lui, G. Tabacaru, Y. Tokimoto, L. Trache, R.E. Tribble, and S. Piskor, 2004 Annual Meeting of the Division of Nuclear Physics of the APS, Chicago, Illinois, (October 2004).

*TRIUMF Weak Interaction Symmetry Test*, **J.R. Musser (for the TWIST Collaboration)**, 2004 Spring Meeting of the APS, Denver, Colorado, (May 2004).

*Precision Mass Measurements in Weak Interaction Studies*, **J.C. Hardy, Invited Talk**, NIPNET International Workshop on High-Precision Mass Measurements, Saariselka, Finland, (April 2004).

*$V_{ud}$  Overview*, **J.C. Hardy, Invited Talk**, From Zero to  $Z^0$ : a Workshop on Precision Electroweak Physics, Fermilab, Illinois, (May 2004).

*CVC Tests and CKM Unitarity*, **J.C. Hardy, Invited talk**, INPC04, International Nuclear Physics Conference, Goteborg, Sweden, (June 2004).

*Superallowed  $0^+ \rightarrow 0^+$  Beta Decay and CKM Unitarity: A New Overview Including More Exotic Nuclei*, **J.C. Hardy, Invited talk**, ENAM04, Exotic Nuclei and Atomic Masses Conference, Pine Mountain, Georgia, (September 2004).

*Standard Model Tests with Superallowed  $\beta$  Decay: Nuclear Data Applied to Fundamental Physics*, **J.C. Hardy, Invited talk**, International Conference on Nuclear Data for Science and Technology, Santa Fe, New Mexico, (September 2004).

*Superallowed Nuclear Beta Decay: Probing the Weak Force with Precision On-Line Measurements*, **J.C. Hardy, Invited talk**, CAARI 2004, the 18<sup>th</sup> International Conference on the Application of Accelerators in Research and Industry, Fort Worth, Texas, (October 2004).

*Precise Branching Ratios in the Superallowed  $\beta$ -Decay of  $^{34}\text{Ar}$* , **V.E. Iacob**, J.C. Hardy, N. Nica, C.A. Gagliardi, G. Tabacaru, L. Trache and R.E. Tribble, APS meeting, Denver, Colorado, (May 2004).

*Precise Measurement of the K-Conversion coefficient for the 80.2 KeV Transition from  $^{193m}\text{Ir}$* , **N. Nica**, J.C. Hardy, V.E. Iacob, S. Raman, C.W. Nestor, Jr., M.B. Trzhaskovskaya, APS meeting, Denver, Colorado, (May 2004).

*Efficiency Calibration for a  $\beta$ - $\gamma$  Coincidence Set-Up: Source Measurements and Monte Carlo Calculations*, **V.E. Iacob**, J.C. Hardy, N. Nica, APS meeting, Chicago, Illinois, (October 2004).

*Resonance Scattering at Drip-Lines*, **V.Z. Goldberg**, LIV International Conference on Nucleus Spectroscopy and Nuclear Structure, Belgorod, Russia, (June 2004).

*Nuclear Structure of  $^9\text{He}$  and  $^7\text{He}$* , **V.Z. Goldberg**, EXON04 Symposium on Exotic Nuclei, St. Petersburg, Russia, (July 2004).

*Surprising Structure Effects in Light Drip-Line Nuclei*, **V.Z. Goldberg, Invited Talk**, Abo Akademii, Turku, Finland, (July 2004).

*Synthesis of Heavy and Superheavy Nuclei with Radioactive Beams: Plans and Expectations*, **G.G. Chubaryan**, International Symposium on Exotic Nuclei, Peterhof, Russia, (July 2004).

*Forecast on Heavy and Superheavy Element Research with Radioactive Beams*, **G.G. Chubaryan**, Department of Physics, University of Jyväskylä, Finland, (November 2004).

*Towards the Critical Behavior for the Light Nuclei by NIMROD Detector*, **Y.G. Ma**, R. Wada, K. Hagel, J.B. Natowitz and the NIMROD Collaboration, **Invited Talk**, SQM2004 conference, Capetown, South Africa, (September 2004).

*Thermometry and Caloric Curves*, **J.B. Natowitz**, **Invited Talk**, The World Consensus Initiative 3 (WCI3) Conference, Texas A&M University, College Station, Texas, (February 2005).

*Reaction Dynamics and Equilibration in Fermi-Energy Heavy Ion Collisions*, **J.B. Natowitz**, **Invited Talk**, ACS Meeting, San Diego, California, (March 2005).

*Forward Rapidity Results with BRAHMS at RHIC*, **K. Hagel** (for the BRAHMS Collaboration), **Invited Talk**, Symposium of Nuclear Physics 2005, Cocoyoc, Mexico, (January 2005).

*Charged Hadron Ratios in  $p + p$  Collisions at  $\sqrt{S_{mn}} = 200\text{GeV}$* , **K. Hagel** (for the BRAHMS Collaboration), **Invited Talk**, DNP Meeting, Chicago, Illinois, (October 2004).

*Forward Physics at RHIC with BRAHMS*, **K. Hagel** (for the BRAHMS Collaboration), **Invited Talk**, Chinese Center of Advanced Science and Technology Summer School and Workshop on QCD and RHIC Physics, Beijing, China, (August 2004).

*Heavy Ion Reaction Studies and the Nuclear Equation of State*, **S.J. Yennello**, ACS national meeting, Philadelphia, Pennsylvania (August 2004).

*Improving Graduate Education in Nuclear Science*, **S.J. Yennello**, 228<sup>th</sup> ACS national meeting, Philadelphia, Pennsylvania (August 2004).

*We Need You: the Top 10 Reasons to Go to Graduate School: Graduate Studies in Science and Engineering an Exciting Beginning to a Great Future*, **S.J. Yennello**, MAES Meeting, Austin, Texas, (November 2004).

*We Need You: the Top 10 Reasons to Go to Graduate School: Graduate Studies in Science and Engineering an Exciting Beginning to a Great Future*, **S.J. Yennello**, UTPan American Meeting, Edinburg, Texas, (November 2004).

*Hot Nuclei, Multifragmentation and the Nuclear Liquid-Gas Phase Transition*, **S.J. Yennello**, 228<sup>th</sup> ACS national meeting, ACS Meeting, San Diego, California, (March 2005).

*Projectile Fragmentation: A Route to Exploring the N/Z Degree of Freedom*, **S.J. Yennello**, ACS Meeting, San Diego, California, (March 2005).

*Isospin and Kinematical Properties of Heavy Residues from the Multifragmentation of Neutron-Rich Systems*, **G.A. Souliotis**, APS Meeting, Denver, Colorado, (May 2004).

*Heavy Residues as Probes of Isospin Dynamics and Equilibration in Deep Inelastic Collisions Around the Fermi Energy*, **G.A. Souliotis**, **Invited Talk**, Nuclear Chemistry Gordon Conference, Colby–Sawyer College, New London, New Hampshire, (June 2004).

*Deep-Inelastic Collisions with Accelerated Fission Fragments from the ANL Californium Source Upgrade*, **G.A. Souliotis**, ATLAS User Group Meeting, Physics Division, Argonne National Laboratory Argonne Illinois, (July 2004).

*Probing the Density Dependence of the Nuclear Symmetry Energy via Heavy-Residue Isoscaling*, **G.A. Souliotis**, DNP Meeting, Chicago, Illinois (October 2004).

*Probing the Nuclear Symmetry Energy via Heavy-Residue Isoscaling*, **G.A. Souliotis**, ACS Meeting, San Diego, California, (March 2005).

*Energy and Isospin Dependence of the Fragments Produced in Multifragmentation*, **D.V. Shetty**, APS Meeting, Denver, Colorado, (May 2004).

*Symmetry Energy and the Isospin Dependent Equation of State*, **D.V. Shetty**, DNP Meeting, Chicago, Illinois, (October 2004).

*Density Dependence of the Symmetry Energy and the Equation of State of Asymmetric Nuclear Matter*, **D.V. Shetty**, ACS Meeting, San Diego, California, (March 2005).

*(N/Z) Equilibration Study: Results*, **Elizabeth Bell**, APS Meeting, Denver, Colorado, (May 2004).

*The N/Z Degree of Freedom and Nuclear Multifragmentation*, **Elizabeth Bell**, Los Alamos National Laboratory, Los Alamos, New Mexico, (November 2004).

*Quasiprojectile Fragmentation Around Mass 40*, **August L. Keksis**, Third RIA Summer School on Exotic Beam Physics, ATLAS Facility, Argonne National Laboratory, Argonne, Illinois, (August 2004).

*Quasiprojectile Fragmentation in the Mass 40 Region*, **August L. Keksis**, ACS Meeting, Philadelphia, Pennsylvania, (August 2004).

*Quasiprojectile Fragmentation Around Mass 40*, **August L. Keksis**, DNP Meeting, Chicago, Illinois, (October 2004).

*A Multiple Ionization in L-Shell Ionizing Collisions*, **V. Horvat**, R.L. Watson, J.M. Blackadar, A.N. Perumal, and Yong Peng, 18<sup>th</sup> International Conference on the Application of Accelerators in Research and Industry, Ft Worth, Texas, (October 2004).

*From Quark-Gluon Plasma to Pentaquark Baryons*, **C.M. Ko**, **Invited Talk**, International Workshop on Pentaquarks, Heavy-Light Hadrons and Dense/Hot Matter, Seoul, South Korea, (May 2004).

*Pentaquark Baryon Production in Nuclear Reactions*, **C.M. Ko**, **Invited Talk**, Workshop on Strangeness and Exotica at RHIC, Brookhaven National Laboratory, New York, (May 2004).

*Production Mechanisms for Pentaquark Baryons*, **C.M. Ko**, **Invited Talk**, International Workshop PENTAQUARK04, SPring-8, Japan, (July 2004).

*Quark Coalescence at RHIC*, **C.M. Ko**, **Invited Talk**, STAR Collaboration Workshop, Beijing, China, (August 2004).

*Theoretical Overview of Relativistic Heavy Ion Collisions*, **C.M. Ko**, **Invited Talk**, 32<sup>nd</sup> International Conference on High Energy Physics, Beijing, China, (August 2004).

*Quark Coalescence in Relativistic Heavy Ion Collisions*, **C.M. Ko**, and V. Greco, **Invited Talk**, Proceedings of XLIII International Winter Meeting on Nuclear Physics, Bormio, Italy, (March 2005).

*Complete Boundary Conditions for the Three-Body Coulomb Scattering Wave Function and New Approach to the Ionization/Breakup Processes*, **A.M. Mukhamedzhanov**, APS meeting, Denver, Colorado, (May 2004).

*A Relation Between Proton and Neutron Asymptotic Normalization Coefficients for Light Mirror Nuclei and its Relevance to Nuclear Astrophysics*, **A.M. Mukhamedzhanov**, APS Meeting, Denver, Colorado, (May 2004).

*Insight the Theory of Trojan Horse I*, **A.M. Mukhamedzhanov**, **Invited talk**, INFN (National Institute of Nuclear Physics) and University of Catania, Catania, Italy, (May 2004).

*Insight the Theory of Trojan Horse II*, **A.M. Mukhamedzhanov**, **Invited talk**, INFN (National Institute of Nuclear Physics) and University of Catania, Catania, Italy, (June 2004).

*Off-Shell Effects in  $p+d \rightarrow p+p+n$  as a Way to Trojan Horse III*, **A.M. Mukhamedzhanov**, **Invited talk**, INFN (National Institute of Nuclear Physics) and University of Catania, Catania, Italy, (June 2004).

*Theory of Resonance Processes in Trojan Horse IV*, **A.M. Mukhamedzhanov**, **Invited talk**, INFN (National Institute of Nuclear Physics) and University of Catania, Catania, Italy, (June 2004).

*Few-Body Problems in Nuclear Astrophysics*, **A.M. Mukhamedzhanov**, 19<sup>th</sup> European Conference on Few-body problems in Physics, Groningen, the Netherlands, (August 2004).

*Indirect Techniques in Nuclear Astrophysics: Trojan Horse*, **A.M. Mukhamedzhanov**, **Invited talk**, Mainz University, Mainz, Germany, (August 2004).

*Asymptotic Normalization Coefficient and Interference of the Resonance and Direct Capture Terms in the Astrophysical Factor for the Hot CNO Process  $^{13}\text{N}(p,\gamma)^{14}\text{O}$* , **A.M. Mukhamedzhanov**, DNP APS Meeting, Chicago, Illinois, (October 2004).

*Few-Body Problems in Nuclear Astrophysics*, **A.M. Mukhamedzhanov**, International Conference: on Nuclear Structure, Astrophysics and Reactions, University of Surrey, Guilford, United Kingdom, (January 2005).

*Subthreshold States in Nuclear Astrophysics and ANC*, **A.M. Mukhamedzhanov**, **Invited talk**, INFN (National Institute of Nuclear Physics) and University of Catania, Catania, Italy, (January 2005).

*New Method of Determination of the Spectroscopic Factors from  $(d,p)$  Reaction*, **A.M. Mukhamedzhanov**, **Invited talk**, Oak Ridge National Laboratory, Oak Ridge, Tennessee, (February 2005).

*Physics of the Subthreshold States in Nuclear Astrophysics*, **A.M. Mukhamedzhanov**, **Invited talk**, Oak Ridge National Laboratory, Oak Ridge, Tennessee, (February 2005).

*Transfer Reactions: Spectroscopic Factors versus ANC's. Reaction Mechanisms for Rare Isotope Beams*, **A.M. Mukhamedzhanov**, **Invited talk**, 2<sup>nd</sup> Argonne/MSU/JINA/INT RIA Workshop, East Lansing, Michigan, (March 2005).

*Hadrons Below and Above  $T_c$* , **R. Rapp**, **Invited Talk**, International Workshop on Tracing Deconfinement in Nucleus-Nucleus Collisions, ECT\* Trento, Italy, (April 2004).

*Charm(onium) Re-Interactions in Nuclear Reactions*, **R. Rapp**, **Invited Talk**, Workshop on Heavy-Quark Production at RHIC at the RHIC-AGS Users Meeting, Brookhaven National Laboratory, Upton, New York, (May 2004).

*Thermal Photons in Strong Interactions*, **R. Rapp**, **Invited Talk**, GSI Darmstadt, Germany, (June 2004).

*Light and Heavy Hadrons in Medium*, **R. Rapp**, **Invited Talk**, University of Frankfurt, Frankfurt, (June 2004).

*The Vector Probe in Heavy-Ion Collisions*, **R. Rapp**, **Invited Talk**, International Workshop for Young Scientists on the Physics of Ultrarelativistic Heavy-Ion Collisions (Hot Quarks '04), Taos Valley, New Mexico, (July 2004).

*Dileptons at RHIC*, **R. Rapp**, **Invited Talk**, International Chinese Center of Advanced Science and Technology (CCAST) workshop, Beijing, China, (August 2004).

*What is the Origin of Mass?*, **R. Rapp**, Physics Department Graduate Orientation, Texas A&M University, College Station, Texas, (August 2004).

*Light and Heavy Hadronic Modes Below and Above  $T_c$* , **R. Rapp**, **Invited Talk**, Argonne National Laboratory, Argonne, Illinois, (October 2004).

*Quark Coalescence and Charm(onium) in QGP*, **R. Rapp**, **Invited Talk**, International Conference on Hard and Electromagnetic Probes of High Energy Nuclear Collisions, Ericeira, Portugal, (November 2004).

*Electromagnetic Radiation and In-Medium Effects*, **R. Rapp**, **Invited Talk**, European Graduate School workshop on Hadrons in Medium, Gießen, Germany, (November 2004).

*Perspectives on RHIC-II: Heavy Ions and Hot and Dense Matter*, **R. Rapp**, **Invited Talk**, RHIC-II Science Workshop, Brookhaven National Laboratory, Upton, New York, (November 2004).

*Light and Heavy Hadronic Modes in Medium*, **R. Rapp**, **Invited Talk**, University of Bielefeld, Bielefeld, Germany, (November 2004).

*Electromagnetic Probes of Medium Effects in Heavy-Ion Collisions*, **R. Rapp**, **Invited Talk**, International Workshop XXXIII on Gross Properties of Nuclei and Nuclear Excitations on Probing QCD with High Energy Nuclear Collisions, Hirschegg, Austria, (January 2005).

*Medium Modifications of the  $\Delta(1232)$* , **H. van Hees**, International Workshop for Young Scientists on the Physics of Ultrarelativistic Heavy-Ion Collisions (Hot Quarks '04), Taos Valley, New Mexico, (July 2004).

*Medium Modifications of the  $\Delta(1232)$* , **H. van Hees**, DNP APS Meeting, Chicago, Illinois, (October 2004).

*Thermalization of heavy quarks in the quark-gluon plasma*, **H. van Hees**, **Invited Talk**, International Workshop XXXIII on Gross Properties of Nuclei and Nuclear Excitations on Probing QCD with High Energy Nuclear Collisions, Hirschegg, Austria, (January 2005).

*Compression Modes and Nuclear Matter Incompressibility Coefficient within Relativistic and Non-relativistic Models*, **S. Shlomo**, **Invited Talk**, International Nuclear Physics Conference (INPC-2004), Goteborg, Sweden, (June 2004).

*The Nuclear Matter Equation Incompressibility Coefficient from Isoscalar Compression Modes*, **S. Shlomo**, **Invited Talk**, The World Consensus Initiative 3 (WCI3) Conference, Texas A&M University, College Station, Texas, (February 2005).

*The Nuclear Matter Equation of State from Compression Modes*, **S. Shlomo**, **Invited Talk**, The 229<sup>th</sup> American Chemistry Society National Meeting, San Diego, California, (March 2005).

*Hadronization via Coalescence*, **V. Greco**, Conference on Hot Quarks 2004, Taos, New Mexico, (July 2004).

*The Search for the Quark-Gluon Plasma in Heavy-Ion Collision*, **V. Greco**, INFN Italian Summer School, Otranto, Italy, (September 2004).

*Signatures of Quark Recombination at RHIC*, **V. Greco**, 1<sup>st</sup> ALICE Italian National Meeting, University of Catania, Catania, Italy, (January 2005).

*Charm and Beauty in the Search for the Quark Gluon Plasma*, **V. Greco**, University of Padova, Padova, Italy, (January 2005).

*The Search for the Quark Gluon Plasma at the Relativistic Heavy Ion Collider*, **V. Greco**, University of Florence, Florence, Italy, (January 2005).

*Studying the Primordial Plasma after Big-Bang through Little Bang*, **V. Greco**, Aerospace Engineering Department, Texas A&M University, College Station, Texas, (March 2005).

## RESEARCH PERSONNEL AND ENGINEERING STAFF

April 1, 2004 - March 31, 2005

### Faculty and Research Group Leaders

Carl A. Gagliardi, Professor of Physics  
John C. Hardy, Professor of Physics  
Che Ming Ko, Professor of Physics  
Akram M. Zhanov, Senior Scientist  
J. B. Natowitz, Professor of Chemistry, Bright Chair  
Ralf Rapp Assist. Prof. of Physics  
Shalom Shlomo, Senior Scientist  
Robert E. Tribble, Professor of Physics, Director  
Rand L. Watson, Professor of Chemistry  
Sherry J. Yennello, Prof. of Chemistry  
Dave H. Youngblood, Professor of Physics

### Research Staff

Henry Clark, Accelerator Physicist (50%)  
Grigor Chubaryan, Research Scientist  
John C. Hagel, Research Scientist (50%)  
Vladimir Horvat, Research Scientist (50%)  
Victor Iacob, Associate Research Scientist  
Yiu-Wing Lui, Research Scientist  
George Souliotis, Assistant Research Scientist  
Livius Trache, Research Scientist  
Maxim Vasilyev, Assistant Research Scientist (80%)  
Ryoichi Wada, Research Scientist

### Visiting Scientists

Juha Arje – From 10/6/04 To 12/15/04  
Florin Carstoiu – From 1/7/05  
Vladilen Goldberg  
Zbigniew Majka – To 6/22/04  
V. Kolomietz – From 1/10/05  
Ian Towner – From 8/3/04 To 9/15/04

### Accelerator Physics And Radiation Line Staff

Henry Clark, Accelerator Physicist (50%)  
Vladimir Horvat, Research Scientist (50%)  
Bruce Hyman, Research Associate  
George Kim, Accelerator Physicist

Don May, Accelerator Physicist  
Dennis Utley, Research Associate (25%)

### Computer Systems Staff

Robert Burch, Jr., Systems Analyst/Sr.  
Microcomputer/LAN Administrator –  
From 4/1/04  
John C. Hagel, Assoc. Research Scientist (50%)  
Maxim Vasilyev, Asst. Research Scientist (20%)

### Engineering Staff

Greg Derrig, Senior Mechanical Engineer  
Robert Olsen, Mechanical Engineer

### Postdoctoral Research Associates

Bijay Agrawal – To 12/23/04  
Narayana P. Appathurai – To 9/30/04  
Lie-Wen Chen – To 9/1/04  
Vicenzo Greco  
Marian Jandel  
Seweryn Kowalski  
Wei Liu – From 2/1/05  
Massimo Mannarelli – From 8/2/04 To 2/28/05  
Thomas Materna  
Ninel Nica  
Dinesh Shetty  
Tapas Sils – From 11/02/04  
Gabriel Tabacaru  
Yoshiaki Tokimoto  
Hendrik van Hees  
Jiansong Wang – To 12/22/04

## STUDENTS

April 1, 2004 - March 31, 2005

### Graduate Students

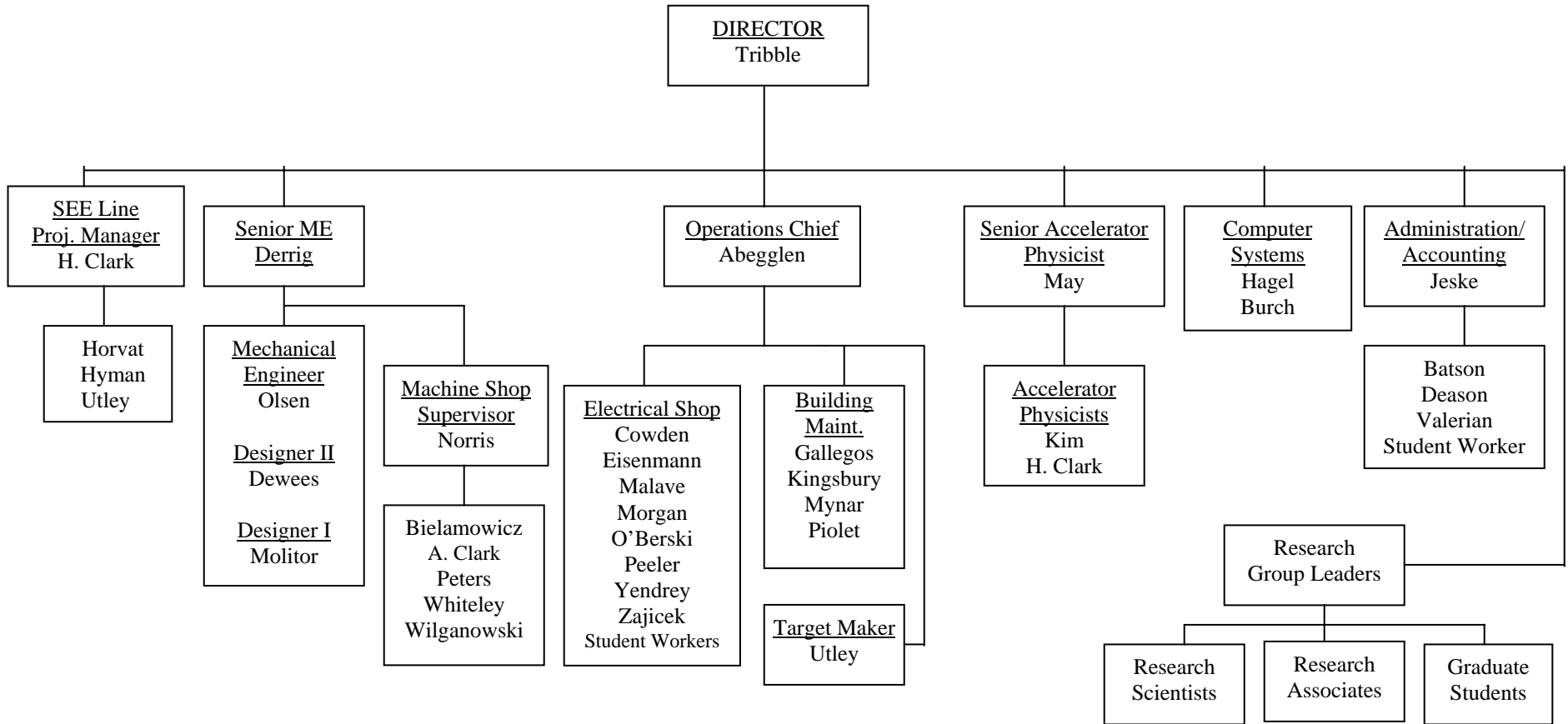
Tariq Al-Abdullah  
Joseph Brinkley  
Xinfeng Chen  
James Drachenberg – From 9/1/04  
Changbo Fu  
John Goodwin – From 9/1/04  
Thomas Henry  
Jennifer Iglie – From 6/1/04  
August Keksis  
Wei Liu – To 12/17/04  
Elizabeth Martin  
Ranjini Murthy – From 10/15/04  
James Musser  
Luciano Pappalardo – To 11/3/04  
Hyo-In Park – From 9/1/04  
Yong Peng  
Fakhriddin Pirlepsov  
Oleksiy Pochivalov  
Nathaniel J. Pogue – From 6/1/04  
Li Jun Qin  
Sarah Soisson  
Brian Stein  
Deqiang Sun – From 6/1/04  
Au Kim Vuong  
Sara Wuenschel – From 6/1/04  
Yongjun Zhai

### Undergraduates and Student Technicians

Michael G. Arvizu – From 7/12/04  
Jaime L. Estes – To 5/7/04  
Joshua Garey  
Stephen Hanssen  
Chelsey Jones – To 5/12/04  
Chelsi Kaltwasser – To 12/17/04  
Meagan Makarenko – From 1/6/05  
Matthew Mccleskey  
Emily Melton – From 6/1/04  
Sarah Parketon – To 10/5/04  
Barrett C. Parker  
Casseday Richers  
Michael Sarahan  
Brandy L. Tucker – From 5/13/04 To 8/3/04  
William D. Wright  
Peter J. Yunker – From 8/2/04  
Kylee Ziegler – From 8/3/04

# ORGANIZATIONAL CHART - CYCLOTRON INSTITUTE

VII-10



**STUDENTS WHO RECEIVED GRADUATE DEGREES  
FROM THESIS WORK CONDUCTED  
AT  
THE CYCLOTRON INSTITUTE**

**April 1, 2004 – March 31, 2005**

<b>Name</b>	<b>Year</b>	<b>Thesis Title</b>	<b>Advisor</b>	<b>First Position</b>	<b>Present Position</b>
Wei Liu	2004	<i>Charmonium absorption and charmed hadron production in hadronic reaction</i>	Che-Ming Ko	Graduate Research Assistant	Post Doc. at Cyclotron Institute, Texas A&M University

## INSTITUTE COLLOQUIA AND SEMINARS

April 1, 2004-March 31, 2005

### 2004

- |              |   |  |
|--------------|---|--|
| April 8      | Dr. Jeffrey W. Martin, Kellogg Radiation Laboratory, California Institute of Technology, Pasadena, California | <i>Ultracold Neutrons</i>  |
| April 20     | Professor J. W. Watson, Department of Physics, Kent State University, Kent, Ohio                              | <i>Short-range Correlations in Nuclei from <math>(p,2p+n)</math> and <math>(e,e'p+N)</math> Measurements</i>         |
| May 10       | Mr. Sean Liddick, NSCL-Michigan State University, East Lansing, Michigan                                      | <i>The Evolution of Shell Structure in the <math>A\sim 60</math> Mass Region</i>                                     |
| May 25       | Dr. Juha Ärje, Department of Physics, Cyclotron Lab., University of Jyväskylä, Jyväskylä, Finland             | <i>IonGuide-ECRIS Facility: Production of Radioactive Ion Beams for K500 MeV Cyclotron</i>                           |
| May 27       | Dr. R. K. Choudhury, Institute of Physics, Bhubaneswar, India   | <i>Study of Heavy Ion Fusion Dynamics from Fission Fragment Angular Distributions</i>                                |
| June 22      | Dr. Raj K. Gupta, Department of Physics, Punjab University, Chandigarh, India                                 | <i>Dynamical Clusterization Process in Hot and Rotating Nuclei Formed in Heavy Ion Reactions</i>                     |
| July 30      | Professor C. O. Dorso, Universidad de Buenos Aires, Buenos Aires, Argentina                                   | <i>Dynamics and Thermodynamics of Excited Drops</i>  |
| August 26    | Dr. Guy Savard, Argonne National Laboratory and University of Chicago, Argonne, Illinois                      | <i>The Proposed ATLAS Californium Source Radioactive Beam Upgrade</i>  |
| September 3  | Dr. Massimo Mannarelli, Cyclotron Institute, Texas A&M University, College Station, Texas                     | <i>Gapless Color Superconductivity</i>   |
| September 10 | Professor Yu. M. Tchuvil'sky, Moscow State University, Moscow, Russia   | <i>Microscopic Theory of Alpha-Particle States in Nuclei, Alpha-Condensate and the Statistics of Alpha-Particles</i> |
| September 17 | Dr. Massimo Mannarelli, Cyclotron Institute, Texas A&M University, College Station, Texas                     | <i>Gapless Color Superconductivity - Lecture II</i>  |

September 17	Professor Juha Aysto, University of Jyväskylä, Jyväskylä, Finland	<i>Towards Precision Mass Measurement of Radioactive Ions with a Penning Trap at IGISOL</i>
September 21	Dr. Rituparna Kanungo, RIKEN Institute, Wako, Japan	<i>Exporing the New Nuclear Structure Near Drip Lines</i>
September 24	Dr. Ralf Rapp, Cyclotron Institute, Texas A&M University, College Station, Texas	<i>Thermal Photons in Strong Interactions</i>
October 4	Dr. Georges Audi, Center for Nuclear and Mass Spectrometry, Orsay, France	<i>Masses, Half-Lives, Spins and Decays of Nuclides</i>
October 5	Dr. Isao Tanihata, Argonne Natinal Laboratory, Argonne, Illinois	<i>What's New with Nuclear Halo's and Neutron Skin's</i>
October 8	Dr. Oded Heber, Department of Particle Physics, Weizmann Institute of Science, Rehovot, Israel	<i>Charged Particle Dynamics in an Electrostatic Ion Trap</i>
October 12	Dr. A. M. Mukhamedzhanov, Cyclotron Institute, Texas A&M University, College Station, Texas	<i>Can Spectroscopic Information be Extracted from Transfer Reactions?</i>
October 19	Professor Konstantin Gridnev, St. Petersburg University, St. Petersburg, Russia	<i>The Nuclear Model of Binding Alpha-Particles</i>
October 22	Dr. Vincenzo Greco, Cyclotron Institute, Texas A&M University, College Station, Texas	<i>The Search for the Quark-Gluon Plasma in Relativistic Heavy-Ion Collisions – Lecture I</i>
October 26	Dr. Aldo Bonasera, Lab. Nat. del sud-INFN, Catania, Italy	<i>Constrained Molecular Dynamics for Fermions</i>
November 4	Mrs. Elizabeth Bell, cyclotron Institute, Texas A&M University, College Station, Texas	<i>N/Z Equilibration</i>
November 5	Dr. Vincenzo Greco, Cyclotron Institute, Texas A&M University, College Station, Texas	<i>The Search for the Quark-Gluon Plasma in Relativistic Heavy-Ion Collisions – Lecture II</i>
November 5	Dr. Hendrik van Hees, Cyclotron Institute, Texas A&M University, College Station, Texas	<i>Charm in Heavy Ion Collisions</i>

November 10	Mr. August L. Keksis, Cyclotron Institute, Texas A&M University, College Station, Texas	<i>Quasiprojectile Fragmentation with 32 and 45 MeV/u <math>^{40}\text{Ar}</math>, <math>^{40}\text{Ca}</math> and <math>^{48}\text{Ca}</math> on <math>^{112}\text{Sn}</math> and <math>^{124}\text{Sn}</math></i>
November 10	Mr. Fakhriden Pirlepsov, cyclotron Institute, Texas A&M University, College Station, Texas	<i>Asymptotic Scattering Wave Function for Three Charged Particles and Astrophysical Capture Processes</i>
November 17	Mr. Yong Peng, Cyclotron Institute, Texas A&M University, College Station, Texas	<i>Systematics of Cross Sections for Target K Vacancy Production in Heavy Ion Collisions</i>
November 17	Mr. Lijun Qin, Cyclotron Institute, Texas A&M University, College Station, Texas	<i>p-A, A-A Collisions with NIMROD</i>
November 19	Professor Ronald Bryan, Department of Physics, Texas A&M University, College Station, Texas	<i>The Low-Energy Nucleon-Nucleon Interaction and the Sigma Meson</i>
November 23	Dr. T. Udagawa, Department of Physics, University of Texas, Austin, Texas	<i>Extension of Direct Reaction Theories to Incomplete and Complete Fusion Reactions</i>
December 1	Mr. Au Kim Vuong, Cyclotron Institute, Texas A&M University, College Station, Texas	<i>New Effective Nucleon-Nucleon Interaction</i>
December 1	Mr. Oleksiy Pochivalov, Cyclotron Institute, Texas A&M University, College Station, Texas	<i>Microscopic Description of Properties of Isoscalar Giant Dipole Resonance in Nuclei</i>
December 1	Mr. Tariq Ai-Abdullah, Cyclotron Institute, Texas A&M University, College Station, Texas	<i>Extracting the ANCs for <math>^{23}\text{Al}</math>, <math>^{22}\text{Mg}+p</math> from the Mirror System <math>^{23}\text{Ne}</math>, <math>^{22}\text{Ne}+n</math></i>
December 3	Dr. Sabin Stoica, National Institute of Physics & Nuclear Engineering, Bucharest, Romania	<i>Recent Results on Neutrino Properties</i>
December 8	Mr. Changbo Fu, Cyclotron Institute, Texas A&M University, College Station, Texas	<i>Determine <math>S_{34}</math> Factor from <math>^7\text{Be}</math> Breakup Reaction</i>
December 8	Mr. Xinfeng Chen, Cyclotron Institute, Texas A&M University, College Station, Texas	<i>Giant Resonance Study by <math>^6\text{Li}</math> scattering</i>

December 10	Dr. Loic Grandchamp, Lawrence Berkeley National laboratory, Berkeley, California	<i>Quarkonium Production in Heavy-Ion Collisions</i>
December 14	Dr. Frances Hanappe, P.N.T.P.M.- Université Libre de Bruxelles, Brussels, Belgium	<i>News from DEMON: Dynamics of Capture Reactions the Tetraneutron Enigma</i>
December 15	Mr. Thomas Henry, Cyclotron Institute, Texas A&M University, College Station, Texas	<i>Thesis Progress on Jet Reconstruction in <math>d+Au</math> and <math>p+p</math> Collisions at RHIC</i>
<b><u>2005</u></b>		
January 18	Dr. Hanan Amro, University of Notre Dame, South Bend, Indiana	<i>Nuclear Reactions with Exotic Nuclear Beams</i>
February 9	Dr. Larry Ahle, Lawrence Livermore National Laboratory, Livermore, California	<i>Stockpile Stewardship and Radioactive Beam Facilities</i>
February 11	Dr. Andrei Kryjevski, University of Washington, Seattle, Washington	<i>Meson Condensates in CFL Superconductors</i>
February 25	Dr. Tapas Sil, Cyclotron Institute, Texas A&M University, College Station, Texas	<i>An Effective Field Theory: Applicability to Nuclear Systems</i>
March 1	Dr. Yu-Gang Ma, Shanghai Institute of Applied Physics, Chinese Academy of Sciences, Shanghai, China	<i>Studies of Nucleon-Nucleon Momentum Correlation Function in the Reactions Induced by Neutron-rich or Proton-Rich Light Nuclei</i>
March 3	Dr. Jeff Blackmon, Physics Division, Oak Ridge National Laboratory, Oak Ridge, Tennessee	<i>Nuclear Physics in Stellar Explosions</i>
March 4	Mr. Fakhriden Pirlepsov, cyclotron Institute, Texas A&M University, College Station, Texas	<i>Asymptotic Scattering Wave Function for Three Charged Particles and Astrophysical Capture Processes</i>
March 10	Dr. Robert Grzywacz, University of Tennessee and Oak Ridge National Laboratory, Oak Ridge, Tennessee	<i>Experimental Studies of the Nuclei Far from Stability with Digital Signal Processing</i>
March 11	Dr. Ralf Rapp, Cyclotron Institute, Texas A&M University, College Station, Texas	<i>Thermal Field Theory and Instantons I</i>
March 17	Professor Nguyen Dinh Dang, RIKEN, Wako, Japan	<i>Particle-Number Conservation with the Self-Consistent RPA</i>

March 22	Dr. Stratos Galanopoulos, National Technical University of Athens, Athens, Greece	<i>Proton Capture Cross Section Measurements in Sr Isotopes Relevant to p-Process Nucleosynthesis</i>
March 24	Dr. Michael Famiano, National Superconducting Cyclotron Laboratory, Michigan State University, East Lansing, Michigan	<i>High Resolution Experiments in Nuclear Astrophysics</i>